Microcirculatory and Myocardial Physiology in Ischaemic Left Ventricualr Dysfunction

De Silva, Kalpa

Awarding institution:
King's College London

Title: Microcirculatory and Myocardial Physiology in Ischaemic Left Ventricualr Dysfunction

Author: Kalpa de Silva

Microcirculatory and Myocardial Physiology in Ischaemic Left Ventricular Dysfunction

Kalpa Gayantha De Silva

Cardiovascular Division
The Rayne Institute
St. Thomas' Hospital
King's College London
London, UK

Submitted for the

Degree of Doctor of Philosophy

To the University of London

2013

ABSTRACT

Introduction

Left ventricular (LV) dysfunction influences, and is affected by, changes in coronary flow. The integrity of the microvasculature is integral in myocardial perfusion and myocyte function, and remains incompletely understood in the context of impaired LV function. The main aim of this thesis was to examine the physiological alterations that occur to the microcirculation and myocardial function following myocardial infarction.

Methods

Simultaneous intra-coronary pressure and Doppler flow assessment with wave intensity analysis performed to determine the energy flux in the coronary circulation was undertaken following percutaneous revascularization, in two distinct cohorts. Firstly, in a group with recent myocardial infarction and secondly in a group undergoing revascularization supported by intra-aortic balloon counterpulsation (IABP) therapy. In a separate group, the electrophysiological alterations occurring following acute myocardial infarction were assessed using a novel trans-coronary epicardial voltage mapping technique.

Results

We demonstrated that the microcirculatory expansion wave in the infarct-related artery is predictive of both infarct size and regional ventricular recovery following revascularization, assessed by cardiac MRI. Intra-aortic balloon inflation was temporally associated with a unique acceleratory aortic-originating compression wave energy. The magnitude of this

wave relates linearly to augmentation of coronary flow velocity during hyperaemic conditions, where autoregulation is 'switched-off'. During basal, 'switched-on' autoregulatory conditions, IABP therapy does not significantly augment flow, due to an increase in microvascular resistance and reduction in microcirculatory expansion wave energy. Trans-coronary electrogram mapping is technically feasible during percutaneous revascularization procedures, with encouraging results in regard to voltage-mapped parameters that may allow prediction of infarcted versus viable tissue.

Conclusion

The microcirculation is integral in the functioning of the myocardium. Wave energy derivatives provide an integrated assessment of microvascular haemodynamics and regional myocardial function. Furthermore, the efficacy of intra-aortic balloon counterpulsation is likely to be dependent on the degree of microvascular dysfunction present, with those whose salient haemodynamics are beyond the autoregulatory range most likely to benefit from mechanical assist support devices. Trans-coronary epicardial voltage mapping may provide a technique for the assessment of myocardial viability following infarction, though further development is required to determine its utility and accuracy.

ACKNOWLEDGMENTS

I would like to thank my supervisors Dr Divaka Perera, Professor Sven Plein and Professor Simon Redwood, for their support, tutelage and encouragement throughout my time in research. I particularly want to thank Dr Perera for his unwavering support, enthusiasm and energy during the microcosm that clinical research represents. This has been greatly appreciated and has nurtured my personal interest in research. In addition, I would like to thank Professor Michael Marber for his advice and support, and Professor Eike Nagel for his supervision in the development of my clinical cardiac MRI training.

All of the studies in this thesis were performed at the cardiac catheter laboratories at St. Thomas' Hospital, London, and I want to thank all of the lab staff, who were always accommodating and willing to help, despite the prolonged nature of many of the study protocols. Furthermore, I am grateful to the cardiac MRI radiographers and administrative staff in both the cardiology and imaging sciences departments.

I would like to thank all of the fellows who I have worked with during my time in research. They provided an important support network and helped me conduct my research by aiding with recruitment and offering suggestions and encouragement when needed.

I owe a great deal to my parents, who have made many personal sacrifices to allow me to pursue my career. I would like to thank them for this, and for the support they have always provided me.

Finally, to my wife, Raakhee, though last in my acknowledgments, is always foremost in my thoughts, and has personally shared in all of the vicissitudes that my research has entailed. I am deeply grateful for her unstinting support, understanding and love throughout my career and during my time in research. Thank you. It is to her that I would like to dedicate this thesis.

TABLE OF CONTENTS

LIST OF FIGURES

1. BACKGROUND

Coronary artery disease remains the most significant cause of mortality in the world, with over seven million deaths per year attributed to this disease process.[1] The study and investigation of the human circulation has been under scrutiny for centuries, however many intricacies of the coronary circulation and its relationship to atherosclerosis remain incompletely understood, particularly in relation to the microcirculation.


EXERCITATIO
ANATOMICA DE
MOTV CORDIS ET SAN-
GVINIS IN ANIMALI-
BVS,
GVILIELMI HARVEI ANGLI,
Medici Regii, & Professoris Anatomiæ in Col-
legio Medicorum Londinensi.
FRANCOFVRTI,
Sumptibus GVILIELMI FITZERI.
ANNO M. DC. XXVIII.

"...It must of necessity be concluded that the blood is driven into a round by a circular motion in living creatures, and that it moves perpetually; and that this is the function of the heart, which by pulsation it performs; and lastly, that the motion and pulsation of the heart is the only cause…"

Figure 1: *An extract from De motu cordis (1628), Dr William Harvey – providing the first written description of the arterial circulation and its dependence on the heart*

1.1 *Physiology of the Human Coronary Circulation*

1.1.1 Autoregulation of Coronary Blood flow in the normal heart

Myocardial perfusion is controlled by various factors acting to regulate the coronary circulation. Coronary blood flow provides the required oxygen supply for any given myocardial oxygen demand across a range of perfusion pressures (Figure 2), increases automatically from a resting level to a maximum level in response to increases in myocardial oxygen demand from physiological stimuli such as exercise, or as a result of neurohumoral or pharmacological hyperemic stimuli. This increase from baseline resting perfusion conditions to maximal flow is termed the coronary flow reserve (CFR). Myocardial perfusion is regulated by three major resistance components, occurring at three respective levels of coronary circulatory anatomy: the epicardial artery, the prearterioles, and the intramyocardial capillary network (microcirculation). In the normally functioning circulation, the resistances across these compartments vary in accordance to the nature of the vessel . The epicardial compartment includes vessels ranging from 0.5mm-5mm. The predominant function of these vessels is to provide capacitance and under normal conditions offer minimal resistance to flow, contributing only 7% to the overall coronary resistance. Alterations in resistance occur at the microcirculatory level, (arterioles <200um in diameter); these are the vessels which exert most control on coronary blood flow to the heart[2] and are responsible for the maintenance of coronary vasomotor tone which allows physiological and pathological stimuli such as exercise, to cause a three to five fold increase in coronary flow.[3]

Whilst the microvasculature can be sub-divided into three distinct anatomical categories (100-200µm, 40-100µm and <30 µm) the mechanisms that regulate the flow of blood within these compartments functionally overlap with one another. There is a tendency for each domain of

microvessel to have a predominant regulating mechanism, and in the event that one mechanism becomes dysfunctional or is inhibited, then other mechanisms become active to compensate. Within the largest arterioles it has been demonstrated that endothelial dependent dilation is the most prominent mode of regulation, with the converse being observed in the smallest vessels.[4] In these larger mircrocirculatory vessels, an increase in flow rate causes vasodilatation and a reduction in flow causes vasoconstriction. Whilst endothelial dependent mechanisms are also present in medium sized arterioles (40μm - 100μm) the main regulating mechanism is dependent on intraluminal pressure changes within vessels. Intraluminal pressure is detected by vascular smooth muscle cell stretch receptors, with resultant vasoconstriction with increasing intraluminal pressure. Conversely a reduction in intraluminal pressure causes compensatory vasodilatation due to smooth muscle relaxation. This pressure sensitive mechanism is known as myogenic control[5]. The smallest arterioles (<30 μm) are regulated by changes in metabolic activity, whereby an increase in metabolic activity leads to vasodilatation.[4] Therefore in the microcirculation, an increase in metabolic activity initially causes the tiny vessels to dilate. This causes a secondary reduction in pressure upstream in the medium sized vessels causing myogenic dilation, leading to increased flow further upstream in the larger arterioles causing endothelial dependent dilation.[6] This auto-regulatory mechanism allows a rapid response to physiological stimuli, with sequential activation from the smallest vessels to the largest arterioles, to maintain or increase myocardial perfusion to match metabolic demand (Figure 3).

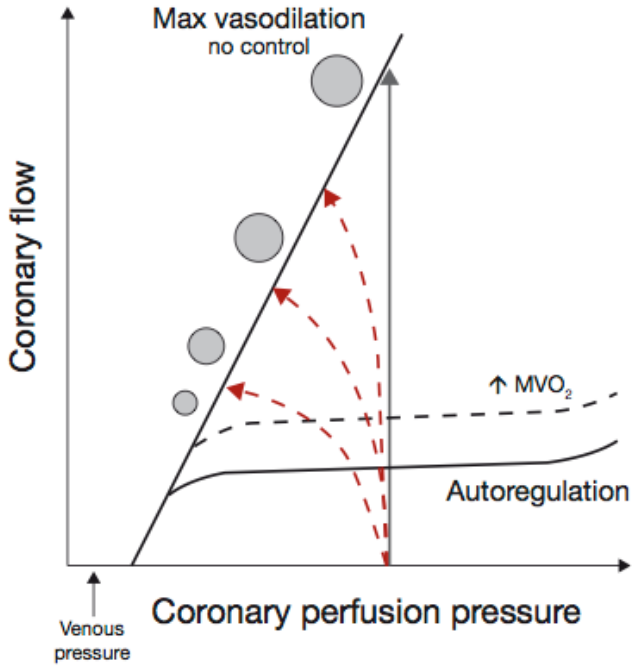

Figure 2: *Haemostatic Coronary Autoregulation - Coronary pressure–flow relationship. At rest, flow is maintained over a large range of physiological pressures by a parallel change in resistance. The dashed line indicates autoregulation at higher oxygen consumption. At maximal vasodilatation, flow can increase up to about five times in the absence of a stenosis (grey vertical line). Control is exhausted and coronary flow depends on perfusion pressure. As vascular tone is minimal, vessel diameter decreases with reduced distending pressure. The nonlinear pressure loss across a stenosis (red dotted lines) significantly reduces the maximal flow that can be achieved. Note that the maximal pressure–flow line has a non-zero intercept, which implies that microvascular resistance is pressure dependant. MVO_2 =myocardial oxygen consumption. (Adapted from Siebes et al)*[7]

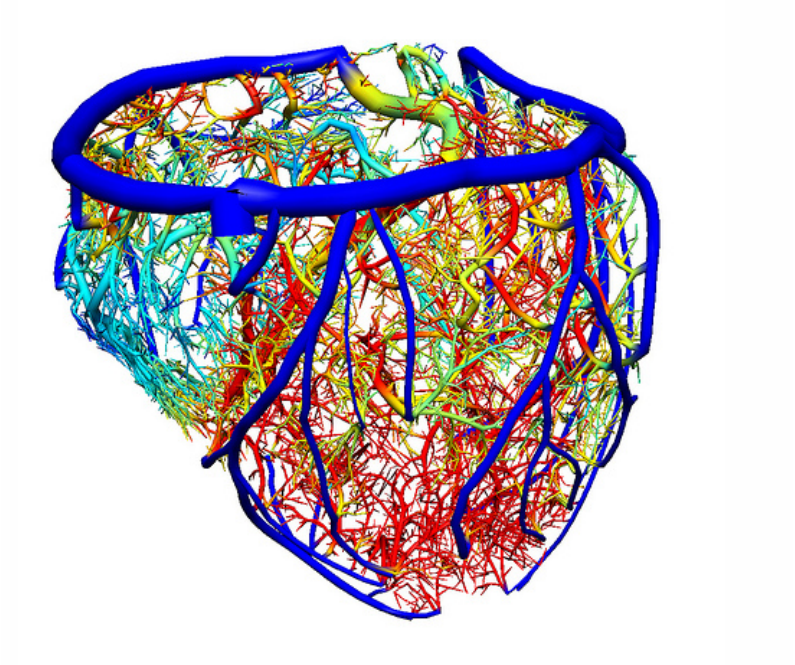

Figure 3: *Computerized representation of the Coronary Microcirculation*
(Image courtesy of Nic Smith, Biomedical Engineering department, Imaging Sciences, King's College London)

1.1.2 Coronary Blood flow in the presence of Coronary artery disease

The Coronary Pressure-flow relationship

Myocardial ischaemia results from an imbalance between myocardial oxygen demand and the supply achievable by the coronary circulatory system. The autoregulatory processes described above normally maintain the basal flow rate at a constant level in response to changing pressure and oxygen demand (Figure 2). Atherosclerosis and subsequent stenoses increase resistance within the epicardial compartment of the circulation. In the presence of a narrowing that causes a critical reduction in vessel lumen area, there is a disruption to the normal haemostatic auto-regulatatory response because of compensatory vasodilatation of the microcirculatory compartment, leading to a diminished or abolished coronary reserve, predisposing to reduced resting coronary blood flow and a mismatch in myocardial oxygen demand and supply. In addition to the affect of coronary disease on the mechanisms of resistance control of the coronary circulation, this is coupled with reduced coronary flow as a direct result of pressure diminution distal to a stenosis. The complex fluid dynamics associated with a stenosed vessel results in the pressure damping and is secondary to two main sources of energy losses - frictional and inertial. The frictional losses occur at the entrance and within the stenotic region. These losses, in accordance to Poiseuille's law, are linearly related to flow (Q). Inertial losses stem from the sudden expansion at the end of a stenosis, causing flow separation, turbulence and eddies (reversal of flow), which is governed by Bernoulli's principle, with these exit losses increasing with square of flow, caused by the convective acceleration in the narrowed segment. Theses two factors result in energy losses producing a consequent pressure loss distal to the stenosis and thus a pressure gradient across the narrowed segment (Figure 4).

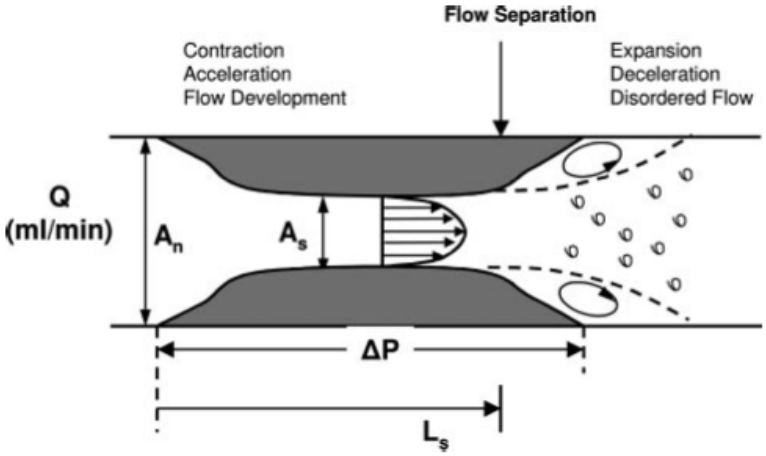

Figure 4: *Fluid dynamics of an epicardial stenosis, and the resultant frictional and inertial energy losses. A_s indicates area of the stenosis; A_n, area of the normal segment; and L_s, effective length of stenosis (up to the point of flow separation). Adapted from Kern et al.*[8]

Gould et al[9] demonstrated the relationship between resting and maximal myocardial blood flow at varying degrees of stenosis severity (Figure 5). It was determined that resting coronary blood flow remains intact with a 40-80% stenosis, but maximal flow will be reduced. Within this range of stenoses, repetitive ischaemia and increased oxygen demand may result in myocardial stunning. A stenosis of more than 80% may, however, reduce resting coronary blood flow and therefore render the myocardium subtended by the diseased vessel hypoperfused, which occurring chronically, results in a reduction in metabolic and contractile function. In the acute setting there is likely to be a degree of over lap between these two physiological states, as a chronically hypoperfused area of myocardium could suffer an acute ischaemic insult and be 'stunned' in addition to the baseline resting state.

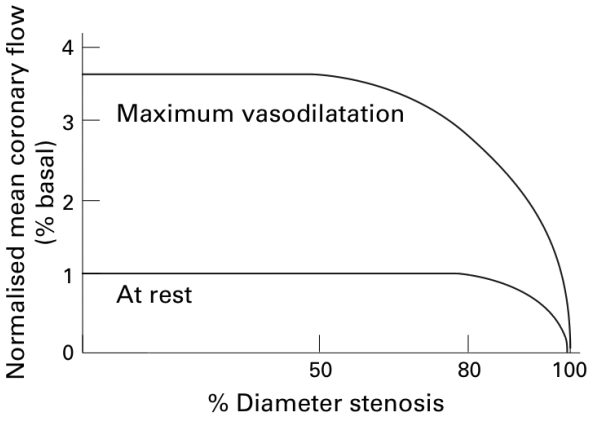

Figure 5: *Relationship of percentage stenosis and coronary flow (Adapted from Gould et al)*[10]

The microcirculation in coronary disease

Epicardial coronary flow was thought to be the most important determinant in myocardial perfusion, however, as described above it has been shown that coronary blood flow is autoregulated in relation to variations in aortic pressure and the metabolic requirements of the myocardium by changes in the resistances of the prearterioles (100-200µm) and arterioles (<100µm) respectively, as described above.[11]

The autoreguatory process present in the normal coronary circulation is altered in the presence of coronary artery disease (CAD). This vasodilatory reserve is progressively weakened in the presence of coronary atherosclerosis, as the coronary resistance is redistributed from the microvasculature to the less elastic epicardial circulation. Ultimately the vasodilator reserve is lost, and relative myocardial hypoperfusion ensues in response to increase myocardial oxygen consumption.

Acute coronary syndromes occur as a result of a prolonged period of myocardial ischaemia subsequent to a reduction in resting coronary flow, leading to a diminished oxygen supply, leading to irrerversible myocardial necrosis. In clinical practice microvascular dysfunction is frequently

observed in the setting of acute coronary syndromes and is likely to have a bidirectional relationship with infarction, as it may be unclear as to whether epicardial atherothrombosis was caused or directly effected by microvascular dysfunction. Frequently, despite the therapeutic goal of establishing patency of the infarct-related epicardial artery is achieved, the myocardial blood flow in the infarcted area is observed to be inadequate, visually represented as the 'no-reflow' phenomenon.[12] This is consequence to the presence of significant microvascular obstruction and dysfunction. Importantly the severity of microvascular dysfunction post infarction has been demonstrated to be an important correlate of left ventricular (LV) functional recovery, cardiovascular morbidity and mortality and is proportionate to infarct size.[13, 14]

In clinical practice microvascular dysfunction is frequently observed in the setting of acute coronary syndromes, especially following reperfusion of acute myocardial infarction. Despite establishing angiographic patency of the infarct-related epicardial artery, myocardial blood flow can remain inadequate, a phenomenon known as 'no-reflow'.[12] No-reflow occurs in up to 30% of patients, and is thought to be a consequence of microemboli and subsequent microvascular obstruction (MVO).[15] The severity of microvascular dysfunction post infarction has been demonstrated to be an important correlate of left ventricular (LV) functional recovery, cardiovascular morbidity and mortality and is proportionate to infarct size.[13, 14] Additionally, MVO has been shown to be a powerful independent predictor of adverse outcome.[14, 16]

Kloner et al. first described to the presence of MVO in a canine coronary artery occlusion-reperfusion model, demonstrating a link between angiographic no-reflow phenomenon and severely damaged intramural microvessels with specific histological features of endothelial cell swelling, protrusions, and decreased pinocytic vesicles.[17] Additional histological changes that have

been suggested to occur during the formation of MVO are the production of reactive oxygen species leading to the disruption of endothelial cells, fibrin and platelet deposition, neutrophil activation, and haemorrhagic red cell extravasation following reperfusion. Epicardial thrombi and microvasculature thrombosis may also result from necrotic plaque particulates being showered distally into the myocardium following plaque rupture or as a result of coronary interventional procedures.[18-21]

1.1.3 Myocardial perfusion and ventricular function

A reduction in coronary blood flow from an occlusive stenosis will, ultimately, cause a reduction in left ventricular contraction and function[22]. The effect of a short non-lethal episode of ischaemia is seen on both a functional and cellular level. The impact of coronary occlusion on LV function depends on the duration of interruption in blood flow. Animal models have shown that, following a short period of epicardial coronary occlusion (15-20 minutes) and subsequent release of the occlusion, the initially ischaemic dysfunctional myocardium remains dysfunctional for a few days before ultimately returning to normal[23]. Furthermore, it has been demonstrated that an ischaemic insult has a direct effect on myocardial cellular function, with a reduction in Adenosine 5-triphosphate (ATP) reserves observed, though a gradual recovery and complete normalisation is typical after one week[24] Myocardial Stunning is a term used for an acute transient non-lethal ischaemic injury that causes left ventricular dysfunction even after reperfusion therapy, with the potential for full functional recovery in due course.[25] The effect of a prolonged period of myocardial ischaemia however, is irrerversible myocardial necrosis. The severity, or transmurality, of infarction is proportionate to the time of ischaemic injury. Kim et al[26] demonstrated, using late-gadolinium enhancement MRI imaging, that necrosis of greater than 50% of the myocardial wall

thickness, in the vast majority, represents myocardium that is irreversibly damaged, and will not regain or improve in functional capacity despite restoration of epicardial blood flow.

1.1.4 Myocardial infarction - Stunning, Hibernation and Viability

Myocardial Stunning

"Stunning" is most frequently observed following a severe episode of ischaemia-reperfusion, leading to a subacute "downregulation" of contractile function in response to reduced regional myocardial blood flow, with gradual recovery in function within hours-to-days of the original ischaemic insult (Figure 6).

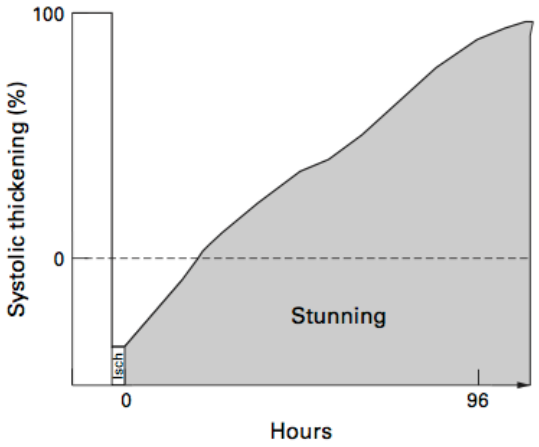

Figure 6: *The effect of a brief coronary occlusion on systolic function in the dog. The dark shaded box indicates a short episode of ischaemia. The myocardium rapidly becomes dyskinetic and following restoration of flow there is a gradual return of function. This period between the episode of ischaemia and recovery of full function is known as stunning. (Adapted from Bolli et al.)*[27]

Hibernating myocardium

The pathophysiology of myocardial hibernation is characterized as a situation of reduced regional contractile function distal to a coronary artery stenosis that recovers after removal of the coronary stenosis. Chronic hibernation develops in response to one or more episodes of myocardial

ischemia-reperfusion, possibly progressing from repetitive stunning with normal blood flow to hibernation with reduced blood flow.

Myocardial Viability

Viable myocardium is defined as dysfunctional myocardium subtended by a diseased coronary artery with limited or absent scarring. This is a prospective definition, which does not require demonstration of functional improvement with revascularisation but suggests the potential for recovery.[28]

Rahimtoola et al[29] first demonstrated the importance of viability assessment prior to the revascularization procedures being undertaken. In a cohort with chronically impaired left ventricular function and resting regional wall motion abnormalities, who underwent coronary artery bypass grafting, long-term improvement in LV function was obtained after the surgical revasularization procedure (Figure 7). This early work concluded, "the challenge, then, is to recognize preoperatively patients in whom LV function will improve".

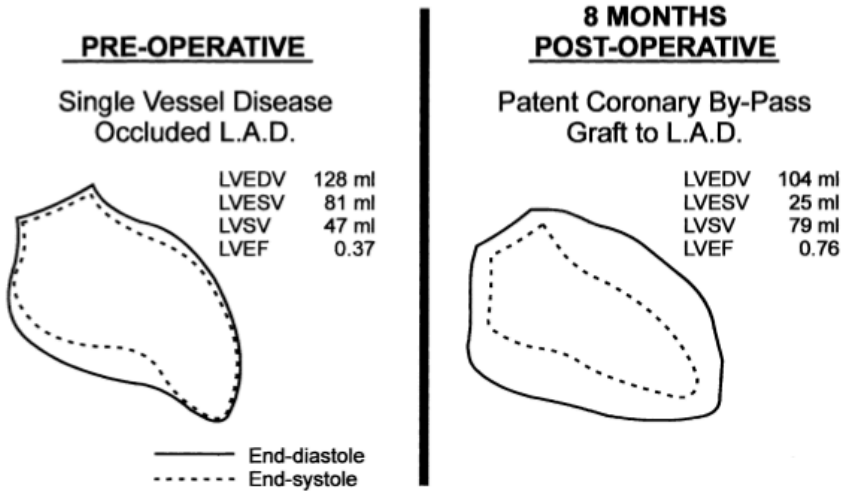

Figure 7: *Demonstration of the effect of revascularization on LV function according to viability – adapted from Rahimtoola et al.*[29]

Since this seminal work there have been a number of experimental observations emphasing the importance of the recognition and understanding of myocardial functional performance in the context of coronary disease, specifically in relation to the field of coronary revascularization. Revascularization of hibernating myocardium has been shown to improve regional and global function, cause postitive remodeling,[30] increase survival and reduce major adverse cardiovascular complicatons such as MI, heart failure and unstable angina. Furthermore, revascularization in the context of chronic left ventricular dysfunction in the absence of significant viable myocardium does not have demonstrable clinical benefit (Figure 8).[31]

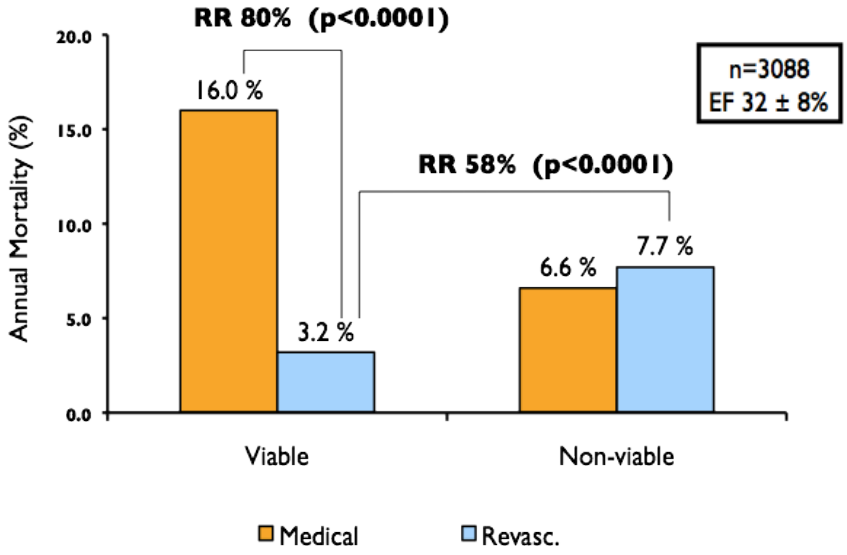

Figure 8: *Myocardial Revascularization stratified according to viability – adapted from Allman et al.*[31]

1.2 *Coronary Physiological alterations in left ventricular dysfunction*

1.2.1 Haemodynamic and Structural Alterations in Hypoperfused Myocardium

The flow-function relation

In myocardium subtended by functionally significant coronary artery disease the fundamental derangement is a reduced myocardial blood flow (MBF), which preferentially affects the subendocardium. Animal investigation has shown that the functional capacity of the subendocardium is the main determinant that governs overall transmural contraction, with the subendocardium receiving more MBF per unit muscle than the epicardium.[32] The extent of the reliance on the subendocardium has been borne out with the demonstration of the fine balance in coupling between subendocardial-MBF (SE-MBF) and function, with only a 20% reduction in SE-MBF resulting in severe regional dysfunction.[33] Reduction in transmural MBF leads to a disproportionate reduction in SE-MBF (Figure 9) with a 25% reduction in overall MBF resulting in a 50% reduction in SE-MBF, and a 50% reduction in MBF causing a 75% diminution in SE-MBF leading to regional akinesis.[34, 35] Whereas a lessening in subepicardial MBF does not similarly correlate to transmural LV wall function.[32]

Whilst the evidence for the "hibernation paradigm" was clear in animal models, until recently, methodology to quantify MBF in humans was not available. Initial studies using Positron emission tomography, had been conflicting, some suggesting that resting flow was not impaired in hibernating myocardium compared with flow in remote myocardium,[36-38] whilst others using the same methodology had found that MBF in hibernating myocardium was significantly reduced (by 20% to 30%) compared with MBF in the remote normal myocardium.[39, 40] However, utilisation of Cardiac magnetic resonance perfusion imaging's high spatial resolution and first-pass perfusion techniques, have provided confirmatory evidence that in patients with CAD with hibernating

myocardium have reduced MBF at rest in the regions subtended by the CAD, with restoration of flow observed following revascularization (Figure 9).[41]

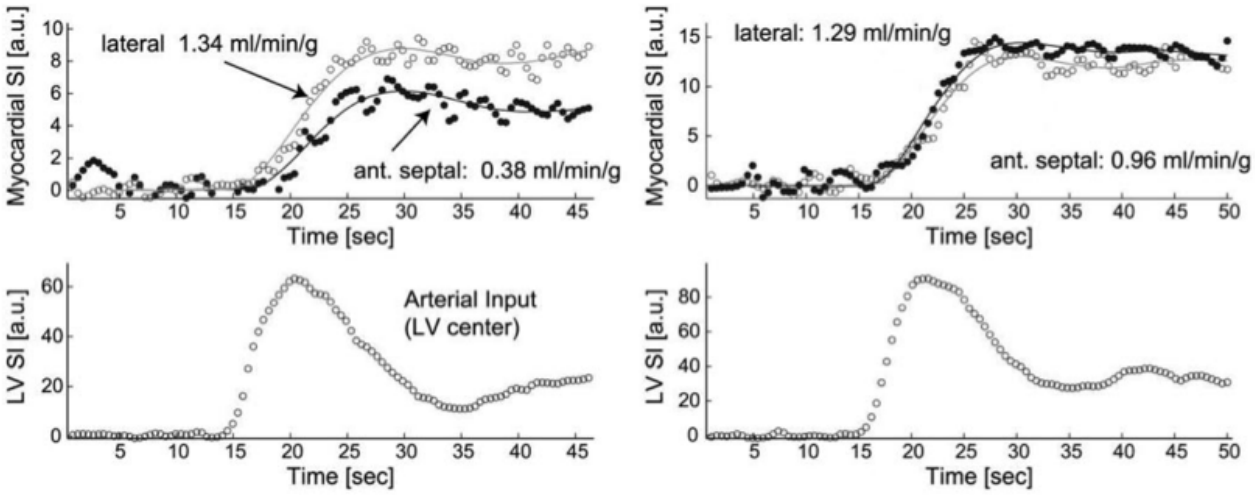

Figure 9: *Myocardial and blood pool signal intensity versus time curves in a patient with a 95% stenosis in proximal left anterior descending coronary artery both before and after PCI. There is reduced resting MBF in the anterior (ant.) septal segment, which improves significantly after PCI. In contrast, resting MBF does not change significantly in the unaffected lateral segment. SI indicates signal intensity; a.u., arbitrary units. (Adapted from Selvanayagam et al).*[41]

Coronary Flow Reserve in hibernating myocardium

Coronary flow reserve (CFR), the ratio of maximal to basal flow is reduced in the presence of an epicardial coronary stenosis. Irrespective of resting flow, CFR is almost always reduced in viable but dysfunctional myocardium, with it more severely deranged in segments with low flow at rest. The severity of CFR reduction has an impact on the ability of viable myocardium to improve its contraction upon inotropic stimulation, as this requires an increase in MBF.

Viable segments without contractile reserve usually have lower CFR than viable segments with contractile reserve. The response of viable segments to these stimuli varies greatly from segment to segment as well as with the intensity and the duration of stimulation. Many viable segments in hibernating myocardium exhibit a biphasic response when challenged by increasing levels of inotropic stimulation.[42] At low levels of stimulation, and provided that sufficient CFR is present, systolic wall thickening usually increases and starts earlier in systole. At higher levels, when the

increase in demand cannot be matched anymore by further increases in MBF, systolic function again deteriorates and can even become worse than at baseline.[43]

1.2.2 Structural Myocardial Adaptations in Chronically Hypoperfused Myocardium

Myocyte

The primary alteration is the depletion of contractile elements in the cardiomyocytes. In some cells, this is limited to the vicinity of the nucleus; whereas in others it is very extended, leaving only few or no sarcomeres at the cell periphery. The space previously occupied by the myofilaments is usually filled with glycogen. The mitochondria are increased in number and display alterations in size and shape. Nuclei are usually tortuous and show uniformly dispersed heterochromatin. Sarcoplasmic reticulum is virtually absent, as are T tubules. At the molecular level, the expression of myosin, actin, titin, and alpha-actinin is usually reduced. Cytoskeletal proteins such as desmin, tubulin, and vinculin are disorganized. The expression of connexin 43, a major gap junction protein, and that of nuclear A-type lamins are also reduced.[43]

Extracellular matrix

The extracellular matrix shows increased amounts of type I collagen, type III collagen, and fibronectin in chronic LVD. Within the widened interstitium, an increased number of vimentin-positive cells (endothelial cells and fibro- blasts) and macrophages can usually be seen.

The severity of the structural changes that affect a chronically dysfunctional myocardium are likely to impact on its ability to respond to an inotropic stimulus and on the speed at which it may or may not recover after revascularization. Segments with less fibrosis or with less severe cardiomyocytic alterations are more likely to improve in function following the administration of dobutamine or after revascularization.[43]

Microcirculation

The integrity of the microcirculation is a primary determinant of myocyte viability. Histological analysis of human dysfunctional myocardium demonstrated that the microvasculature was better preserved in segments that improved in function after revascularization than in those that remained dysfunctional.[44] Microvascular dysfunction often follows a period of epicardial coronary obstruction, due to a combination of luminal obstruction, endothelial damage and autonomic dysfunction.[45] The extent and reversibility of microvascular injury strongly influences the degree of resulting myocardial damage.[46] Following revascularisation of an epicardial lesion causing myocardial infarction, microvascular function has been found to predict the subsequent recovery of contractile function. Using myocardial contrast echocardiography (MCE) to evaluate microvascular perfusion,[47] microvascular integrity has been shown to predict improvement in wall motion, four weeks following an AMI, in patients with a patent IRA.[48] More recently, the rate and extent of gadolinium uptake on contrast-enhanced MRI imaging has evolved as a technique for detecting microvascular obstruction (MVO).[14] Patients with MVO on MRI have been found ultimately to have less functional recovery, more adverse remodelling and worse clinical outcomes than those with intact microvasculature.[49]

1.2.3 Mean-per-beat Physiological Parameters in the Identification of Myocardial Dysfunction

Coronary Flow Reserve (CFR)

CFR, the ratio between hyperaemic and resting coronary flow, is considered a surrogate of microvascular function, in the absence of an epicardial obstruction to flow. Using cine angiography to measure coronary flow, Suryapranata et al demonstrated that CFR following successful angioplasty was strongly correlated with subsequent myocardial recovery.[50] Many investigators have found similar associations between intracoronary Doppler-derived CFR and myocardial

viability,[51-53] although others have failed to do so.[54, 55] One possible explanation for this discrepancy is that CFR may not have accurately reflected microvascular function in these series, owing to the confounding effects of residual epicardial disease. More recently Belesin et al[56] studied a group of patients that had suffered a myocardial infarction 3.7 ± 6.3 months previously, underwent pre- and post- PCI CFR analysis and compared this to dobutamine echocardiography. The study concluded that an improvement in CFR by >0.8 had a sensitivity and specificity of 83% and 93% respectively (p<0.001), in predicting LV recovery. Further to this, the post PCI CFR value was also observed to independently predict myocardial recovery (p=0.001), confirming the notion that in the absence of residual stenosis in the IRA, the greater the final CFR the less microvascular dysfunction has occurred, which in turn predicts a better functional outcome. This confirmed the previously made assertion that a low CFR after angioplasty is a poor prognostic sign, both for restenosis as well as for the improvement in myocardial function.[57-59] Whilst this and many of the other studies examining the potential of CFR as a marker of viability, were assessed distant to the index infarction, Kitabata et al[60] studied an acute cohort, who underwent CFR assessment of the IRA, using a dual Doppler-pressure sensor tipped wire, immediately after PPCI, when presenting with an anterior MI. The intra-coronary measurements were then correlated against late-gadolinium enhanced CMR imaging, semi-quantitatively analyzing the anterior segments with a transmurality score (Grade 0 – 0%, Grade 1 – 0-25%, Grade 2 – 25-50%, Grade 3 – 50-75%, Grade 4 - 75-100%), defining the severity, or transmural extent of infarction (TEI), which has been validated to predict LV functional recovery post infarction.[61, 62] The cohort, subdivided into those who had suffered a transmural infarction (Grade 4) and non-transmural infarction (Grades 0, 1, 2 and 3). In those with transmural infarctions peak CK was significantly higher (<0.0001) and CMR visualized microvascular obstruction was more frequent (62% vs. 16%, p<0.03). A low post-PCI CFR correlated with the enzymatic infarct size along with the CMR determined infarct size. CFR values were significantly lower in the transmural cohort compared to the non-transmural group (1.14 ±

0.19 vs. 1.75 ± 0.48, p=0.002). Receiver operator characteristic (ROC) curve analysis for CFR in predicting transmural infarction was within the acceptable range for a diagnostic test, at 0.848. Though CFR measurement is predictive of myocardial recovery in numerous studies, there are a number of inherent limitations with this technique. The measurements are required to be taken post-PCI, meaning that, in the setting of an asymptomatic subject recently post infarction, it cannot be used as a clinical utility to predict viability and then guide whether revascularization is required. Furthermore, post-PCI CFR assessment in the ACS setting introduces a number of potential factors that could disrupt the accuracy of the tool; these include PCI related distal embolisation into the microvasculature, platelet plugging, thrombus formation, and microvasculature compression by oedematous myocardial tissue. For these reasons, CFR measured post PCI is unlikely to be a reliable method of myocardial viability assessment. A paucity of data in the current literature in regards to the role of pre-PCI CFR assessment suggests that further investigation is required to determine whether this surrogate could be of use in determining viability in the acute setting.

Both CFI and CFR as indices used to interrogate the coronary microvasculature are measured either during (CFI) or after (CFR) PCI. If the intention was to assess preservation of myocardial viability post infarction, to potentially guide and tailor an interventional strategy, these would not be feasible, as both produce retrospective answers to the question of viability.

Fractional Flow Reserve (FFR)

Fractional flow reserve of the myocardium (FFR_{myo}, commonly abbreviated to FFR) is the ratio of maximal myocardial blood flow achievable in the presence of an epicardial stenosis (Q_s) to the maximal myocardial blood flow in the hypothetical case of a completely unobstructed coronary artery (Q^N). Assuming that microvascular and coronary collateral resistances are minimal and constant during maximal hyperaemia, FFR can be derived from simultaneous measurement of

distal coronary, aortic and central venous pressures (P_d, P_a, P_v respectively), obviating the need to directly measure myocardial flow, where FFR = Q_s/Q^N = (P_d - P_v)/ (P_a - P_v).[63, 64] As an unobstructed epicardial coronary artery poses negligible resistance to flow, the normal value for FFR is 1.0 and values below 0.75 reliably predict reversible ischaemia (100% specificity) in patients with normal left ventricular function.[65] Furthermore, it has been shown that a FFR of 0.75 can be used to distinguish patients who would benefit from revascularisation from others whose coronary disease can safely be managed with medical therapy.[66]

The concept of deriving indices of flow from coronary pressure alone is attractive for it's simplicity but rests firmly on the assumption that microvascular resistance is both constant and minimal during pharmacological hyperaemia. The clinical studies used to validate FFR were based on patients with stable coronary disease and preserved left ventricular (LV) function, in whom microvascular function is thought to be intact. More recently, the utility of FFR has been explored in other settings, including patients with recent myocardial infarction or impaired LV function. De Bruyne et al studied 57 patients 20 ± 27 days after AMI and found that a FFR threshold of 0.75 identified flow heterogeneity on SPECT imaging with a sensitivity and specificity of 82% and 87% respectively.[67] Even more acutely (3.7 ± 1.3 days) following AMI, Samady et al found that a FFR threshold of 0.75 discriminates inducible ischaemia on SPECT or MCE with good accuracy.[68] Furthermore, it has been suggested that FFR reflects the mass of viable myocardium present following AMI; despite a similar degree of epicardial stenosis on angiography, patients with scar had higher FFR values than those with viable myocardium on SPECT imaging (Figure 10). The authors proposed that for a fixed coronary stenosis, FFR increases following myocardial infarction and necrosis, due to a decrease in maximal myocardial flow achievable (Q^N), although this assertion is yet to be verified experimentally. Hence FFR may be a function of the epicardial resistance to flow (which affects Q_s) as well as the mass of remaining viable myocardial tissue (which affects Q^N via microvascular changes), with values below a certain threshold identifying

patients who would benefit from revascularisation, as they have a functionally significant epicardial lesion subtending viable myocardium. De Bruyne et al suggest that this threshold is 0.75,[67] although this study did not directly assess functional recovery, quantify the mass of viable myocardium or clarify whether FFR would predict functional recovery of myocardium following acute infarction. Belesin et al[56] undertook a study to further delineate the function of FFR in a recent AMI cohort, examining a population 3.7 ± 6.3 months post infarction. FFR measurements taken before and after PCI were correlated with two-dimensional echocardiography and dobutamine stress echocardiography at 6 ± 1 month's follow-up. Similar to De Bruyne's work, there was a clear correlation between enzymatic infarct size (Peak CK) and an increase in FFR value ($r = 0.47$, $p = 0.003$). Further to this, an FFR of <0.71 before angioplasty, on regression analysis was found to have a ROC area under the curve of 0.808, with a high sensitivity, of 88%, but a poor specificity, of 69%. An interesting observation was the change in FFR (ΔFFR) between pre- and post- PCI also correlated with echocardiographic myocardial recovery ($p = 0.001$), however the sensitivity was only 69% with a specificity of 88%.

The major limitation with the body of work in identifying whether FFR would be an accurate marker of viability is that most of the patients studied are relatively remote from the index event, meaning the impact of acute microvascular dysfunction may not have been fully appreciated, therefore further investigation is required.

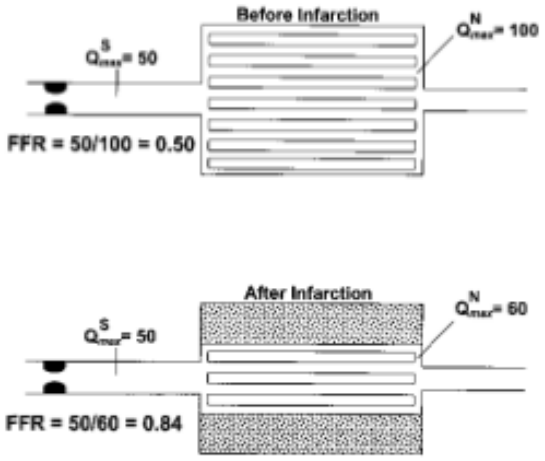

Figure 10: *Schematic of a coronary stenosis, depicting the dependence of FFR and on the mass of viable myocardium the coronary artery subtends – adapted from De Bruyne et al.*[67]

Index of Microvascular resistance (IMR)

The second is the Index of Microvascular Resistance (IMR), defined as the ratio of mean distal coronary pressure and the inverse of mean hyperaemic transit time (T_m), a correlate of absolute flow, derived from a coronary thermodilution curve following intra-coronary injection of cold saline, (IMR = $P_d/(^1/T_m)$ simplified to $P_d \times T_m$. Fearon et al demonstrated the utility and feasibility of IMR, in a STEMI cohort, as an 'in-lab' marker of viability, where the measurements were taken immediately after PPCI. An IMR value ≥32 U, the median IMR value in the study, correlated with both peak CK ($p<0.0001$) and echocardiographic wall motion score at 3 months (WMS) ($p=0.002$), with Pearson correlation coefficients, R, of 0.67 and 0.59 respectively, suggesting these markers of infarct size and severity had a linear relationship with IMR.[69] Lim et al[70] furthered this, confirming that a low IMR post infarction related to the presence of more viable myocardial tissue, as identified by FDG-PET imaging, and corresponded with a greater improvement in LV recovery 6 months post infarction, with a ROC area under the curve being 0.89, confirming the diagnostic potential of the method.

The major limitation of coronary thermodilution, and therefore IMR, is that it ignores the contribution of collateral flow and although the IMR value can be adjusted for collateral supply by

including a measurement of coronary wedge pressure,[71] is likely to be less accurate than H-MR. Unlike thermodilution techniques, Doppler measurements allow analysis of phasic coronary flow, which provides further independent parameters of microvascular function. The relationship between intracoronary pressure and flow during a single cardiac cycle can be represented by a pressure-flow loop. Both the slope (Slope Index of Flow-Pressure, SIFP) and intercept (zero flow pressure, P_{zf}) of the hyperaemic diastolic pressure-flow curve has been found to correlate with microvascular integrity.[72, 73] Interestingly, several small studies have recently suggested that P_{zf} is much better than CFR and is comparable to h-MR at predicting viability following AMI[54, 60]. However as calculation of P_{zf} requires off line analysis, this is not a feasible tool in day-to-day clinical practice. The difficulty with the Doppler based h-MR derivative of microvascular function relates to the technical aspect of obtaining adequate flow traces to allow accurate measurements, this is likely to be operator dependent, with those who have experience using this type of instrument being able to obtain accurate readings on a regular basis.

Hyperaemic Microvascular resistance (HMR)

Independent interrogation of microvascular resistance requires simultaneous measurement of distal coronary pressure and flow. With the advent of dual modality pressure and flow sensor-tipped guidewires in the past decade, two comparable indices of microvascular resistance have been described, which utilize different measurements of coronary pressure (Index of Microvascular Resistance) and pressure and flow (Hyperaemic Microvascular Resistance).

The first is Hyperaemic Microvascular Resistance (HMR), which is the ratio of mean distal coronary pressure (P_d) to Average Peak Flow Velocity (APV) obtained from intracoronary pressure and Doppler sensors respectively (h-MR = P_d /APV).[55] In the same study as described above, Kitabata et al[60] utilized this technique to determine the value in predicting CMR and enzymatic (CK) determined infarct size. The microvascular resistance index (MVRI, the synonym used in the study

for HMR) was reduced in transmural infarction compared to non-transmural infarction (3.70 ± 0.98 mmHg cm^{-1}s vs. 2.17 ± 0.84 mmHg·cm^{-1}s, p=0.0004). There was a significant linear relationship between peak CK-MB (r=0.77, p<0.0001) and infarct size defined by CE-CMR (r=0.78, p<0.0001). The ROC area under the curve was 0.885, and with a cut-off of 3.25 mmHg cm^{-1}s, the sensitivity, specificity, and predictive accuracy for MVRI were 75%, 89%, and 85%, respectively. Concluding that MVRI immediately post PCI strongly correlated with enzymatic, CE-CMR infarct size and is able to predict transmural from non-transmural infarction.

Table 1 below summarises the invasive physiological markers of myocardial function.

Study	Year	n	Marker Used	Study group	Procedure time/ Stage of measurement	Follow-up	Comparator	Outcome(s)	p
Suryapranata et al[53]	1994	22	CFR	STEMI post lysis	Within 4 hours of lysis; post PCI measurement	10 days	LV angiography	Predicts LV recovery	0.00003
Lee et al[17]	2000	70	CFI_P	STEMI	Within 12 hours of symptom onset; post PCI measurement	1 month	Echo WMS	Increased CFI_P Predicts improved LV recovery	<0.01
Yamamoto et al[44]	2001	48	CFI_P	STEMI	Within 24 hours of symptom onset; pre- and post-PCI measurements	n/a	MCE	Increased CFI_P predicts poor LV recovery	<0.01
De Bruyne et al[74]	2001	57	FFR	NSTEMI/ STEMI	20±27 days (Range 6 to 570 days)	3-12 days	SPECT	Low Pre-PCI FFR predicts reversible defects on SPECT	<0.001
Samady et al[75]	2006	48	FFR	NSTEMI/ STEMI	3.7±1.3 days; Pre- and post- PCI measurements	11±9 weeks	SPECT/ MCE	Low Pre-PCI FFR predicts reversible defect with SPECT and MCE	<0.001; <0.001
Belesin et al[58]s	2008	46	FFR CFR	NSTEMI/ STEMI	3.7±6.3 months post infarction; Pre- and Post PCI measurements	6 months	Low-dose dobutamine Echo	High pre-PCI FFR predicts CK derived infarct size	0.003
								Low Pre-PCI FFR predicts LV recovery	<0.001
								ΔFFR predicts LV recovery	<0.001
								ΔCFR predicts LV recovery	<0.001
Fearon et al[65]	2008	29	IMR	STEMI	Within 12 hours of symptom onset; post PCI measurement	3 months	Echo WMS and Peak CK	Predicts LV recovery	0.002
								CK derived infarct size	<0.0001
Lim et al[66]	2009	40	IMR	Anterior STEMI	Mean of 346±274 mins from symptom onset; post PCI measurement	6 months	Echo WMS and FDG-PET	Predicts LV recovery	<0.001
								Predicts amount of viable myocardium	<0.001
Kitabata et al[62]	2009	27	HMR CFR	Anterior STEMI	Within 12 hours of symptom onset; post PCI measurements	n/a	CE-CMR; Transmurality score	HMR Predicts infarct size;	<0.0001
								HMR differentiates transmural/ non-transmural infarction	0.0004
								CFR Predicts infarct size	<0.0001
								CFR differentiates transmural/ non-transmural infarction.	0.002

Table 1: *Invasive Coronary Physiology Indices Predicting Viability*

1.3 Phasic coronary flow Assessment – Wave Intensity Analysis (WIA)

1.3.1 Theoretical Background

The phasic nature of coronary blood flow was first described by Gregg and Sabiston.[74] The relationship and effect of cardiac contraction on coronary flow was later hypothesized in the 'intra-myocardial pump' theory.[75] This suggested that myocardial contraction forms an impediment to coronary blood flow by compressing the vessels embedded within the cardiac muscle. A new method for investigating coronary arterial pressure and flow waveforms has been developed based upon wave intensity analysis (WIA).[76] Parker et al extrapolated a mathematical technique, termed method of characteristics, which was widely used in the field of gas dynamics. WIA is a time-domain method and assumes that every wave can be reconstructed by the superposition of an infinite number of wavefronts. No assumption regarding the periodicity of the interrogated signals or the linearity of the system under investigation is necessary. Therefore within the coronary circulation WIA assesses the shape of a pressure and flow waveform during a cardiac cycle represents the phasic coronary flow in terms of the resultant energy transfer produced. The sum of a series of the traveling wavefronts, allow the origin and nature of the pressure and flow changes in arteries to be determined. Quantification of these wavefronts, by WIA, represents an adept method for the study of the coronary-cardiac interaction and its resultant effects on coronary pressure and flow, as it is able to, simultaneously, demonstrate changes in both coronary haemodynamics and cardiac performance and determine the relative contributions of the aortic and microcirculatory contributions to coronary blood flow.

1.3.2 Mathematical Derivation of Wave Intensity

Net wave intensity (dI) represents the flux of energy carried by a wave per cross sectional area of a vessel, which is determined by the product of change in pressure (P) and velocity at a single location.

$$dI = dP \times dU \quad (1)$$

Wave intensity (dI) within the coronary circulation can be can be differentiated into component waves, propogated either, by the upstream, aortic-end (dI_+) of the vascualture or the downstream, microcirculatory (dI_-), defined as:

$$dI = dI_+ + dI_- \quad (2)$$

In order to separate and quantify the waves present in the coronary circulation using wave intensity, a local measure of wave speed, c, is required. A single-point technique was used in the measurements obtained in this thesis. This uses simultaneous measurement of pressure and flow to determine wave speed in the following equation, where the sums are taken over an integer number of cardiac cycles, where ρ is the density of blood.

$$c = \frac{1}{\rho}\sqrt{\frac{\Sigma dP^2}{\Sigma dU^2}} \quad (3)$$

Waves originating from the proximal end of the circulation (dI_+) and the distal end of the artery (dI_-) were calculated as follows:

$$dI_{+} = \frac{1}{4\rho c}\left(\frac{dP}{dt} + \rho c \frac{dU}{dt}\right)^2 \quad (4)$$

or

$$dI_{-} = -\frac{1}{4\rho c}\left(\frac{dP}{dt} - \rho c \frac{dU}{dt}\right)^2 \quad (5)$$

The separated waves are uniquely characterized by their effect on the blood mass, with compressions waves increasing pressure and expansion waves decreasing pressure.

Therefore the waves can be classified into four types; forward compression wave (FCW), forward expansion wave (FEW), backward compression (BCW) and backward expansion wave (BEW).

The WIA profile within the coronary circulation has a typical morphology, with forward waves arising from the left ventricular cavity entering the epicardial coronary vessel via the aorta, whilst backward waves orginate from the microcirculatory vessels embedded within the myocardium.[77] Figure 11 below shows the typical coronary WIA profile, with the compression waves occurring during the systolic contraction phase of the cardiac cycle and the expansion waves occurring during the diastolic relaxation.

The WI analysis performed for this thesis was done using a custom-made code on Matlab software. This used Savitzky-Golay[78] polynomial filtering and ensemble averaging of the respective selected beats analysed, to calculate net coronary wave intensity, normalizing for the sampling rate, calculated as:

$$dI = dP_d/dt \times dU/dt \quad (6)$$

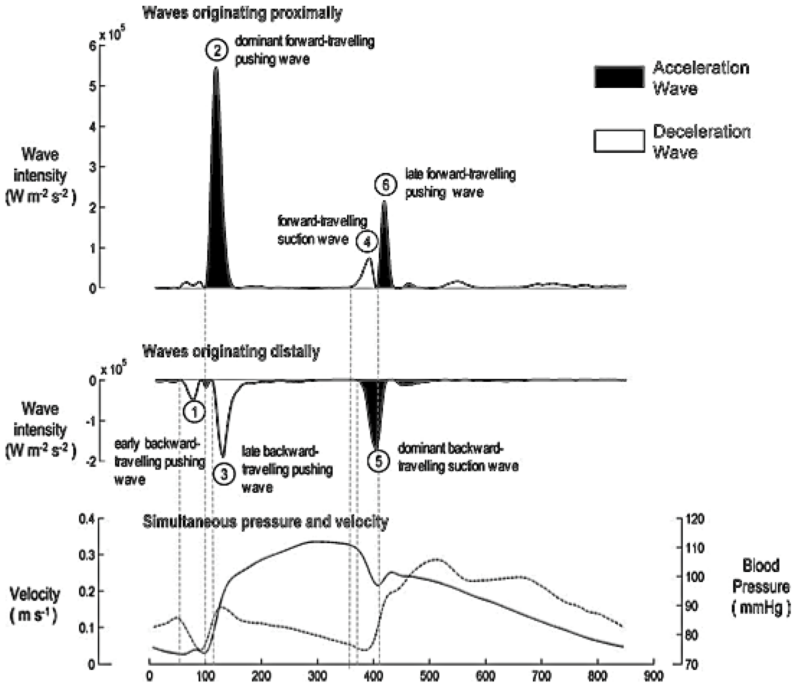

Figure 11: *Typical Coronary Wave Intensity waveform – Adapted from Davies et al.*[79]

1.3.3 Wave Intensity Waveforms and their Clinical Applications

The increased awareness of the utility of WI in its application to coronary flow along with the advancements made with dual Pressure-Doppler sensor tipped intra-coronary wires (ComboWire, Volcano Therapeutics, Inc, USA) (Figure 12), have allowed simultaneous pressure and velocity data to be obtained, enabling this body of work to expand in recent times.

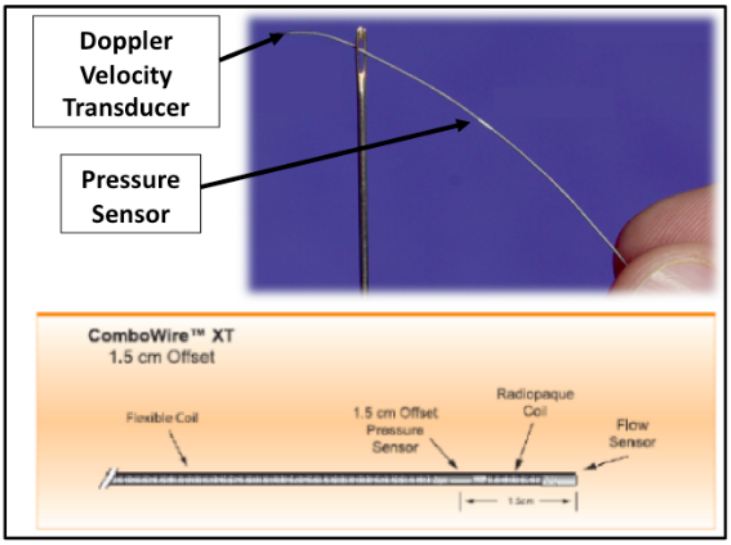

Figure 12: *0.014" Dual-sensor guide wire, Combowire® (Volcano Therapeutics, USA). On this wire (model"9515), the Doppler velocity transucer, situated at the tip of the wire is offset by 15mm from Pressure sensor*

The methodology has been adopted to increase the understanding of pressure and flow in systemic arteries[80-83] and then in coronary arteries of animal models.[84] Latterly the techniques have been used in humans to confirm the typical wave intensity waveform present in unobstructed coronary arteries, and the effects on the waveform morphology in the presence of left ventricular hypertrophy.[79] In brief, the typical waveform pattern seen during each cardiac cycle consists of up to 6 waves, 3 forward directed (from the proximal, aortic end) and 3 backward directed (from the distal, microvascular circulation), recurring in the same sequence beat-to-beat, each occurring during different phases of ventricular systole or diastole. The 6 waves can be described according to whether they are 'compressive', resulting from the force of the ventricle during systole or 'expansile' (during diastole). Figure 11 illustrates the typical coronary wave intensity pattern. The first wave is the backward compression wave (BCW – labeled 1), as the pressure increases during the onset of systole, the microvasculature is mechanically compressed, causing a decelerating wave. As the pressure continues to increase in systole, a forward compression wave (FCW – labeled 2) occurs, from the aortic end, accelerating coronary flow. Simultaneously with FCW, is a further BCW (labeled 3), causing deceleration, because of

continued microvascular compression, however the net wave intensity is positive, resulting in forward accelerating flow. As systole ends, the pressure imparted from the left ventricle is reduced, therefore causing a forward originating suction (or expansion) wave (FEW – labeled 4), this is decelerating in nature. During the same phase of the cardiac cycle, the compressive force previously exerted on the microvasculature is reduced, therefore allowing the microcirculation to expand, causing a backward expansion wave (BEW – labeled 5), accelerating flow. The final waveform is a late forward directed compression wave (late FCW – labeled 6), caused by the transient increase in aortic pressure because of the closure of the aortic valve, causing further acceleration.

Conceptually, consideration of the energy flux present during a cardiac cycle, as opposed to flow or pressure alone, has resulted in a fundamental difference in the understanding of the behavior of the cardiac-coronary interaction. Previously it was assumed that forward directed flow would result in acceleration of flow within a coronary vessel, however this has been demonstrated to not necessarily be the case, as with the second forward directed wave (labeled 4 in figure 5), occurring at the end of systole, where there is a pressure drop, causing a proximally originating suction wave or forward expansion wave (FEW), with resultant deceleration, however this is counteracted by the backward expansion wave (BEW) as a result in reduced mechanical ventricular compression of the microvascular tree, which causes a net acceleration in the coronary circulation. The nature and origin of coronary flow as determined by WIA is further summarized in figure 13 below.

Pressure	Velocity	Wave Origin	Wave Nature
↑	↑	Aortic End (Proximal)	Accelerating
↑	↓	Distal end (Microcirculatory)	Decelerating
↓	↑	Distal end (Microcirculatory)	Accelerating
↓	↓	Aortic End (Proximal)	Decelerating

Figure 13: *Determining the origin and nature of coronary flow according to wave origin*

The extent of microvascular dysfunction following an ACS directly correlates with the severity of myocardial necrosis and irreversibility of left ventricular dysfunction, theoretically also causing a reduction in the microvascular driven component of coronary flow. Wave intensity analysis was utilized to assess variances in coronary flow in a cohort of patients with recent ACS, demonstrating the effect of microvascular dysfunction on coronary flow, in varying degrees of infarct size.

1.4 *Electrophysiological alterations in left ventricular dysfunction*

Profound electrophysiological changes occur in the myocardium following acute coronary occlusion, including a decrease in action potential amplitude and duration, diminution of the resting membrane potential and a reduction in the rate of depolarization[85-87]. Prolonged ischaemia results in a core of necrotic myocardium with increased electrical resistance due to uncoupling of gap junctions[88]. Several studies have shown that electrical signals from infarct related myocardial territories (either in isolation or coupled with assessment of mechanical function) can be used to differentiate healthy, necrotic and ischaemic myocardium[89, 90].

1.4.1 Endocardial Myocardial Mapping

In a canine coronary occlusion model, left ventricular endocardial electrogram amplitudes were found to be significantly lower in chronic infarction areas as opposed to healthy zones.[91, 92] Similarly, hibernating myocardium has been shown to have preserved electrical activity, within an intermediate voltage range, which has reduced voltages compared to control regions in pigs[93]. In clinical studies, a gradation on endocardial voltages has been noted, with lowest amplitudes in those with fixed perfusion defects on Single Photon Emission Computed Tomography (SPECT) imaging (suggestive of non-viable myocardium) and mildly reduced endocardial voltages in those with reversible perfusion defects, in relation to each other and to normal tissue[94].

Early work in this field aimed to define scarred versus normal myocardium, however subsequent studies have demonstrated the presence of an electrical continuum of endocardial voltage amplitudes, grading scarred, hibernating (viable) and healthy myocardium, identified by functional Fluorodeoxyglucose (FDG) Positron Emission Tomography (PET) and SPECT scanning.

Furthermore, these voltages are predictive of recovery in both regional and global ventricular function, following revascularisation with PCI. The unipolar electrogram amplitudes were

significantly different and reproducible amongst normal regions, regions with reduced perfusion but preserved metabolism and regions with scar, that the Area under the curve (AUC) of Receiver Operator Characteristics (ROC) analysis was 0.84, suggesting its diagnostic ability, with a sensitivity and specificity of 77% and 75% respectively.[95]

Although absolute endocardial voltages are lower in scarred than viable myocardium, considerable overlap was noted in the early studies, with many regions yielding unipolar voltages in the "grey zone" between 7 and 12mV. The accuracy of the method was enhanced by simultaneous assessment of mechanical function (Electromechanical mapping, EMM) or by normalising voltages to those recorded from healthy unaffected myocardium[96]. One of the sources of this grey zone is the limited transmural resolution of the techniques previously used, especially the ability to differentiate subendocardial from transmural scar. Using 1.5 Tesla delayed-enhancement magnetic resonance imaging, Perin et al were able to define the unipolar voltage thresholds for varying severities of myocardial infarction transmurality, thereby minimizing the degree of voltage overlap previously seen, underlining the accuracy of electromechanical mapping to detect viability. Distinct voltage cut-offs were observed, differentiating normal myocardium to subendocardial or transmural infarction. A threshold of 7.9mV to identify subendocardial infarction from normal myocardium was associated with a sensitivity and specificity of 80%, whilst the threshold for distinguishing transmural infarction was 6.9mV, with a sensitivity and specificity of 93% and 88% respectively. Perin et al concluded that endocardial voltage assessment is a 'valuable tool for diagnostic evaluation of myocardial viability, particularly when decisions involving high-risk revascularisation procedures are frequently entertained on an immediate basis', such as in post-myocardial infarction patients.[97]

A further limitation of endocardial electrical mapping derives from the relationship between the transmurality of infarction and the potential for contractile recovery following revascularisation.

Ischaemia preferentially affects the endocardium and in the event of prolonged coronary occlusion, a wavefront of necrosis progressively spreads from the endocardium to epicardium[98].

1.4.2 Epicardial Myocardial Mapping

There is growing evidence that the transmural extent of infarction is one of the strongest predictors of viability and it is generally accepted that functional recovery occurs following revascularisation when the endocardial scar occupies less that 50% of the thickness of myocardium[61, 99]. Areas of subendocardial scar, which have viable but dysfunctional mid and epicardial segments may have low endocardial voltage potentials. Endocardial mapping in such regions could yield a false-negative assessment of viability, which may erode the accuracy of the technique overall. On the other hand, epicardial electrical activity is relatively normal in these regions and as such, an epicardial electrical mapping technique would be expected to predict functional recovery more reliably. Reddy et al[100] demonstrated the achievability of epicardial electrogram assessment; combining epicardial and endocardial electroanatomic mapping in a porcine model with chronic infarction, as a method of scar-substrate mapping for ventricular tachycardia. This demonstrated that epicardial scar mapping, through direct epicardial contact, via a subxyphoid approach to access the pericardial space and subsequent insertion of a mapping catheter, was feasible and accurate, and established a proof-of-principle that epicardial mapping can delineate scar. An elegant human clinical validation of this concept has recently been provided by Vahlhaus et al, who measured epicardial electrograms (by direct myocardial contact) in 34 patients, at the time of coronary artery bypass surgery.[101] Viability was determined by assessing the change in segmental wall motion on echocardiography at 7 months following the procedure. They demonstrated that non-viable segments were characterized by prolonged bipolar signal duration (22.8 ± 0.5ms vs. 15.4 ± 0.4ms, $p<0.001$) and reduced bipolar voltage (3.6 ± 0.3mV vs.

13.1 ± 0.3mV, p<0.001). Using a dichotomous voltage of 5.9mV, the epicardial electrograms predicted functional recovery with 83% sensitivity and specificity.

The studies by Reddy et al and Vahlhaus et al demonstrated the potential of epicardial mapping, although both used surgical placement of the epicardial electrodes on the surface of the heart, and as a technique itself, this has no clinical diagnostic utility, as both are very invasive and only applicable once a patient undergoes surgery. However, epicardial electrograms can also be obtained via the coronary artery during cardiac catheterisation. Epicardial ECGs are recorded via an intracoronary guidewire, to monitor ST segment shift during PCI.[102-104] More recently, electrograms obtained from coronary guidewires have been used to guide ablation of scar-related Ventricular Tachycardia during electrophysiology procedures.[105, 106] Segal et al describe a series of cases where unipolar electrograms obtained from the guidewire were recorded during VT in the circumflex, obtuse marginal, diagonal and posterior descending arteries, enabling ablation by alcohol or radiofrequency ablation.[106] Absolute unipolar and bipolar voltages, as well as those normalised to the highest voltages recorded from control regions, have been shown to predict myocardial viability.[101, 107]

1.5 Aims & Objectives

The main focus of this thesis was to investigate the effects of coronary artery disease and myocardial infarction on the intrinsic physiological mechanisms that underpin myocardial perfusion and function.

Furthermore, it aimed to identify and develop invasive physiological markers of myocardial integrity and coronary circulatory function. Specifically examining the effects of acute and chronic myocardial infarction on microcirculatory, coronary and myocardial physiology, assessing these changes using, invasively obtained intra-coronary pressure and flow patterns, in conjunction with non-invasively obtained, cardiac magnetic resonance imaging, with visualization of the effects on the myocardium. The CMR protocol categorized size and extent of infarction and identified regional wall motion defects following ACS, with the protocols being developed to ensure optimal imaging acquisition, in this heterogenous population. The results of the relationship between the invasively determined pressure-flow derived wave intensity indices and late-gadolinium determined infarction are presented in Chapter 3.

Additonally, in patients with chronic ischaemic cardiomyopathy undergoing percuteanous coronary revascularization, we investigated the physiological effects of adjunctive intra-aortic balloon counter-pulsation support on the coronary circulation using pressure-flow derived indices of assessment. Specifically aiming to examine and describe the inter-relationship between coronary auto-regulatory mechanisms and the efficacy of counterpulsation mechanical assist devices.

Furthermore, we performed feasibility studies examining the effects of infarction on the electrical integrity of myoctye function as a possible determinant of infarct severity identified during revascularization procedures, via the novel implementation of a trans-coronary electrogram mapping technique.

The principle apparatus required for the studies involving patients presenting with acute coronary sydromes were 3 Tesla cardiac magnetic resonance imaging assessment of infarct size and extent, along with two distinct modalities of invasive physiological assessment obtained during cardiac catheterization. The first was utilizing phasic analysis of simultaneously obtained pressure and flow measurements within the coronary circulation, whilst the second was adopting mean-per-beat derived indices in the assessment of coronary and microcirculatory function. The second, was the adaptation of a coronary angioplasty guide-wire to allow trans-coronary electrogram measurements to be obtained during PCI procedures, to assess myocardial infarction. The developmental process and analytical techniques used for both of these techniques is outlined in the methods section in chapter 2.

Key Hypotheses Under Investigation in this Thesis

1. Myocardial infarction related microcirculatory dysfunction can be identified and quantified using phasic pressure-flow derived wave intensity analysis.
2. The efficacy of Intra-aortic balloon counter-pulsation therapy is intrinsically linked to the presence or absence of coronary auto-regulatory mechanisms, which are principally governed by the microcirculation.
3. Trans-coronary electrogram assessment of infarct size is a feasible method of assessing electrical integrity of the myocardium during percutaneous coronary intervention procedures.

2. METHODS AND TECHNIQUES USED IN THIS THESIS

2.1 Introduction

This chapter outlines some of the specific techniques used in this thesis, encompassing the development of the techniques used and including preliminary data that were obtained for internal validation and reproducibility purposes and to fine-tune methods prior to their use in the main clinical and exploratory studies.

2.2 Haemodynamic Methods during Cardiac Catheterization

2.2.1 Assessment of intra-coronary pressure and flow

2.2.1.1 Simultaneous Intra-coronary Pressure and Flow Measurements

Invasive interrogation of the coronary circulation with single modality pressure or Doppler sensor wire technology has allowed a vast array of investigations to be performed within the coronary circulation. Coronary Flow Reserve (CFR) is a marker than can be assessed using either modality, with flow velocity measured directly using a Doppler sensor tipped guidewire (CFR_V), or via a thermodilution (CFR_P) based approach using a pressure wire, where the transit time of room temperature bolus of saline is measured as it passes through the coronary artery as a surrogate of flow. CFR_P represents a robust assessment of myocardial flow and correlates well with the direct measure (CFR_V).[69] However, CFR_P and CFR_V are limited, by being affected by the concurrent haemodynamic conditions. Additionally, CFR_P is also degraded, in the presence of a stenosis, by anatomical variances such as the presence of significant collateral circulation.[108] Single modality technology remains steadfast in its clinical applicability, with the utilization of pressure wire technology

in the clinical arena, through Fractional Flow Reserve (FFR), which has been widely implemented as an invasive measure of functional significance of epicardial coronary stenoses, with compelling clinical outcome data to support its use.[109, 110] Nonetheless, the ability to simultaneously interrogate pressure and flow allows a greater degree of precision in the understanding of the inter-relationship between the microcirculation and the epicardial conduit vessels. The ability to assess pressure and flow has been borne out by continued technological developments, from the inception of direct coronary velocity assessment through high-frequency, 20MHz, pulsed Doppler, catheter based methods.[111] Subsequently allowing the direct measure of the two integral parameters, with the use of two separate wires used in tandem, though this led to considerable electrical cross-talk, limiting this methods use.[112] Latterly, the development of the dual-sensor ComboWire® (Volcano Therapuetics™, USA, Figure 12) has seen the introduction of a multi-piezoelectric crystal Doppler sensor and pressure sensor, mounted on a 0.014inch high fidelity guidewire, which is offset by 1.5cm, providing continuous wave Doppler signals, at a sampling frequency of 200KHz, to be measured simultaneously with intracoronary pressure. This has provided the basis of numerous seminal investigations into the, hitherto, incompletely understood nature of the coronary and microvascular haemodyanmics.[113-115] Most importantly the affects on, and by, the microcirculation have been elucidated in greater detail, with an enhanced appreciation of the importance of direct measurement of microvascular resistance when evaluating coronary haemodynamics. Whilst the index of microvascular resistance (IMR) had been developed as a pressure derived marker of microcirculatory resistance, obtained via the same thermistor based thermodilution technique and is subject to assumptions relating to the presence or absence of coronary collaterals. The dual-sensor modality has allowed the development of both means-per-beat

indices, such as the hyperaemic microvascular resistance (HMR) representing a directly measured marker of resistance, and the application of mathematical models in its use in phasic analyses such as wave intensity analysis (Figure 14).

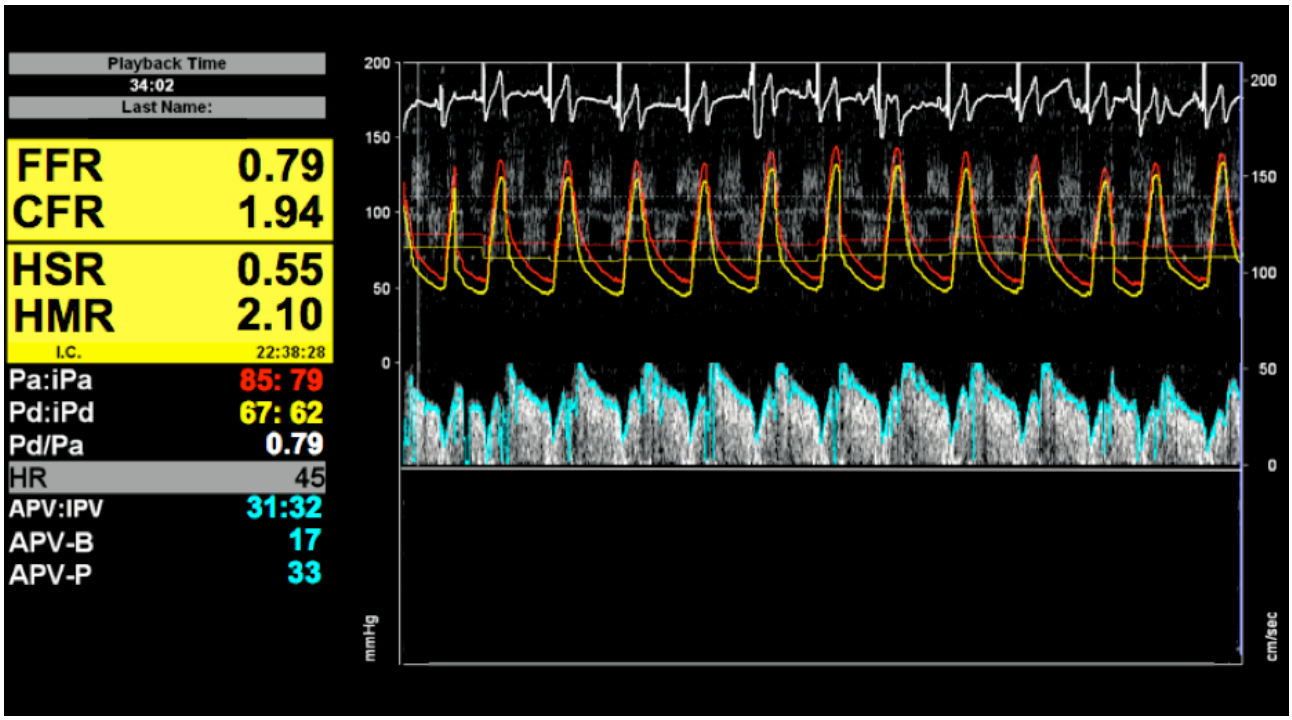

Figure 14: *Simultaneous intra-coronary pressure and Doppler velocity recordings. Red line = aortic pressure, yellow line = distal coronary pressure and blue line = Doppler derived velocity.*

2.2.1.2 Reproducibility and Variance assessment of Pressure and Flow indices

Aim

To assess reproducibility and variance for of the measurement of intra-coronary pressure and flow using the dual-sensor ComboWire at baseline and during adenosine induced hyperaemia.

Methods

Consecutive patients who required invasive functional assessment of the haemodynamic significance of a coronary stenosis using a pressure wire were recruited. The lesion was crossed with a 0.014" ComboWire with the tip positioned in the distal vessel. Three sequential baseline measurements of pressure and flow were recorded at ten second intervals. The patient was then given intra-coronary boluses of adenosine to induce maximal hyperaemia. The dose of adenosine was sequentially up-titrated, with the maximum tolerable dose dictated by the onset of atrio-ventricular conduction block or systemic symptoms (up to 60mcg were administered in the Right and up to 96mcg in the Left Coronary Arteries respectively) used for subsequent measurements. Coronary flow velocity, measured by the average peak velocity (APV), was allowed to return to the basal value, with a minimum of three measurements taken using the maximal tolerated dose. All tracings were continuously recorded and analyzed off-line using dedicated software (StudyManager, Volcano Corp, USA).

Analysis

Basal and hyperaemic average peak velocity (APV) was measured as the average instantaneous velocity (IPV) taken over 3 cardiac cycles. Additionally, during maximal

hyperaemia, the pressure measurements in the distal coronary (P_d) and aorta (P_a) were also recorded. From these values fractional flow reserve (FFR= P_d/P_a), coronary flow reserve (CFR= APV_{peak}/APV_{basal}), hyperaemic stenosis resistance index (HSR=P_a-P_d/APV_{peak}) and hyperaemic microvascular resistance (HMR=P_d/APV_{peak}) were calculated. All arterial pressure values were corrected to venous pressure measurements taken from a catheter in the right atrium.

From the 3 sets of values recorded for each vessel (base and peak measurements) the outlier was excluded and the statistical analysis performed on the 2 closest sets of values. Variability was calculated as the standard deviation of the differences/mean. Bland-Altman plots were then used to record the mean difference and standard error (Figure 15).

Results

Fourteen vessels in 8 patients were examined in the study (Table 2). Measurements were successfully taken in 13 vessels (5 LAD, 5 Cx and 3 RCA), with two operators performing the studies. One set of data was unusable due to poor quality of the traces.

	Absolute mean±SD	Variability (%)	Mean difference	95% CI	Standard Error
Base APV	19±7.9	7.8	2.16	0.3-4	2.2
Peak APV	33.5±11.5	7.3	3.43	1.1-5.8	3.2
P_a	73.3±11.8	2.5	2.56	0.1-5	3.3
P_d	58±10.7	2.9	2.57	0.2-2.9	2.9
FFR	0.79±0.16	1.7	0.02	-0.004-0.05	0.05
CFR	1.8±0.6	8.4	0.2	0.03-0.3	0.17
SR	0.67±1	12.3	0.05	0.006-0.1	0.27
MR	2±0.72	7.3	0.21	0.02-0.4	0.2

Table 2: *Variability results for Simultaneously obtained Pressure-Flow (ComboWire) measurements*

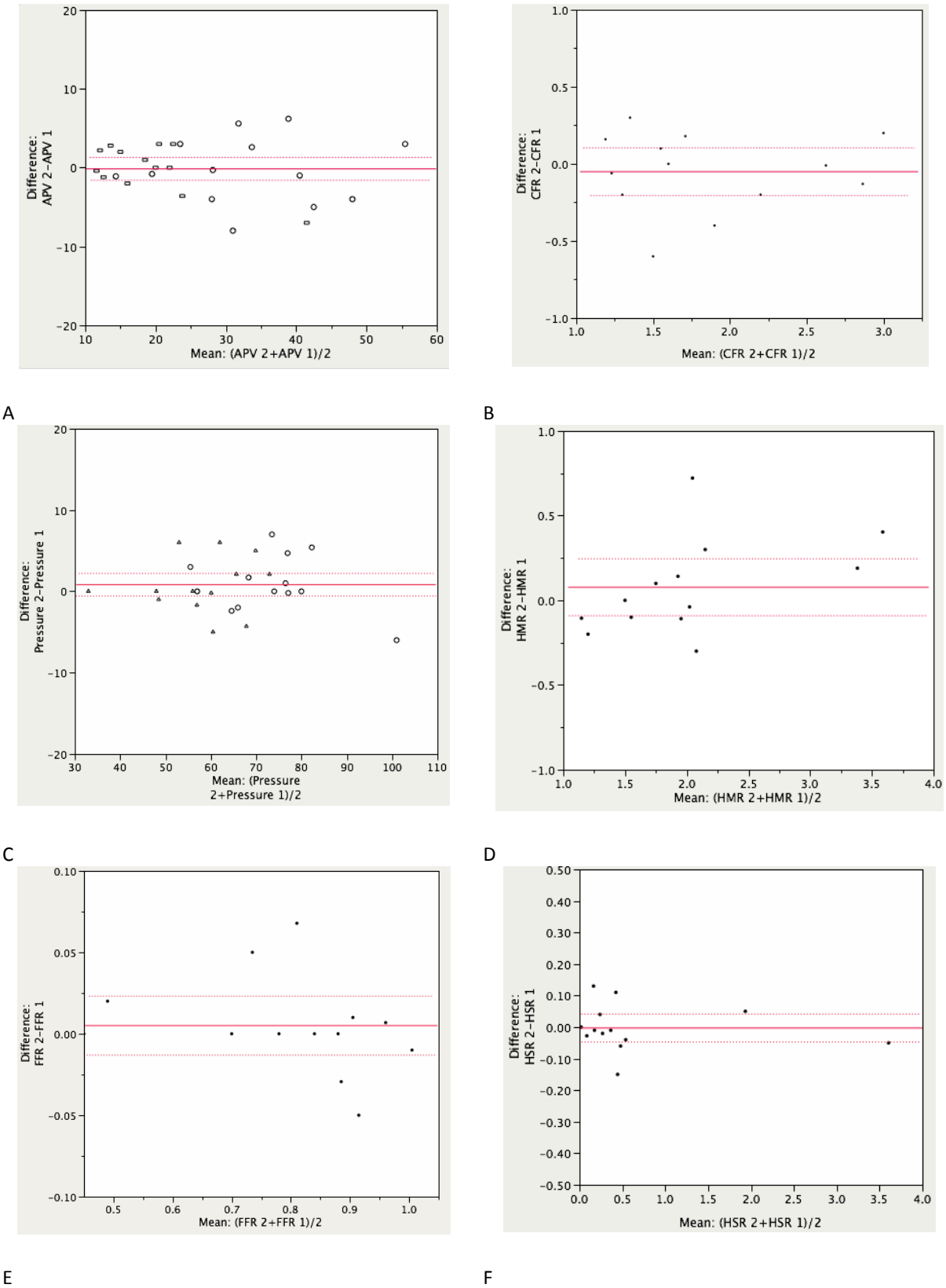

Figure 15: *Bland-Altman Plots showing mean difference and standard error (SE) for (A) Average Peak Veolcity (APV), (B) Coronary flow reserve (CFR), (C) Pressure measurements, (D) Hyperaemic Microvascular resistance (HMR), (E) Fractional Flow Reserve (FFR), (F) Hyperaemic Stenosis Resistance (HSR)*

Conclusion

These data suggest a high degree of reproducibility with low variance for Combowire measurements in our institution that compare well to results from other centres published in the literature.

2.2.2 Development of Pressure-Flow Acquisition Protocol

The initial study protocol planned to obtain pressure and flow measurements during a 2-minute infusion of Intravenous adenosine, to induce hyperaemia. However, initial pilot studies revealed that whilst hyperaemia was invariably achieved using this method, repeated Doppler-Pressure measurements, to interrogate the artery sufficiently, were not possible, without repeating the 2-minute infusion a number of times. This was not feasible, as it meant the patients receiving repeated adenosine infusions, and being subject to its side effects. Therefore the protocol was adapted to use intracoronary adenosine, with incremental doses starting from 18mcg to 60mcg in the right coronary artery and 36mcg to 96mcg in the left coronary system. As documented previously[116] the dosage was titrated up towards the maximum tolerated to ensure hyperaemia was achieved in each patient, without causing side effects such as atrio-ventricular delay. To ensure accurate dosing of IC adenosine, the guiding catheter is required to be fully engaged with the ostium of the coronary tree being interrogated. This allows direct introduction of drug in to the coronary vessel, limiting the possibility of dilution secondary to loss of drug in to the aorta, a consistency in all measurements undertaken across a cohort of patients.

Optimizing Intracoronary Measurements

The quality of the pressure-flow data obtained determines the accuracy and validity of the phasic wave intensity data, as this relies on changes over time within both indices to extroploate into wave profiles. The 0.014 inch ComboWire (Volcano Corp, USA) used to obtain this data (Figure 12) has a pressure sensor at the tip of the wire and a Doppler velocity sensor 1.5cm proximal to this. Acquisition of flow velocity data can be both time consuming and fraught with variation. Intra-coronary wire position can be with either 'anterograde' or 'retrograde' recording of flow signals. Anterograde signals are obtained when the wire is placed directly into the coronary artery, resulting in the Doppler and Pressure sensors positioned sequentially within the artery (Figure 16). Retrograde recordings are obtained when the tip of the wire is manipulated and coiled, so the pressure and Doppler sensor are adjacent to each other within the artery (Figure 17). The retrograde position allows for a more stable flow velocity signal, with reduced vessel wall artifact and also less variation in amplitude whilst in a fixed position during IC boluses of adenosine, unlike when performed with the anterograde approach. Therefore in order to limit variation in the quality of the data acquired, all procedures were performed with the wire in the 'retrograde' position, wherever possible.

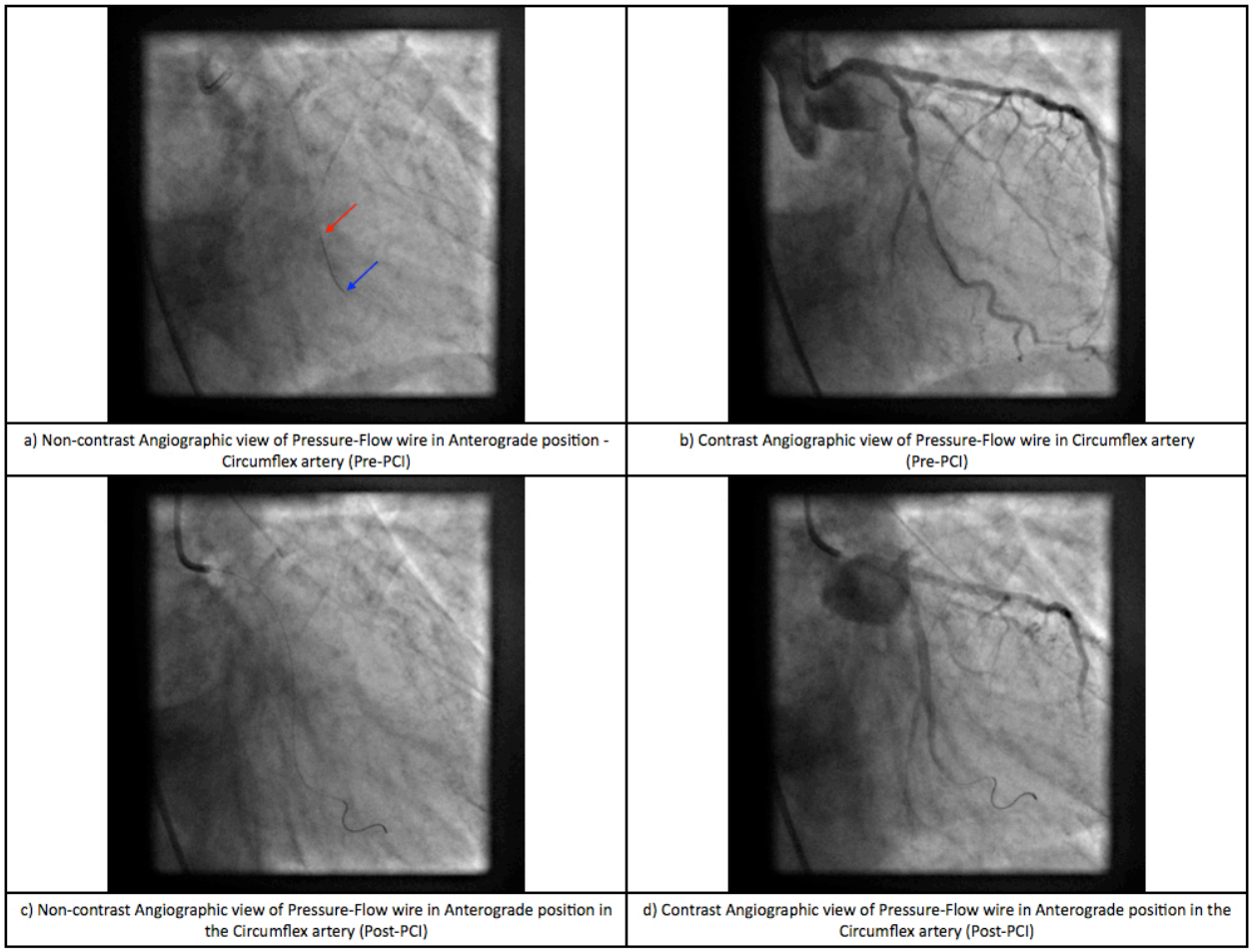

Figure 16: *Anterograde recording position within the Circumflex Artery. a) Non-contrast angiographic view (Pre-PCI), with red arrow highlighting Pressure sensor and blue arrow highlighting the Doppler sensor. b) Contrast view, Pre-PCI. c) Non-contrast view Post PCI. d) Contrast view post PCI.*

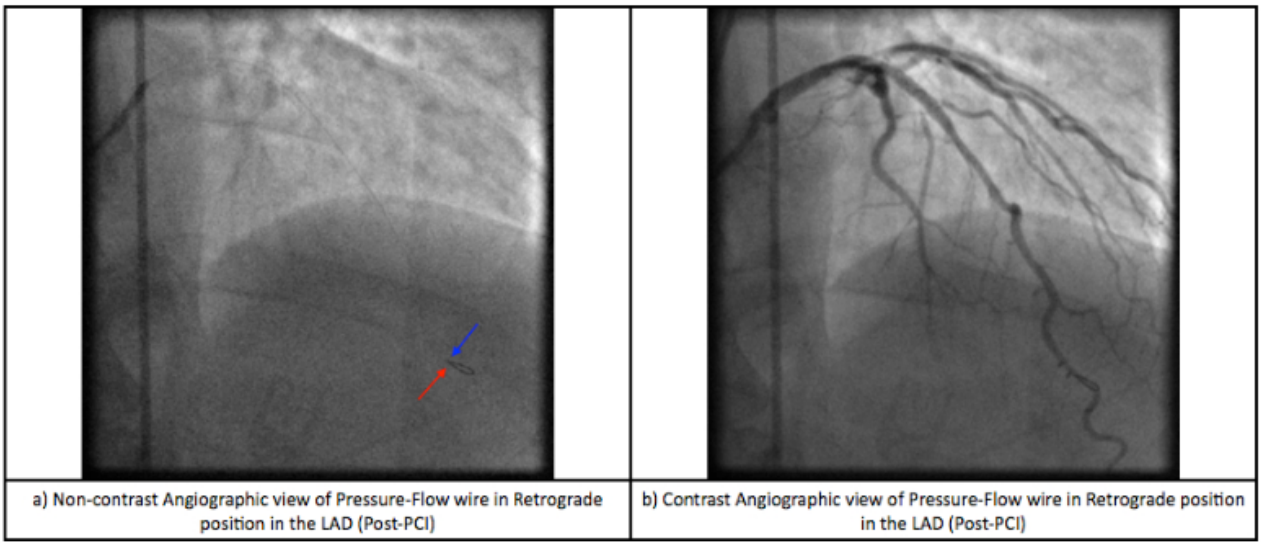

Figure 17: *Retrograde pressure-flow wire in the left Anterior descending artery; a) non-contrast angiographic view, Red arrow highlighting Pressure sensor, blue arrow highlighting Doppler sensor. Note that this position allows sensors to be adjacent to each other, minimizing any delay in respective data acquisition. b) Contrast view of LAD.*

Intra-coronary Pressure and Doppler Measurements

Coronary pressure and flow measurements were carried out using a dual pressure and Doppler sensor-tipped wire, ComboWire® (Volcano Corporation, USA) as described previously.[8, 115]. Briefly, following calibration and normalisation to aortic pressure, the tip of a 0.014-inch sensor-tipped guidewire will be advanced across the lesion and distal coronary pressure and Doppler measurements will be carried out at baseline and hyperaemia, with simultaneous measurement of aortic and central venous pressures (P_a, P_v) via the guide catheter and a right atrial diagnostic catheter respectively. Maximal hyperaemia was induced by a intra-coronary bolus of Adenosine, ranging from 24-72mcg per bolus. Whilst the dual-sensor wire allows simultaneous measurements, there is an intrinsic fixed delay of approximately 63 milliseconds between the pressure and flow traces. For the purposes of the measurements obtained this was corrected for, to ensure more accurate data representation. The following parameters means per beat parameters were calculated**:** 1)Fractional Flow Reserve, FFR = P_d/ (P_a at hyperaemia (pre+post PCI), 2) Coronary Flow Reserve, CFR = $APV_{hyperaemia}$ / $APV_{baseline}$ (pre+post PCI), 4) Hyperaemic Microvascular Resistance, h-MR = P_d / $APV_{hyperaemia}$. The WIA data was calculated specifically investigating the the predominating wave energies, 1) Backward expansion wave, BEW, 2) Forward compression wave, FCW and 3) Backward compression wave.

The use of intra-coronary pressure and flow assessment as detailed above is demonstrated in the studies outlined in chapter 3 (3.1-3.3).

2.3 Trans-coronary electrogram assessment of myocardial infarction

2.3.1 Methodological Background

The recording of a Trans-coronary electrogram (TCM) has a similar method to a standard 12-lead surface ECG; the electrogram is a result of potentials created within the myocardium, detected at the interface between the epicardial artery wall and epicardial layer of the myocardium and is a result of the summation of depolarisation and repolarisation of the many myocardial fibres in the adjacent area. The effects of summing all the electrical activity in the heart can be represented by an electrical dipole whose magnitude and direction is constantly changing (Figure 18). The scalar magnitude of the ECG is then the product of the dipole and the electrode orientation. Profound electrophysiological changes occur in the myocardium following acute coronary occlusion, including a decrease in action potential amplitude and duration, diminution of the resting membrane potential and a reduction in the rate of depolarization[85-87]. Prolonged ischaemia results in a core of necrotic myocardium with increased electrical resistance due to uncoupling of gap junctions[88]. TCM's may be able to detect these anomalies in electrical conduction and have the potential of correlating them with the severity of myocardial necrosis and subsequent myocardial viability.

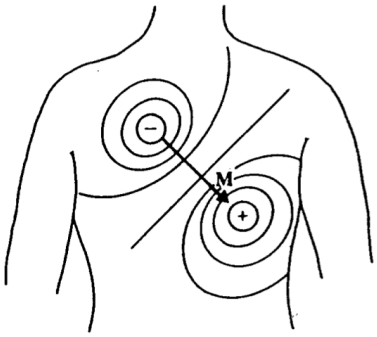

The dipole consists of the points of equal positive and negative charge separated from one another and denoted by the dipole moment vector M

Figure 18: *Approximate dipole field of the heart at the peak of the R wave.*

2.3.1.1 Ex-vivo Guide-wire Resistance Testing

Background:

The nature of the trans-coronary electrogram mapping technique relies on the intrinsic electrical conductive properties of the angioplasty guide-wire being used for the PCI procedure. As there are a wide variety of wires in clinical use, the optimal wire, in terms of its innate electrical properties is not known. We conducted an ex-vivo study to higlight the wires that may be more appropriate for epicardial unipolar mapping.

Aim:

1. To assess the variances in electrical resistance between different coronary guide-wires.

2. Determine whether there is a difference between those with hydrophilic coating and uncoated wires when used in measurement trans-coronary electrograms.

Hypothesis:

1. Uncoated guidewires will have less electrical resistance and are therefore more suitable to measure epicardial electrograms.

Methods:

Ex-vivo experimentation of each guide-wire, passing direct current (D.C) through the wire connected to a Digit Volt meter (DVM) to determine the resistance (Ohm) of each wire. Each wire was measured three times with the mean resistance calculated for each.

Results:

One uncoated and two coated standard angioplasty guidewires were tested; a further rotational atherectomy wire was also tested, acting as a high resistance reference wire, for comparison. The hydrophilic coated guidewires had a mean resistance of 28.7Ω and 36.1Ω respectively, compared to a mean of 19.3Ω for the uncoated wire (Table 3).

One-way ANOVA testing was performed, along with Tukey's multiple comparison testing to assess the significance of the difference in electrical resistances between the wires. This analysis demonstrated a significant difference in resistance between the uncoated and both coated angioplasty guidewires, p=0.0001.

Guide-wire	Coated/ Uncoated	Dimensions	Type of coating	Manufacturer	Resistance (Ω)
Balanced Middleweight (BMW) ™	Uncoated	0.014"x 180cm	n/a	Boston Scientific	19.3
Luge™	Coated	0.014"x182cm	Hydrophillic	Boston Scientific	28.70
Whisper LS™	Coated	0.014" x190cm	Hydrophillic	Abbott Vascular	36.08
RotaWire™ (as reference)	Uncoated	0.009"x325cm	n/a	Boston Scientific	81.72

Table 3: *Electrical Resistance of Intra-coronary guidewires*

Limitations

The ex-vivo experiment was performed with the assumption that electrical resistance is constant and does not change within each intra-coronary guidewire. However impedance, a measure of both resistance and reactance; where reactance is derived from the combination of capacitance and inductance properties of the material. Impedance is a result of changing

frequency of electrical impulses, which occurs during the passage of alternating current (A.C), which is routinely used in the cardiac catheterization laboratory. Therefore, impedance testing is potentially a more accurate method of determining the exact resistance effect of each wire. However, the current testing method sufficiently highlights the general differences in the resistive properties of wires routinely used in PCI procedures.

Conclusion

The uncoated angioplasty guide-wire has less intrinsic electrical resistance and therefore would be more suited to measuring trans-coronary electrograms than hydrophilic coated wires.

2.3.2 Development and refinement of the Trans-coronary mapping experimental protocol

Filter Selection

Modern ECG monitors offer multiple filters for signal processing. The most common settings are 'monitor' and 'diagnostic' modes. In monitor mode, the low frequency filter or high-pass filter (signals *above* a designated threshold are allowed to pass) are set at either 0.5 Hz or 1 Hz and the high frequency filter or low-pass filter (signals *below* a designated threshold are allowed to pass) is set at 40 Hz. These settings limit artifact for routine cardiac rhythm monitoring. The high-pass filter helps reduce wandering baseline and the low-pass filter helps reduce 50 or 60 Hz electrical main power supply noise. In diagnostic mode, the high-pass filter is set at 0.05 Hz, which allows accurate ST segments to be recorded. The low-pass filter is set to 40, 100, or 150 Hz. Consequently; the monitor mode ECG display is more filtered than diagnostic mode, because its pass-band is narrower. Therefore the 'diagnostic'

settings used to obtain TCM's were a high-pass filter of 0.05Hz and a low pass filter of 100Hz, which are the standard settings on the vast majority of 12-lead ECG machines. Figure 19 shows the effects of frequency distortion on the capture electrogram recording.

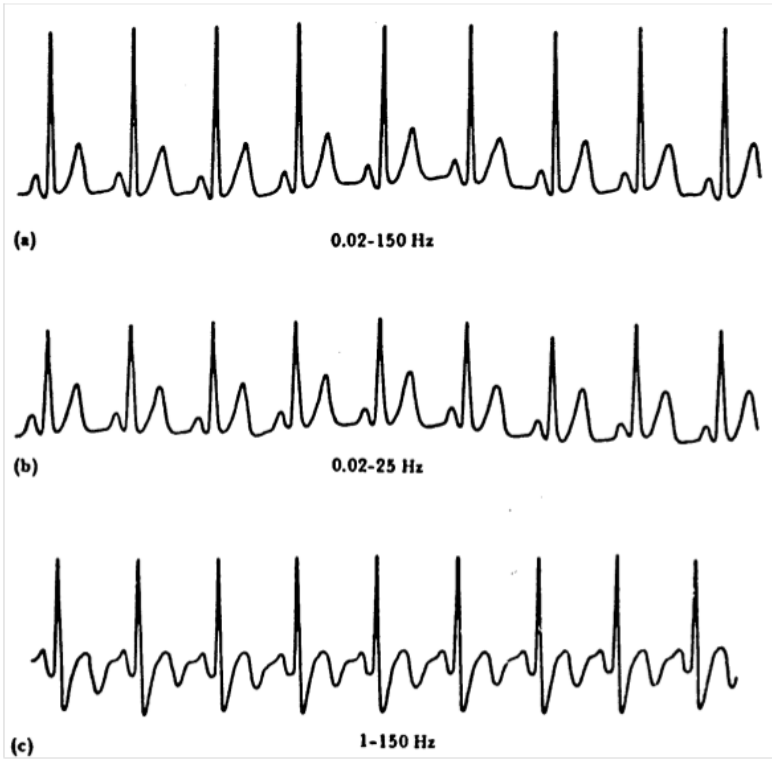

a) True ECG, **b)** Low Pass Filtered (High frequency distortion),
c) High pass Filtered (Low frequency distortion)

Figure 19: *Effects of Frequency distortion on an ECG*

Trans-coronary electrogram (TCE) Monitoring

As the filter settings, described above, used to obtain TCE's were identical to those used in standard 12-lead surface ECG machines, this was also used to obtain TCE's in the cath lab, as it was felt this would be a simple, and transferable method for TCM as a future clinical utility, Figure 20 shows a schematic of how the electrical connection is made to a 12 lead ECG machine. However, the integrated electrophysiological systems in place within cath

labs serve as better modes of obtaining the TCM data, and allow more detailed post processing of the electrogram data. Therefore after initial pilot data was obtained using the 12-lead ECG system, the protocol was changed to allow TCE's to be measured from the Siemans Sensis EP system (Figure 21) shows the connection method to the Sensis system). The EP system allows multiple filter settings to be recorded simultaneously during each case.

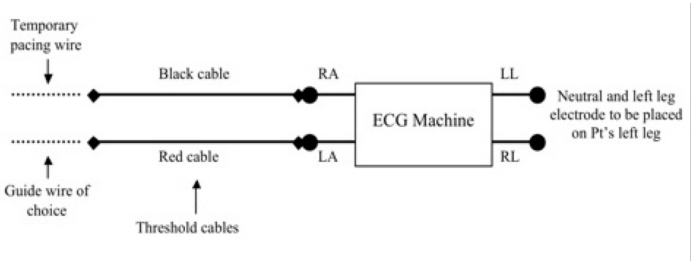

Figure 20: *Schematic of Trans-coronary Electrogram via 12-lead ECG machine*

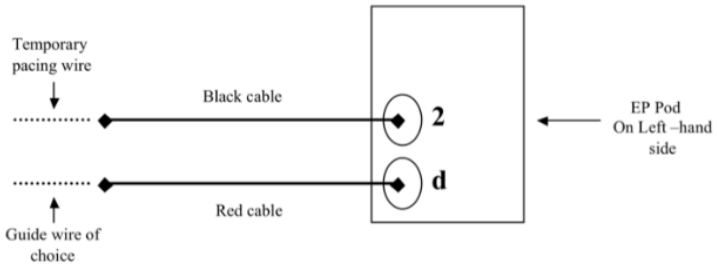

Figure 21: *Siemans Sensis Electrophysiology system TCM Connection*

The cath lab system has been adapted to allow additional measurements to be obtained, and standardized during all cases, with four filter settings routinely measured during each case. These are shown in Figure 22: and are as follows:

Trace 1. Guide wire vs. Temporary wire in IVC with standard filters (0.05/100Hz)

Trace 2. Guide wire vs. Temporary wire in IVC with EP filters (30/500Hz)

Trace 3. Guide wire vs. Wilson's central terminal (WCT)

Trace 4. Temporary wire in IVC vs. Wilson's central terminal

The instantaneous voltages can be calculated from recordings on the EP workstation and caliper marking a point in time (at the maxima and minima on trace 1). Whilst, also measuring the instantaneous voltages at each mark on the surface ECG Leads I, II and II and on trace 1 and trace 4, using Einthoven's formula, the absolute value of WCT voltage at these instants in time can be deduced. By deducting lead I, II and III voltages from trace 4, will give the absolute value of the IVC "far field" voltage at these instants. Therefore, WCT voltage – [I + III – II voltage] should equal zero, if the resultant voltage is not zero, then this is a result of the intrinsic far-field voltage detected. Deducting this far-field voltage from the initially measured "maxima and minima" will enable the absolute local intracoronary value to be identified. We have shown that trace 4 (TPW in IVC vs. WCT) is negligible and therefore the trans-coronary unipolar voltage at any given position is seen in trace 1.

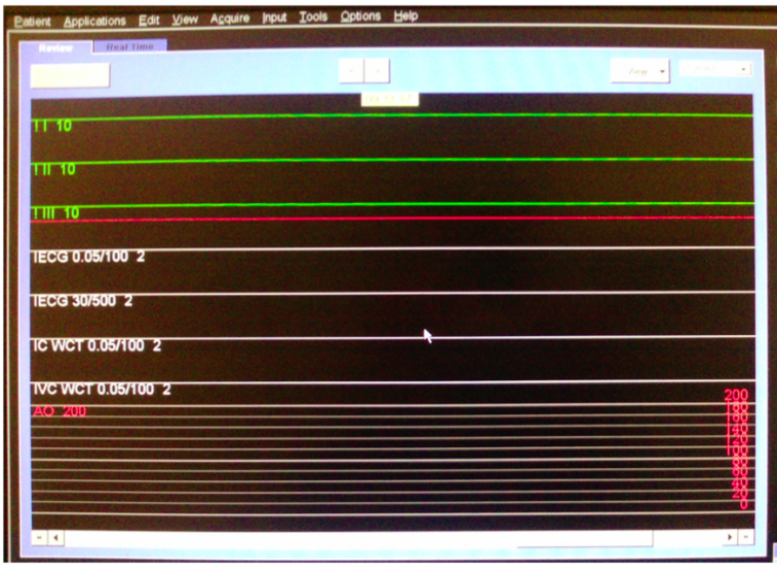

Figure 22: *Adapted Electrophysiology System (SENSIS) system view; Developed specifically for the study, showing the four new electrogram monitoring modes (white text) and standard leads (green text)*

Improving spatial localization of unipolar electrogram - Insulation of guide-wire

Bipolar electrogram voltage maps are the preferred mode of assessing myocardial scar.[96] However, the ability of wavefront direction to influence bipoloar electrogram amplitude is a potential limitation,[117] and subsequently, a wavefront that is perpendicular to the recording dipole will have less amplitude than one that is parallel to it. Whilst unipolar electrograms are not subject to this directional dependance, they are limited by containing substantial far-field electrical signal. As described above, the choice of high-pass filtering, eliminates this to a large extent. However, using the trans-coronary mapping technique, the length of the guidewire, the positive electrode, is potentially a source of increased far-field signal. Therefore, to minimise this, the wire is insulated, by an over-the-wire balloon, which remains uninflated, allowing the distal tip of the wire (5-10mm) to act as the unipolar sensing electrode. Figure 23 below shows and example of an electrogram signal obtained within an LAD, following PCI. The use of the insulation leads to an decrease voltage, reducing the far-field component of the trace.

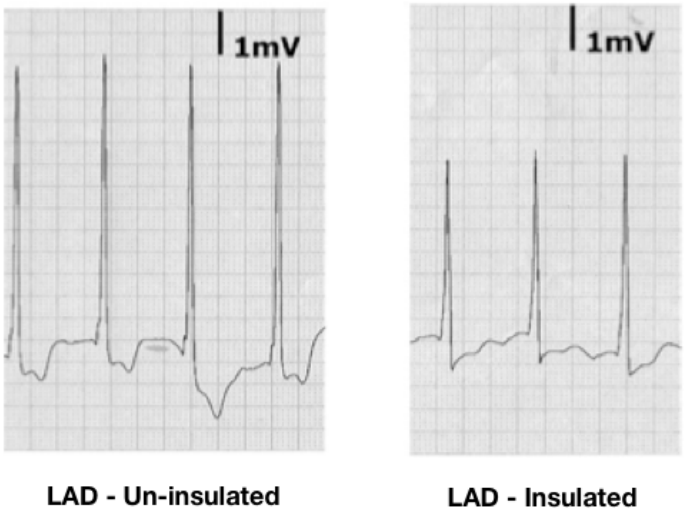

Figure 23: *Effect of insulation of the angioplasty guidewire during trans-coronary electrogram mapping. Showing the increased amplitude obtained with increased electrical insulation afforded by the over-the-wire balloon*

Trans-coronary Electrogram Acquisition protocol

Following intubation of the target coronary artery by a suitable angioplasty guide catheter, an uncoated 0.014-inch coronary guidewire was advanced into the distal vessel. The tip of the guidewire was sequentially positioned in the major epicardial branches beyond the lesion and finally in the distal epicardial vessel. An un-inflated monorail angioplasty balloon was then passed over the wire to insulate all but the distal 5-10mm of the wire while recording electrical signals, to optimise localisation of these signals and minimize the far-field component of the unipolar electrogram. A temporary pacing wire will be inserted via the femoral venous sheath and the tip advanced just into the IVC; this will act as the indifferent electrode (Figure 24). Using 'crocodile' clips, the red pacing connector is placed into port 'd' of the Sensis system. The operator will then places the red 'crocodile' clip on the end of the coronary wire, which will act as the positive electrode. The black pacing cable connector is placed into the port labelled '2' and the operator places the black 'crocodile' clip on the end of the TPW, acting as the negative electrode.

The proximal ends of the intracoronary guidewire and the pacing wire will be connected to limb lead inputs in the Siemans Sensis® Electrophysiology monitoring system, with unipolar voltage recordings obtained.

Electrograms will also be obtained from a control region, with the guidewire positioned at various points in an angiographically unobstructed coronary artery, to obtain electrograms from normal myocardium, as a patient normalised reference. The position of the guidewire tip will be recorded in relation to a conventional segmental coronary reference system.

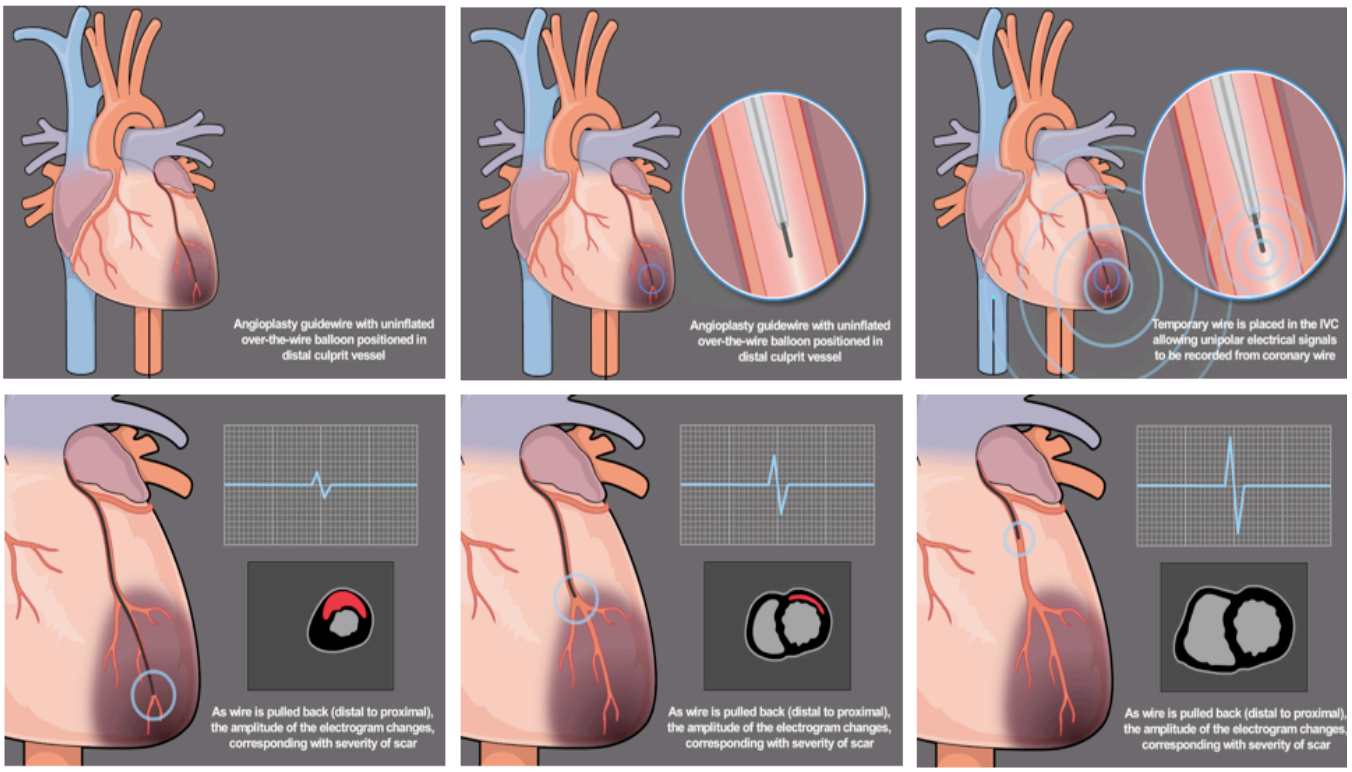

Figure 24: *Schematic of the Trans-coronary electrogram mapping technique with depiction of the expected pathophysiological relationship of unipolar electrogram amplitude with late-gadolinium enhancement-CMR scar imaging (bottom row)*

2.4 Cardiac Magnetic Resonance Imaging methods

2.4.1 Basic Principles

Magnetic resonance (MR) imaging is dependent upon the distribution and concentration of hydrogen nuclei within the body and on the physical and chemical environment of those nuclei. The basis of MR imaging and the acquisition of the images involve complex physical principles, which are beyond the scope of this chapter. In summary, when a patient enters the core of the magnet within a scanner, hydrogen nuclei align with and *precess* about the axis of the magnetic field. This precession can be altered by application of additional small magnetic field pulses. The application of these pulses in a controlled manner (in the form of *pulse sequences)* means that signals can be received and processed to produce an image of

the spatial distribution of the spins or protons within the body. Multiple types of pulse sequences can be used for different imaging protocols to define cardiac structure, tissue characterisation, or measurement of cardiovascular function; all can be employed within a single study. The unique ability to provide such a comprehensive assessment of cardiac form and function, together with the lack of exposure to ionising radiation to patients makes CMR a very useful non-invasive imaging modality.[118]

In the past decade, MRI has become the clinical reference standard for the measurement of myocardial contractile function and viability. Several different markers of viability can be derived from MRI studies, based on either morphological or functional parameters. In addition, MRI methods are becoming available that allow assessment of tissue oedema and microvascular obstruction.

Cine (Contractile function) Imaging

MRI allows accurate measurement of global and regional contractile function of both ventricles. The high spatial resolution, excellent tissue contrast and three-dimensional coverage of the heart result in very low variability of MRI measurements of contractile function, which significantly enhances the statistical power when used to assess viability in research studies. Given that can be data acquired in any imaging plane, the main cardiac axes can be reliably reproduced, facilitating longitudinal follow-up of regional contractile function. Analogous to dobutamine-stress echocardiography, contractile reserve can also be assessed with dobutamine-MR (Dob-MR). The combination of an end-diastolic wall thickness of >5.5mm and systolic wall thickening on stress of >1mm are accepted markers of viability. When both these parameters are combined, Dob-MR has been shown to have a sensitivity

and specificity for predicting functional recovery following revascularisation that is at least comparable to Dobutamine stress echo and FDG-PET (Figure 25).[119]

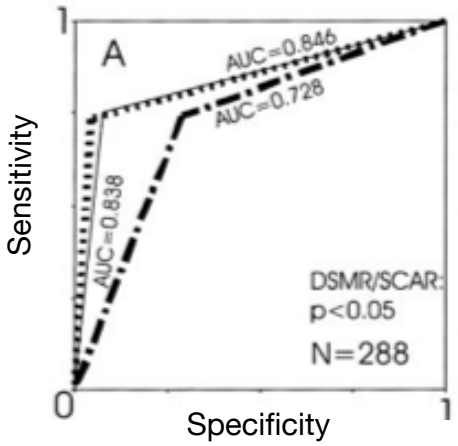

Figure 25: *Additive value of low-dose Dobutamine cine imaging with late-gadolinium enhancement imaging in detecting viable myocardium (Adapted from Wellnhofer et al)*[120]

Late-Gadolinium Enhancement

Late-gadolinium enhanced (LGE) MRI is currently the reference standard for the in vivo assessment of myocardial fibrosis and necrosis. LGE-MRI has been well validated in animal models and the clinical utility of LGE-MRI in delineating viable myocardium has been demonstrated in numerous studies by direct comparison with other markers of viability including contractile reserve, perfusion, metabolism, electromechanical mapping and histology (Figure 26). The very high spatial resolution and complete cardiac coverage allows volumetric quantification as well as precise transmural localisation of scar.[121]

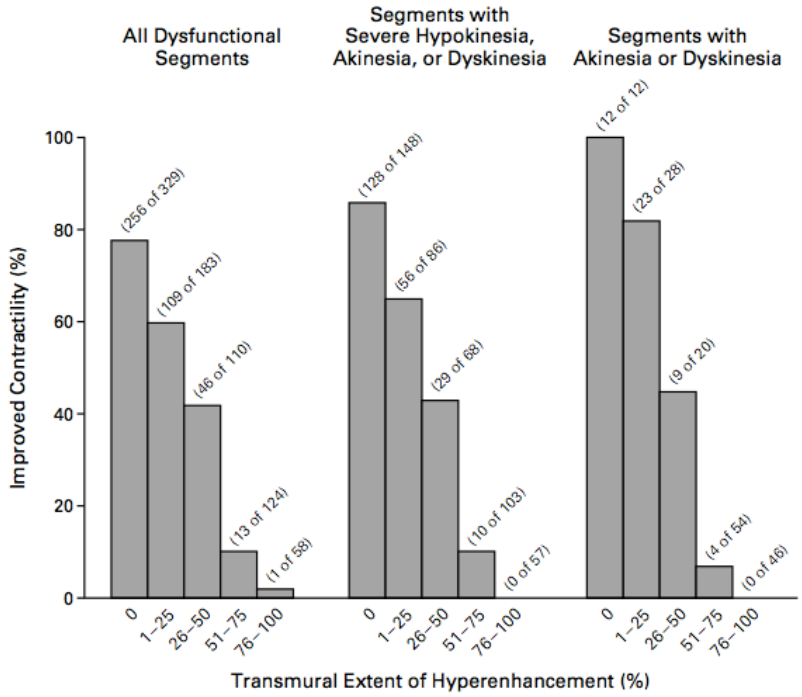

Figure 26: *Demonstration of the variability in recovery depending upon the transmurality of infarction. (Adapted from Kim et al)*[26]

Most current gadolinium-based contrast media are extracellular agents, with rapid distribution within the intravascular and interstitial space, but exclusion from the intracellular space of intact myocytes. In the context of acute myocardial injury, the cell membranes can no longer exclude the contrast from the intracellular space and injured myocardium therefore takes up and retains more contrast agent than viable myocardium. In addition, clearance of contrast agent from injured myocardium is reduced (Figure 27). The CMR technique of late-gadolinium enhancement (LGE) makes use of these differences in the distribution volume of the contrast agent and with appropriate imaging parameters depicts acutely infarcted myocardium as an area of hyper-enhanced myocardium compared to regions of non-infarcted myocardium.[122] Due to its high spatial resolution and tissue contrast LGE imaging can accurately depict the extent and transmurality of myocardial injury after acute myocardial infarction including microinfarcts as low as 1 gram of tissue.[123] In addition,

the pattern of hyperenhancement can be used to differentiate infarction from other types of acute injury such as myocarditis.[123, 124] In the presence of MVO, MRI contrast media do not reach the infarct core affected by the reperfusion injury. On LGE images, the MVO zone therefore appears as a dark core residing within a hyper-enhanced infarct zone (Figure 28). The appearance of the MVO on LGE imaging is a highly dynamic process and due to contrast agent diffusion into the infarcted core, the size of the dark MVO core reduces with increasing imaging time from contrast injection. Often, LGE images are therefore acquired at 1-2 minutes delay after contrast administration, when the MVO appears largest. However, it is not certain, when the optimal time is to image MVO and some studies have suggested that imaging at 10 minutes is most predictive of remodelling.[125] The transmurality of LGE and the amount MVO present are both inversely related to the eventual left ventricular (LV) ejection fraction and predicts the likelihood of recovery of regional wall motion.[26, 126]

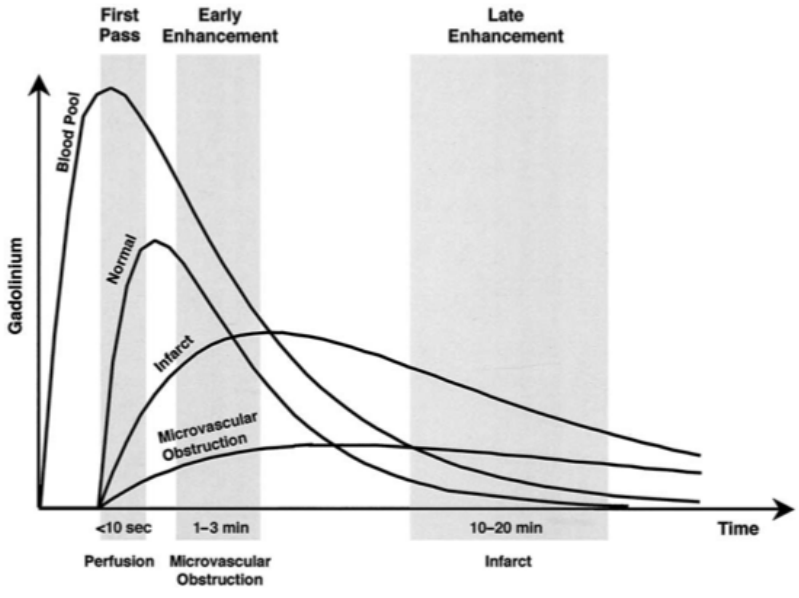

Figure 27: *Gadolinium contrast kinetics and CMR imaging modalities.*

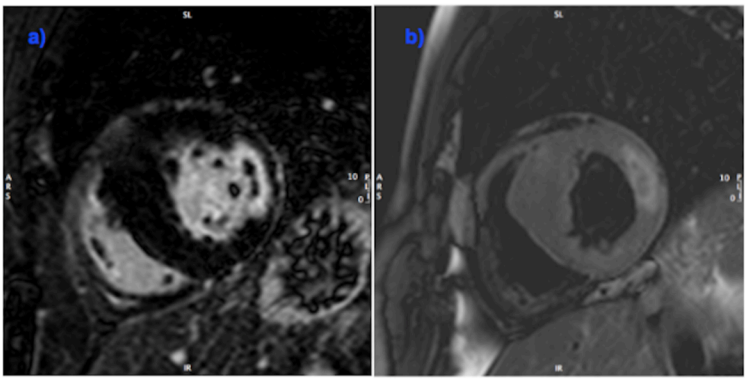

Figure 28: *Myocardial infarction with microvascular obstruction: A) Lateral wall LGE with MVO. B) T2-weighted image showing oedematous region with dark core in area of MVO, suggesting intramyocardial hemorrhage.*

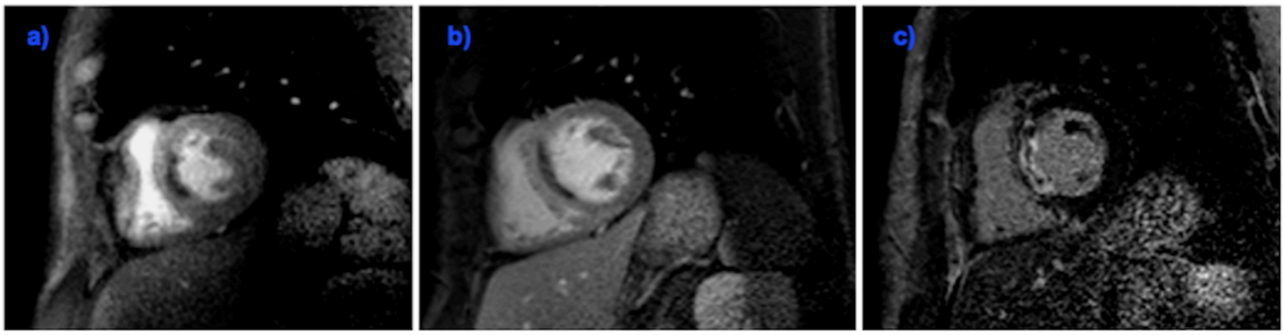

Figure 29: *CMR of a patient presenting with an AMI 2 days ago and with 'no-relow' observed during angiography. A) First-pass perfusion images acquired at rest show a septal wall defect in the area of MVO. B) Early gadolinium enhancement (EGE) acquired 2 minutes after first pass perfusion shows a similar defect caused by MVO. C) LGE images acquired 10 minutes later delineate the infarct zone in white and a smaller MVO (due to contrast diffusion into the MVO over time).*

T2 weighted imaging

One of the pathophysiological consequences of acute ischaemia is an increase in unbound water in the ischaemic tissue.[127] T2-weighted CMR (T2w CMR) is sensitive to the water content of tissue and therefore allows the delineation of acutely ischaemic myocardium. The area of high signal on T2w CMR has been shown to accurately correlate with the area at risk assessed by microspheres.[127] Additionally, increased myocardial T2 signal may be observed within 30 minutes of ischemia onset — detecting myocardial injury prior to both troponin and LGE (Figure 30).[128] Some controversy remains about the precise mechanism of hyperenhacement on T2w CMR in acute ischaemic injury and T2w CMR methods have lower

signal to noise ratio than LGE methods and may be more prone to flow and motion related artefacts.[129] Expertise is therefore needed for the acquisition and interpretation of T2w images. In patients who have severe microvascular dysfunction, reperfusion injury can result in a haemorrhagic transformation of the infarct core, often seen following PCI, which has independent adverse effects on LV remodelling.[130] Haemorrhage present within the myocardium lowers T2 signal, allowing these areas to be identified as a hypointense core within the infarct.[131]

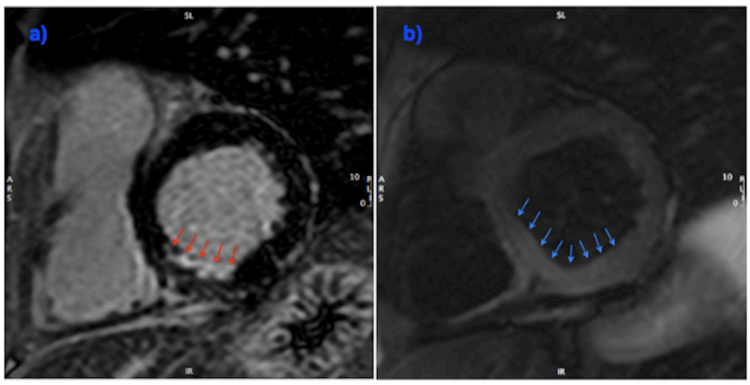

Figure 30: *Infarction and Area at Risk: A) LGE image - subendocardial inferior myocardial infarction. B) T2-weighted image of "area at risk."*

Myocardial Salvage Index

Mortality following myocardial infarction is related to several factors, one of which is the amount of myocardium subtended by the infarct-related vessel; the hypoperfused area at risk (AAR) as a result of the ischaemic insult.[132, 133] Combined, LGE and T2 weighted CMR allow the distinction between infarcted and potentially viable myocardium; LGE delineates the former, whilst T2- imaging determines the latter. These methods therefore permit the calculation of a myocardial salvage index (MSI) by CMR, by correcting the amount of necrotic myocardium for the extent of AAR. From a microcirculatory perspective this index is a marker of irreversibly damaged microvasculature (LGE) and potentially viable

microvasculature (T2w CMR), if timely reperfusion occurs, with this salvage of myocardium being the principal mechanism by which patients with recent myocardial infarction benefit from reperfusion therapies.[134] Eitel et al have recently prospectively demonstrated that MSI is a strong independent predictor of both major adverse cardiovascular events and mortality at six months and in the longer term (median of 19 months) following reperfused STEMI.[135, 136]

2.4.2 Methods Used to Assess infarct size

Cardiac magnetic resonance (CMR) is the reference standard for assessment of ventricular function and size and extent of myocardial infarction. CMR allows accurate measurement of global and regional contractile function of both ventricles. The high spatial resolution, excellent tissue contrast and three-dimensional coverage of the heart result in very low variability of CMR measurements of contractile function, which significantly enhances the statistical power when used to assess viability in research studies.

Three methods of infarct assessment were utilized during the experiments presented in this thesis. The first measure of infarction was through cine, contractile function, imaging, which assesses the global and regional wall motion acquired in any imaging, plane, with the main cardiac axes reliably reproduced, facilitating accurate longitudinal follow-up of regional contractile function. This was performed during the resting state and also with a low-dose dobutamine infusion. Experimental and clinical studies have shown that myocardial dysfunction caused by hibernation or stunning, present following a myocardial infarction, can be transiently reversed by positive inotropic stimulation.[137] During dobutamine infusion, systolic wall thickness increases in viable, but not in scarred myocardium.

The second technique, which is unique to CMR imaging, is late-gadolinium enhancement (LGE) imaging, described in detail in chapter 1. Gadolinium-based contrast media are generally extracellular agents, which rapidly distribute within the intravascular and interstitial space, but are absent from the intracellular space of intact myocytes. In the context of acute myocardial injury, the cell membranes can no longer exclude the contrast from the intracellular space and injured myocardium therefore takes up and retains more contrast agent than viable myocardium. In addition, clearance of contrast agent from injured myocardium is reduced. The CMR technique of late-gadolinium enhancement (LGE) makes use of these differences in the distribution volume of the contrast agent and with appropriate imaging parameters depicts acutely infarcted myocardium as an area of hyper-enhanced myocardium compared to regions of non-infarcted myocardium.

The final modality was T2-weighted imaging, which relies on the patho-physiological consequence of acute ischaemia causing a rise in the unbound water within the myocardium. T2-weighted CMR (T2w CMR) is sensitive to the water content of tissue and therefore allows the delineation of acutely ischaemic myocardium, with the area of high signal on T2w CMR has been shown to accurately correlate with the area at risk assessed by microspheres.[127]

The two experiments that compared invasive indices of infarction, wave intensity and trans-coronary electrograms were compared directly to these three modalities, with the results presented in chapters 3.1 and 4 respectively.

2.4.3 Semi-quantitative versus quantitative CMR analysis

2.3.2.1 Development of CMR analysis

A semi-quantitative analysis of wall motion and transmurality of late gadolinium enhancement was initially adopted to determine the size and extent of infarction. Schuijf et al[138] had previously suggested that semi-quantitative methods of CMR assessment had a good correlation to the quantitatively determined equivalents, with a 90% agreement, and a coefficient of variability, $\kappa = 0.90$.

The two scores being used were the wall motion score (WMS), to visually assess regional wall motion abnormalities (RWMA's) in the cine CMR images, and the transmurality score (TMS), which identified the percentage of transmural scar thickness. The 5-point wall motion score was calculated as follows, where 1 = normal, 2 = hypokinesis, 3 = akinesis, 4 = dyskinesis and 5 = aneurismal (Figure 31a). The TMS was 4-point score, where 0 = no LGE, 1 =1-25%, 2 = 26-50%, 3 =51-75% and 4 = 76-100% (Figure 31b).[139] Abnormal LGE defined as myocardium displaying higher signal intensity than the surrounding myocardium.[26] These scoring systems were stratified in accordance to the American Heart Association 16-segment model of myocardial territories (Figure 32).[140]

WMS	RWMA
1	Normal
2	Hypokinesis
3	Akinesis
4	Dyskinesis
5	Aneurysmal

a) Wall Motion Score

TMS	% LGE
0	None
1	1-25
2	26-50
3	51-75
4	76-100

b) LGE Transmurality Score

Figure 31: *Wall motion and Transmurality Scores*

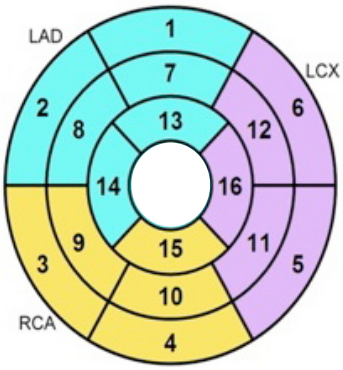

Figure 32: *American Heart Association 16 segment model*

Methods

Study Patients:

Inclusion criteria

To mirror the cohort of patients planned to be recruited for the main ACS studies, the inclusion criteria was consistent with this. 1) Acute myocardial infarction (AMI) >2 and <7 days before scheduled PCI or coronary angiography proceeding to PCI, including patients who have received thrombolysis for an acute STEMI (AMI is defined as symptoms of ischaemia lasting at least 20 minutes with ST deviation (elevation or depression) of at least 1mm and significant elevation in cardiac biomarkers; TnT >0.5. or TnI >5). 2) One or more coronary lesions of at least 75% diameter stenosis (on visual inspection of coronary angiograms) that are suitable for PCI.

Seven patients presenting with acute coronary syndromes, had CMR prior to planned coronary angiography and PCI. Two independent reviewers scored each score respectively, to minimise potential bias being introduced in the analysis of the images.

Results

The mean Troponin T was 1.9 ± 0.7. 112 segments were analysed according to the AHA model. 75 segments had normal wall motion, 23 were hypokinetic, and 14 were akinetic, with no dyskinesis or anerysmal segments identified. When WMS in hypokinetic segments was compared with TMS, a large degree of heterogeneity was observed, with 43% (n=10) having 51-75% transmurality of scar, though 13% (n=3) had no demonstrable scar with hypokinesis observed in the WMS analysis (Figure 33). However, the presence of akinetic segments was associated with greater than 50% LGE in 93% (n=12) of those identified. Table 4 below shows the WMS comparison to TMS in full.

Transmurality Score (%LGE)	Wall Motion Score					
	1	2	3	4	5	Total
0 (0)	66	3	0	0	0	69
1 (0-25)	6	4	0	0	0	10
2 (26-50)	3	3	1	0	0	7
3 (51-75)	0	10	1	0	0	11
4 (76-100)	0	3	12	0	0	15
Total	75	23	14	0	0	112

Table 4: *Transmurality Scores Stratified against Wall motion Scores*

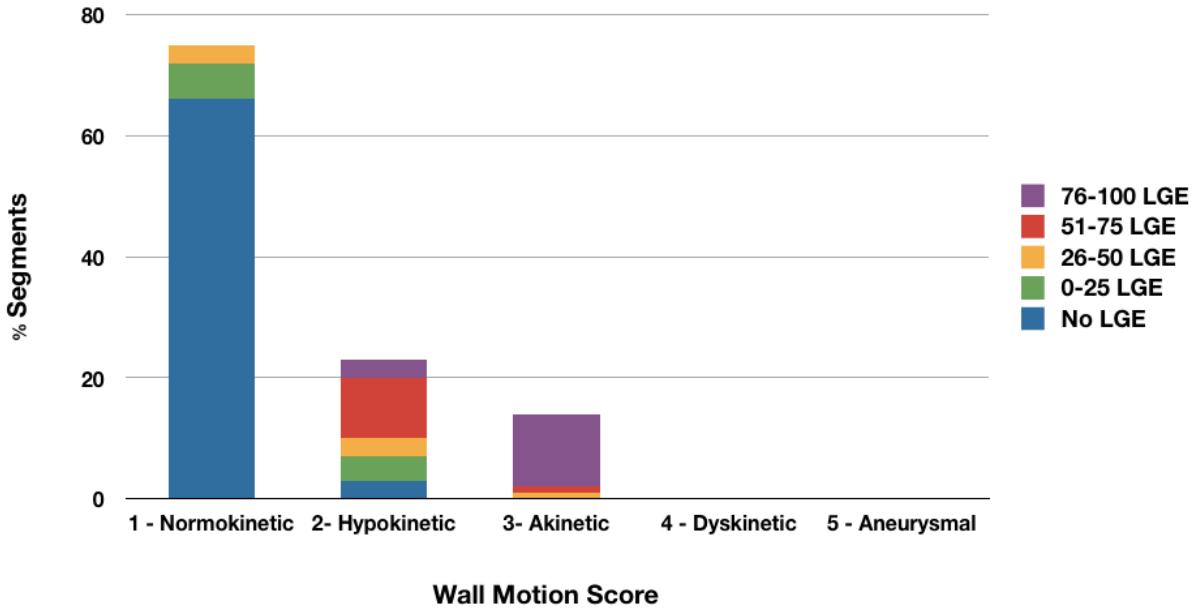

Figure 33: *Graphical representation of TMS versus WMS*

Discussion of technique and modifications

The results of this pilot study suggested that those identified to have hypokinesis had a varying range of infarct transmurality. In addition a recent meta-analysis of CMR imaging in the assessment of myocardial viability suggested that LGE has a better sensitivity and negative predictive value than wall motion scoring for predicting recovery.[141]

To ensure accurate assessment of both wall motion and LGE derived scar quantification of the two parameters was considered a suitable addition to the analysis plan. Whilst continuing to assess these markers visually, quantification would allow reproducible measurements, particularly relevant when used to assess change over time.

With the use of a specially designed CMR analysis platform CMR 42 (Circle Cardiovascular Imaging, Calgary, Canada), the area of hyperenhancement can be quantitatively determined

using a previously described signal intensity method.[26, 138] A region of interest (ROI) is placed in an area of remote myocardium. Infarcted tissue is then defined as an area of myocardium with signal intensity greater than 5 standard deviations (s.d) compared to the remote ROI on LGE imaging. Endo-epi-cardial contours were drawn (excluding papillary muscles) to derive total LV mass. Infarct mass was expressed as the absolute mass of infarcted tissue (in grams) and a percentage of the total LV mass (Figure 34).

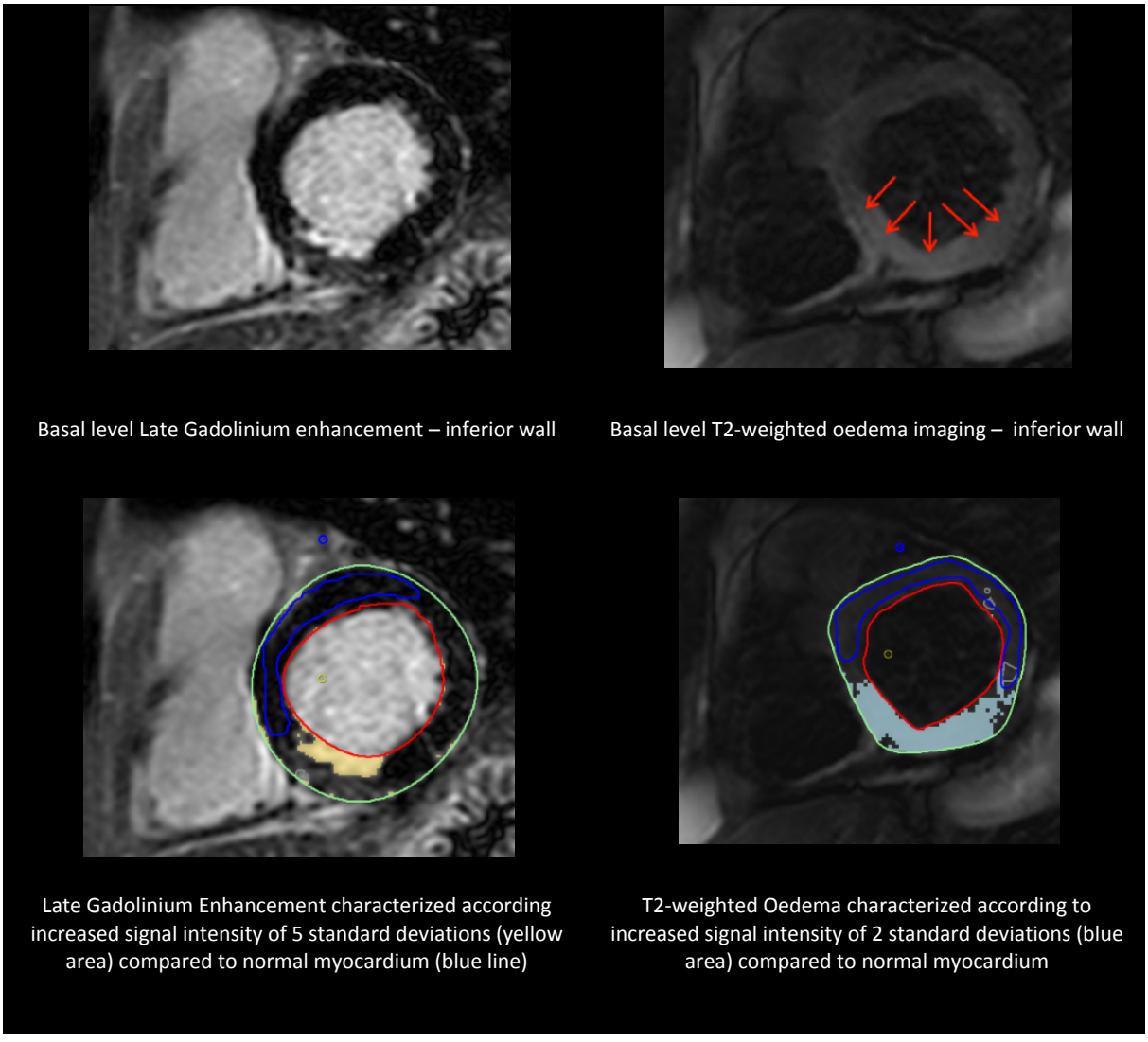

Figure 34: *Quantification of late-gadolinium enhanced and T2-weighted images*

Quantification of regional wall thickening was performed as previously described.[26, 142] Endo- and epicardial contours in diastole (first image of the cine series) and systole (identified as the phase with smallest LV volume) were drawn for the entire ventriclular cavity (Figure 35).

Figure 35: *Quantitative analysis of wall motion and wall thickening, using endo- and epi- cardial planemetry to identify*

The area of infarction on the cine images was identified by comparing the identical corresponding LGE images. Percentage wall thickening was automatically calculated by determining the absolute differences in wall thickness between end-diastole and end-systole. This method facilitated the recovery of function following revascularization was defined as the percentage change in regional wall thickening (%WT) in the infarct area, at follow-up, compared to the index study. Significant recovery in function post

revascularization was characterized as an increase in regional WT by ≥30% (%WT), identifying likely clinically relevant ventricular remodelling (Figure 36).[142, 143]

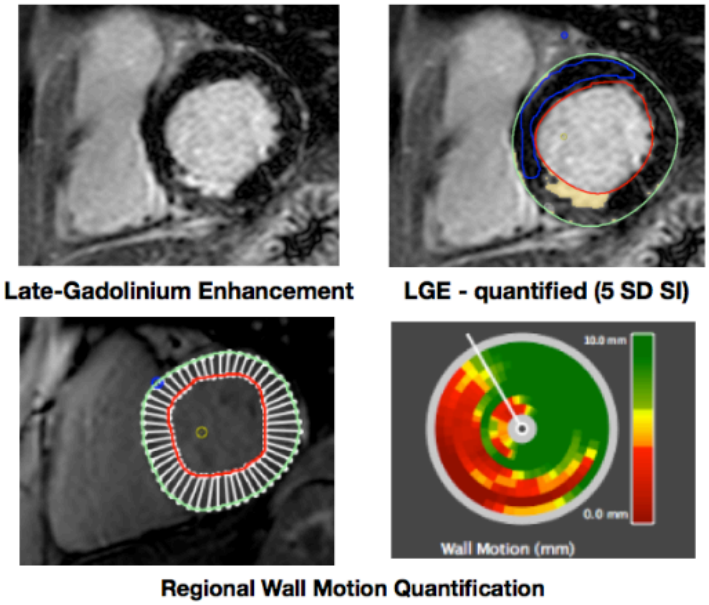

Figure 36: *Regional wall motion quantification in relation to LGE derived area of infarction*

2.4.4 CMR Scanning Protocol

All scans were performed on a dedicated 3 Tesla cardiac MRI scanner (Achieva, Phillips Healthcare, Best, Netherlands) using dual-RF transmission technology and a 32-channel phase array body coil. Cine images were acquired using a standard steady state free precession (SSFP) cine technique in two-, three- and four-chamber orientations and in a left-ventricular (LV) short-axis stack covering the LV from apex to base. A T2-weighted short axis stack, with the same geometry as the cine images, was performed, ranging from 9-13 slices. A three-slice SSPP cine sequence was performed after a 4-minute intravenous infusion of 5mcg/kg/min Dobutamine, repeated at 10mcg/kg/min dose. Late gadolinium enhanced (LGE) imaging was performed using an inversion recovery fast gradient echo sequence 10-20 min after the intravenous administration of 0.2 mmol/kg body weight of gadobutrol

(Gadovist, Bayer Schering Pharma, Berlin, Germany), depending on the nature of the patient, with prolonged times utilized in patients presenting with acute coronary syndromes, to minimize the possible risk of odematous tissue being misinterpreted as LGE derived scar.[144] A stack of images was acquired in the same LV short axis orientation as the cine images to ensure registration between cine CMR and infarct measurements. LGE acquisition was guided by a Look-Locker sequence with a typical pre-pulse delay of 200-330ms. Figure 37 provides a schematic of the protocol.

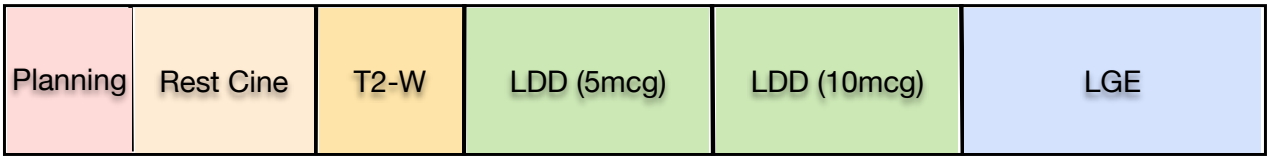

Figure 37: *CMR protocol assessing infarct size and viability following an acute coronary syndrome*

3. CORONARY PHYSIOLOGY STUDIES

PART A:

CORONARY PHYSIOLOGICAL ADAPTATIONS IN THE PRESENCE OF LEFT VENTRICULAR DYSFUNCTION: INSIGHTS FROM CORONARY WAVE INTENSITY ANALYSIS

3.1 CORONARY WAVE ENERGY: A NOVEL PREDICTOR OF FUNCTIONAL RECOVERY FOLLOWING MYOCARDIAL INFARCTION

Kalpa De Silva[1], Paul Foster[1], Antoine Guilcher[2], Michael Marber[1], Simon Redwood[1], Sven Plein[3,4], Divaka Perera[1]

Affiliations:

[1] King's College London BHF Centre of Excellence, NIHR Biomedical Research Centre at Guy's and St. Thomas' NHS Foundation Trust, Cardiovascular Division, The Rayne Institute, London, UK

[2] Department of Clinical Pharmacology, St. Thomas' NHS Foundation Trust, London, UK

[3] King's College London BHF Centre of Excellence, NIHR Biomedical Research Centre and Welcome Trust and EPSRC Medical Engineering Centre at Guy's and St. Thomas' NHS Foundation Trust, Division of Imaging Sciences, The Rayne Institute, London, UK

[4]Multidisciplinary Cardiovascular Research Centre, Leeds Institute of Genetics, Health and Therapeutics University of Leeds, Leeds, UK.

3.1.1 ABSTRACT

BACKGROUND

Revascularization following acute coronary syndromes (ACS) provides prognostic benefit, provided that the subtended myocardium is viable. The microcirculation and contractility of the subtended myocardium affect propagation of coronary flow, which can be characterized by wave intensity analysis (WIA). The study objective was to determine in ACS whether early WIA-derived microcirculatory (backward) expansion wave energy (BEW) predicts late viability, defined by functional recovery.

METHODS

31 patients (58±11 yrs) were enrolled following Non-ST elevation myocardial infarction (NSTEMI). Regional left ventricular (LV) function and late-gadolinium enhancement (LGE) were assessed by cardiac MRI (CMR), before and 3 months following revascularization. The BEW was derived from WIA of phasic coronary pressure and velocity in the infarct-related artery (IRA) while mean values were used to calculate Hyperaemic Microvascular Resistance (hMR).

RESULTS

12-hour Troponin T, LVEF and percentage LGE mass were 1.35±1.21 µg/L, 56±11%, and 8.4±6.0% respectively. The IRA BEW was inversely correlated to LGE infarct mass ($r = -0.81$, $p < 0.0001$) and strongly predicted regional LV recovery ($r = 0.68$, $p=0.001$). By ROC analysis, a BEW threshold of 2.8 W m^{-2} s^{-2} x 10^5 predicted functional recovery with sensitivity and

specificity of 0.91 and 0.82 (AUC 0.88). hMR correlated with LGE mass (r = 0.48 , p=0.03) but not LV recovery (r = - 0.34, p=0.07).

CONCLUSION

The microcirculation-derived Backward Expansion Wave is a new index that correlates with the magnitude and location of infarction, which may allow the prediction of functional myocardial recovery. Coronary WIA may facilitate myocardial viability assessment during cardiac catheterization.

Key words

Wave intensity analysis; acute coronary syndromes; myocardial viability; microvascular function; left ventricular remodeling

3.1.2 INTRODUCTION

Coronary revascularization improves mortality and morbidity following an acute myocardial Infarction (AMI), provided that the myocardium subtended by the diseased artery is viable.[31, 145] Non-ST elevation MI (NSTEMI) accounts for two-thirds of all AMI presentations[146] and is usually treated by initial pharmacological stabilization followed by coronary angiography with a view to revascularization, ideally within 96 hours of symptom onset.[147-149] This expedited treatment algorithm is designed to reduce the risk of recurrent myocardial infarction but as a consequence most patients do not undergo non-invasive assessment of left ventricular function and/or myocardial viability prior to cardiac catheterization. At present, there are no invasive tools for assessing myocardial viability in the catheterization laboratory, as an adjunct to coronary angiography. A real-time invasive physiological index of viability would enable personalized and instantaneous risk stratification following ACS, with revascularization targeted to those who are likely to derive long-term benefit.

An important determinant of myocardial viability and tissue perfusion is the integrity of the microcirculation.[48, 150, 151] The severity of microvascular dysfunction influences left ventricular (LV) functional recovery, cardiovascular morbidity and mortality following ACS.[13, 14, 152] The advent of pressure and Doppler sensor-tipped guidewire technology has allowed detailed in vivo interrogation of microcirculatory physiology and these techniques have demonstrated that microcirculatory compromise correlates with infarct size following ST-elevation myocardial infarction (STEMI).[60, 153] Wave intensity analysis (WIA) of phasic coronary pressure and flow profiles has allowed further characterization of the

microcirculation and its impact on coronary flow in a number of stable clinical settings.[79, 154] These studies demonstrate that mechanical impedance of the coronary microcirculation by the myocardium is the predominant factor that governs myocardial perfusion, with a backward travelling (microcirculatory) expansion wave (BEW) identified as being the most influential in generating diastolic coronary flow.[75, 155, 156] Wave intensity analysis has not previously been used to assess the effect of myocardial infarction on the energy transfer within the coronary circulation.

3.1.3 AIMS

The aims of our study are to assess the correlation between microcirculatory wave energy and the extent of myocardial infarction and to assess the utility of this novel physiological index to predict recovery of ventricular function following revascularization. We also compared the BEW with hyperaemic microvascular resistance (hMR), the invasive reference standard for measuring microvascular function.

3.1.4 STUDY DESIGN

3.1.4.1 Inclusion Criteria

Patients scheduled to undergo urgent coronary angiography and revascularization 2-7 days after presenting with an NSTEMI, defined as symptoms of ischemia lasting at least 20 minutes (chest pain score >4)[157] in conjunction with significant elevation in cardiac biomarkers (defined as a TnT >0.20ug/L) identified twelve hours after symptom onset, were eligible for inclusion into the study (Figure 38). This cohort of patients was selected as they have an extremely heterogenous degree of microvascular dysfunction following infarction and therefore provide a diverse group for invasive physiological marker

assessment of microvascular function and subsequent myocardial recovery.

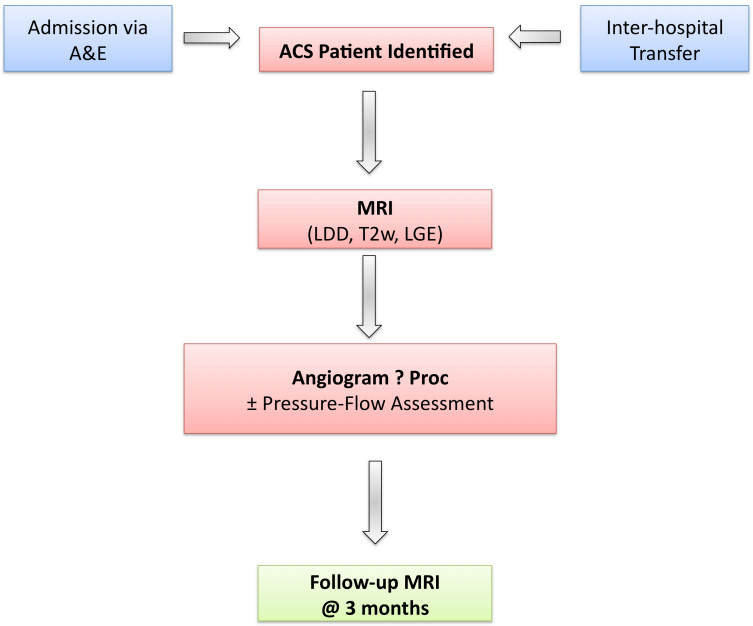

Figure 38: *Patient Recruitment Stream*

3.1.4.2 Exclusion Criteria

To ensure that CMR findings reflected acute myocardial injury, patients were not enrolled if they had suffered a prior myocardial infarction. Additional exclusion criteria were a prior diagnosis of valvular disease, previous PCI or CABG surgery, an occluded infarct related artery (IRA) at time of angiography, persistent arrhythmias or hemodynamic instability. Patients with contraindications to CMR at study entry, such as pacemakers, implantable defibrillators, claustrophobia, or metallic intracranial implants, were also excluded.

3.1.4.3 Ethical Approval

The study protocol was approved by the institutional research ethics committee (REC ref 08/H0802/143). All participants were provided with an information sheet detailing the study protocol prior to obtaining informed consent.

3.1.4.4 Cardiac catheterization and intra-coronary measurements

All patients where preloaded with aspirin (300mg) and clopidogrel (600mg). Interventional cardiologists performing the catheterization procedures were blinded to the information obtained from the preceding CMR. Coronary angiography was performed using a standard Judkins technique. Intracoronary nitroglycerin was administered before diagnostic angiography and intracoronary physiological measurements. Identification of the infarct-related artery (IRA) was based on the presenting 12-lead electrocardiogram and angiographic findings. Hemodynamic measurements were obtained, where possible prior to percutaneous coronary intervention (PCI), in the IRA, and then immediately following PCI. Measurements were then carried out in an angiographically normal reference coronary artery (with less than 10% diameter stenosis), supplying a myocardial territory remote to the infarct region. All measurements were obtained during intra-coronary adenosine induced hyperaemia ((up to 60mcg for Right and 96mcg for Left coronary arteries respectively). Aortic pressure (P_a) was measured via the coronary guiding catheter. Intracoronary pressure (P_d) and average peak velocity (APV) were measured via a 0.014-inch dual pressure-Doppler sensor guidewire (ComboWire® Volcano Corp, CA, USA), the tip being positioned in the distal vessel. Simultaneous pressure and Doppler measurement were repeated at least 3 times in each location and condition to reduce acquisition error (Figure 39).

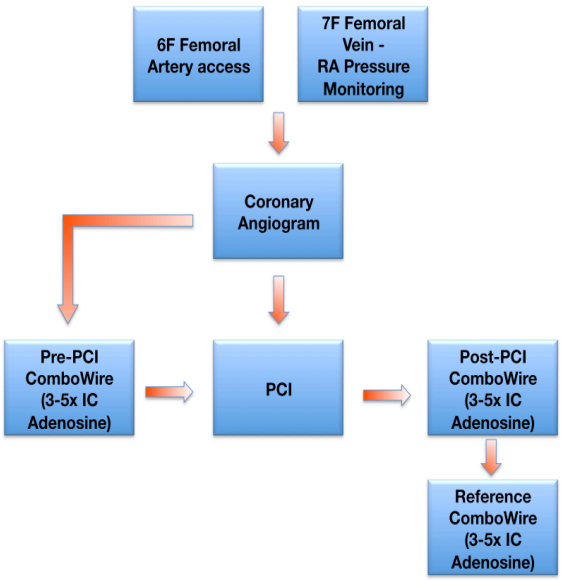

Figure 39: *Schematic of the Cardiac Catheter Laboratory Protocol*

3.1.4.5 Data analysis

Hemodynamic data analysis

Phasic pressure and flow

Data were sampled at 250 Hz and analyzed off-line, using a customized programme developed on Matlab (Mathworks, Inc, Natick, Mass). A Savitzky-Golay convolution method[78] was adopted, using a polynomial filter to refine the derivates of the P_a and v signals. Three to six consecutive cardiac cycles were selected for resting and hyperaemic conditions, gated on the ECG R wave-peak, with ensemble averaging of P_a, P_d, APV, and HR. For the purposes of wave intensity analysis it has been considered that diastole commences with the onset of ventricular relaxation, signified by the dichrotic notch on the arterial pressure waveform, as previously described.[156] Net coronary wave intensity (dI) was calculated from the time-derivatives of ensemble-averaged coronary pressure and flow velocity (U) as $dI = dP_d/dt \times dU/dt$.[76, 79] Coincident (microcirculation-derived) backward and (aorta-derived) forward propagating waves were separated assuming blood density to be

1050 (kg/m^3) and estimating coronary wave speed using the sum of squares method.[76, 158] The peak energy (in W m^{-2} s^{-2} x 10^5) carried by the three most prominent wave energies identified were analysed and included in this manuscript. These were the positive, forward directed (aorta-derived) compression wave (FCW), occurring at the onset of systole; the concurrently occurring negative (backward, microcirculation-derived) compression wave (BCW) and the backward expansion waves (BEW), the first negative wave occurring at the onset of ventricular relaxation, identified by the onset of diastole (Figure 40). The investigators who performed the data analyses were blinded to all clinical patient data.

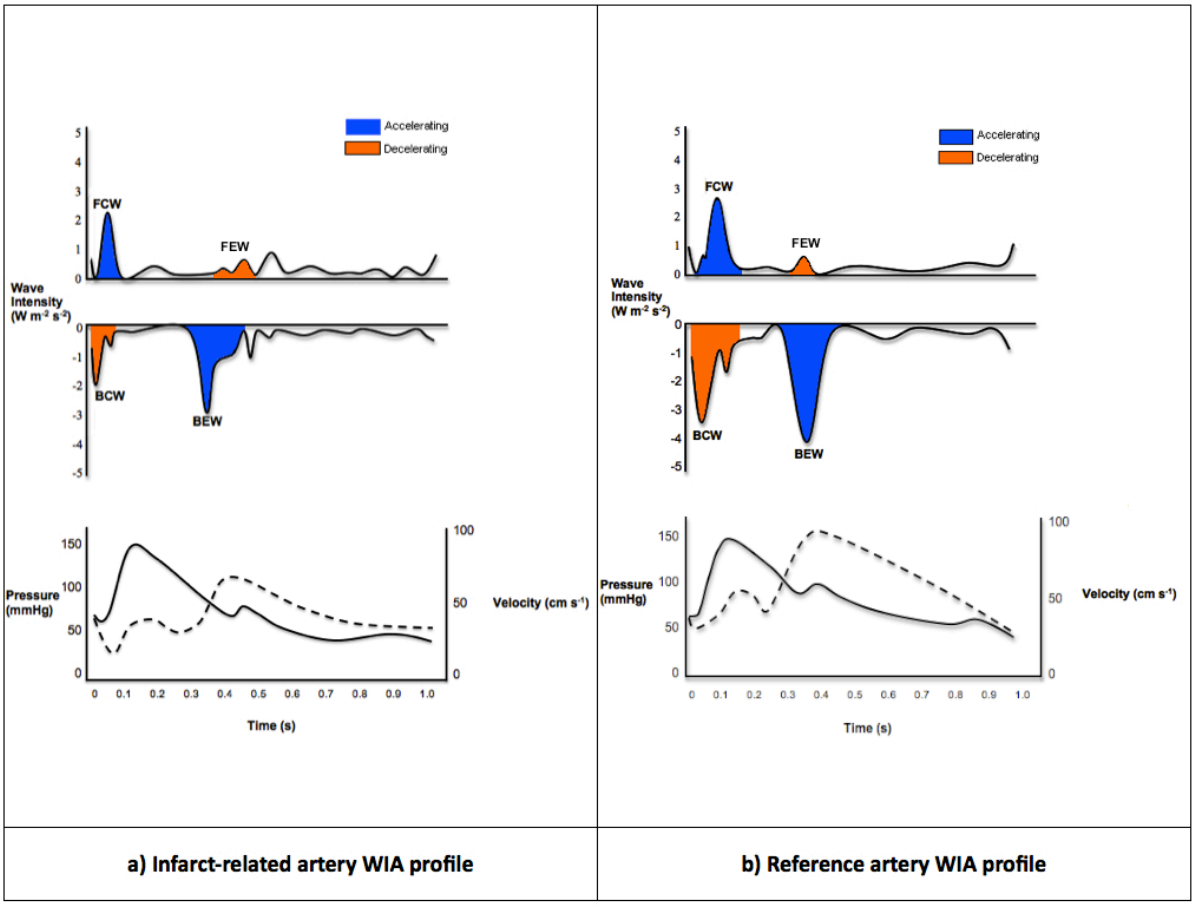

Figure 40: *Example of the differences observed between infarct-related artery and reference artery wave intensity profiles; a) Infarct-related artery (IRA) WIA profile (LAD); b) Remote reference vessel (Cx) WIA profile. (solid line is pressure, dashed line is velocity).*

Mean-per-beat pressure and flow

Hyperaemic microvascular resistance (hMR) was calculated as the ratio of mean P_d to APV (mmHg cm^{-1} s) during maximal hyperaemia, obtained through simultaneous intra-coronary pressure-flow measurements, during 3-6 consecutive cardiac cycles.[55, 60]

Cardiac Magnetic Resonance Imaging

Index CMR studies were performed prior to emergent angiography and PCI. The scans were performed on a dedicated 3 Tesla cardiac MRI scanner (Achieva, Phillips Healthcare, Best, Netherlands) equipped with dual-RF transmission technology and a 32-channel phase array body coil. Cine images were acquired using a standard steady state free precession (SSFP) cine technique in two-, three- and four-chamber orientations and in a left-ventricular (LV) short-axis stack covering the LV from apex to base. The acquisition pulse sequence provided a typical spatial resolution of 1.8 x 1.8 x 8 mm with a 2mm inter-slice gap and a temporal resolution of 50 frames per second. Area at risk was assessed using a T2- weighted sequence; a short-axis stack covering the whole ventricle using T2-weighted triple inversion recovery breath-hold pulse sequence was performed (slice thickness 8 mm; repetition time 2 RR intervals; echo time 99 ms; image matrix 145x192). Late gadolinium enhanced (LGE) imaging was performed using an inversion recovery fast gradient echo sequence 15-20 min after the intravenous administration of 0.2 mmol/kg body weight of gadobutrol (Gadovist, Bayer Schering Pharma, Berlin, Germany), to ensure optimised infarct delineation in the ACS setting.[144] A stack of images was acquired in the same LV short axis orientation as the cine images to ensure registration between cine CMR and infarct measurements. LGE acquisition was guided by a Look-Locker sequence with a typical pre-pulse delay of 200-330ms. Follow-up scans were performed between 3-4 months, using an identical acquisition protocol.

CMR Analysis

Quantitative analysis was performed offline, by blinded observers, using dedicated CMR viewing software (CMR 42, Circle Cardiovascular Imaging, Calgary, Canada). The area of hyperenhancement was quantitatively determined using a previously described signal intensity method,[26, 138] where oedematous tissue derived from the T2-W sequence is defined as having a signal intensity of greater than 2 standard deviations (S.D) compared to a region of interest (ROI) in an area of remote normal myocardium, whilst infarcted tissue is defined as an area of myocardium with LGE signal intensity greater than 5 S.D (Figure 41). Endo-epicardial contours were drawn (excluding papillary muscles) to derive total LV mass. Infarct mass was expressed as the absolute mass of infarcted tissue (in grams) and as the percentage of the total LV mass.

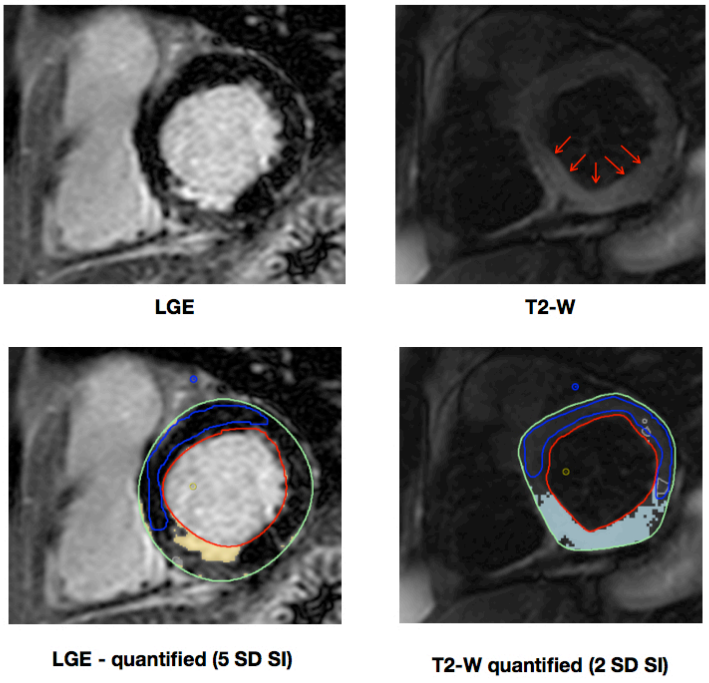

Figure 41: *Quantitative Analysis of T2-Weighted and Late-gadolinium enhancement using a signal intensity method.*

Quantification of regional wall thickening was performed as previously described (Figure 42).[26, 142] Briefly, endo- and epicardial contours in diastole (first image of the cine series) and systole (identified as the phase with smallest LV volume) were drawn for the entire ventriclular cavity. The area of infarction on the cine images was identified by comparing the identical corresponding LGE images. Percentage wall thickening was automatically calculated by determining the absolute differences in wall thickness between end-diastole and end-systole. Recovery of function following revascularization was defined as the percentage change in regional wall thickening (%WT) in the infarct area, at follow-up, compared to the index study. Significant recovery in function post revascularization was characterized as an increase in regional WT by ≥30% (%WT), identifying likely clinically relevant ventricular remodelling.[142, 143]

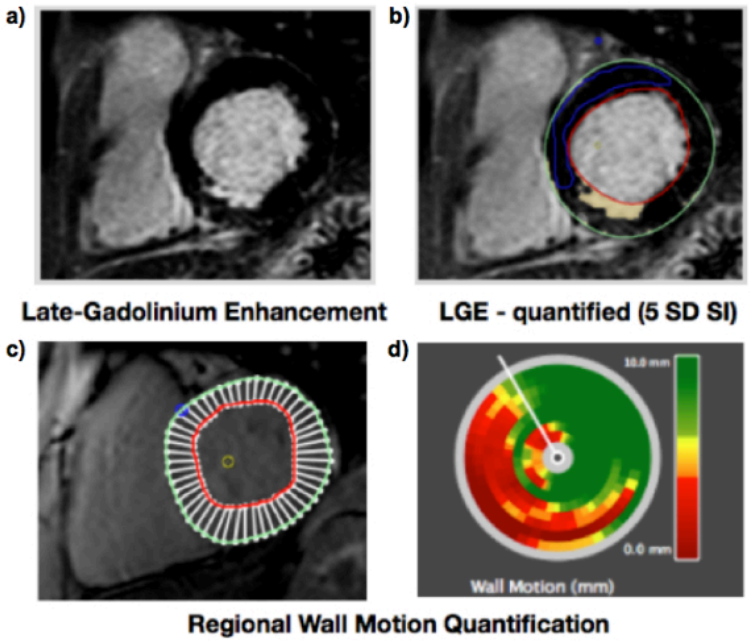

Figure 42: *Cardiac CMR infarction and regional wall thickness quantification; a) Inferior late-gadolinium enhancement (LGE); b) Quantified LGE using signal intensity threshold analysis; c) Segmentation of ventricular cavity; d) Polar map representation of the regional differences in wall thickening*

3.1.4.6 Statistical Analysis

Statistical analysis was performed using IBM SPSS version 20. Pearson correlation analysis was used to identify the relationship between WIA derived separated wave energies and infarct size and recovery in function following PCI. Continuous variables were compared, assuming a non-parametric distribution, using the Wilcoxon signed rank test and the Mann-Whitney test for paired or unpaired comparisons, respectively. A two-tail test for significance was performed in all analyses, whereby $p \leq 0.05$ was considered statistically significant. Coefficient of variability (CV) analysis of the Doppler-pressure measurements was performed on the constituent pressure and velocity components – Pd and APV, along with the microvascular resistance surrogate, HMR. CV was calculated as the standard deviation of the differences divided by the mean in two consecutively obtained data sets. Inter-observer reproducibility for these measures was assessed using a single measure intra-class correlation coefficient. Percentage recovery in ventricular function was assessed according to whether ≥30% recovery in regional wall thickening was observed following PCI.[142, 143] Using this characterization, Receiver operator characteristic (ROC) analysis was performed to determine the optimal cut-off value and subsequent sensitivity and specificity for diastolic microcirculatory wave intensity (BEW), and hMR, in predicting regional recovery in function, with the difference between the two indices, assessed using the Delong ROC comparison analysis.[159] Data are presented as mean ± standard deviation, unless otherwise specified.

3.1.5 RESULTS

BASELINE CHARACTERISTICS

Thirty-one NSTEMI patients were recruited to the study, with 9 subsequent exclusions, 3 – claustrophobia during CMR, 2 – requiring surgical revascularization, 1 - inadequate quality of Doppler-pressure trace**,** and 3 - neither CMR or angiographic features of an ACS (Figure 43). Twenty-two (18 men, 57±10 yrs) completed both the CMR and intra-coronary pressure and Doppler measurements, after enrolment 77±46 hours following symptom onset. 12-hour Troponin T was 1.35±1.21 µg/L. Quantitatively determined percentage diameter stenosis of the culprit lesion was 79±15% in the IRA (Table 5). Patients were scanned 4±2 hours prior to angiography (4±1 days following symptom onset). LV ejection fraction was 56% (IQR 31-68%) and hyperenhanced infarct mass was 8.4 ± 6.0g, which corresponded to 8.0 ± 6.1% of total left ventricular mass (Table 6). Both parameters of infarct size, mass and % LV mass, correlated linearly with TnT (R= 0.61, , p=0.003 and R=0.67, p=0.001, respectively).

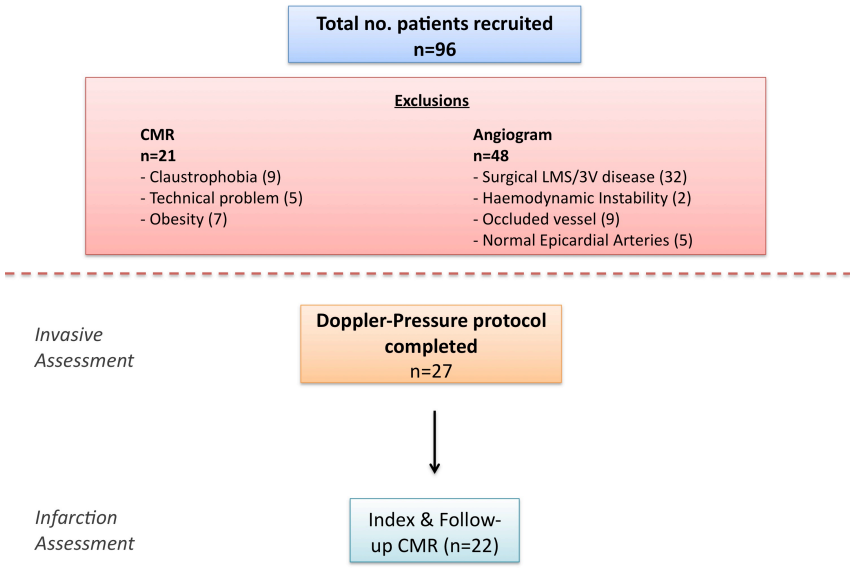

Figure 43: *Patient recruitment analysis*

Variable	Total	≥30% Recovery in WT	≤30% Recovery in WT	p value
No. completed protocol	22	11	11	n/a
Age, Median (IQR)	57 (51-67)	56 (47-71))	58 (52-79)	0.27
Medical History				
Male, n (%)	18 (82)	10 (82)	8 (73)	0.16
Hypertension, n (%)	10 (45)	5 (45)	5 (45)	1.0
Diabetes mellitus, n (%)	3 (14)	1 (9)	2 (18)	0.56
Hypercholesterolemia, n (%)	15 (68)	8 (73)	7 (64)	0.66
Smokers, n (%)	8 (36)	2 (18)	6 (55)	0.05
BMI[*] (kg/m^2), Median (IQR)	26 (25-28)	26 (21-31)	27 (23-32)	0.64
Prior MI[†], n (%)	0 (0)	0 (0)	0 (0)	n/a
Previous PCI[‡], n (%)	0 (0)	0 (0)	0 (0)	n/a
Type of ACS				
NSTEMI[§], n (%)	22 (100)	11 (100)	11 (100)	1.0
Duration from Symptom onset to CMR[‖], Median Hrs (IQR)	46 (43-76)	45 (39-164)	47 (44-172)	0.09
Duration from Symptom onset to angiogram, Median Hrs (IQR)	48 (48-78)	45 (45-72)	50 (46-210)	0.14
Cardiac Biomarkers				
Peak Troponin T (µg/L), Median (IQR)	1.35 (0.40-1.21)	0.89 (0.22-1.59)	1.63 (0.61-4.2)	0.08
Infarct-related artery				
LAD/Cx/RCA[#], n	14/3/5	6/4/1	7/3/1	n/a
Pre-PCI QCA[**], Median % (IQR)	78 (71-88)	77 (70-85)	78 (72-87)	0.11
Post-PCI FFR[††], Median (IQR)	0.94 (0.91-0.98)	0.93 (0.91-0.95)	0.94 (0.92-0.97)	0.25
Medications (on discharge), n (%)				
ASA	22 (100)	11 (100)	11 (100)	1.0
Clopidogrel	22 (100)	11 (100)	11 (100)	1.0
Beta-blocker	21 (95)	10 (91)	11 (100)	0.95
ACE-inhibitor (or ARB)	22 (100)	11 (100)	11 (100)	1.0
Statin	22 (100)	11 (100)	11 (100)	1.0
Calcium antagonist	6 (27)	4 (36)	2 (18)	0.16
Thiazide diuretic	4 (18)	2 (18)	2 (18)	1.0

[*] Body Mass Index
[†] Myocardial Infarction
[‡] Percutaenous coronary intervention
[§] Non-ST-elevation myocardial infarction
[‖] Cardiac Magenetic Resonance
[#] Left anterior descending/circumflex/right coronary artery
[**] Quantitative coronary angiography
[††] Fractional flow reserve

Table 5; *Baseline Characteristics*

	Index Presentation	Follow-up	*p value*
No. completed protocol	22	22	*n/a*
Time of MRI following symptom onset (days), Median (IQR)	2 (2-3)	93 (89-97)	*n/a*
Volumetric Analysis			
LVEDV* (ml), Median (IQR)	129 (106-149)	103 (90-128)	*0.02*
LVESV† (ml), Median (IQR)	58 (46-81)	47 (36-57)	*0.04*
LVEF‡ (%), Median (IQR)	56 (31-68)	57 (34-67)	*0.55*
Quantitative Infarct size characterization			
Infarct mass (g), Median (IQR)	7.6 (2.6-11.2)	6.2 (2.1-10.3)	*0.06*
Infarct mass % of left ventricular mass, Median (IQR)	7.1 (2.6-11.3)	6.0 (2.3-11.1)	*0.08*
Quantitative Regional Wall Analysis			
Wall thickening, percentage, Median (IQR)	48 (27-52)	70 (43-84)	*0.0001*
Improvement in Wall thickening %, Median (IQR)	-	23 (4-36)	*n/a*

* Left ventricular end-diastolic volume
† Left ventricular end-systolic volume
‡ Left ventricular ejection fraction

Table 6: *Cardiac CMR Data*

Coronary Hemodynamic Indices

a. Coronary Wave Intensity Analysis

IRA microcirculatory expansion wave energy (BEW) inversely correlated with TnT (R =-0.70, p<0.0001), and LGE infarct mass (R = -0.81, p < 0.0001) (Figure 44). The systolic compression waves in the IRA were also inversely correlated with TnT and infarct mass, albeit less strongly than the BEW; R = -0.33, p=0.001 and R = -0.57, p=0.01 respectively for the IRA BCW and R = 0.31, p=0.01 and R= -0.56, p=0.01 respectively for the IRA FCW.

In contrast, REF microcirculatory energy (BEW) did not correlate with either TnT or LGE mass (R= 0.02, p=0.46, and R = 0.10, p=0.65) and BCW (R = -0.31, p=0.17, R= -0.007, p=0.97 respectively). Similarly no correlation was present with REF FCW; (R= -0.36, p=0.10 and R = -

0.05, p=0.80, respectively).

When considering the relationship between IRA wave energy and myocardial area at risk derived from T2-W enhanced imaging, no correlation is observed with any of the three prominent waveforms; BEW (R =-0.33, p=0.19), FCW (R=-0.43, p=0.06) and BCW (R=-0.22, p=0.39).

LV ejection fraction was proportional to the IRA aorta-derived systolic FCW (R= 0.55, p=0.008 respectively) and to a lesser extent, the distally originating systolic BCW (R = 0.43, p=0.04). The diastolic BEW showed no such relationship, R= 0.23, p=0.30.

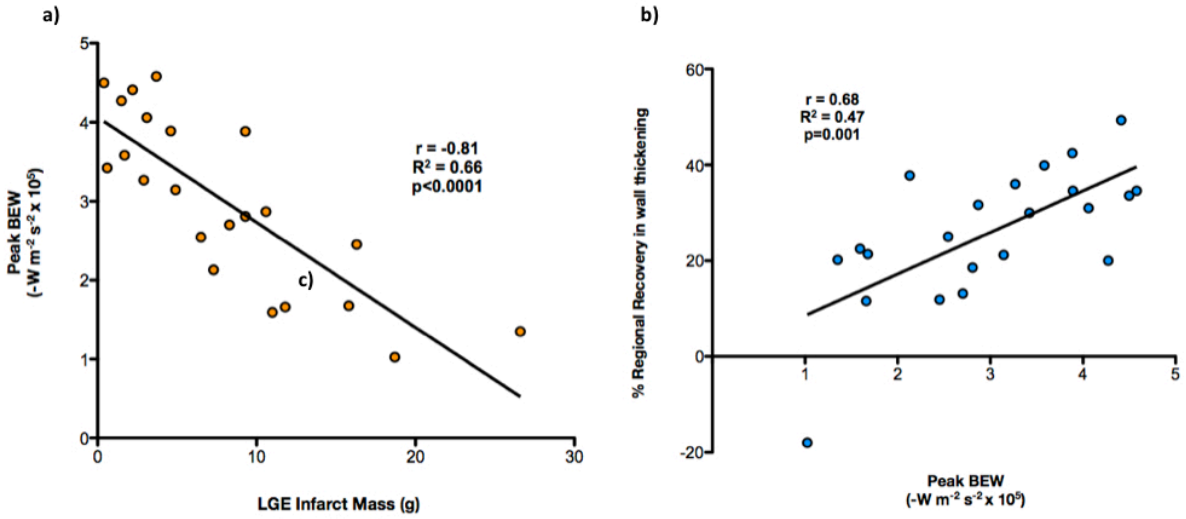

Figure 44: *Backward Expansion Wave (BEW) versus infarction and wall thickening parameters; a) Infarct-related artery (IRA) BEW vs. Absolute LGE mass; b) Regional improvement in wall-thickening vs. IRA BEW*

Pre-PCI measurements were obtained in a subset of 11 patients of the overall cohort. Pre-PCI BEW showed a trend toward an inverse correlation with TnT and LGE mass seen in the post-PCI setting, however these correlations were not statistically significant (R =-0.54,

p=0.08 and R =-0.52, p=0.10). There was an attenuation of all waveforms when measured in the presence of a stenosis, in comparison to the post-PCI values, though these were not significantly reduced (BEW p=0.11, FCW p=0.08 and BCW p=0.13). Figure 45 highlights the mean magnitude reduction observed in BEW energy (1.96±0.65 versus 2.31±0.73 x W m^{-2} s^{-2} x 10^{5}), whilst figure 46 depicts the relationship with post-PCI BEW.

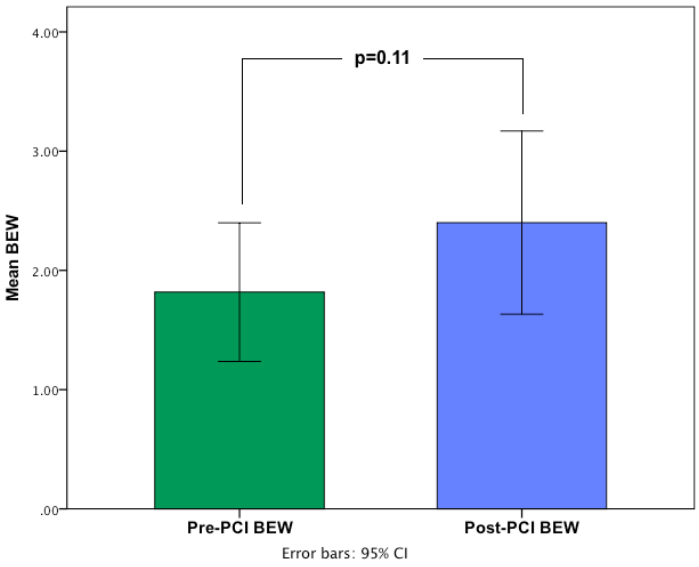

Figure 45: *Attentuation of BEW in the presence of a stenosis*

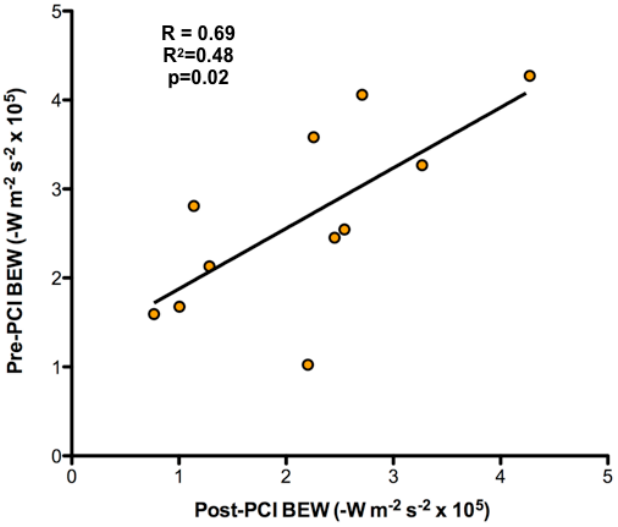

Figure 46: *Pre-PCI versus Post-PCI Backward Expansion Wave Energy*

A comparison was made between measurements performed during baseline and hyperaemic conditions. BEW continued to have an inverse relationship with myocardial infarction mass derived by troponin (R=-0.69, p=0.004) and LGE (R = -0.72, p=0.003). The basal IRA BEW energy showed a non-significant trend to be increased compared to hyperaemic BEW (3.12 (2.10-4.01) vs. 3.01 (2.04-3.93) W m^{-2} s^{-2} x 10^5, p=0.12). Both IRA FCW (2.51 (1.98-3.51) vs. 2.47 (2.12-3.31) W m^{-2} s^{-2} x 10^5, p=0.46) and BCW (1.79 (1.20-2.51) vs. 1.85 (1.41-2.58) W m^{-2} s^{-2} x 10^5, p=0.51) had a similar magnitude to their hyperaemic equivalents. An inverse correlation with both TnT and LGE was noted with basal IRA BCW (R= -0.27, p=0.04 and R= -0.39, p=0.02), though this was less statistically significant than when measured during hyperaemia. Basal FCW showed a linear trend with TnT (R = 0.29, p=0.01) and LGE (R=-0.48, p=0.01), with similar statistical significance as when observed during hyperaemia.

b. Hyperaemic microvascular resistance

HMR (P_d/APV) in the IRA was 2.44±1.07 mmHg cm^{-1} s compared to 2.0±0.56 mmHg cm^{-1} s in the reference vessel, p=0.001. IRA HMR directly correlated with both TnT release (R= 0.46, p=0.04) and LGE infarct mass (R = 0.48, p=0.03). Reference HMR showed no correlation with either marker of infarct size; TnT ; R = 0.31, p=0.18 or LGE R = 0.22, p=0.23 respectively.

	Infarct-related artery	Reference artery	*p value*
Wave Intensity Analysis (W m^{-2} s^{-2} x 10^5)			
Aortic-originating energies			
FCW*, Median (IQR)	2.47 (2.12-3.31)	3.01 (2.77-3.82)	*0.01*
Microcirculatory-originating energies			
BCW†, Median (IQR)	1.85 (1.41-2.58)	2.33 (1.42-2.78)	*0.006*
BEW‡, Median (IQR)	3.01 (2.04-3.93)	3.98 (2.29-3.77)	*0.001*
Means per beat derivatives			
hMR§ (mmHg cm^{-1} s), Median (IQR)	2.34 (1.73-2.93))	1.90(1.52-2.59)	*0.001*

* Forward compression wave
† Backward compression wave
‡ Backward expansion wave
§ Hyperaemic microvascular resistance

Table 7: *Wave Intensity and Mean-per-beat Data*

c. Variability and inter-observer reproducibility

APV, P_d and HMR had a coefficient of variability of 8.7, 2.7 and 7.3% respectively. The single measure intra-class coefficients for these measures were 0.74, 0.88 and 0.77 respectively.

LEFT VENTRICULAR REMODELING

LV remodeling was assessed by CMR 101±29 days post revascularization. LV ejection fraction at follow-up was 57% (IQR 34-67%). Positive remodeling was seen in the ventricular volumes, with the end-diastolic volume decreasing from 128 ±30ml to 116 ±25ml (p=0.02). End-systolic volume similarly reduced from 62±22ml to 47±17ml (p=0.04). There was a trend to a reduced volume of hyperenhancement at follow-up, in terms of absolute infarct mass (8.4 ± 6.0g versus 7.5±4.7g, p=0.06) and relative to overall LV mass (8.0±6.1% versus 7.4±4.2%, p=0.08). At baseline, median regional %WT in the infarct territory was 48% (IQR 19-69%) improving to 70% (IQR 38-94%), p<0.0001, post revascularization, with a median improvement of 23% (IQR -18-49%) (Table 6).

The microcirculation-derived diastolic BEW was strongly predictive of both, initial baseline wall thickening (R=0.83, p<0.0001) and the eventual change in regional wall thickening (%WT) (R= 0.68, p=0.001) (Fig 3b), as was the distally originating systolic BCW (R=0.62, p=0.002 and R = 0.52, p=0.02 respectively). There was a statistically non-significant association between baseline and improvement in %WT in respect to the aorta-derived systolic FCW (R=0.44, p=0.07 and R = 0.48, p=0.06 respectively). Additionally, there was an inverse relationship between IRA hMR and baseline wall thickening (R=-0.52, p=0.02), although this was not statistically significant when associated with regional recovery function (R= -0.34, p=0.07).

By ROC analysis, the optimum BEW threshold for predicting recovery of regional function was 2.81 W m^{-2} s^{-2} x10^{5}. Values above this threshold predicted improvement in %WT with sensitivity and specificity of 0.91 and 0.82 respectively (AUC 0.88). The optimal hMR value for predicting recovery was ≤2.41 mmHg cm^{-1} s and the corresponding sensitivity, specificity and AUC were 0.82, 0.64, 0.68 respectively (Figure 47). The Delong ROC comparison test confirmed the superior predictive accuracy of BEW compared to hMR (p=0.05). In patients in whom the BEW was greater than 2.81, the likelihood of recovery in function was significantly higher than in those patients in whom the BEW was less than or equal to 2.81 (p=0.001), compared to the equivalent optimum hMR value of ≤2.41 (p=0.12) (Figure 48 a & b).

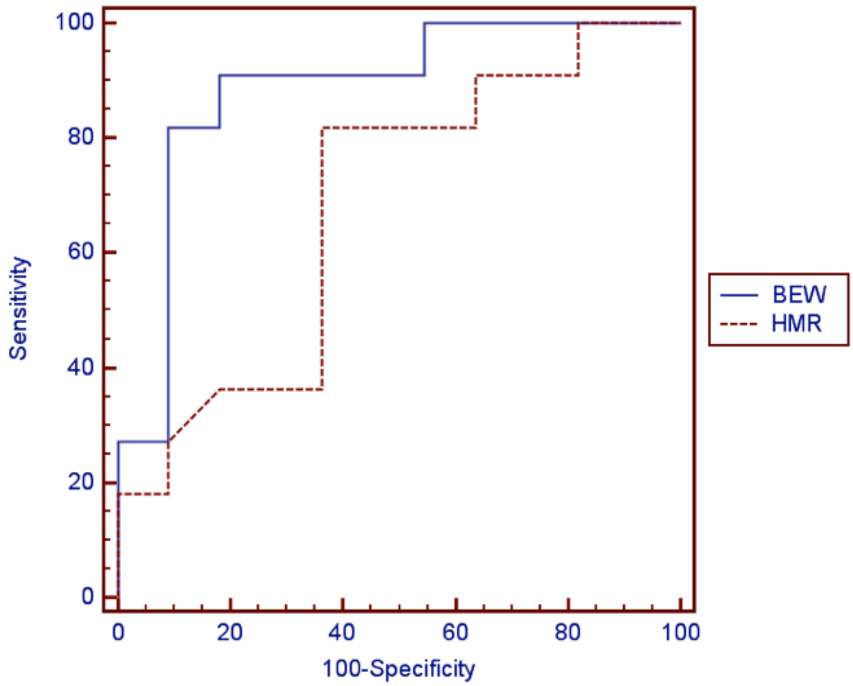

Figure 47: *Receiver Operator Characteristics analysis (n=22); a) Accuracy of BEW and hMR in predicting ≥30% improvement in Regional Wall thickening –area under the curve (AUC) for prediction of functional recovery were 0.82 and 0.68 respectively. The optimal cut-off values were >2.81 $Wm^{-2}s^{-2}$ x 10^5 for BEW and <2.41 mmHg cm^{-1} s for hMR.*

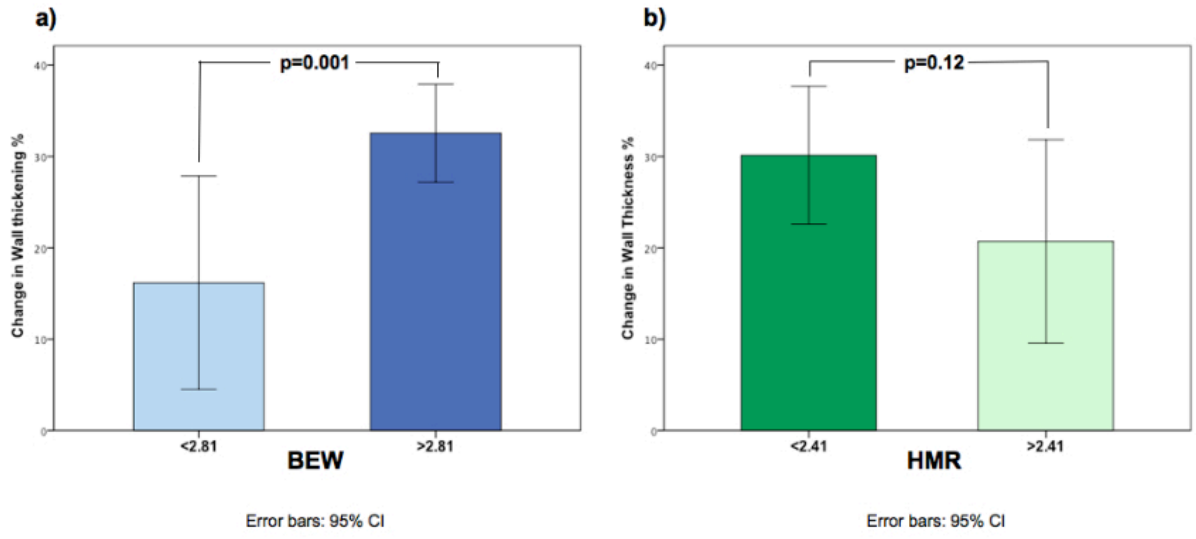

Figure 48: *Regional improvement in wall-thickening identified by optimal a) BEW b) HMR cut-offs based on ROC analyses*

3.1.6 DISCUSSION

Our study indicates that the magnitude of the backward expansion wave energy in the infarct-related artery is strongly predictive of myocardial recovery following an NSTEMI, highlighting its potential utility as an index of myocardial viability that can be obtained during cardiac catheterization. Furthermore, we have demonstrated that the BEW is reduced following acute coronary syndromes, in proportion to the magnitude of infarction

Phasic WIA versus means-per-beat assessment of microvascular function

The ability to prospectively risk stratify patients following myocardial infarction is paramount to optimization of outcome. The severity of microvascular dysfunction post infarction has been demonstrated to be an important correlate of LV functional recovery, cardiovascular morbidity and mortality and is proportionate to infarct size.[13, 14, 48] Coronary flow reserve (CFR) and fractional flow Reserve (FFR) following AMI have both been found to be predictive of myocardial recovery, albeit with variable accuracy.[52, 53, 56, 67] However, supportive evidence correlating FFR with viability is limited in the acute setting, when microvascular derangement is at its peak, potentially affecting the accuracy of FFR in this context. The dependence of CFR on prevailing hemodynamic conditions and epicardial coronary disease has also limited its applicability. Consequently, both measures have been largely superseded by more specific indices of microvascular resistance, which have been more consistently associated with myocardial viability. Fearon et al[153] first demonstrated the utility of the Index of microvascular resistance (IMR) in evaluating the microcirculation, confirming that it was an independent predictor of infarct size and LV recovery following STEMI. These findings

have subsequently been reproduced by several investigators who have assessed IMR after successful primary PCI.[70, 160] Similarly, Kitabata et al[60] demonstrated that the Doppler-based index hMR is predictive of infarct size and recovery in function following reperfusion of STEMI. However, it should be noted that these indices have previously only been evaluated in the setting of acute STEMI. To our knowledge, the current study is the first reported evaluation of hMR as a measure of myocardial recovery following NSTEMI. Our findings suggest that the correlation between hMR and either infarct size or the likelihood of recovery of regional function many not be as strong as it is following STEMI. While this difference may relate to the smaller extent of infarction in our NSTEMI population compared to the previous STEMI studies, it is possible that microvascular resistance alone may not be an adequate measure of myocardial viability in NSTEMI.

The use of wave energetics to analyze phasic coronary pressure and flow represents a paradigm shift in evaluating microvascular function and has the potential to provide more detailed insights into the determinants of myocardial perfusion than the traditional means-per-beat methods. This may explain the superior diagnostic accuracy of the BEW, which interrogates microvascular function as well as regional contractility, the co-determinants of myocardial viability.

Pre-PCI versus post-PCI coronary WIA

The results presented above highlight the potential of this techniques ability to be utilized as a parameter measured before PCI, guiding the selection of patients for revascularization according to the presence of significant myocardial viability, but more universally to allow identification of those patients that additional pharmaco-adjunctive therapy, to alleviate and

improve microvascular dysfunction, could be utilised.[161] However, whilst simultaneously assessing pressure and Doppler flow is feasible it remains more challenging due to the natural reduction in coronary flow velocities as a consequence of the presence of a stenosis. We have demonstrated that pre-PCI measurements is feasible and safe to assess BEW before PCI and furthermore, that there is a close correlation between BEW derived from measurements taken before and after PCI ($r=0.70$ $p=0.01$; where $BEW_{pre} = 0.68 \times BEW_{post} + 1.2$ W m^{-2} $s^{-2} \times 10^5$). However, the presence of a stenosis will alter the coronary wave speed and therefore may alter the accuracy of the separated wave energies obtained when adopting the single-point assessment of wave speed, as performed in this study. Further investigation into the affects of stenoses is required to determine the accuracy of WIA in the ACS setting.

Diastolic Wave Energy: the Backward Expansion Wave

The myocardial-microvascular interaction is pivotal in governing coronary pulsatile flow and transmural myocardial flow distribution. While aortic pressure is the main determinant of coronary arterial pressure and flow, the relationship is complex and non-linear, with various models alluding to the impendence of systolic coronary flow by the contraction of myocardium surrounding the intramyocardial microcirculation have been postulated.[75,155] [74,162] The Backward expansion wave (BEW) is the dominating microcirculatory wave energy that propagates coronary flow and therefore myocardial perfusion, during diastole.[79, 154] [79, 154] The BEW occurs as a result of diastolic relaxation of the microvasculature, creating a 'suction' effect, subsequently accelerating flow within the microvascualar bed. It can therefore be considered an integrated measure of the myocardial-microvascular interaction. The effect of varying microvascular resistance on this wave, with both pharmacological

vasodilation[163] or enhanced LV lusitropy, results in a decreased compressive force on the microcirculation, thereby increasing the magnitude of the BEW.[84] Davies et al demonstrated a 30% reduction in the magnitude of the BEW in patients with hypertension-related LV hypertrophy, a population known to have globally impaired microvascular function and LV lusitropy, when compared to a group of matched controls.[79]

Myocardial ischemia and infarction affects both aspects of the myocardial-microvascular interaction, namely contractility and microvascular function[164], making the BEW wave an attractive tool for evaluating this relationship. The reduction in BEW amplitude following infarction found in our study of NSTEMI mirrors the previous observations of the impact of infarction on diastolic coronary flow in the setting of STEMI.[165] Iwakura et al[166] demonstrated the aberrant nature of diastolic flow following infarction, observing a disproportionate attenuation of diastolic flow velocity deceleration compared to systolic flow. In our study, the spatial heterogeneity of contractility and microvascular function following infarction is reflected in the differences between IRA and remote vessel wave energies (Figure 40). BEW magnitude was significantly reduced, by 26%, in the infarct region compared to the non-infarct zone (Table 7). Furthermore, the IRA BEW magnitude was predictive of regional LV recovery, whereas the REF BEW, remote from the infarct zone, was not related to the likelihood of recovery.

Systolic Wave Energies - Backward and Forward Compression Waves

The forward compression wave energy occurs at the onset of systole, and is an accelerating energy driven from the aortic-end of the circulation, primarily resulting from the pressure transmitted by ventricular contraction. Sun et al,[84] examined this association, in an animal

model, using WIA to measure the effect of pacing-induced pacing-induced perturbations in LV function to show increasing LV contraction increased the ventricular driving force, coronary pressure and subsequently the magnitude of FCW. We have demonstrated for the first time in patients, that alterations of LV ejection directly relate to the resultant FCW energy, with those having a low LVEF having a reduced FCW energy. Furthermore, the weaker association of FCW with infarct size compared to BEW or BCW may reflect the fact that its primary determinant, LVEF, is a global measure of systolic function, which is affected by diminished contractility in the infarct zone as well as compensatory hypercontractility in the remote zones.

The backward travelling, microcirculatory compression wave (BCW) is the other significant wave in systole. It is decelerating in nature and arises from the compressive force on the microcirculation during systole, with the net difference between FCW and BCW determining flow during systole. The linear relationship observed with LVEF confirms that BCW is governed by the extrinsic compression exerted by the myocardium on the microvasculature. As BCW represents regional systolic contractility, it is also a predictor of infarct size, though to a lesser extent than the diastolic BEW. The relative amplitudes of FCW and BCW thus reflect the opposing effects of LV contraction on coronary perfusion pressure and compression of the microcirculation during systole.

3.1.7 LIMITATIONS

This was a small, single centre study but is the first in human study to examine the relationship and effects of recent myocardial infarction on coronary wave intensity. Despite being a cross-sectional study, patients with prior MI, and those with CMR signs suggestive of non-ischemic myocardial disease or valvular heart disease were excluded, to minimise confounders. Furthermore, we have used a sum-of-squares method to derive coronary wave speed, which in turn was used to separate wave energies.[158] This technique has been validated in subjects with normal coronary arteries and its applicability in the setting of ACS and obstructive epicardial disease is unknown.

Additionally, whilst the data presented here were obtained at a center with considerable interventional experience in intra-coronary hemodynamic assessment techniques with specific relevance to utilization of the dual-sensor pressure-flow wire, we believe this technology remains a reproducible method of invasively interrogating the coronary circulation, which could be adopted more widely in the interventional community.

Finally, the eventual infarct size in this NSTEMI population was relatively modest. However, the utility of BEW at predicting viability is expected to be even better with larger infarctions but this requires prospective validation.

3.1.8 FUTURE WORK

In the present study we assessed the utility of wave intensity analysis provides a unique insight into the coupling of vascular and myocardial function in the presence of acute regional left ventricular dysfunction. Whilst major advances have been made in the treatment of acute myocardial infarction, with improved adjuvant pharmacotherapy and stent technology evolving and markedly improving the morbidity and mortality following

myocardial infarction, methods of improving acute microcirculatory dysfunction are lacking. In conjunction with any potential therapy, is the necessity for a robust and sensitive method of assessing the efficacy of potential treatments on the microvascular function. Whilst mean pressure and flow indices, such as IMR and HMR, are currently adopted to interrogate the microcirculation, the microcirculatory (backward) expansion wave (BEW) may provide a more complete marker of regional myocardial function coupled with microvascular haemodynamics. The efficacy of future pharmacological agents, particularly those with intra-coronary preparations, could be assessed using this surrogate of microvascular function.

3.1.9 CONCLUSION

Microcirculatory expansion wave energy is a new index that, in this homogenous acute coronary syndrome cohort, has been shown to specifically and quantitatively assess the magnitude and location of infarction and may allow the prediction of late myocardial recovery following ACS. Coronary wave intensity analysis may provide an accurate adjunctive method of assessing myocardial viability during cardiac catheterization, following ACS.

3.2 CORONARY AND MICROVASCULAR PHYSIOLOGY DURING INTRA-AORTIC BALLOON COUNTERPULSATION

Kalpa De Silva[1], Matthew Lumley[1], Antoine Guilcher[2], Sven Plein[3,4], Michael Marber[1], Simon Redwood[1], Divaka Perera[1]

Affiliations:

[1]King's College London BHF Centre of Excellence, NIHR Biomedical Research Centre at Guy's and St. Thomas' NHS Foundation Trust, Cardiovascular Division, The Rayne Institute, London, UK

[2]Department of Clinical Pharmacology, St. Thomas' NHS Foundation Trust, London, UK

[3]Department of Biomedical Engineering, Division of Imaging Sciences and Biomedical Engineering, King's College London BHF Centre of Excellence, NIHR Biomedical Research Centre and Welcome Trust and EPSRC Medical Engineering Centre at Guy's and St. Thomas' NHS Foundation Trust, The Rayne Institute, London, UK

[4]Multidisciplinary Cardiovascular Research Centre, Leeds Institute of Genetics, Health and Therapeutics University of Leeds, Leeds, UK.

3.2.1 ABSTRACT

BACKGROUND

IABP is the most commonly utilized circulatory support device, although its efficacy in certain scenarios has been questioned. The impact of alterations in microvascular function on intra-aortic balloon pump (IABP) efficacy has not previously been evaluated in humans. The objective of this study was to identify the effect of coronary autoregulation on myocardial perfusion during IABP therapy.

METHODS

Thirteen patients with ischemic cardiomyopathy (LVEF 34±8%) undergoing PCI were recruited. Simultaneous intracoronary (IC) pressure (P) and Doppler-flow (U) measurements were undertaken in the target vessel following PCI, during unassisted and IABP assisted conditions. Coronary autoregulation was modulated by the use of IC adenosine, inducing maximal hyperaemia. Wave intensity analysis characterized the coronary wave energies associated with balloon counterpulsation.

RESULTS

IABP device inflation and deflation were temporally associated with two novel diastolic coronary waves travelling from the aorta; an acceleratory forward compression wave (IABP-FCW) caused by IABP inflation and a deceleratory forward expansion wave (IABP-FEW) associated with device deflation. During basal conditions, despite an increase in mean distal coronary pressure (82.4±16.1 vs. 88.7±17.8 mmHg, p=0.03), there was no change in average peak velocity (APV) or the velocity time integral (VTI) with IABP therapy (30.6±12.0 vs.

26.6±11.3 cm s^{-1}, p=0.59 and 28.3±10.0 vs. 22.8±7.5 cm, p=0.51, respectively). Basal microvascular resistance (bMR) increased with IABP therapy (2.32±0.52 vs. 3.27±0.41 mmHg cm^{-1} s, p=0.001). In contrast, when autoregulation was disabled by maximal hyperaemia, IABP therapy led to an increase in average peak velocity (APV) (39.4±10.5 vs. 44.7±17.5 cm s^{-1}, p=0.002) and velocity time integral (VTI) (25.8±15.1 vs. 32.4±15.7 cm, p=0.009), which was linearly related with the wave energy of IABP-FCW (R^2=0.71, p=0.01).

CONCLUSION

Autoregulation ameliorates the effect of IABP on coronary flow. However during hyperaemia IABP augments myocardial perfusion, principally due to a diastolic forward compression wave caused by balloon inflation, suggesting IABP would be of greatest benefit when microcirculatory reserve is exhausted.

Key words

Wave intensity analysis; intra-aortic balloon pump; microvascular function; left ventricular dysfunction.

3.2.2 INTRODUCTION

In excess of one-third of all coronary revascularization procedures occur in the context of underlying impaired left ventricular function, with an associated increase in morbidity and mortality.[167-169] The intra-aortic balloon pump (IABP) is commonly utilized during percutaneous coronary intervention (PCI) with the aim of increasing coronary blood flow through augmentation of the diastolic aorto-coronary pressure gradient. Additionally, IABP therapy decreases myocardial oxygen demand, by reducing the end-diastolic pressure, and, therefore, the after-load, making it an attractive means of ameliorating ischemia and consequently enhancing cardiac output. However, recent randomized control data, in clinical scenarios where IABP therapy is commonly employed, have shown limited efficacy with routine placement of the device.[170-172] The physiological basis for this lack of benefit remains unclear, but may relate to the interaction of the device with the innate hemostatic coronary auto-regulatory mechanisms that govern myocardial perfusion, particularly in regard to the vasomotor control at the level of the microcirculatory resistance vessels. IABP therapy may only provide additional haemodynamic support when myocardial perfusion is outside the normal physiological range, when auto-regulation has been pathologically disabled, in conditions such as profound cardiogenic shock or persistent ischemia.

Regional and global left ventricular perfusion and function are closely related to the microvascular integrity of the relevant myocardial territories, with microvascular dysfunction leading to left ventricular impairment and vice versa. The advent of pressure and Doppler sensor-tipped guide-wire technology has allowed detailed in vivo interrogation of

microcirculatory physiology. [60, 153] Wave intensity analysis (WIA) of phasic coronary pressure and flow profiles has allowed further characterization of the microcirculation and its impact on coronary flow in a number of stable and acute clinical settings.[79, 154, 173] These studies demonstrate that mechanical impedance of the coronary microcirculation by the myocardium is the predominant factor that governs myocardial perfusion, with a backward travelling (microcirculatory) expansion wave (BEW), and a forward travelling (aortic) compression wave (FCW) identified as being the most influential in generating diastolic coronary flow.[75, 155, 156] Wave intensity analysis has not previously been used in humans to assess the effect of IABP counter-pulsation therapy on the energy transfer within the coronary circulation.

3.2.3 AIMS

The aim of this study was to characterise the effects of IABP therapy on the coronary circulation by simultaneously assessing coronary flow, microvascular resistance and wave energy. Using these indices, we assessed whether microcirculatory auto-regulation modulates the effects of IABP therapy in patients with chronic ischemic cardiomyoapthy undergoing PCI.

3.2.4 STUDY DESIGN

3.2.4.1 Inclusion Criteria

Patients scheduled to undergo high-risk single-vessel or multi-vessel PCI were considered for inclusion into the study. High-risk was defined as the presence of impaired left ventricular function (ejection fraction <40% on cardiac magnetic resonance imaging (MRI), echocardiography or left ventricular angiography) and a large amount of myocardium

subtended by stenosed vessels, characterized by the British Cardiovascular Intervention Society Jeopardy score (BCIS JS) of 6 or greater. The BCIS Jeopardy score has been described previously, [174] but in brief, it is a modification of the Duke Jeopardy Score,[175] which allows broader classification of coronary anatomy, including left main coronary artery stenoses and bypass grafts (the total score ranges from 0-12).

3.2.4.2 Exclusion criteria

Exclusion criteria were a prior diagnosis of significant aortic valvular disease, non-ischemic cardiomyopathy, severe peripheral artery disease precluding insertion of the IABP catheter, an acute coronary syndrome within the preceding 48 hours or cardiogenic shock.

3.2.4.3 Ethical Approval

The study protocol was approved by the UK NHS research ethics committee (Ref: 11/H0804/10). All participants were provided with an information sheet detailing the study protocol prior to obtaining informed verbal and written consent.

3.2.4.4 Cardiac catheterization, IABP and intra-coronary measurement protocol

All patients where preloaded with aspirin (300mg) and clopidogrel (600mg). Coronary angiography was performed using a standard Judkins technique via a femoral artery approach. A 40cc IABP catheter (Maquet Cardiovascular, Germany) was inserted via the contra-lateral femoral artery and deployed in the descending aorta distal to the left subclavian artery origin at the start of the procedure and counterpulsation was commenced at 1:1 augmentation ratio. Intracoronary nitroglycerin was administered before diagnostic

angiography and intracoronary physiological measurements, to ensure maximal epicardial arterial vasodilatation. Haemodynamic measurements were obtained in the target vessel (TV) immediately following PCI. Aortic pressure (P_a) was measured via the coronary guiding catheter. Intracoronary pressure (P_d) and average peak velocity (APV) were measured via a 0.014-inch dual pressure and Doppler sensor-tipped guidewire (ComboWire® Volcano Corp, CA, USA), the tip being positioned in the distal vessel. Simultaneous pressure and Doppler measurements were repeated at least 3 times for each condition to reduce acquisition error, ensuring the resumption of steady state between measurements, defined as a return of APV to the baseline value.

First, basal measurements were obtained (with autoregulation "switched on") during 1:1 IABP-augmentation. Then, measurements were obtained after transiently disabling autoregulation, with 1:1 IABP-augmentation. Autoregulation was disabled by inducing maximal hyperaemia via sequentially increasing doses of intracoronary Adenosine, with the maximum tolerable dose dictated by the onset of atrio-ventricular conduction block or systemic symptoms (up to 60mcg were administered in the Right and up to 96mcg in the Left Coronary Arteries respectively). Basal and hyperaemic measurements were then repeated in unassisted conditions, after placing the IABP on 'stand-by' mode, and allowing at least four minutes for return of basal steady state conditions.

3.2.4.5 Data Analysis

Haemodynamic data analysis

Phasic pressure and flow analysis

Data were sampled at 200 Hz and analyzed off-line, using a customized programme developed on Matlab (Mathworks, Inc, Natick, Mass). A Savitzky-Golay convolution method[78] was adopted, using a polynomial filter to refine the derivates of the P_a and APV signals. Three to six consecutive cardiac cycles were selected for resting and hyperaemic conditions, gated on the ECG R wave-peak, with ensemble averaging of P_a, P_d, APV, and HR. For the purposes of wave intensity analysis it has been considered that diastole commences with the onset of ventricular relaxation, signified by the dichrotic notch on the arterial pressure waveform, as previously described.[156] Net coronary wave intensity (δI) was calculated from the time-derivatives (δt) of ensemble-averaged coronary pressure and flow velocity (U) as $\delta I = \delta P_d/\delta t \times \delta U/\delta t$.[76, 79] Coincident (microcirculation-derived) backward and (aorta-derived) forward propagating waves were separated assuming blood density to be 1050 (kg/m^3) and estimating coronary wave speed using the sum of squares method.[76, 158] The peak energies (in $W\ m^{-2}\ s^{-2} \times 10^5$) carried by the three most prominent wave energies identified were analysed. These were the positive, forward (aorta-derived) compression wave (FCW), occurring at the onset of systole; the concurrently occurring negative backward (microcirculation-derived) compression wave (BCW) and the backward expansion waves (BEW), the first negative wave occurring at the onset of ventricular relaxation, identified by the onset of diastole. Additionally, the waveforms that were associated with inflation and deflation of the IABP balloon in diastole were also analyzed. Total wave energy (area under the curve) was also determined, to identify the relative changes occurring during unassisted

and IABP-assisted conditions. The investigators who performed the data analyses were blinded to all clinical patient data.

Pulse wave and Mean-per-beat pressure-flow analysis

Pulse wave analysis was performed using custom-made programmes (Matlab, MathWorksInc, Natick, ME) in both unassisted and assisted aortic arterial waveforms. The area under the systolic phase of the pressure tracing (tension time index, TTI), and diastolic phase, (diastolic time index, DTI), were determined using the dichrotic notch (Figure 49). TTI relates to myocardial oxygen demand and DTI to coronary perfusion.[176] The Buckberg index (BI) was also calculated, providing a ratio of myocardial oxygen demand and supply, which is the quotient of diastolic to systolic pressure-time integral, representing afterload (TTI) and potential subendocardial blood supply (DTI) respectively.[176] To assess the affect of the IABP-device on the timing of the cardiac cycle, diastolic time fraction (DTF) was calculated. This represents the ratio of time in diastole to duration of a complete heart cycle.

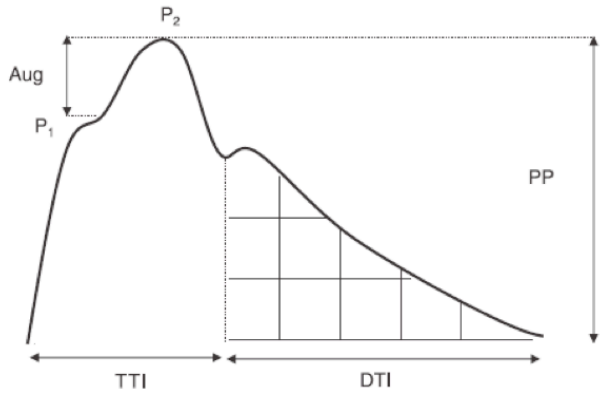

Figure 49: *Arterial Pressure Waveform – Pulse Wave parameters; Two systolic peaks are labelled P1 and P2. The area under the curve (AUC) during systole is the tension time index (TTI), and AUC during diastole is diastolic time index (DTI).*

Velocity time integral was calculated as follows;

$$VTI = \sum_{t-start}^{t-end} v_t \times \delta t$$

where t represents time during the cardiac cycle from t_{-start} to t_{-end}, v_t is the instantaneous flow velocity at time t, and δt represents the interval between successive measurements.

Hyperaemic and non-hyperaemic (basal) microvascular resistance (hMR and bMR respectively) were calculated as the ratio of mean P_d to APV (mmHg cm^{-1} s) during maximal hyperaemia or basal conditions respectively, obtained through simultaneous intra-coronary pressure-flow measurements, during 3-6 consecutive cardiac cycles.[55, 60]

3.2.4.6 Statistical Analysis

Statistical analysis was performed using IBM SPSS version 20. D'Agostino and Pearson omnibus normality test was performed to ensure a non-skewed distribution. Two-way analysis of variance (ANOVA) without replication was performed for each measured variable when comparing to at least two different (nominal) conditions. Correlation analysis was used to quantify the relationship between variables. A two-tail test for significance was performed in all analyses; $p \leq 0.05$ was considered statistically significant. Data are represented as mean ± standard deviation, unless otherwise stipulated.

3.2.5 RESULTS

Baseline Characteristics

Thirteen patients with ischemic cardiomyopathy were recruited, 11 (aged 67±11) with an LVEF 34±8% completed the study protocol. Two patients became haemodynamically compromised during the procedure and did not complete the study protocol and were therefore excluded from the final analysis. 82% (n=9) were hypertensive, 91% (n=10) were hypercholesterolemic and all had prior myocardial infarction. The high-risk nature of this cohort was typified by the elevated logistic EuroScore (11±5%) and significant degree of coronary artery disease burden, with a mean BCIS JS of 9±2. Patient characteristics are outlined in Table 8.

Variable	n
Age, Mean (±SD)	67 (11)
Medical History	
Male, n (%)	8 (73)
Hypertension, n (%)	9 (92)
Diabetes mellitus, n (%)	7 (64)
Hypercholesterolemia, n (%)	10 (92)
Smokers, n (%)	6 (54)
BMI[*] (kg/m^2), Mean (±SD)	27 (4)
Prior MI[†], n (%)	11 (100)
Previous PCI[‡], n (%)	5 (45)
Peripheral Vascular Disease, n (%)	4 (36)
Left Ventricular Ejection Fraction, Mean % (±SD)	34 (8)
Logistic EuroScore, Mean % (±SD)	11 (5)
Coronary Artery Disease	
One-vessel, n (%)	0 (0)
Two-vessel, n (%)	8 (73)
Three-vessel, n (%)	3(27)
Left Main Stem, n (%)	4 (36)
Left anterior descending, n%)	7 (64)
Circumflex, n (%)	4 (36)
Right coronary artery, n (%)	5 (45)
BCIS-Jeopardy Score, Mean (±SD)	9 (2)

[*] Body Mass Index
[†] Myocardial Infarction
[‡] Percutaenous coronary intervention

Table 8: *Patient Characteristics*

Effects of Hyperaemia on Unassisted Coronary Haemodynamics

Heart rate, aortic and distal coronary pressure remained unchanged during intra-coronary adenosine induced hyperaemia (p=0.41, p=0.93 and p=0.26 respectively). There was a reduction in microvascular resistance (MR), (R^2=0.61, p=0.003) with a corresponding increase in coronary flow (APV) (R^2=0.62, p=0.01). Furthermore, there was an increase in the microcirculatory (backward) travelling expansion wave (BEW) (R^2=0.57, p=0.02). Table 9 provides a summary of the haemodynamic observations.

	Basal ('Switched on' autoregulation)			Hyperaemic ('Switched off' autoregulation)		
	Unassisted	IABP-assisted	*p value*	Unassisted	IABP-assisted	*p value*
Mean-per-beat derivatives						
HR (bpm)[*]	66.3±14.1	66.4±12.3	*0.87*	69.2±14.2	69.1±12.6	*0.85*
P_a (mmHg)[†]	92.6±17.4	95.4±20.4	*0.03*	93.4±16.4	92.1±15.4	*0.01*
P_d (mmHg)[‡]	82.4±16.1	88.7±17.8	*0.04*	82.4±16.1	89.7±14.4	*0.02*
APV (cm s^{-1})[§]	32.3±11.1	26.6±11.3	*0.08*	39.4±10.5[+]	44.7±17.5[^]	*0.002*
MR (mmHg cm^{-1} s)[||]	2.32±0.52	3.27±0.41	*0.001*	2.21±0.42[+]	2.25±0.78[^]	*0.45*
Pulse Wave Analysis						
VTI (cm)[#]	26.8±12.3	22.8±7.5	*0.51*	25.8±15.1	32.4±15.7	*0.009*
DTF[**]	0.65±0.07	0.64±0.08	*0.87*	0.60±0.09	0.61±0.09	*0.33*
DTI[††]	43.9±11.9	54.2±13.4	*0.007*	39.5±13.0	46.5±14.5	*0.01*
TTI[‡‡]	30.1±15.2	27.8±6.8	*0.08*	31.4±11.6	27.9±8.7	*0.11*
BI[§§]	1.70±0.68	2.08±0.57	*0.03*	1.31±0.37	1.91±0.56	*0.01*
Wave Intensity Analysis (W m^{-2} s^{-2} x 10^5)						
Systolic Wave Energies						
FCW[||||]	+1.70±0.40	+1.82±0.51	*0.27*	+1.75±0.46	+1.78±0.55	*0.34*
BCW[##]	-0.32±0.20	-0.55±0.31	*0.06*	-0.48±0.25	-0.36±0.18	*0.17*
Diastolic Wave Energies						
BEW[***]	-2.21±0.64	-1.62±0.67	*0.004*	-2.43±0.63[+]	-1.98±0.76[^]	*0.07*
IABP-FCW[†††]	n/a	+1.82±0.90	*n/a*	n/a	+1.86±0.67	*n/a*
IABP-FEW[‡‡‡]	n/a	+0.95±0.81	*n/a*	n/a	+0.91±0.76	*n/a*

HR (bpm)[*] - Heart rate
P_a (mmHg)[†] - Mean aortic pressure
P_d (mmHg)[‡] - Mean distal coronary pressure
APV (cm s^{-1})[§] - Average peak velocity
MR (mmHg cm^{-1} s)[||] - Microvascular resistance
VTI (cm)[#] - Velocity time integral

DTF[**] - Diastolic time fraction

DTI[††] - Diastolic time integral

TTI[‡‡]- Tension time index
BI[§§] - Buckberg index
FCW[||||] - Forward travelling compression wave
BCW[##] - Backward travelling compression wave
BEW[***] - Backward travelling expansion wave
IABP-FCW[†††] - Intra-aortic balloon pump associated forward travelling compression wave
IABP-FEW[‡‡‡] - Intra-aortic balloon pump associated forward travelling expansion wave

'+' Denotes statistically significant changes in parameters observed during unassisted basal vs. hyperaemic conditions (APV p=0.01, MR p=0.003, BEW p=0.02).'^' Denotes statistically significant changes in parameters observed during IABP-assisted basal vs. hyperaemic conditions (APV p=0.005, MR p=0.0001, BEW p=0.03).

Table 9: *Coronary Mean and Phasic Haemodynamic data*

IABP Effects with 'Switched on' Autoregulation

Systemic and Pulse wave parameters

During basal conditions heart rate remained unchanged following the introduction of IABP device (66.3±14.1 vs. 66.4±12.3 bpm, p=0.87). Mean aortic pressure (P_a) altered significantly with balloon-pump assistance (92.2±16.4 vs. 95.4±20.4 mmHg, p=0.03). A non-significant trend in reduction of TTI was observed (30.1±15.2 vs. 27.8±13.9, p=0.08) with balloon augmentation. While the device did not alter the duration of diastole, with DTF remaining unchanged (0.65±0.07 vs. 0.64±0.08 secs, p=0.87), diastolic pressure-time index, DTI, increased in conjunction with diastolic augmentation of mean aortic pressure with counterpulsation therapy (43.9±11.9 vs. 54.2±13.4, p=0.007). The ratio of myocardial oxygen supply (DTI) to demand (TTI), the Buckberg index (BI), increased (1.70±0.68 vs. 2.08±0.57, p=0.03)

Mean coronary indices

Whilst balloon pump augmentation led to an increase in distal coronary pressure (82.4±16.1 vs. 88.7±17.8 mmHg, p=0.04), there was no corresponding change in mean flow velocity (APV) (32.3±11.1 vs. 26.6±11.3 cm s^{-1}, p=0.08) in the presence of a functioning autoregulation. Similarly VTI remained unchanged during basal IABP-assisted conditions (26.8±12.3 vs. 22.8±7.5 cm, p=0.51). Microvascular resistance during basal conditions (bMR) was observed to increase significantly during counterpulsation therapy (2.32±0.5 vs. 3.27±0.41 mmHg cm^{-1} s, p= 0.001).

Coronary Wave Intensity Analysis

The three previously described wave energies (FCW, BCW and BEW) were identified in all patients. Additionally coronary wave intensity analysis of the circulation during IABP counter-pulsation showed two additional wave energies (Figure 50) relating to the inflation and deflation of the balloon. Inflation resulted in an aortic-originating (forward travelling) accelerating compression wave (IABP-FCW), with the subsequent deflation of the balloon causing an aortic-originating (forward travelling) decelerating expansion wave (IABP-FEW). Furthermore, during balloon-pump assistance peak BEW was reduced compared to unassisted conditions (-2.21±0.64 vs. -1.62±0.67 W $m^{-2}s^{-2}x10^{5}$, p=0.004). During unassisted conditions, the relative acceleratory energies provided by FCW and BEW were 39% and 61% respectively, whilst during IABP-assistance, FCW was 36%, BEW reduced to 30%, with the IABP-FCW accounting for 34% of total wave energy.

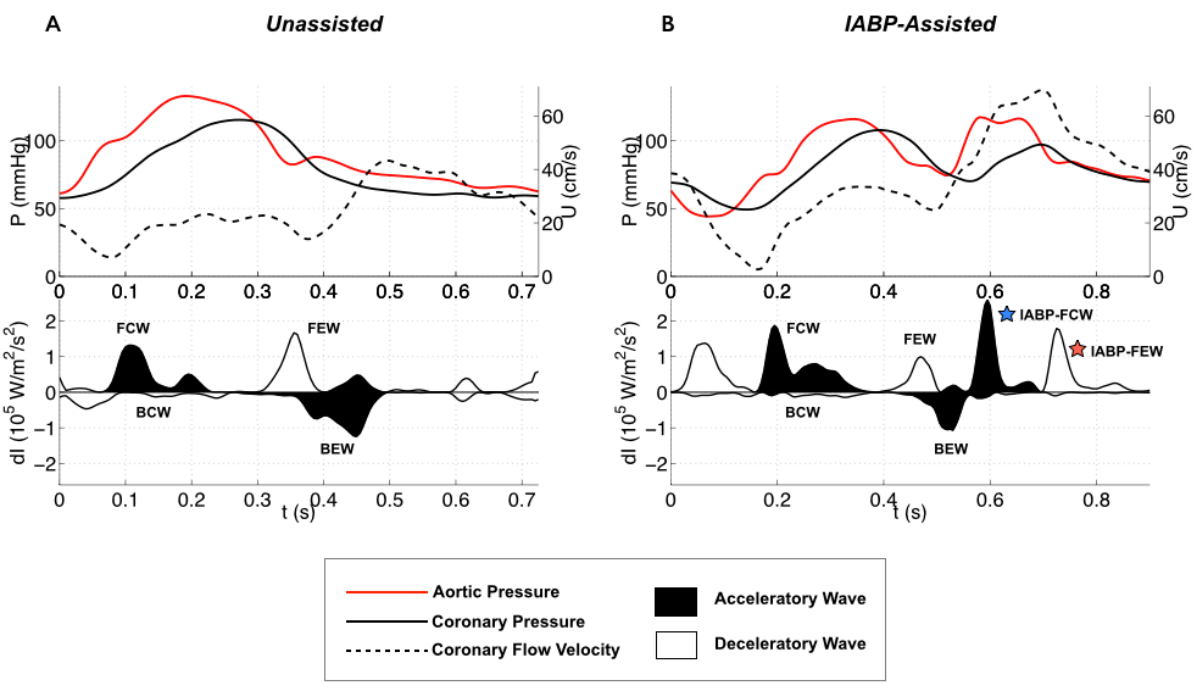

Figure 50: *IABP Wave Intensity Profile: A – WIA profile during unassisted conditions demonstrating the four wave energies previously described. B – WIA profile during IABP-assisted conditions, highlighting the temporally related wave energies with device inflation (IABP-FCW) and deflation (IABP-FEW).*

IABP Effects with 'Switched off' Autoregulation

Systemic and Pulse wave parameters

Balloon counter-pulsation during intra-coronary adenosine induced hyperaemia did not alter the heart rate (69.2±14.2 vs. 69.1±12.6 bpm, p=0.85), DTF (0.60 ±0.09 vs. 0.61±0.09 sec, p=0.33) or mean Pa (93.4±16.4 vs. 92.1±15.4 mmHg, p=0.57) compared to unassisted conditions. TTI was reduced (although this was not statistically significant; 31.4±11.6 vs. 27.9±8.7, p=0.11) and there was an increase in DTI (39.5±13.0 vs. 46.5±14.5, p=0.01), with a corresponding increase in BI (1.31±0.37 vs. 1.91±0.56, p=0.01), mirroring observations during basal conditions.

Mean coronary indices

Similar to basal conditions, balloon-pump assistance in the hyperaemic setting was accompanied by an increase distal coronary pressure (82.4±16.1 vs. 89.7±14.4 mmHg, p=0.02). However in contrast to the basal state, there was an increase in APV (39.4±10.5 vs. 44.7±17.5 cm s^{-1}, p=0.002). Furthermore, VTI was observed to increase during balloon assistance (25.8±15.1 vs. 32.4±15.7, p=0.009) (Figure 51). Hyperaemic microvascular resistance was unchanged in unassisted and assisted conditions, 2.21±0.42 vs. 2.25±0.78 mmHg cm^{-1} s, p=0.45 (Figure 52).

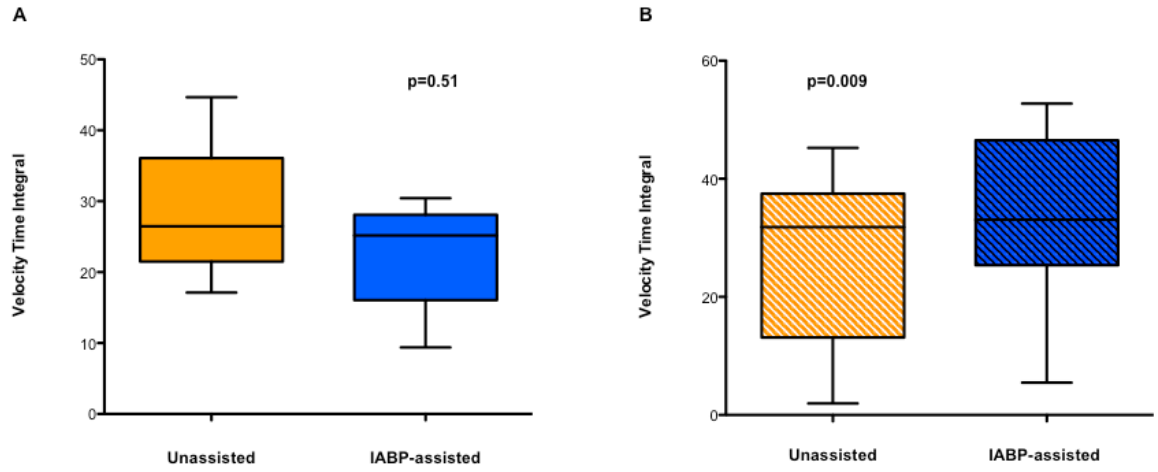

Figure 51: *Veloticty Time Integral during unassisted and IABP-assisted conditions; A – during basal conditions; B – during hyperemic conditions*

Coronary Wave Intensity Analysis

Augmentation of coronary flow with balloon counterpulsation ($\Delta APV = APV_{IABP} - APV_{unassisted}$) related proportionately with the IABP-FCW wave energy ($p=0.001$, $R^2=0.71$) (Figure 53) with maximal hyperaemia; there was no relationship between these parameters in basal conditions. IABP-FEW also related with augmentation of APV ($p=0.003$, $R^2=0.60$). Mulitple linear multiple regression, confirmed that augmentation in APV was primarily as a result of IABP-FCW, $p=0.01$ rather than IABP-FEW, $p=0.14$, with $\Delta APV = 2.2 \times 10^{-5}(FEW) + 5.7 \times 10^{-5}(FCW) + 6.13$. The dominant microcirculatory wave, BEW, remained tended to decrease during hyperaemic balloon-pump assistance (2.43 ± 0.63 vs. 1.98 ± 0.76 W m^{-2} s^{-2} x 10^5, $p=0.07$) compared to unassisted conditions.

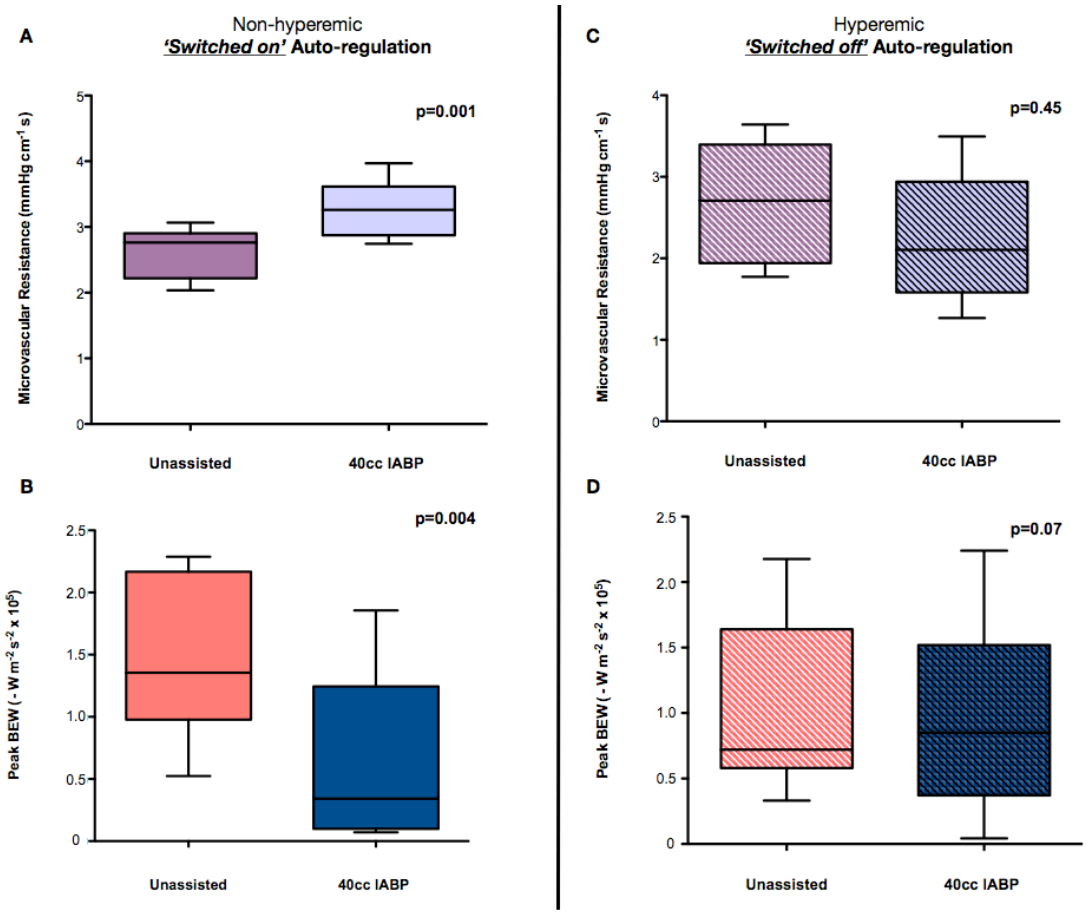

Figure 52: *Relationship of Microvascular Resistance (MR) with Microcirculatory (backward) expansion wave (BEW): A & B: MR and BEW during basal conditions. C & D: MR and BEW in hyperaemia*

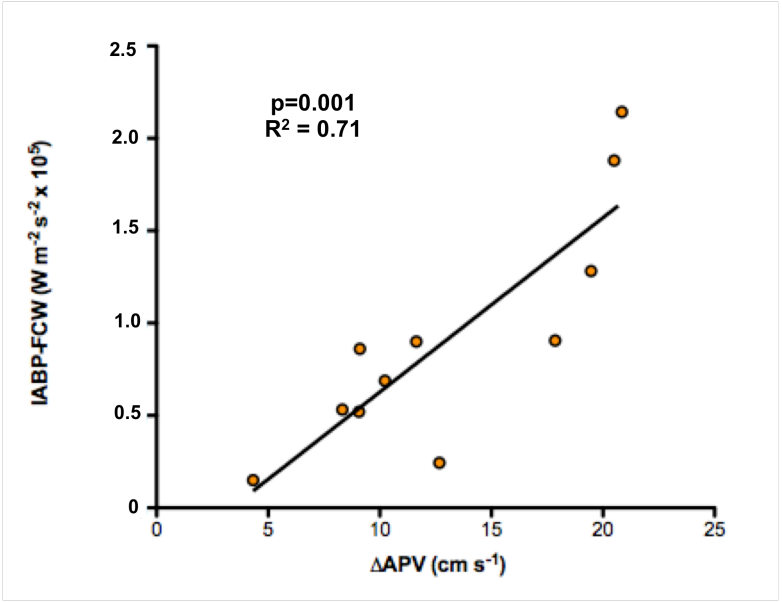

Figure 53: *IABP-FCW relationship with hyperaemic coronary flow velocity; During hyperaemia, with autoregulation disabled, IABP device inflation is associated with an acceleratory wave energy (IABP-FCW) which is linearly related to coronary flow (APV).*

3.2.6 DISCUSSION

We have comprehensively characterized the effects of intra-aortic balloon counterpulsation on coronary and microvascular haemodynamics, including the first clinical application of coronary wave intensity analysis in this setting. Using these techniques, we have shown that the effects of IABP therapy are intimately linked to innate microvascular function and that the processes of autoregulation may ameliorate the potential benefits of this therapy. However, when autoregulation is disabled, IABP therapy was seen to augment myocardial perfusion. These findings help to explain the results of recent randomized control trials of balloon counterpulsation and also indicate the potential utility of this therapy in clinical scenarios accompanied by exhausted microcirculatory reserve.

Coronary Autoregulation and IABP

Coronary blood flow is tightly controlled and matched to the oxygen demands of the heart by adapting the calibre of the coronary resistance arteries, via inter-related processes involving mechanisms intrinsic to the vascular wall, as well as metabolic and neurohumoral factors.[177, 178] The two major determinants of coronary flow are coronary arterial pressure and myocardial oxygen consumption. Coronary autoregulation is the mechanism that maintains coronary flow independent of arterial pressure for a given level of oxygen consumption or changing oxygen requirements at a constant perfusion pressure.[179] In the presence of an epicardial coronary stenosis there is intra-mural microcirculatory vasodilatation, reduction in resistance, accommodating for the reduction in pressure distal to the stenosis.[115] Ischemia ensues as a result of the inability of this vasodilatory response

to match the oxygen requirements, because the threshold of maximal mirocirculatory vasodilatation has been exceeded, and resistance cannot be reduced any further. Therefore in the presence of persistent ischemia, the autoregulatory mechanisms are completely exhausted, so that myocardial flow becomes proportional to perfusion pressure. This condition of minimal resistance is mimicked by pharmacological administration of adenosine, which causes maximal vasodilatation and reduction in resistance (MR), switching 'off' the normal autoregulatory pathways. During this state, we have demonstrated that IABP therapy leads to an increase in distal coronary pressure, which proportionately increases coronary flow. However, when autoregulation is intact, the counterpulsation-related increase in P_d is accompanied by an increase in microvascular resistance, as a consequence of which coronary flow remains unchanged.

Clinical data on IABP efficacy and the impact of autoregulation

The efficacy of IABP therapy has come in to question in recent years in light of several randomized control trials that have failed to demonstrate the efficacy of routine IABP placement in different clinical settings. The first of these was BCIS-1,[170] a trial of elective IABP use in patients who were haemodynamically stable at the outset, but were at increased risk of major complications during PCI. Routine placement of IABP did not alter the incidence of major adverse cardiovascular and cerebrovascular events (MACCE), compared to those randomised to have unassisted PCI. Given that most patients enrolled in BCIS-1 are likely to have had perfusion pressures within the autoregulatory range and that patients with active ischemia and shock were excluded, the findings of the current study may explain why a strategy of routine IABP placement in unselected patients failed to show benefit. On the

other hand, one in eight patients who were randomized to receive unsupported PCI suffered haemodynamic compromise sufficient to warrant rescue IABP insertion. There is a signal that those requiring 'bail-out' may be patients at the extreme end of the spectrum of diminished physiological reserve, severity of coronary artery disease and therefore microvascular dysfunction. The CRISP AMI trial,[180] assessed the role of routine use of IABP in patients presenting with large anterior STEMI's within 6 hours of symptom onset without cardiogenic shock . Pre-procedure IABP insertion failed to reduce infarct size in this study. Although this result appears to be at odds with the physiological observations seen in the current study, this lack of effect may have been due to the relatively brief period of counterpulsation prior to mechanical reperfusion being achieved. From our observations, the sub-group who stand to gain most benefit from counterpulsation therapy may be those that had persisting ischemia despite reperfusion and analysis of this subset of patients in CRISP-AMI may be instructive.

The most recent of these RCT's was IABP-SHOCK II, which assessed the utility of IABP in acute myocardial infarction complicated by cardiogenic shock.[172] A strategy of elective IABP insertion failed to reduce 30-day mortality in this study. Although hypotension is central to the clinical diagnosis of cardiogenic shock, it is interesting to note that systolic blood pressure was in excess of 90mmHg in approximately 50% of all patients enrolled in IABP SHOCK II, falling within the normal range of coronary auto-regulation. Applying the observations of our current study, it could be postulated that the presence of a working auto-regulatory system may have limited the effect of IABP therapy in many patients of the IABP-SHOCK II cohort.

The effect of autoregulation on the efficacy of mechanical haemodynamic support may also be applicable to devices that aim to directly unload the left ventricular cavity. Remmelink et

al[181] previously observed, in a cohort of patients undergoing PCI with LV dysfunction with adjunctive Impella® device (Cardiotechnik, Aachen, Germany) support, that during basal conditions, increased distal coronary pressure did not lead to an augmentation of coronary flow, though a linear increase was evident during hyperaemic conditions. Analogous with the current study, an increase in basal microvascular resistance, due to the presence of a functioning microcirculatory auto-regulation, diminished the beneficial effect of the device.

Wave Intensity Analysis of IABP counter-pulsation

Kolyva et al[182, 183] previously demonstrated the effect of the IABP balloon on aortic haemodynamics during *in vivo* and *ex vivo* experiments, delineating the unique ability of WIA in assessing the haemodynamic effects of the device, highlighting the relationship of device inflation and deflation to wave propagation in the aorta. The current study represents the first application of WIA to pressure and flow measurements in the coronary circulation during counterpulsation in humans. We have demonstrated that IABP therapy is associated with a characteristic WIA morphology, with two unique diastolic waves observed, the first, a further forward compression wave, corresponds with inflation of the balloon, and the second with balloon deflation. These novel parameters allow comprehensive assessment of the effects of IABP therapy integrated with innate microvascular and contractile function and may prove to be useful in future counterpulsation research, aimed at distinguishing responders from non-responders and for assessing the relative efficacy of newer iterations of pulsatile assist devices.

Using these techniques, we have demonstrated that IABP-augmentation of aortic and distal coronary pressure does not necessarily translate to an improvement in coronary flow or perfusion of the heart, as previously thought. Instead, we have shown that the energy driving myocardial perfusion during counterpulsation is entirely different to the patterns in unassisted conditions, with the added beneficial energy of the IABP-FCW being offset by a decrease in the BEW (in turn due to an increase in microvascular resistance due to autoregulation) such that net coronary flow remains unchanged. In contrast, during hyperaemic conditions, when autoregulation is disabled, there is no diminution of the BEW during counterpulsation, such that the effect of the IABP-FCW and the BEW are summative, resulting in augmentation of coronary flow. In the presence of hyperaemia, the energy from the balloon inflation (IABP-FCW) related linearly to the increase in peak coronary flow velocity (ΔAPV). These observations may explain the lack of benefit seen when the IABP is employed prophylactically rather than in cases when auto-regulatory mechanisms have been rendered dysfunctional, such as in the presence of persistent ischemia or shock.

3.2.7 LIMITATIONS

This was a small, single centre study, but is the first in human study to describe the relationship and effects of the use of intra-aortic balloon counter-pulsation on coronary wave intensity and the effects of modulating coronary auto-regulation on the utility of IABP therapy. As a consequence of the small sample sizes and the use of unadjusted statistical tests adopted within the studies, there is potential for a type 1 error affecting the results. Therefore, further investigation is warranted to confirm these initial findings.

3.2.8 CONCLUSION

WIA can be used to characterize balloon-pump assisted coronary flow. Autoregulation ameliorates the effect of IABP on coronary flow by increasing microvascular resistance in response to increased distal coronary pressure. However, during hyperaemic conditions, IABP augments myocardial perfusion, principally due to a diastolic forward compression wave caused by balloon inflation. These findings suggest IABP will be of greatest benefit when regional microcirculatory reserve is exhausted despite the concomitant reduction in cardiac work.

3. CORONARY PHYSIOLOGY STUDIES

PART B:

REFINING WAVE INTENSITY ANALYSIS

3.3 IMPACT OF CORONARY WAVE SPEED ON WAVE INTENSITY ANALYSIS

Kalpa De Silva[1*], M. Cristina Rolandi[2*], Matt Lumley[1], Brian Clapp[1], Maria Siebes[2], Divaka Perera[1]

[*]I would like to acknowledge the work of Cristina Rolandi, who is joint first author on this body of work.

Affiliations:

[1] King's College London BHF Centre of Excellence, NIHR Biomedical Research Centre at Guy's and St. Thomas' NHS Foundation Trust, Cardiovascular Division, The Rayne Institute, London, UK

[2]Biomedical Engineering and Physics, Academic Medical Center, University of Amsterdam, Amsterdam, The Netherlands

3.3.1 ABSTRACT

INTRODUCTION

The technique of wave separation during wave intensity analysis (WIA) requires that wave speed is known. This is currently estimated using the single-point technique (*SPc*), a sum of squares mathematical model and has not previously been validated in the coronary circulation. This study is the first to directly measure coronary wave speed (D_C) in humans and compare it to the *SPc*.

METHODS

In 14 patients undergoing cardiac catheterization, intracoronary pressure was measured in an unobstructed epicardial coronary artery using a high-fidelity catheter equipped with two pressure sensors located Δs = 5 cm apart. Directly measured wave speed was calculated as D_c, where $D_c = \Delta s/\Delta t$, where Δt is the time delay between the two pressure signals. Intracoronary pressure (P) and flow velocity (U) were measured simultaneously with a dual-sensor guide wire to derive SP_c, where $SP_c = 1/\rho \cdot \sqrt{(\sum dP^2/\sum dU^2)}$, ρ = blood density. All signals were recorded at baseline and at hyperemia induced by intracoronary adenosine. Energies of the backward (BW) and forward (FW) separated waves of wave intensity were compared using *SPc*, *Dc* and baseline *SPc*.

RESULTS

SPc at baseline (16.8±1.5 m/s) did not significantly differ from *Dc* (15.9±1.8 m/s), p=0.44 . During hyperemia, *SPc* dropped by 40%, while *Dc* remained unchanged. The BEW energy assessed at hyperemia with *SPc* was 7% lower than when derived with *Dc* while the FCW and

BCW were respectively 17% and 30% higher. When using baseline *SPc* no differences in wave energies were observed.

CONCLUSION

While *SPc* appraises wave speed under resting conditions, it underestimates wave speed during hyperemia, leading to potential errors in calculation of individual wave energies. However, our results suggest that baseline *SPc* can be used for WIA during hyperemia, extending its validity to study coronary physiology.

Key Words

Coronary arteries, coronary artery haemodynamics, wave intensity analysis, pulse wave velocity.

3.3.2 INTRODUCTION

Parker and Jones'[76] seminal description of separating forward and backward waves within the aorta was based upon the method of characteristics solution of the one-dimensional conservation equations for flow in arteries. The ability to separate waves, when performing wave intensity analysis described in this initial work and in the wave intensity analysis performed in this thesis relies on the accurate estimation of wave speed. Wave speed is akin to arterial pulse wave velocity, which has been shown previously to be an important marker of vascular pathology associated with the risk of cardiovascular events,[184, 185] and has a linear relationship with vessel dispensability which is altered by factors which alter wall stiffness such as age, diabetes mellitus, vascular disease, distending pressure and vascular tone.[186-189]

The most robust method of measuring wave speed is the "foot-to-foot" method. This relies upon measurement of the time taken (δt) for a pressure wave to travel between two sites a known distance apart (δs). The pressure curves at the two positions may be acquired simultaneously with two separate pressure sensors, or, alternatively, with one sensor moved between two positions with subsequent gating to the R wave of the ECG. The time delay (δt) is measured between the arrival of an identifiable point on the pressure wave, such as the "foot" and wave speed (c), calculated as follows: $c = \delta s/\delta t$. By their nature, these measurements can only indicate the average wave speed over the distance between the measurement sites and, because the properties of arteries can vary significantly throughout the arterial tree, making this technique prone to error. Parker et al therefore demonstrated a method that could determine the local wave speed from the simultaneous measurement of pressure and velocity at the same site are preferable.

The mathematical theory underpinning this single point measure is summarized and outline below.

Changes in flow, U, result in a change in pressure, P, within a vessel. Propagated down stream (forward) with speed U + c, and upstream (backward) U – c, where c = the wave speed.

Wave speed in its basic terms a function of the density of blood and the distensibility of the vessel, where;

$$c = 1/\sqrt{\rho D} \quad (7)$$

where D, the distensibility of blood is;

$$D = (1/A).dA/dP \quad (8)$$

Where A is the cross-sectional area of the artery.

From the Newtonian law of conservation of mass and momentum, the 'water-hammer' equation encompasses the simple relationship between the changes in pressure and velocity across the wave fronts.

$$dP_{\pm} = \pm \rho c \, dU_{\pm} \quad (9)$$

where ρ is the density of blood and the +/- signs refers to forward or backward travelling waves respectively. As the forward and backward waves are additive ;

$$dP = dP_{+} + dP_{-} \quad (10)$$

$$dU = dU_{+} + dU_{-} \quad (11)$$

Calculation of the forward and backward incremental wave fronts from the measured ΔP and ΔU;

$$dU_{\pm} = \pm \tfrac{1}{2}(dP/\rho c \pm dU). \quad (12)$$

$$dP_{\pm} = \tfrac{1}{2}(dP \pm \rho c\, dU), \tag{13}$$

Wave speed has become a fundamental parameter in performing coronary wave intensity analysis (WIA).[190] Provided that wave speed is known, WIA allows the separation of individual upstream and downstream components of measured traveling waveforms. In the case of the coronary arteries, this has provided a valuable tool for studying the interaction between the myocardial function, epicardial circulation and intra-mural microcirculation.[191]

When considering forward and backward waves, the wave intensity dI = dP x dU. Waves are classified by the sign of the change in pressure that they produce, compression waves have dP >0 and expansion waves have dP<0. Extrapolation from the water-hammer equation (equation 9 above), forward compression causes acceleration, dU >0, whilst forward expansion leads to deceleration, dU<0. In contrary to this, backward compression waves cause deceleration and the expansion waves cause acceleration. However the wave intensity of all forward waves is positive and all backward waves is negative, where $dI = dI_+ + dI_-$, reflecting the net importance of the forward and backward components during each instant in the cardiac cycle.

As shown above the mathematical basis of wave intensity analysis lies in the estimation of wave speed. Subsequently Parker et al[76] and latterly Khir et al[192] demonstrated that during the onset of systole, there are no backward waves, with the water-hammer principle suggesting there should be a linear relationship between the change in pressure and the change in velocity, meaning a P-U loop plotted over a cardiac cycle will show the onset of systole having a linear relationship, with the slope equalling ρc, figure 54 below.

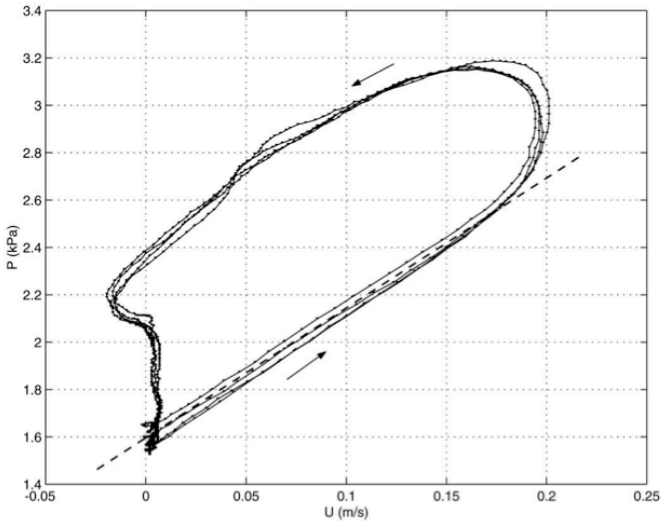

***Figure 54**: PU loop in a human main pulmonary artery – adapted from Parker et al.*[76]

In the coronary arteries hemodynamic interactions and wave reflections alter the linearity of the pressure-velocity relation meaning that this approach cannot be used. The wave speed information is still present but cannot be derived directly from the water hammer method described above. P-U loop requires a unidirectional wave period, derived from the slope of a linear portion of a P-U loop that, in the systemic arteries, occurs at the beginning of systole. In the coronary arteries this method is not applicable because such a period does not exist, as forward and backward waves are generated continuously during both contractile and relaxation phases of a cardiac cycle. Davies et al[158] described the single-point estimate of wave speed (SPc), deriving a formula for calculating wave speed not dependent on the linearity of the pressure- velocity relation yet remains compatible with the water hammer equation for linear pressure-velocity relations.

$$c = \frac{1}{\rho}\sqrt{\frac{\Sigma dP^2}{\Sigma dU^2}} \qquad (14)$$

This single-point technique uses simultaneously acquired pressure (P) and velocity data (U) from a single position within a vessel. It allows wave speed derivation in the coronary arteries not previously possible, as it does not require the vessel length to allow two separate measurements to be obtained nor does it rely on a period during which there is only a single wave impulse, which does not exist within the coronary circulation. The initial validation of this technique suggested a good correlation with the gold standard foot-to-foot method measurement, when compared within the aorta, with a correlation coefficient of 0.72 (P = 0.05), mean difference (single-point foot-to-foot) of 0.9 m/s, and standard deviation of the difference of 1.4 m/s.

Whilst *SPc* has been shown to provide an accurate assessment of wave speed within the aorta. Its applicability has been extrapolated to the coronary arteries during baseline conditions. However, to date, this has only been validated by indirect comparison with wave speed measured in the aorta. [193] Recent demonstration that intrinsic assumptions that underpin the *SPc* determined wave speed may not always applicable in the coronary arteries, especially downstream of a stenosis or at maximum hyperemia. [194] Kolyva et al demonstrated that the local wave speed calculated by the single point technique in a diseased coronary vessel decreased following percutaneous revascularization of a proximal stenosis. The previously held assumption was that wave speed increased following stent deployment and mechanical improvement of flow, as a consequence of restoration or increase in distending pressure. Similarly, at maximum vasodilatation of the microcirculatory resistance vessels, induced by adenosine administration, a decrease in local wave speed (as estimated by SPc) in

the conductance epicardial vessels was observed although the properties of these vessels would not have been expected to be altered.

Furthermore, direct measurements of wave speed in animal experiments have shown that whilst coronary wave speed is not affected by vasodilatation of the microcirculation induced by adenosine,[195, 196] it may be influenced by factors that affect wall stiffness, such as age, vascular disease, vascular tone and transmural pressure. [197-202] We hypothesize that, as measured in animals and contrary to what is predicted by *SPc*, coronary wave speed in humans is not affected by microcirculatory dilatation induced by adenosine.

3.3.3 AIMS

1. To assess wave speed in the human epicardial coronary vessels by direct measurement at rest and during adenosine induced maximal hyperemia.
2. To determine the effect on coronary wave speed with nitroglycerine induced vasodilatation of the epicardial vessels and the effect of decreasing transmural pressure produced by the use of a Valsalva maneuver

3.3.4 STUDY DESIGN

Patients were recruited and the studies were performed at St. Thomas' hospital. The data of high-fidelity dual pressure and flow tracings (Millar catheter) were performed at the Amsterdam Medical Centre. Wave intensity analysis was performed at both sites to assess consistency of the data acquired.

3.3.4.1 Inclusion Criteria

Patients, with stable angina symptoms, scheduled to undergo coronary angiography with a view to proceeding to percutaneous coronary intervention were screened for the study. Patients were recruited if there was at least one unobstructed (<30% diameter stenosis) coronary vessel.

3.3.4.2 Exclusion Criteria

Exclusion criteria were patients under the age of 18, the presence of an angiographic stenosis of greater than 50% diameter stenosis, recent myocardial infarction (<six weeks), significant valvular heart disease, a prior diagnosis of a non-ischaemic cardiomyopathy, or the presence of decompensated heart failure.

3.3.4.3 Ethical Approval

The study protocol was approved by the St. Thomas' hospital research ethics committee (Ref: 10/H0808/58). All participants were provided with an information sheet detailing the study protocol prior to obtaining informed verbal and written consent.

3.3.4.4 Cardiac catheterization and intra-coronary measurement protocol

All patients were preloaded with aspirin (300mg) and clopidogrel (600mg). Heparin was administrated at the beginning of the procedure (70 IU/kg). Coronary angiography was performed using a standard Judkins technique via a femoral artery approach. An 8 French guiding catheter was inserted via the femoral artery engaging the coronary ostium. A 5-in-6 "mother and child" system, HeartRail (Terumo, Japan), was inserted over an un-inflated monorail angioplasty balloon. The 2.5F high-fidelity dual-sensor pressure catheter (Mikro-

Cath™, Millar Instruments, Houston, Texas), which is not primarily designed for intracoronary use, was then advanced to the tip of the HeartRail catheter, which in turn was then withdrawn, to minimize the risk of coronary trauma during insertion of the Mikro-Cath, and positioned in an angiographically normal coronary vessel (Figure 55). Moreover, the only vessels that were felt to compliant enough to accommodate this intra-coronary equipment were included, meaning a straight segment of coronary vessel was needed for inclusion. The two simultaneous intra-coronary pressure waveforms (P1 and P2), obtained 5 cm apart from each other, were then continuously recorded. These pressure signals were amplified with the associated Millar equipment and digitally recorded at a sampling frequency of 5 kHz (MP150, Biopac Systems Inc., Goleta, CA). The signals were digitized at a sampling frequency of 5 kHz. Distal intracoronary pressure (Pd) and blood flow velocity (U) were measured via an additional 0.014-in dual-sensor Pressure-Doppler flow guide-wire (Combowire®, Volcano Corp., San Diego, CA). The wire was inserted through the HeartRail catheter and advanced until the pressure sensor on the Combowire, was aligned adjacent to the distal pressure sensor on the Mikro-Cath, P2. Once the Mikro-cath and Combowire are in place, the guiding catheter is pulled back to the coronary ostium to record aortic pressure (Pa). The Combowire was manipulated until an optimal and stable velocity signal was obtained. Pd and U were processed with the associated instrument console and digitized at a sampling frequency of 200 Hz (Figure 56). An electronic bookmark was applied on both the data acquisition systems in order to synchronize the data.

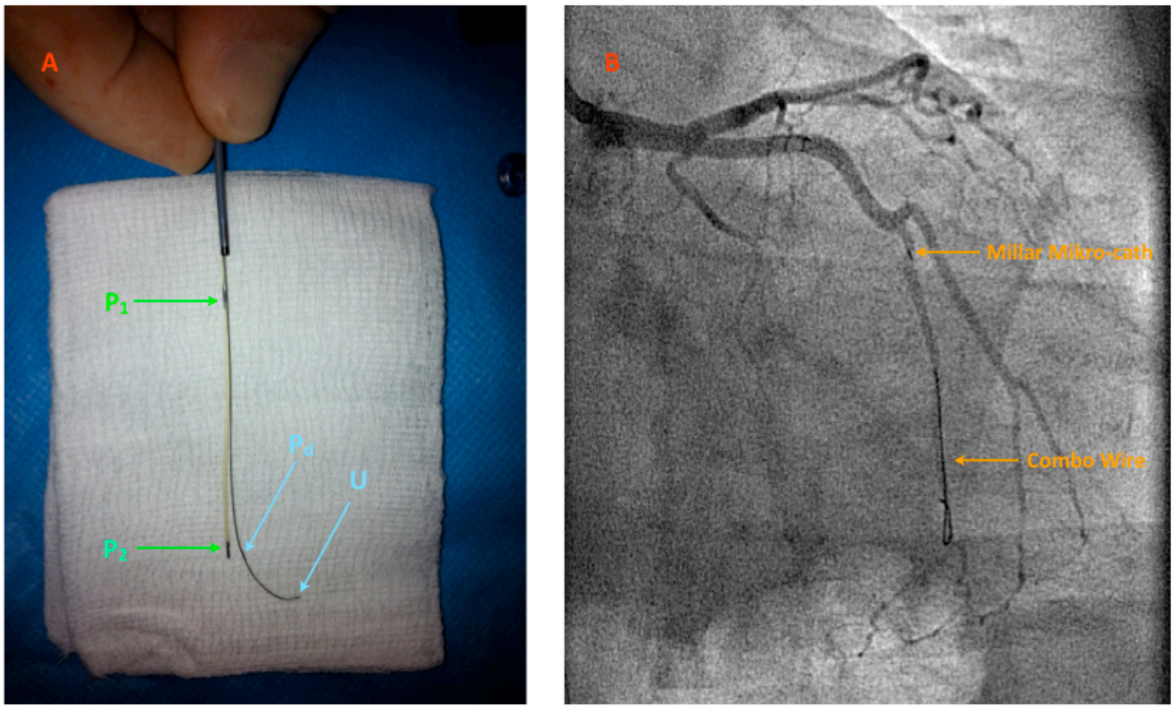

Figure 55: *A. Millar catheter and ComboWire. P1 and P2 representing the proximal and distal pressure sensors on the Millar, respectively. P_d representing the pressure sensor measuring distal coronary pressure, and, U representing the Doppler-flow sensor at the tip of the ComboWire.*

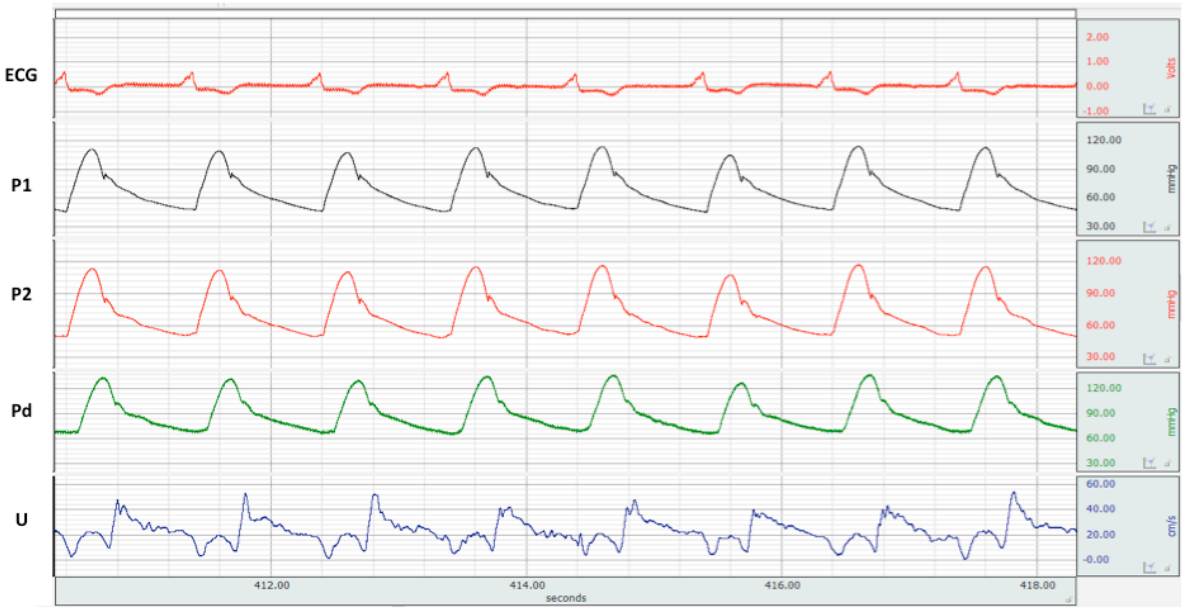

Figure 56: *Continuous Recording of ECG, Millar catheter pressures (P1 and P2) and ComboWire distal coronary pressure (Pd) and Doppler-derived velocity (U)*

Haemodynamic measurements were obtained at resting conditions and during maximal hyperemia induced by intracoronary adenosine injection (12-84 µg). These measurements

were repeated 30 seconds after the intracoronary administration of 1 mg of nitroglycerin. At rest, a sub-group of patients were also asked to perform a Valsalva maneuver (VM) by exhaling against the closed glottis, in order to investigate wave speed with induced changes in vessel trasmural pressure (Figure 57). After obtaining all the measurements in the coronary artery, the Combowire was moved to the aorta so that a comparison between coronary and aortic wave speed could be performed.

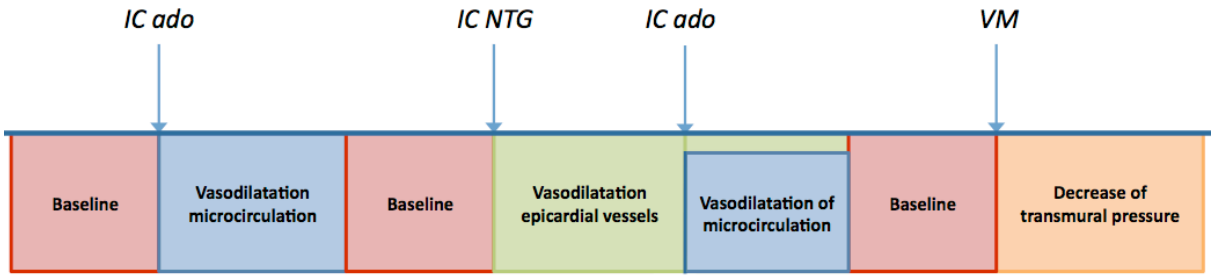

Figure 57: *Study Protocol. IC Ado = bolus of intra-coronary adenosine. IC NTG = intra-coronary bolus of 1mg nitrate. VM = patient asked to perform a valsalva maneuvre*

3.3.4.5 Data Analysis

Quantitative coronary angiography (QAngio XA v. 7.2, Medis Medical Imaging Systems, Leiden, The Netherlands) was performed to obtain the diameter profile of the study vessel. From the continuous recordings (Figure 56), 10-25 heart cycles were selected at resting conditions and 2-5 heart cycles at maximal hyperemia. 2-3 beats were selected at maximum strain of the Valsalva maneuver.

Wave speed was calculated per beat with two different methods and then averaged over the selected beats for each condition. The first approach is based on the direct measurement of the time delay between the two pressure waveforms recorded with the Mikro-Cath (*Dc*); the second way is with the single point technique (*SPc*) as described by Davies et al. [193].

Derivation of wave speed with direct measurement

The hemodynamic recordings were analyzed using the Acqknowledge software (Acqknowledge, Biopac Systems Inc., Goleta, CA). Wave speed was calculated as:

where Δs is the distance between the two pressure sensors that corresponds to 0.05 m; and Δt is the time delay between the two waveforms. The time delay Δt was calculated from the respective times of the dicrotic notch of the two pressure waveforms recorded with the Mikro-cath, P1 and P2. The time point of the dicrotic notch was determined from the local maximum of the second derivative of the respective pressure signal (Figure 58). The second derivative was obtained by passing the pressure signal through two first-order Blackman high-pass filters with a cutoff frequency of 50 Hz.

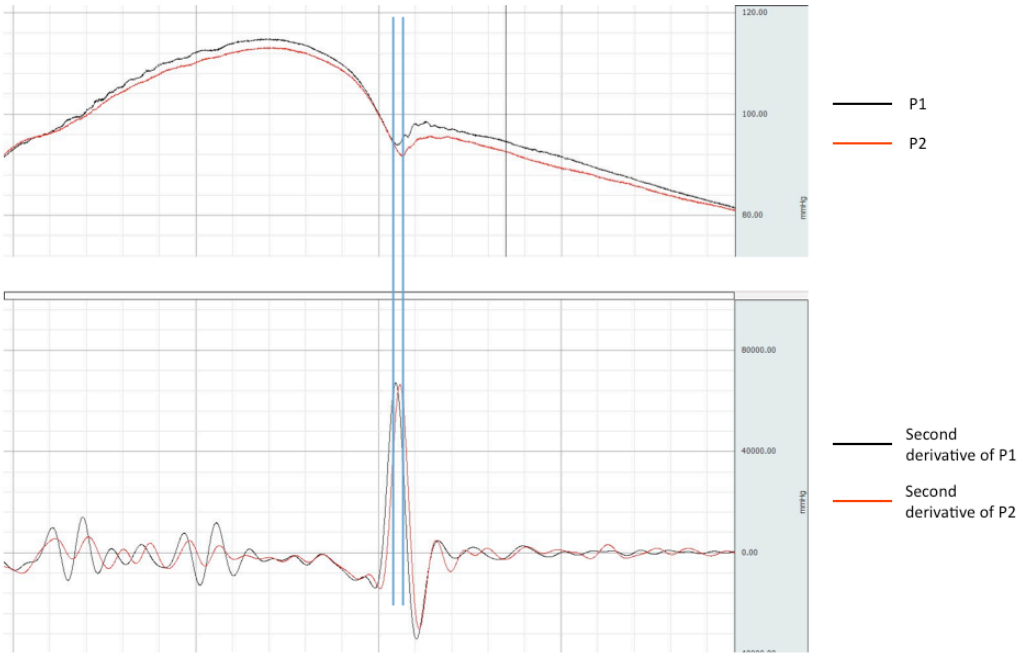

Figure 58: *Dichrotic notch analysis for direct wave speed calculation*

Derivation of wave speed with the single point technique

The hemodynamic signals were analyzed using a custom-made program (Delphi v. 2010, Embarcadero, CA, USA). The wave speed was calculated as:

Time derivatives were obtained after smoothing the raw signals with a Savitzky-Golay filter [203] and then ensemble averaged over each cycle. Density of blood, ρ, was assumed to be constant and taken to be 1060 $kg \cdot m^{-3}$.

Wave Intensity Analysis

Wave intensity (dI) is defined as the product of incremental changes in local pressure (dP) and flow velocity (dU). Coincident forward (dI+) and backward (dI−) travelling waves are superimposed to form the net wave intensity at the measuring location [204].

Net wave intensity (in $Wm^{-2}s^{-2}$) was calculated from the ensemble-averaged cycles at maximum hyperemia and normalized for the sampling rate as described in the methods section (chapter 2). The effect of wave speed on the separated wave intensity, $dI_{\pm}$ was derived using as wave speed *Dc*, *SPc* and *SPc* obtained from baseline recordings.

Coincident (microcirculation-derived) backward and (aorta-derived) forward propagating waves were separated. The energy carried by the four most predominant waveforms was quantified by integrating the area under each of the separated dominant waves. These were the positive, forward directed (aorta-derived) compression wave (FCW), occurring at the onset of systole; the concurrently occurring negative (backward, microcirculation-derived) compression wave (BCW); the backward expansion waves (BEW), the first negative wave occurring at the onset of ventricular relaxation, identified by the onset of diastole and the

forward expansion wave, which a positive deflection occurring as a result of slowing of ventricular contraction leading to a suction effect at the aortic-end of the circulation.

3.3.4.6 Statistical Analysis

All values are expressed as mean ± standard error of the mean unless specified otherwise. Comparison of the different conditions (rest vs hyperemia and with or without nitroglycerin) was performed for each wave speed estimation method using ANOVA with repeated measures followed by contrast analysis (SPSS v. 19.0, IBM, Armonk, NY). Each wave speed method, during the same conditions, were compared with a paired t-test. Relationships between variables were investigated with linear regression analysis (Grapher v. 8.7, Golden Software Inc., Golden, CO). A value of $p<0.05$ was considered statistically significant.

3.3.5 RESULTS

BASELINE CHARACTERISTICS

Fourteen patients were recruited, with a mean age of 67 ± 10 years (44-83). The study vessels were only minimally diseased with a diameter stenosis of 12±7%. The average coronary vessel diameter was 3.0 ± 1.4 mm and the majority of the measurements were taken in the right coronary artery (Table 10).

Patient Characteristics	*n (%)*
Age (±SD)	*68 ± 10*
Male sex	*9 (64)*
Diameter reduction (%)	*12 ± 7*
Study vessel (LAD/LCX/RCA)*	*2/3/9*
Coronary risk factors	
Diabetes	*0*
Hypertension	*10 (71)*
Hypercholesterolemia	*10 (71)*
Prior myocardial infarction	*3 (21)*
LV function (good/poor/unknown)	*7/1/6*
Smoking History	*6 (42)*
Medication	
ACE inhibitors	*10 (71)*
Aspirin	*14 (100)*
β-blockers	*8 (57)*
Calcium antagonists	*5 (36)*

Table 10: *Baseline Characteristics;* *LAD, left anterior descending artery; LCX, left circumflex; RCA, right coronary artery. Values are expressed as mean±SD

The simultaneous coronary haemodynamic measurements, with the Mikro-Cath and the Combowire, were possible in all the patients. In one patient the derivation of the *SPc* in the aorta was not possible because the flow velocity signal was of poor temporal quality. In one patient adenosine was not injected after nitroglycerine administration so no data were available at this condition. Figure 59 below demonstrates the mean haemodynamics recorded throughout the study protocol and its relationship to the varying pharmacologic states.

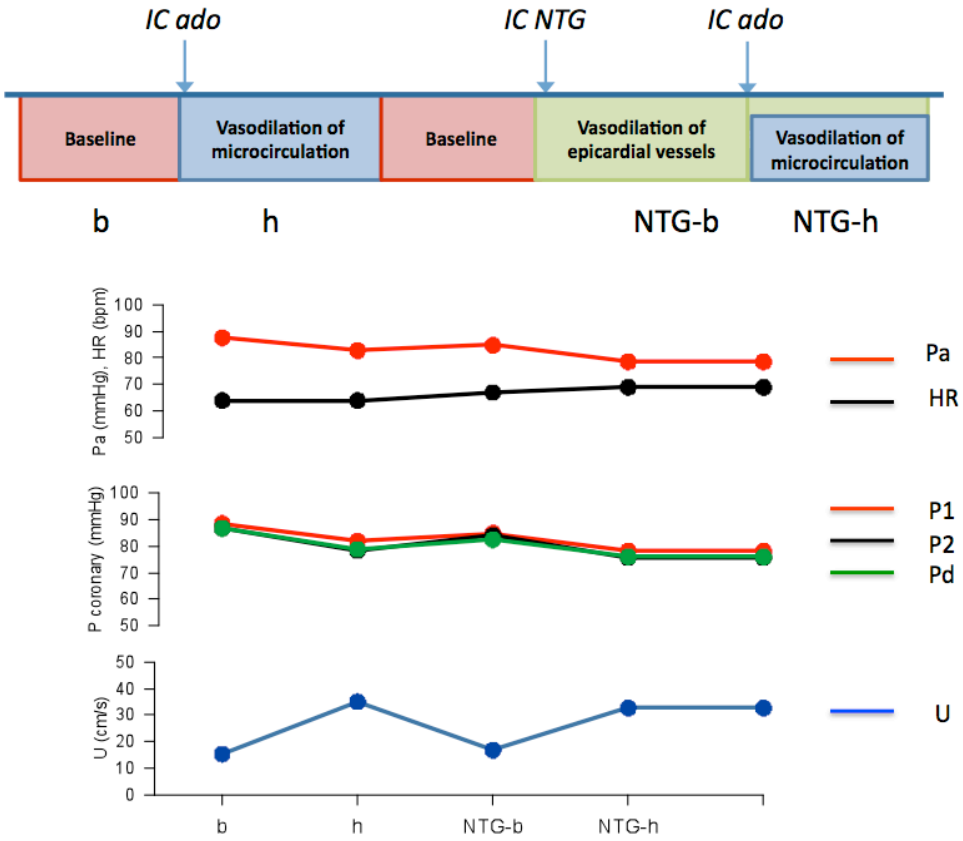

Figure 59: *Mean haemodynamic signals during the varying vascular conditions*

Direct and Single-point estimates of Coronary Wave Speed

Figure 60 shows a representative measurement sequence and the derived per beat wave speed for the two methods. The aortic pressure signal shows two short periods where adenosine was injected into the coronaries and the catheter was flushed. The subsequent vasodilatation is evident by the three-fold increase in flow velocity. The coronary pressures were not affected by the adenosine injection. *Dc* remained constant at approximately $10ms^{-1}$ during the entire period. *SPc* was similar to *Dc* during basal conditions, before and after hyperemia, but was observed to reduce markedly corresponding to the increase in flow velocity during adenosine induced hyperaemia.

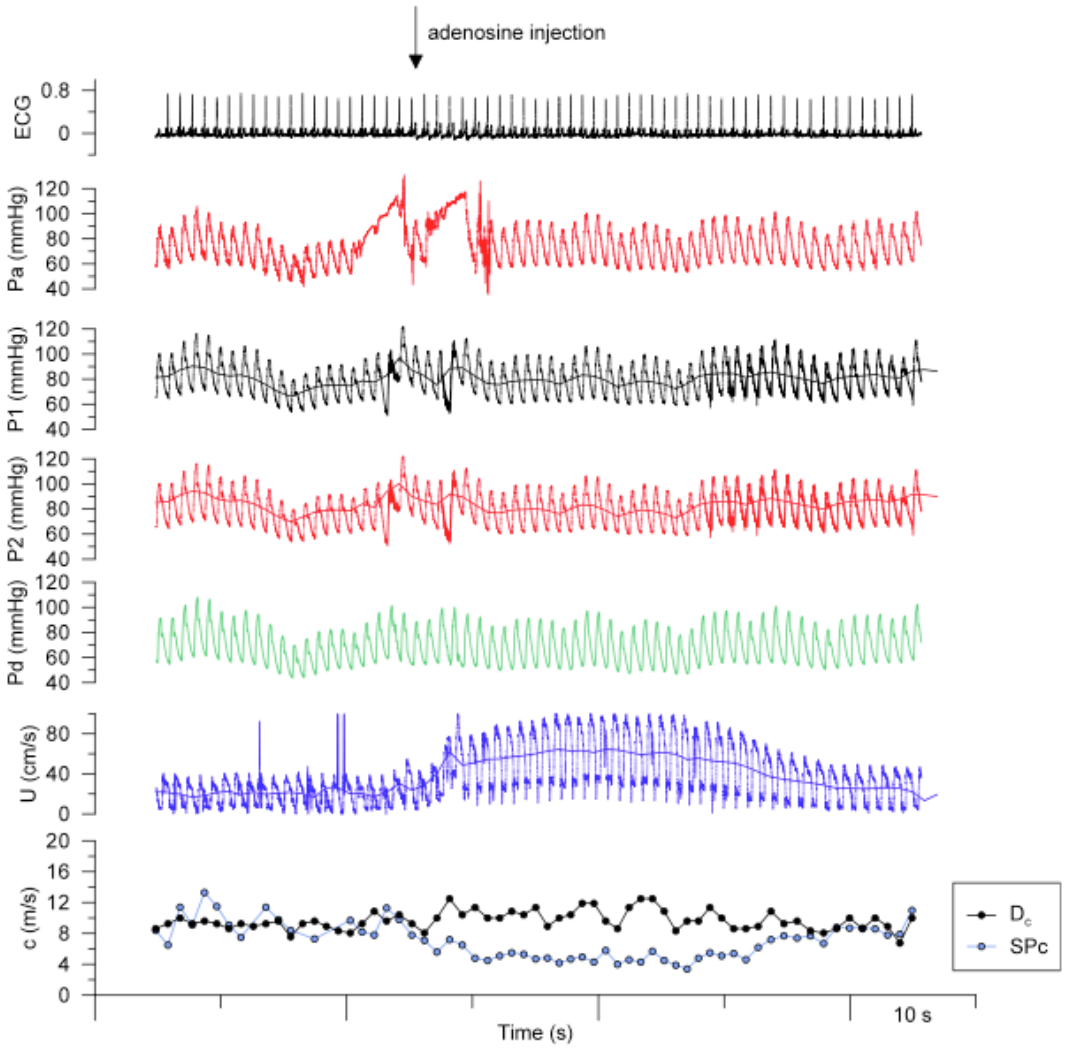

Figure 60: *Haemodynamics signals recorded during an intra-coronary adenosine bolus injection and the respective SPc and Dc per beat wave speeds*

The overall response of hemodynamic variables during the four steps of the protocol is summarized in Table 11. HR was not affected by adenosine but rose by 4% with nitroglycerine ($p<0.05$). Aortic pressure was not affected by nitroglycerine but decreased by 7% following the sequential adenosine injections ($p<0.05$). P1, P2 and Pd followed decreased by around 5% after IC nitrate bolus ($p<0.05$) and approximately 10% with adenosine ($p<0.01$). Adenosine injection caused a two-fold increase in flow velocity, observed with adenosine-only and adenosine plus NTG. NTG bolus was associated with an increase in flow velocity by 10%.

	Base (n=14)	Hyp (n=14)	NTG-base (n=14)	NTG-hyp (n=13)
HR (bpm)	64 ± 3	65 ± 4	67 ± 4	69 ± 5*
Pa (mmHg)	88± 5	83± 5*	85± 4*	79± 4*
P1 (mmHg)	89± 5	81± 5*	84 ± 5*	77 ± 5*
P2 (mmHg)	87± 4	78± 5*	83± 4*	75± 5*
Pd (mmHg)	87± 5	78± 5*	82± 4*	76± 4*
U (cm/s)	15.2 ± 1.0	34.7 ± 3.6*	16.8 ± 1.1*	32.7* ± 3.3*

Table 11: *Hemodynamic variables during the 4 steps of the protocol.*
Values are means ± sem. * p<0.05compare to baseline values

The corresponding average variation in wave speed with the two methods is depicted in Figure 61. At baseline, the two methods yielded statistically similar results: *Dc*=15.9 ± 1.8 m s^{-1} and *SPc* = 16.8 ± 1.5 m s^{-1} (p=0.44). At maximum hyperemia *SPc* markedly dropped by almost 40% to 10.5 ± 0.9 m s^{-1} (p<0.001) while *Dc* remained unchanged (Figure 62).

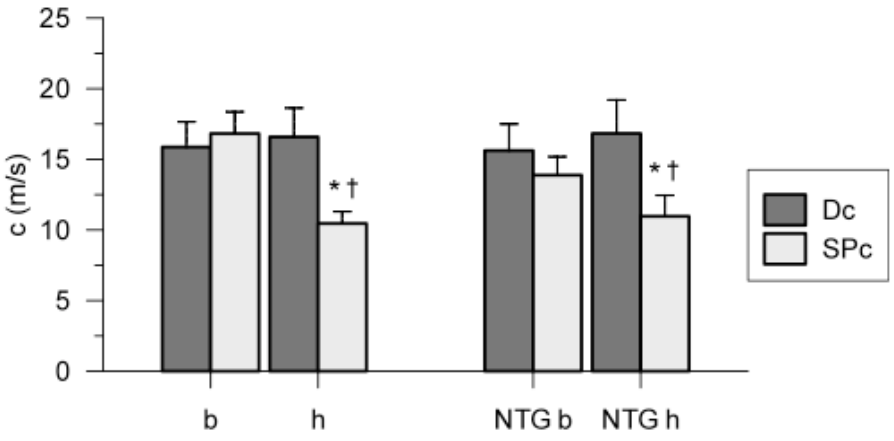

Figure 61: *Effect of conductance and resistance vessel vasodilatation on Dc and SPc*

At baseline *SPc* and *Dc* have comparable values. Nitrates do not affect either *SPc* or *Dc*. With or without nitrates, administration of adenosine causes a decrease of *SPc* by almost 40% while *Dc* is unaffected. * p<0.005 with respect to the relative baseline; † p<0.05

Bland-Altman analysis confirmed the uniformity of the two methods for coronary wave speed determination at baseline (Figure 62), showing an average difference of 0.96 ± 4.47 m/s (p=0.44).

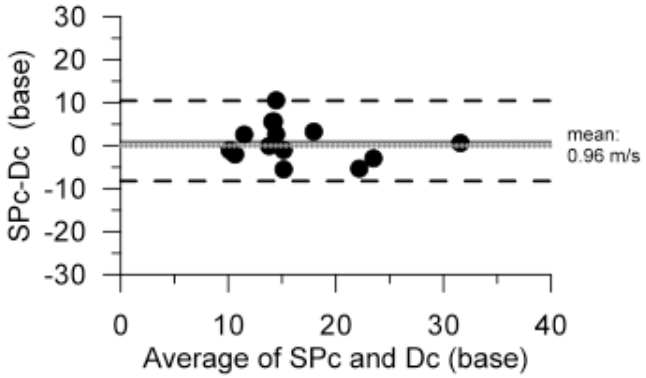

Figure 62: *Comparison of Dc and SPc at baseline*

The average of the difference between *SPc* and *Dc* at maximum hyperemia was -6.1 ± 7.3 m/s (Figure 63 A) and this underestimation of wave speed with *SPc* was greater at higher measured wave speed *Dc* (r=0.89, p<0.0001) (Figure 63 B).

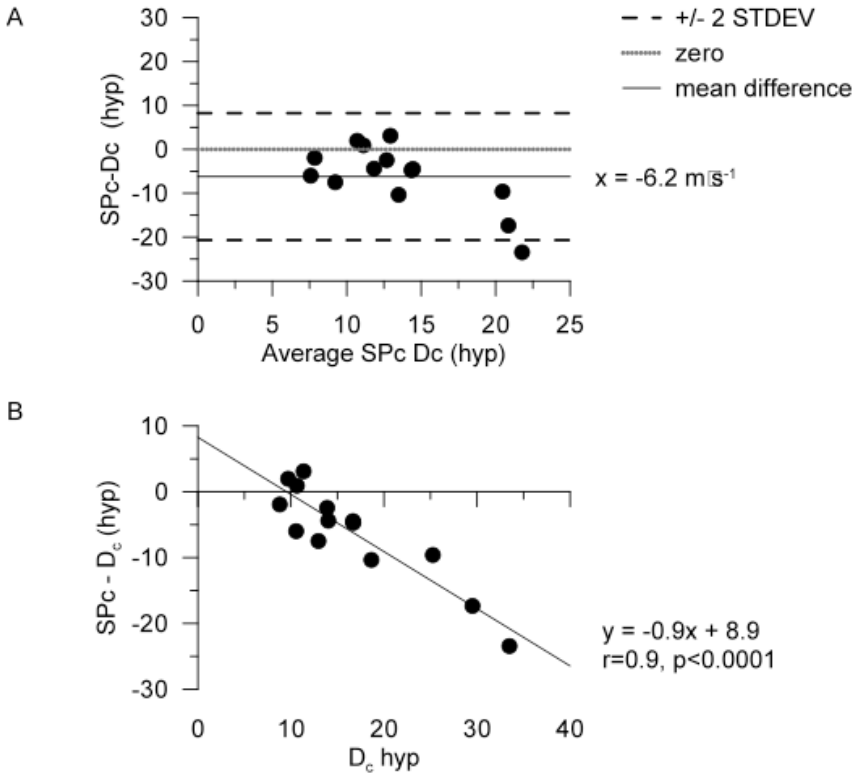

Figure 63: *A. Bland-Altman plot comparing Dc and SPc at maximum hyperaemia ;SPc is 6.2m/s slower than Dc. B. Relationship between Dc and the difference between the two wave speed estimates (Higher the measured wavespeed Dc, the larger the degree of underestimation made by SPc)*

No differences were found in the mean haemodynamics and wave speed values at baseline at beginning of the protocol and at the baseline between adenosine and nitroglycerine injections. Thus all the comparisons of nitroglycerine were performed comparing to the beginning baseline. No changes in *SPc* or *Dc* were observed between the two baselines with or without nitrates. The effect of adenosine injection on *SPc* and *Dc* in conjunction with nitrates was similar to that observed prior to nitrate administration, with *SPc* diminishing from 13.9 ± 1.3 m/s to 10.9 ± 1.6 m/s ($p<0.01$), while *Dc* did not change significantly (15.6 ± 2.0 m/s to 16.8 ± 2.5 m/s, $p<0.05$).

Directly measured wave speed at maximum hyperemia did not differ from *SPc* at baseline. Bland-Altman analysis (Figure 64) confirms that baseline SPc wave speed and hyperaemic Dc wave speed are similar in magnitude with no significant difference detected.

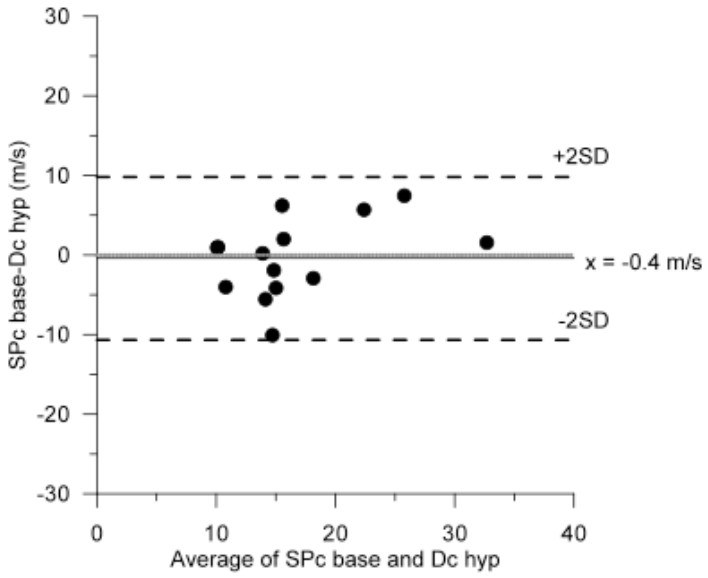

Figure 64: *Bland-Altman analysis comparing Dc at maximum hyperaemia and SPc at baseline – no differences were observed between the two measures.*

Coronary Wave Speed and Accuracy of Separated Wave Intensity Analysis

Underestimation of *SPc* derived wave speed during hyperaemia leads to an underestimation of the area of the separated BEW that was significantly (7%) lower than when estimated with *Dc* ($p<0.05$) (Figure 65). In contrast, hyperaemic *SPc* wave speed causes an increase in the BCW and FCW by 30% and 17% respectively ($p<0.02$). The FEW was not significantly affected. In contrast, when using the baseline *SPc*, which is unchanged from the Dc determinant, for wave separation at maximal hyperemia, no differences with respect to the ones generated with the measured *Dc* were observed (Figure 6).

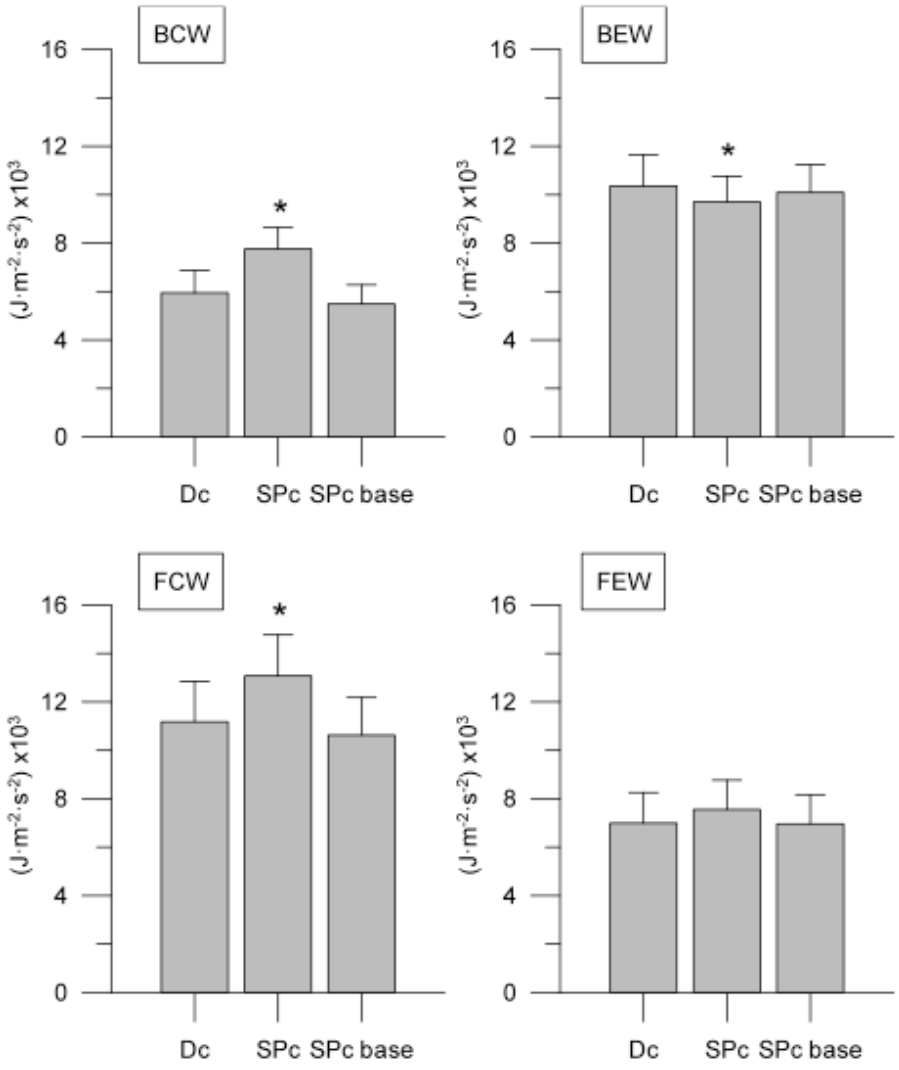

Figure 65: *Separated wave energies at maximum hyperaemia derived by SPc or Dc. (*P<0.05).*

Wave Speed during Valsalva Manouvre

A subset of six patients performed a Valsalva maneuvers (VM). Figure 66 (A) represents the coronary pressure and measured wave speed during two consecutive VM. The effect of the VM on the systemic and coronary circulation is demonstrated by the typical course of the pressure waveform (top signal in Figure 66 A). At the onset of strain, coronary pressure increased, due to the sudden rise of pressure in the thoracic cavity. With continued strain, reduced venous return impedes filling of the left ventricle and produces a decreased blood pressure. Subsequent to exhalation, intra-thoracic pressure reduces abruptly to the individual's normal value, inducing a reduction in blood pressure before returning to the baseline pressure. The bottom panel of Figure 66 (A) depicts the corresponding per beat measured wave speed during the VM. During the strain phase, in conjunction with the decline of transmural pressure (defined as coronary inner pressure minus outside thoracic pressure), *Dc* decreases from baseline and returns slowly, after exhalation, to baseline pressure, in parallel with the changes in transmural pressure.

The average wave speed trends estimated by *SPc* and *Dc*, at baseline and during maximal VM induced strain are depicted in Figure 66 (B). No differences were observed between *SPc* and *Dc* at baseline or during VM strain. However, wave speed, during maximal strain, was lower in both methods ($p<0.01$); *SPc* decreased from 15.1 ± 1.2 m/s to 7.1 ± 0.8 m/s and *Dc* diminished from 14.7 ± 2.1 m/s to 8.3 ± 1.0 m/s.

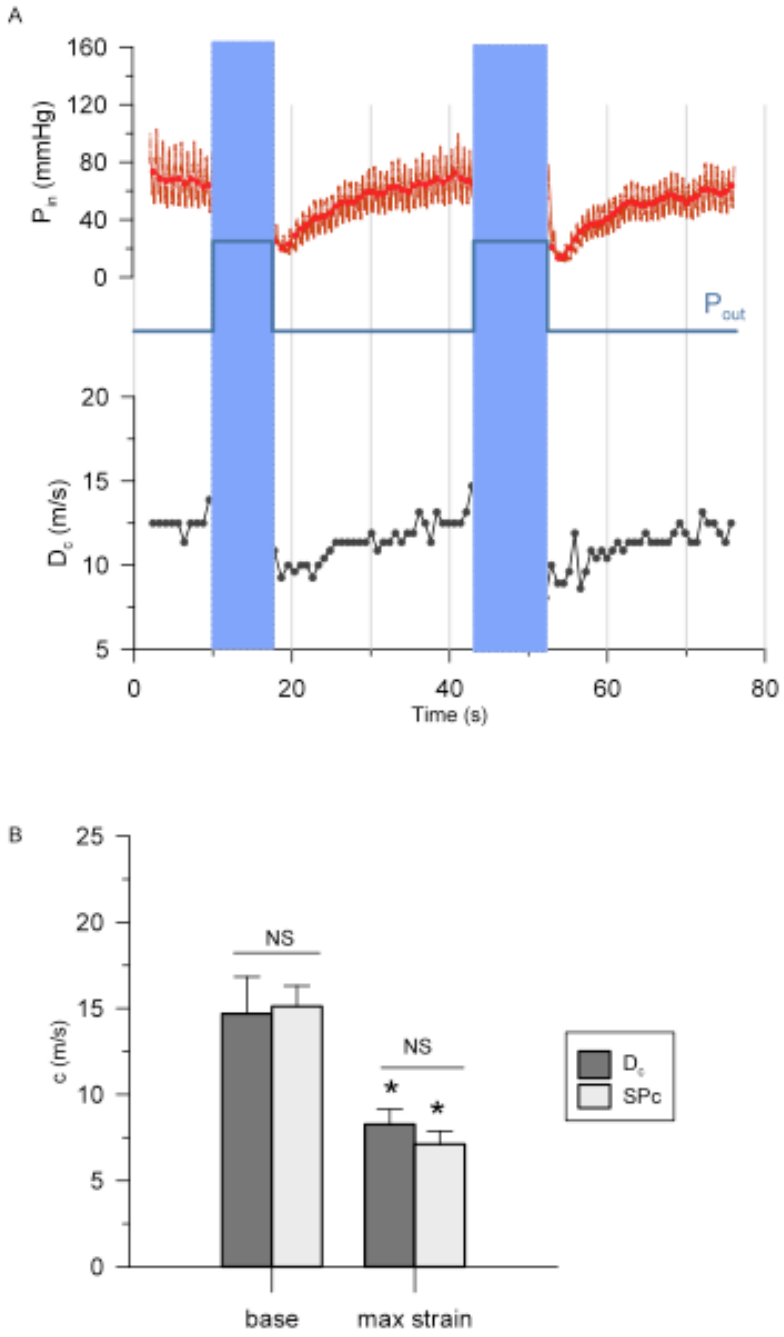

Figure 66: *Effect of valsalva maneouvure (VM) on coronary wavespeed*
A. *Per beat wave speed variation during two consecutive VM's. Coronary pressure behaves as expected by a typical VM. Thoaric pressure is highlighted by the bold blue region to depict the hypothesised transmural pressure decrease during strain of the VM. Measured coronary wave speed changes in parallel with transmural pressure. Thoracic pressure was not measured directly. The changes shown in* P_{OUT} *are not to scale and are for illustrative purposes.* ***B.*** *Average SPc and Dc at baseline and at maximum strain of the VM. Dc matches with SPc during maximal strain. Both SPc and Dc were smaller at the maximal strain of the VM than at baseline.*

Coronary and aortic Wave Speed

Coronary and aortic wave speeds were linearly related ($p<0.02$, $r=0.7$) (Figure 67). Coronary wave speed estimated with *SPc*, during basal conditions, were approximately 35% higher in magnitude than the aortic equivalent (12.0 ± 1.4 m s^{-1} vs. 16.8 ± 1.5 m s^{-1}, $p<0.05$).

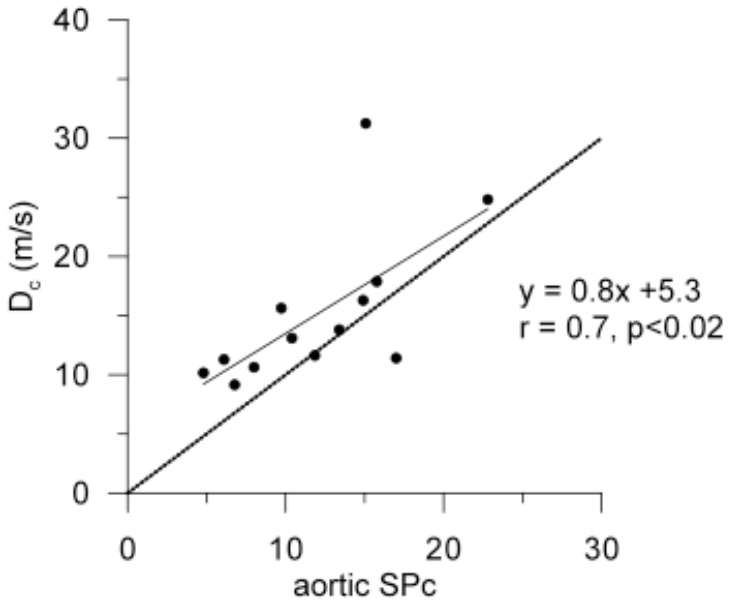

Figure 67: *Correlation between measured wave speed (Dc) and aortic single-point assessment(SPc)*

3.3.6 DISCUSSION

This study represents the first in-vivo human comparison of the single-point (*SPc*) method and a directly calculated time-delay method (*Dc*) of estimating coronary wave speed. Our study confirms that during baseline haemodynamic conditions, in human coronary arteries, coronary wave speed calculated by *SPc* agrees with the *Dc* estimation of wave speed, both having a mean value of approximately 16 m s^{-1}. However during adenosine induced maximal hyperaemic vasodilatation, *Dc* measured coronary wave speed remains unchanged compared to baseline conditions, whilst *SPc* substantially decreases. Importantly our experiment also identifies that at baseline *SPc* is not numerically different from *Dc* during maximal hyperemia.

Effects of Hyperaemia on Single-point estimate of wave speed

The estimated *SPc* coronary wave speed observed in this study was similar in magnitude to that previously identified by Davies et al [193, 205] during basal conditions and Kolyva et al [205] during hyperaemic conditions. Furthermore, baseline wave speed by *Dc* or *SPc* were found to be no different, confirming that *SPc* can be used to accurately determine coronary wave speed during basal conditions. However, during hyperaemic conditions, whilst direct measurement remained unchanged, as observed in previous animal models [195] [196], the *SPc* estimate of wave speed was markedly reduced. This observed reduction replicated the results of previous work by Kolyva et al[205], showing that the administration of adenosine caused a decline in *SPc*. However, as the effect of adenosine is primarily on the resistance vessels in the microcirculation, this should have no affect on the wave speed measured within a conductance epicardial artery. For the first time we have demonstrated that the decrease observed with *SPc* is an anomaly of the technique rather than a valid physiological

phenomenon, evidenced by the stable wave speed calculated by the reference standard *Dc* method.

Nitroglycerin induced epicardial vasodilatation and coronary wave speed

Harder et al[206] provided a physiological explanation for the effects of NTG and adenosine on the epicardial and microcirculation respectively, in terms of the effects on the calcium-dependent action potential present in coronary vasculature smooth muscle. Adenosine was observed to abolish the calcium-dependent action potential in small coronary arteries but had no effect on the action potential in large coronary arteries. In contrast, NTG abolished the calcium-dependent action potential in large coronary arteries without affecting the action potential in small arteries. IC NTG has subsequently been utilized for over three decades aiding diagnostic coronary angiography and interventional procedures, with Fieldman et al documenting the increase in epicardial artery vessel diameter with introduction of increasing doses of NTG during coronary angiography.[207] Systematic visual assessment of the angiographic vessel diameter was not performed in the current study, as it represents a rudimentary assessment of change in vessel diameter. IC haemodynamic changes, however, confirmed there was an increase in coronary flow velocity and reduction in pressure, with no alteration in wave speed following IC injection of NTG. These findings can be explained by two physiological principles governing pressure and flow within the cardiovascular system. Firstly, Poiseulle's law suggests that with a constant driving pressure ($\Delta P = Pa-Pd$) flow is directly proportional to the fourth power of the vessel radius. In view of the unobstructed nature of the coronary vessels examined and therefore constant driving pressure, the observed increase in coronary flow velocity infers an increase in vessel diameter. Secondly, according to Laplace's law, an increased vessel diameter and increased

flow velocity leads in a compensatory reduction in intra-luminal pressure, which maintains a constant wall tension, which in turn will lead to the observed constant wave speed.

In variance with the constant wave speed during NTG observed during the current study, Davies et al previously described a decrease in *SPc* immediately following NTG injection [193] . The likely explanation for this difference is in the timing of when the measurements after NTG injection where performed. Following introduction of NTG there is a reactive hyperaemia, and measurement at this stage will lead to an apparent reduction in *SPc*. To minimize the effect of this, measurements in the current study were performed at least thirty seconds after injection, allowing coronary flow to stabilize and become constant.

Effect of transmural pressure alterations by the Valsalva Manouvre

To further assess the accuracy of *Dc* and *SPc* in determining epicardial coronary wave speed a subset of patients performed a valsalva manouvre (VM) to alter the intra-luminal pressure and observe the resultant affect on wave speed. A VM increases the intra-thoracic pressure but concurrently decreases the aortic and coronary vessel luminal pressure, and hence decreases transmural pressure. Previous studies have confirmed a decrease in both aortic and coronary wave speed is seen during a VM [208, 209]. The current study reaffirmed this physiological principle, with a significant reduction in wave speed detected by both *Dc* and *SPc*. Both Dc and SPc were able to detect the reduction in wave speed during maximal strain and increased transmural pressure, with no difference in accuracy between the two modalities.

Wave Speed and Coronary Wave Intensity Analysis (WIA)

Wave speed estimated from simultaneously obtained pressure and flow data during basal conditions is a robust approximation for use in the derivation of coronary wave intensity to simultaneously obtained pressure and flow data. However if values obtained during hyperaemia are used a number of inaccuracies in the separated wave intensity profiles may occur as a consequence. The diastolic, microcirculatory-originating (backward) expansion wave (BEW) is likely to be underestimated and both the aorta-originating (forward) and microcirculatory-originating (backward) compression waves will be overestimated. Therefore highlighting a definite limitation in the utility of the *SPc* technique in its application in WIA. However, importantly, the *SPc* technique can continue to be used for phasic intra-coronary data analysis, as the baseline value determined through this method can be used for analysis in both basal and hyperaemic states.

3.3.7 LIMITATIONS

This was a small, single centre study but is the first in human study to compare a direct foot-to-foot method of determining coronary wave speed with the established single-point surrogate method. Despite being a cross-sectional study, patients with prior MI, and prior diagnoses of suggestive of non-ischaemic myocardial disease or valvular heart disease were excluded, to minimize confounders. Intra-coronary guide-wires and catheters can potentially obstruct flow and provoke ischaemia that could affect local reflexes of autonomic control of smooth muscle, which may alter wave transmission characteristics. However, no patients encountered symptoms or ECG changes suggestive of ischaemia during the study, making this unlikely to have affected the results. Furthermore, the methodology adopted in this

study represents the most accurate way of assessing and comparing direct (Dc) and indirect (SPc) wave speed in the human coronary circulation with currently available technology. Davies et al's definition of wave speed was obtained via derivation of the sum of dP and dU over 50 cardiac cycles. In this study, for consistency with *Dc*, which is calculated on a per-beat basis, was derived *SPc* per cycle and then averaged *SPc* over the number of selected beats during each condition. As no change in heart rate was observed in consecutive beats, summing the dP and dU over all the cycles or averaging the results of each beat give comparable results. However, whilst the SPc method used in this study represents a deviation from the original experiment, the mean wave speeds obtained, by both methods, were similar to that observed in previous studies, suggesting that the analysis methodology has not altered the accuracy of the results and subsequent conclusions made.

The time delay method remains the most robust and reliable method for assessing coronary wave speed. It is based on having a fixed distance between two sites of measurement within an artery, Δs, and knowing the time delay between the two pressure curves, Δt. For the purpose of this study, we considered Δs to be an equal and constant distance between the two pressure sensors on the Millar catheter. However, this assumption may not always be true in tortuous coronary arteries. However, any potential error would be extremely small and if one considered measurements obtained in a vessel of 0.5 cm diameter, the error on Δs would be less than 1% and is unlikely to significantly alter the final derivation of wave speed. Additionally, the time delay Δt is typically estimated by identification of a recognizable point on the pressure waveform, where there are unidirectional waves. Measurements within the aorta use the easily identifiable, 'foot' of the pressure wave. However in the coronary arteries this is not as well defined because at the onset of systole there are waves emanating from both the aorta and the microcirculation, which leads to a

large degree in variability in the results obtained. The dichrotic notch is the other time point readily identifiable on the pressure waveform. Whilst the use of the dichrotic notch in the time delay method of estimating wave speed has not previously been validated, we have shown that during basal conditions, *Dc* and *SPc* are numerically similar and this represents a potentially less variable time-point on pressure waveforms, that should be utilized in experiments of a similar nature. In the presence of fluctuations in flow, only small changes are observed in the foot-to-foot method, whilst the SPc would be more sensitive to these changes. Finally, transient heart rate reduction observed during valsalva manouvre may have resulted in a reduction in wave speed determined by the *Dc* method.

3.3.8 CONCLUSION

The single-point estimate of wave speed (*SPc*) reliably appraises wave speed in angiographically normal vessels under resting conditions, but markedly underestimates true wave speed during hyperemia, leading to inaccuracies in separated energy wave intensity analysis. However, *SPc* assessed during basal conditions can be extrapolated to WIA during hyperemia in normal vessels, therefore allowing it to be adopted accurately in coronary physiological assessment in both basal and hyperaemic conditions.

3.3.9 ACKNOWLEDGEMENTS

This work was done in conjunction with the Biomedical Engineering department, Amsterdam Medical Centre, University of Amsterdam, Netherlands. I would therefore like to thank and acknowledge the work of my co-investigator, Cristina Rolandi and also the additional supervision of Dr Maria Siebes.

4. TRANS-CORONARY VOLTAGE MAPPING

Trans-coronary Electrogram Mapping during Percutaneous Coronary Intervention: A Novel Electrophysiological Assessment of Myocardial Infarction

4. TRANS-CORONARY ELECTROGRAM MAPPING DURING PERCUTANEOUS CORONARY INTERVENTION: A NOVEL ELECTROPHYSIOLOGICAL ASSESSMENT OF MYOCARDIAL VIABILITY

Kalpa De Silva[1], Asela Bandara[1], Julian Bostock[1], Eike Nagel[2], Michael Marber[1], Jaswinder Gill[1], Simon Redwood[1], Sven Plein[2,3], Divaka Perera[1]

Affiliations:

[1] King's College London BHF Centre of Excellence, NIHR Biomedical Research Centre at Guy's and St. Thomas' NHS Foundation Trust, Cardiovascular Division, The Rayne Institute, London, UK

[2] King's College London BHF Centre of Excellence, NIHR Biomedical Research Centre and Welcome Trust and EPSRC Medical Engineering Centre at Guy's and St. Thomas' NHS Foundation Trust, Division of Imaging Sciences, The Rayne Institute, London, UK

[3]Multidisciplinary Cardiovascular Research Centre, Leeds Institute of Genetics, Health and Therapeutics University of Leeds, Leeds, UK.

4.1.1 ABSTRACT

BACKGROUND

Revascularization following acute coronary syndromes (ACS) provides prognostic benefit, provided that the subtended myocardium is viable. Profound electrophysiological changes occur in the myocardium following acute coronary occlusion. Surgically obtained direct contact epicardial mapping has previously shown a strong relationship with regional myocardial recovery. We examined the utility of a novel trans-coronary electrogram mapping (TCM) method in detection of the electrical anomalies occurring acutely following ACS, during percutaenous coronary intervention (PCI), specifically determining whether TCM can predict infarct size or area at risk.

METHODS

21 patients (57±10 yrs) were enrolled following Non-ST elevation myocardial infarction (NSTEMI). Myocardial infarct size was determined by late-gadolinium enhancement (LGE) and T2-weighted (T2-w) imaging used to assess for myocardial area at risk on cardiac MRI (CMR). TCM was performed utilizing the distal-end of a standard angioplasty guide-wire, insulated by an un-inflated over-the-wire balloon, as the electrode sensor. A unipolar circuit was created with a temporary pacing wire, placed sub-diaphragmatically in the venous system, acting as the indifferent electrode. The epicardial surface underlying the infarct-related artery (IRA) and in a normal reference vessel were each sequentially mapped (distal to proximal) following planned IRA-PCI.

RESULTS

12-hour Troponin T, LVEF and percentage LGE mass were 1.35±1.21 μg/L, 56±11%, and 8.4±6.0% respectively.). The degree of TCM electrogram gradient from distal to mid-vessel inversely correlated to both LGE infarct mass (r = -0.868, p=0.05) and T2-W oedema estimation (r = -0.897, p=0.04), with the more attenuated signals identifying larger areas of infarction and area at risk. The reference territory had significantly larger peak-to-peak voltages (p=0.05).

CONCLUSION

Trans-coronary mapping of the epicardial surface of the myocardium is technically feasible during PCI procedures, and provides novel electrophysiological data following myocardial infarction. The reduction in electrogram gradient from within the IRA vessel correlates with infarct size and area at risk. Further work is needed to develop the technique and assess its accuracy, however, TCM may facilitate myocardial viability assessment during cardiac catheterization.

Key words

Wave intensity analysis; acute coronary syndromes; myocardial viability; microvascular function; left ventricular remodeling

4.1.2 INTRODUCTION

Coronary revascularization improves mortality and morbidity following an acute myocardial Infarction (AMI), provided that the myocardium subtended by the diseased artery is viable.[31, 145] Non-ST elevation MI (NSTEMI) accounts for two-thirds of all AMI presentations[146] and is usually treated by initial pharmacological stabilization followed by coronary angiography with a view to revascularization, ideally within 96 hours of symptom onset.[147-149] This expedited treatment algorithm is designed to reduce the risk of recurrent myocardial infarction but as a consequence most patients do not undergo non-invasive assessment of left ventricular function and/or myocardial viability prior to cardiac catheterization. At present, there are no invasive tools for assessing myocardial viability in the catheterization laboratory, as an adjunct to coronary angiography. A real-time invasive physiological index of viability would enable personalized and instantaneous risk stratification following ACS, with revascularization targeted to those who are likely to derive long-term benefit.

Profound electrophysiological changes occur in the myocardium following acute coronary occlusion, including a decrease in action potential amplitude and duration, diminution of the resting membrane potential and a reduction in the rate of depolarization, which are all potential markers of identifying severity of infarction and degree of residual viability.[85-87]. Previous studies have shown that electrical signals from infracted myocardial territories (either in isolation or coupled with assessment of mechanical function) can be used to differentiate healthy, necrotic and ischaemic myocardium.[89, 90] These demonstrations have

relied on endocardial electrical assessment, which is not routinely accessible during PCI procedures. Conversely, a novel trans-coronary electrogram mapping (TCM) technique can be performed percutaneously to assess electrical activity from the epicardial surface, having been successfully utilized to identify regions of scar during ventricular tachycardia ablations previously.[106] However, adoption of the TCM technique during PCI following myocardial infarction to assess the electrophysiological alterations that occur in this setting has not previously been undertaken.

4.1.3 AIMS

The aims of the study are to determine if trans-coronary voltage mapping is feasible to do during percutaneous coronary intervention. Additionally, to examine which electrogram parameters correlate with infarct size, assessed against a biomarker marker surrogate of infarction (Troponin T), and late-gadolinium enhancement cardiac MRI imaging.

4.1.4 STUDY DESIGN

4.1.4.1 Inclusion Criteria

Patients scheduled to undergo urgent coronary angiography and revascularization 2-7 days after presenting with an NSTEMI, defined as symptoms of ischemia lasting at least 20 minutes (chest pain score >4)[157] in conjunction with significant elevation in cardiac biomarkers (defined as a TnT >0.20ug/L) identified twelve hours after symptom onset, were eligible for inclusion into the study.

4.1.4.2 Exclusion Criteria

To ensure that CMR findings reflected acute myocardial injury, patients were not enrolled if they had suffered a prior myocardial infarction. Additional exclusion criteria were a prior diagnosis of valvular disease, previous PCI or CABG surgery, an occluded infarct related artery (IRA) at time of angiography, persistent arrhythmias or hemodynamic instability. Patients with contraindications to CMR at study entry, such as pacemakers, implantable defibrillators, claustrophobia, or metallic intracranial implants, were also excluded.

4.1.4.3 Ethical Approval

The study protocol was approved by the institutional research ethics committee (Rec ref 08/H0802/143). All participants were provided with an information sheet detailing the study protocol prior to obtaining informed consent.

4.1.4.4 Cardiac catheterization and trans-coronary electrogram measurements

All patients where given loading doses of aspirin (300mg) and clopidogrel (600mg) as per standard clinical practice, prior to coronary intervention. Coronary angiography was performed through a 6F sheath via a femoral artery approach. A 7F venous sheath was placed in the femoral vein at the outset of the procedure, to be used for obtaining electrogram measurements following PCI. 0.5mg-1mg intracoronary nitroglycerin was administered as per routine practice after selective intubation of each coronary system, to reduce the effect of coronary vasospasm.

The method and extent of PCI was at the discretion of the operator, including type of stent (BMS or DES), and adjunctive use of mechanical assist support devices. The decision to perform PCI was made before TCM measurements were obtained and were not used to guide intervention. Following PCI to the target IRA lesion, an uncoated 0.014-inch coronary guidewire was advanced across the stented lesion into the distal epicardial vessel. An un-inflated over-the-wire angioplasty balloon (1.25mm) was then passed over the wire to electrically insulate all but the distal 5-10mm of the wire, optimizing localization of the signals and minimizing far-field interference (Figure 23). A temporary pacing wire was inserted via the 7F femoral venous sheath, and placed sub-diaphragmatically in the inferior vena cava, acting as an indifferent electrode (Figure 68). The proximal end (external to the patient) of the intracoronary guidewire and the pacing wire were connected to the postive and negative inputs on an electrophysiology monitoring system (Siemans Sensis®), with unipolar voltage electrograms continuously recorded. Electrograms were obtained from with the IRA assessing the infarcted region and also in a reference myocardial territory

(angiographically unobstructed (<30% diameter stenosis) coronary artery), with the guide-wire positioned in the distal portion (distal-third) of the vessel and sequentially pull backed to the mid (middle-third) and the proximal-third of vessel (Figure 69).

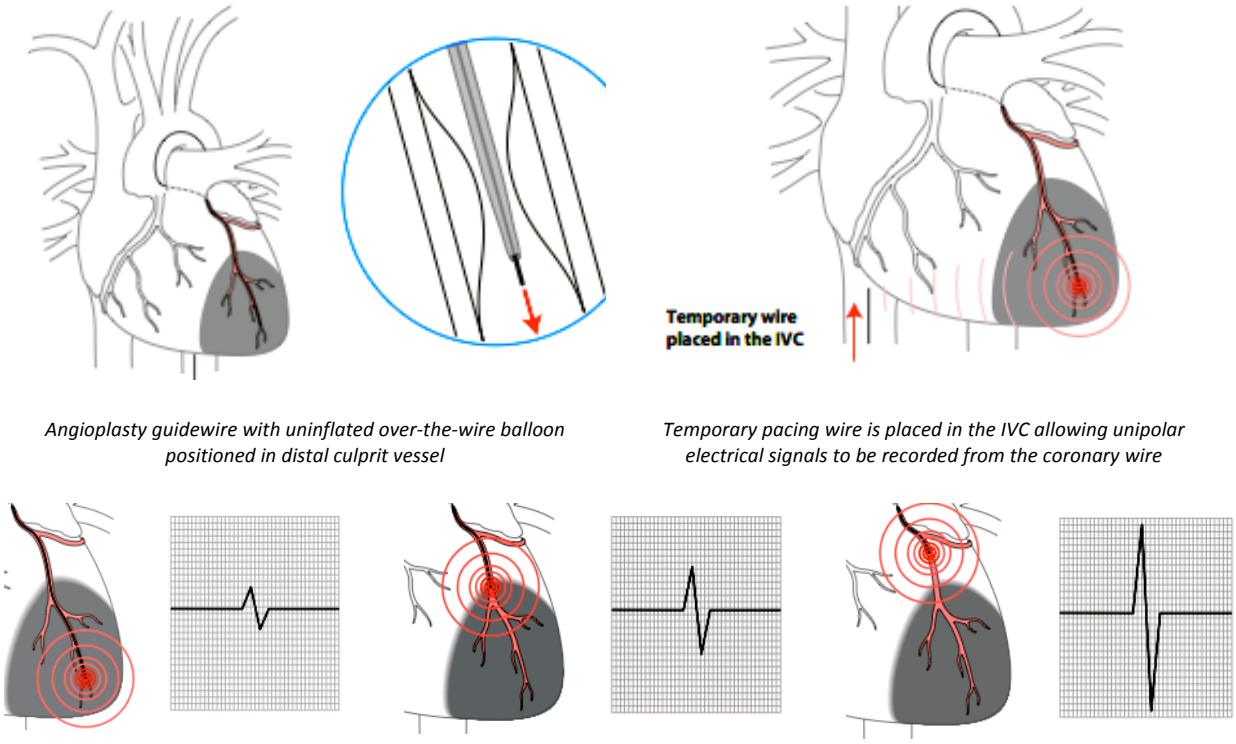

Angioplasty guidewire with uninflated over-the-wire balloon positioned in distal culprit vessel

Temporary pacing wire is placed in the IVC allowing unipolar electrical signals to be recorded from the coronary wire

As the wire is pulled back (distal to proximal), the amplitude of the electrogram changes, Corresponding with the severity of scar (a) Apex (b) Mid-ventricle (c) Base

Figure 68: *Schematic showing how to obtain a Trans-coronary Electrogram. The three panels at the bottom represent the concept of reducing electrical activity with a greater transmurality of infarction*

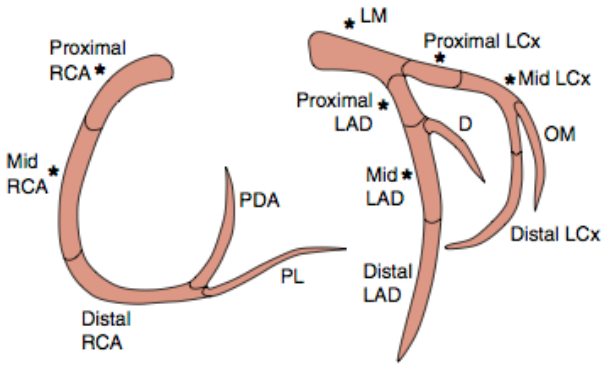

Figure 69: *Diagrammatic representation of coronary anatomy – highlighting each vessel being segmented into three sections; distal, mid and proximal. (Adapted from White et al)*[210]

Figure 70 shows an example of a 3-point trans-coronary electrogram in a patient who had a apical-anterior infarction (Trop T 1.42μg/L), recorded at 50mm/s.

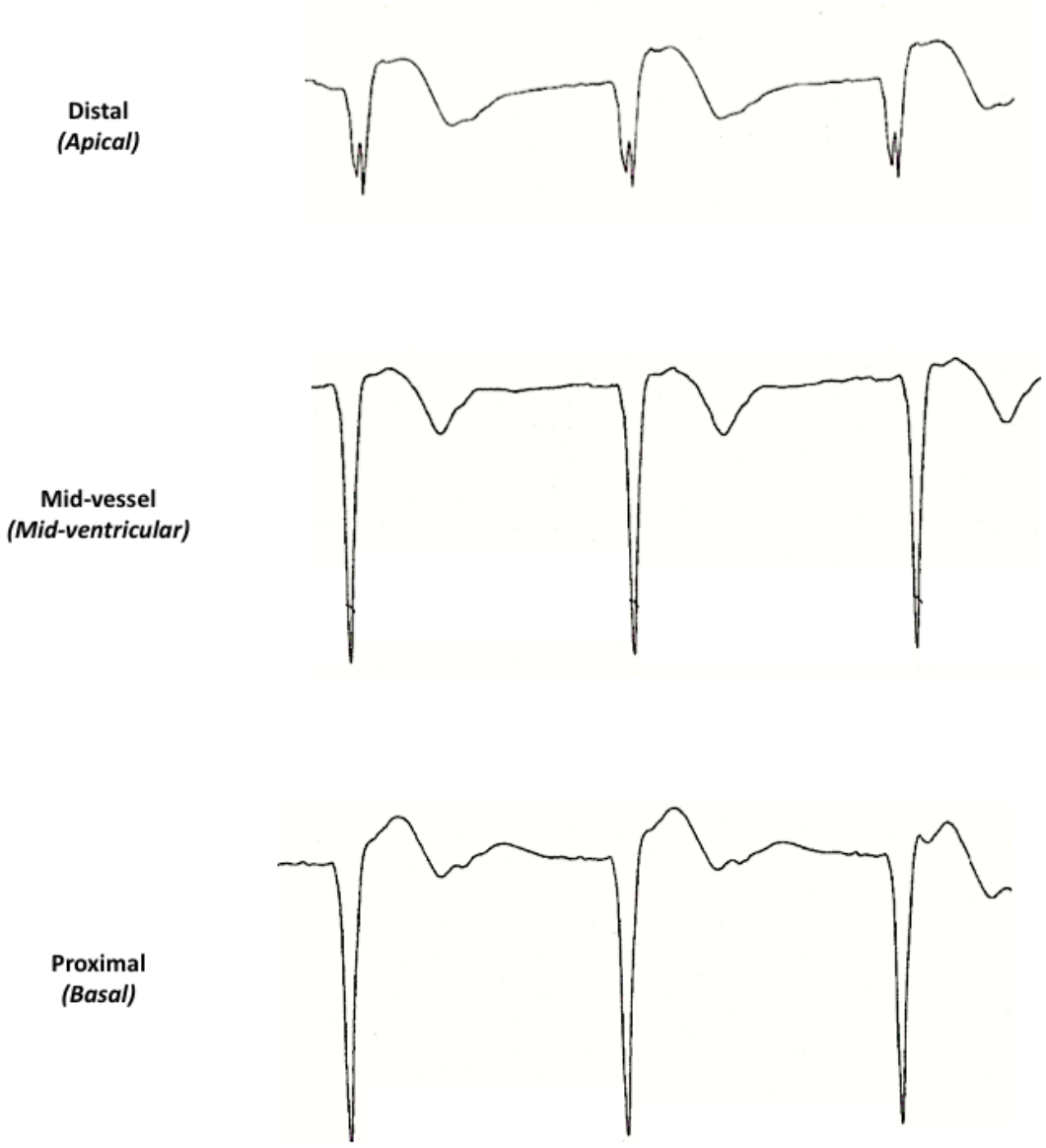

Figure 70: *3-point Trans-coronary electrogram from the LAD of an apical-anterior myocardial infarction with a step-up in electrical amplitude observed at the mid-ventricular level. Measured peak-to-peak amplitudes were: Distal 6.7mV, mid-vessel 12.2mV and proximal 12.6mV. Electrogram areas were: Distal 0.41mV.s, Mid-vessel 0.79 mV.s, proximal 0.81 mV.s.*

Protocol developments

A technical development was made to the measurement protocol to enhance the spatial resolution of the data acquired, by performing a graduated 'pull-back' of the insulated guide-wire, performed at 1cm intervals from the distal to proximal vessel. The pullback distance was calculated by the external distance of the wire measured against a sterilized ruler. The current catheter laboratory protocol is summarized in figure 71.

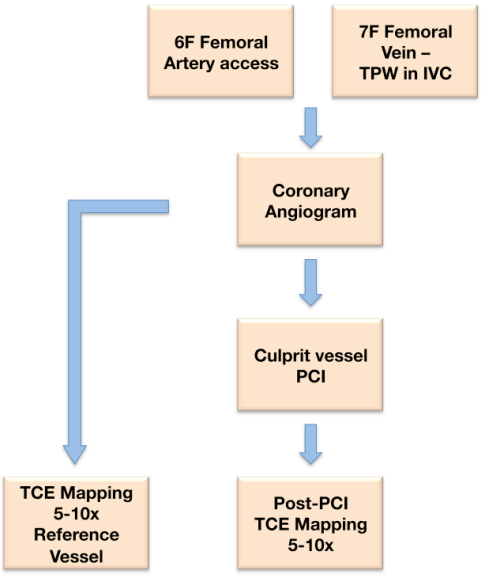

***Figure 71**: Trans-coronary electrogram mapping cardiac catheterization laboratory protocol*

4.1.4.5 Data analysis

Electrogram data analysis

Data were sampled using a high-pass filter of 0.05Hz and a low pass filter of 100Hz, to minimize external electrical interference, with the data subsequently analysed offline. Unipolar voltages were then generated by the electrical vectors formed between the two wires (intra-coronary guide-wire and temporary pacing wire), as described in the methods section (Chapter 2).

Previous voltage mapping analysis in this setting has focussed on peak-to-peak amplitude and its relation to non-viable and viable myocardium.[93-95, 101, 211] In this study, each patient had a three-point vessel map, with the following five electrogram parameters assessed (Figure 72): the amplitude of the positive deflection above the isoelectric line (A), negative deflection below isoelectric line (B), peak-to-peak amplitude (C), and electrogram duration (msec) (D) and the electrogram area in mV.msec.

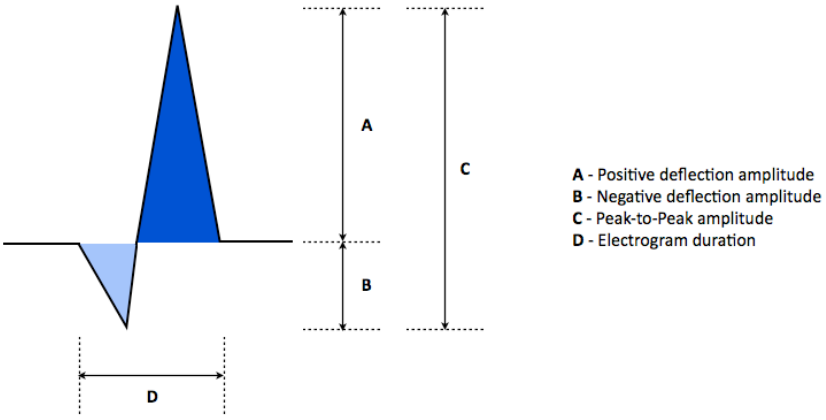

Figure 72: *Electrogram vectors analysed. Each component A-D were correlated with markers of infarction. Additionally the total area (dark blue + light blue) was calculated in mV.sec.*

Additionally, to previous documented analysis, derivation of an individualised voltage map for each myocardial territory, by obtaining a 'gradient' of electrical activity was determined by (1) subtracting (2) dividing the distal voltages (or area) from that obtained in the mid-vessel, anatomically corresponding with the apical to mid myocardial territories.

Infarct size assessment

Biomarker

Troponin T (TnT) obtained twelve hours following onset of ischaemic chest pain symptoms was used as the biomarker to estimate infarct size. Whilst serial measurement of troponin 72-hours following symptom onset represents a more accurate identifier of infarct size, an assay taken at 12-hours remains a good surrogate.[212]

Cardiac Magnetic Resonance Imaging

Index CMR studies were performed prior to emergent angiography and PCI. The scans were performed on a dedicated 3 Tesla cardiac MRI scanner (Achieva, Phillips Healthcare, Best, Netherlands) equipped with dual-RF transmission technology and a 32-channel phase array body coil. Cine images were acquired using a standard steady state free precession (SSFP) cine technique in two-, three- and four-chamber orientations and in a left-ventricular (LV) short-axis stack covering the LV from apex to base. The acquisition pulse sequence provided a typical spatial resolution of 1.8 x 1.8 x 8 mm with a 2mm inter-slice gap and a temporal resolution of 50 frames per second. Area at risk was assessed using a T2- weighted sequence; a short-axis stack covering the whole ventricle using T2-weighted triple inversion

recovery breath-hold pulse sequence was performed (slice thickness 8 mm; repetition time 2 RR intervals; echo time 99 ms; image matrix 145x192). Late gadolinium enhanced (LGE) imaging was performed using an inversion recovery fast gradient echo sequence 15-20 min after the intravenous administration of 0.2 mmol/kg body weight of gadobutrol (Gadovist, Bayer Schering Pharma, Berlin, Germany), to ensure optimised infarct delineation in the ACS setting.[144] A stack of images was acquired in the same LV short axis orientation as the cine images to ensure registration between cine CMR and infarct measurements. LGE acquisition was guided by a Look-Locker sequence with a typical pre-pulse delay of 200-330ms. Follow-up scans were performed between 3-4 months, using an identical acquisition protocol.

CMR Analysis

Quantitative analysis was performed offline, by blinded observers, using dedicated CMR viewing software (CMR 42, Circle Cardiovascular Imaging, Calgary, Canada). The area of hyperenhancement was quantitatively determined using a previously described signal intensity method,[26, 138] where oedematous tissue derived from the T2-W sequence is defined as having a signal intensity of greater than 2 standard deviations (S.D) compared to a region of interest (ROI) in an area of remote normal myocardium (Figure 73), whilst infarcted tissue is defined as an area of myocardium with LGE signal intensity greater than 5 S.D (Figure 73). Endo-epi-cardial contours were drawn (excluding papillary muscles) to derive total LV mass. Infarct mass was expressed as the absolute mass of infarcted tissue (in grams) and as the percentage of the total LV mass.

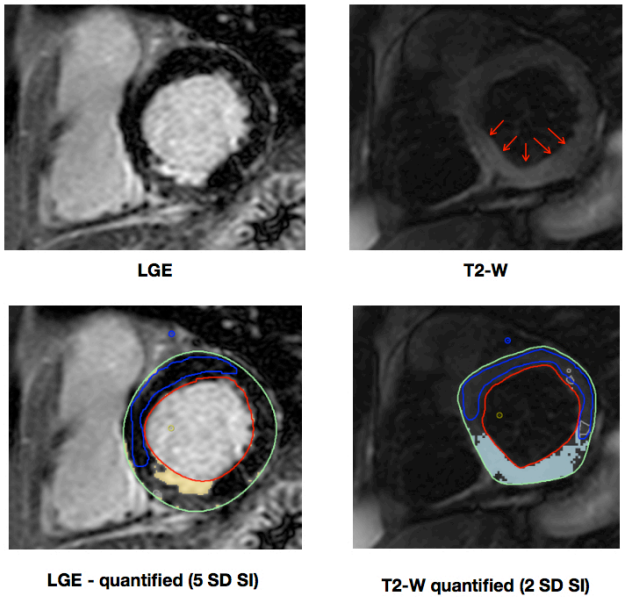

Figure 73: *Quantitative Cardiac MRI Analysis of T2-Weighted oedema (area at risk) and Late-gadolinium enhancement (region of infarction) using a signal intensity method.*

4.1.4.6 Statistical Analysis

Statistical analysis was performed using IBM SPSS version 20. Pearson correlation analysis was used to identify the relationship between TCM derived data and infarct size and area at risk. Continuous variables were compared, assuming a parametric distribution, using Paired or unpaired t-tests. A two-tail test for significance was performed in all analyses, whereby $p \leq 0.05$ was considered statistically significant.

4.1.5 RESULTS

BASELINE CHARACTERISTICS

Twenty-one NSTEMI (59±11 years) patients completed the three-point TCM protocol with 12-hour Troponin T as the marker of infarct size. Ten patients underwent the CMR and TCM protocol 67±34 hours following symptom onset, with patients scanned 4±2 hours prior to angiography. Figure 74 shows the recruitment stream with all exclusions. Mean 12-hour Troponin T was 2.37±1.79μg/L. Quantitatively determined percentage diameter stenosis of the culprit lesion was 81±13% in the IRA (Table 12). CMR derived hyper-enhanced infarct mass was 9.4 ± 6.2g, which corresponded to 7.2 ± 5.3% of total left ventricular mass. Both LGE parameters of infarct size, mass and % LV mass, correlated linearly with TnT (R= 0.64 p=0.002 and R=0.69, p=0.001, respectively). LV ejection fraction was 52±32% and did not relate to the three-point trans-coronary electrograms assessed in this study.

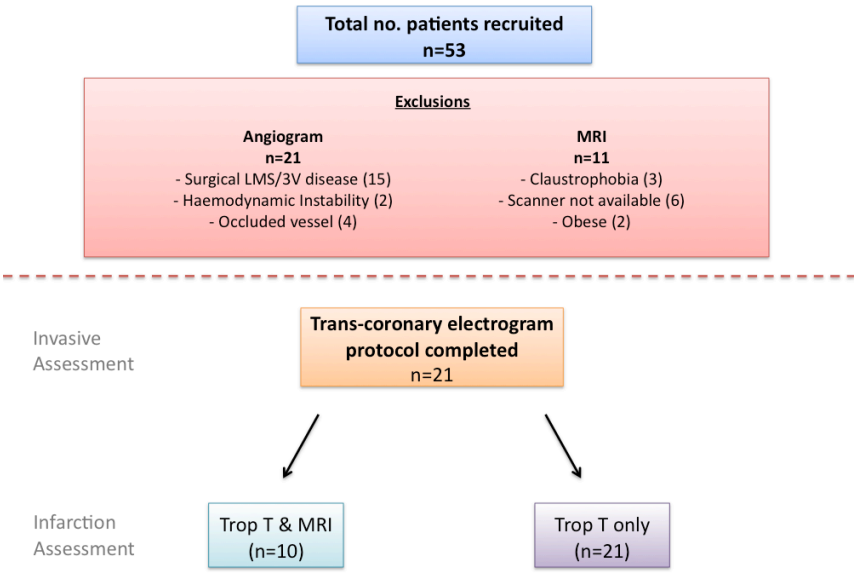

Figure 74: *Trans-coronary Electrogram Mapping study recruitment activity*

No. Recruited	21
Age, mean (±SD)	59 (±11)
Medical History	
Male, n (%)	18 (82)
Hypertension, n (%)	8 (38)
Diabetes mellitus, n (%)	1 (5)
Hypercholesterolaemia, n (%)	8 (38)
Smokers, n (%)	8 (38)
BMI (kg/m^2), Mean (±SD)	27.0 (2.2)
Prior MI, n (%)	0 (0)
Previous PCI, n (%)	0 (0)
Type of ACS	
NSTEMI , n (%)	21 (100)
Time from Symptom onset - Procedure, Mean Hrs (±SD)	67 (±34)
Cardiac Enzymes	
Peak Troponin T (µg/L), Mean (±SD)	2.37 ± 1.79
Culprit Vessels	
LAD/Cx/RCA, n	15/4/2

Table 12: Patient Characteristics

TRANS-CORONARY ELECTROGRAM MAPPING ANALYSIS

Relationship of Infarct-related artery trans-coronary electrogram with markers of infarction and oedema

a. Distal vessel TCM Electrograms

The mean electrogram amplitudes for the positive, negative and peak-to-peak voltages were 7.3±5.6mV, 4.2±3.2mV and 11.3±9.9mV respectively. The positive and negative components of IRA distal TCM electrogram had no relationship with TnT (R=-0.42, p=0.11 and R=-0.36,

p=0.13 respectively). However, the distal peak-to-peak amplitude tended to inversely correlate with TnT (R=-0.46, p=0.06). Figure 75 shows a case example of alteration in peak-to-peak amplitude in conjunction with infarction. Duration of the distal electrogram showed no relationship with TnT identified size of infarction (R=-0.20, p=0.44). Similarly total electrogram area was not predictive of TnT magnititude (R=-0.24, p=0.37).

None of the five parameters assessed related to LGE-infarct mass or oedema mass on T2W imaging (Table 13).

Parameter	Culprit Artery Site	n	Positive (mv)	Negative (mV)	Total (mV)	Duration (ms)	Area (mV.s)
T2EM	Proximal	1	-	-	-	-	-
	Middle	5	**0.743** (0.150)	**0.211** (0.733)	**0.818** (0.090)	**0.237** (0.701)	**0.773** (0.125)
	Distal	6	**0.187** (0.723)	**0.585** (0.223)	**0.572** (0.235)	**0.482** (0.333)	**0.397** (0.435)
T2EM:TMM	Proximal	1	-	-	-	-	-
	Middle	5	**0.662** (0.223)	**0.319** (0.601)	**0.858** (0.063)	**0.156** (0.802)	**0.818** (0.091)
	Distal	6	**0.822*** (0.044)	**0.305** (0.556)	**0.478** (0.337)	**0.287** (0.581)	**0.584** (0.224)
LGEM	Proximal	2	-	-	-	-	-
	Middle	8	**-0.126** (0.766)	**-0.010** (0.980)	**-0.118** (0.780)	**0.285** (0.493)	**-0.078** (0.854)
	Distal	9	**0.241** (0.532)	**0.167** (0.667)	**-0.230** (0.551)	**-0.393** (0.295)	**0.194** (0.417)
LGEM:TMM	Proximal	2	-	-	-	-	-
	Middle	8	**0.175** (0.679)	**-0.154** (0.716)	**0.032** (0.939)	**-0.023** (0.958)	**0.059** (0.890)
	Distal	9	**0.526** (0.146)	**-0.137** (0.726)	**0.037** (0.924)	**-0.368** (0.330)	**0.194** (0.616)

*Table 13: Two-tailed Pearson's correlation test of cardiac MRI parameters. Bold font represents Pearson correlation coefficient, R, with corresponding p values shown below. *p<0.05. The number of patients available for proximal analysis was too small to conduct test. (T2EM = T2 enhanced mass, T2EM:TMM = T2 enhanced mass to total myocardial mass ratio, LGEM = late gadolinium enhanced mass (g), LGEM : TMM = late gadolinium enhanced mass to total myocardial mass ratio).*

b. Mid-vessel TCM Electrograms

Mean mid-vessel voltages were greater than in the distal vessel, 8.4±6.1mV, p=0.03, 5.6±4.7mV, p=0.04 and 13.9±10.1mV, p=0.02 for positive, negative and peak-to-peak deflections respectively. Similarly to distal TCM, electrogram parameters for the focal mid-vessel TCM showed no relationship with TnT (positive, R=-0.46, p=0.13, negative, R=0.18, p=0.58, peak-to-peak, R=-0.25, p=0.43, duration, R=-0.45, p=0.14, and area, R=0.12, p=0.72) or LGE mass (positive, R=0.18, p=0.68, negative, R=-0.15, p=0.72, peak-to-peak, R=0.03, p=0.94, duration, R=-0.02, p=0.96, and area, R=0.06, p=0.89). Additionally, no significant relationship was observed with T2-W oedema mass, with any of the five electrogram factors investigated (positive, R=0.66, p=0.22, negative, R=0.32, p=0.60, peak-to-peak, R=0.86, p=0.10, duration, R=0.16, p=0.80, and area, R=0.81, p=0.09.

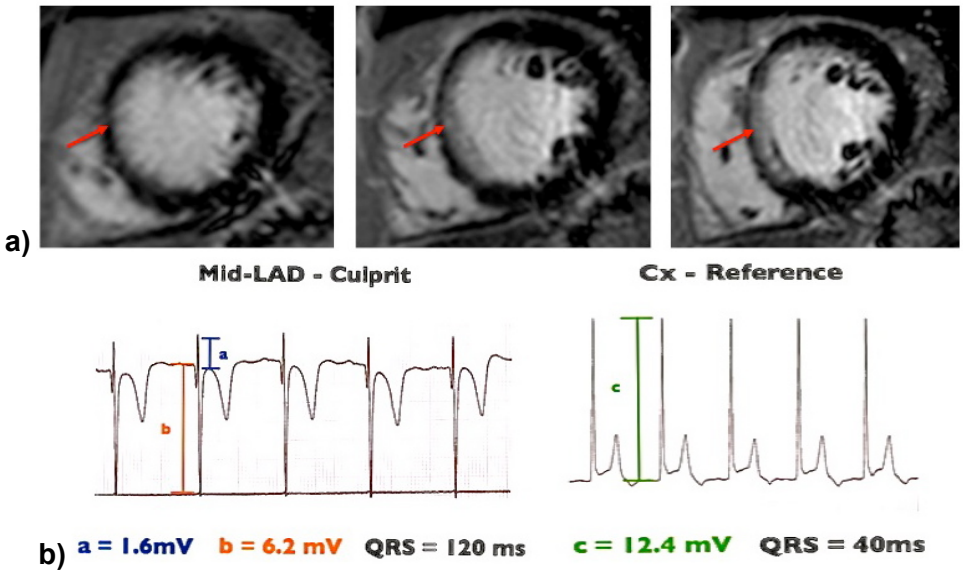

Figure 75: *ACS Trans-coronary Electrogram case*
a) Late-gadolinium enhancement CMR shows anterior-septal apical – basal 50-75% transmurality of infarction (Red arrows). b) Trans-coronary electrogram measurements from LAD showing reduced voltages compared to reference vessel - Circumflex (Electrograms not to scale).

Apical versus mid-myocardial TCM

The majority of infarction identified on CMR extended from mid to apical wall. A comparison was, therefore, made between the amplitudes of the distal and mid-vessel components of the TCM electrograms. Figure 76 shows the trend of increasing electrical activity in the mid-vessel/wall compared to the distal vessel/apical wall, though these were not statistically significant, there was a trend in increasing amplitude in recordings obtained from the mid-vessel.

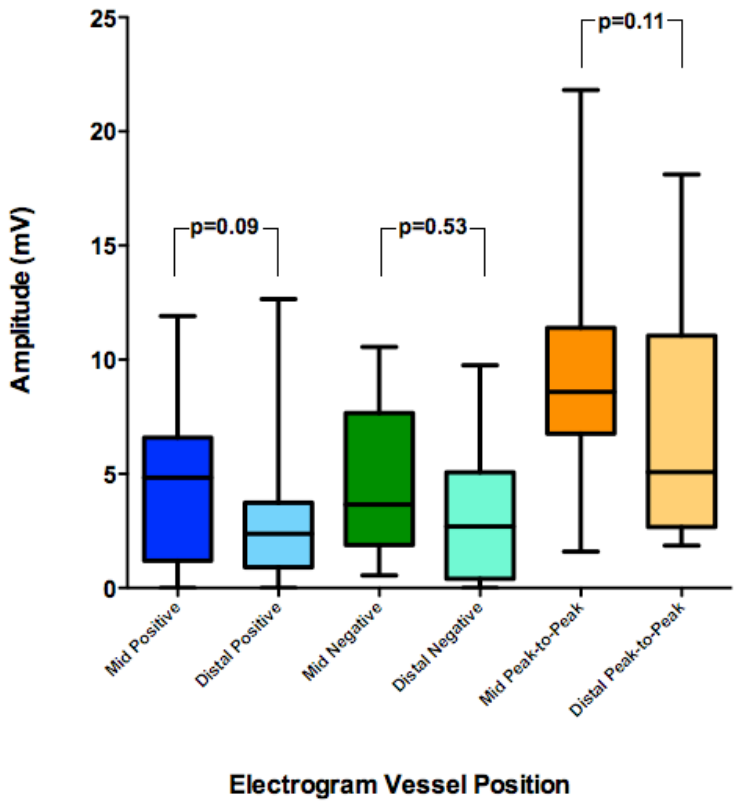

Figure 76: *Infarct-related vessel Trans-coronary electrogram Amplitude variation*

Whilst there was no difference in electrogram duration between the two regions (p=0.66), the distal complexes had a smaller area compared to matched mid-vessel recordings (p=0.01), with a mean difference of 0.09 mV.msec between the two regions.

Infarct-Related Artery Voltage Gradients

The areas beneath the distal electrograms were substracted from the mid-vessel electrograms (Mid_{TCM} – $Distal_{TCM}$) to determine the electrical gradient, along the IRA. This paramater correlated with both LGE mass (R=-0.87, p=0.05) and area at risk measured by T2-W oedema (R=-0.90, p=0.04). The mid to distal ratio of areas (Mid_{TCM} : $Distal_{TCM}$) did not show any correlation with TnT (R=-0.33, p=0.35), LGE (R=-0.46, p=0.42), or T2W (R=-0.54, p=0.35).

Trans-coronary electrogram 'pull-back' gradients

Four additional patients underwent TCM using a 'pull-back' method, allowing more detailed epicardial electrical assessment. The relative changes of postive and negative inflections, and overall amplitude were assessed, to determine whether this would provide a more robust method of epicardial voltage mapping. Figure 77 shows an example of a patient with the composite positive and negative inflections plotted against distance within the infarct-related and reference coronary vessels. Which reinforces the observations of a voltage gradient between distal and middle portions of the culprit and reference vessels. Furthermore, the proportions between positive and negative inflections suggest there are unique electrical signatures between vessels. This method is likely to represent a more integrated approach of assessing unipolar voltage mapping from the epicardial surface.

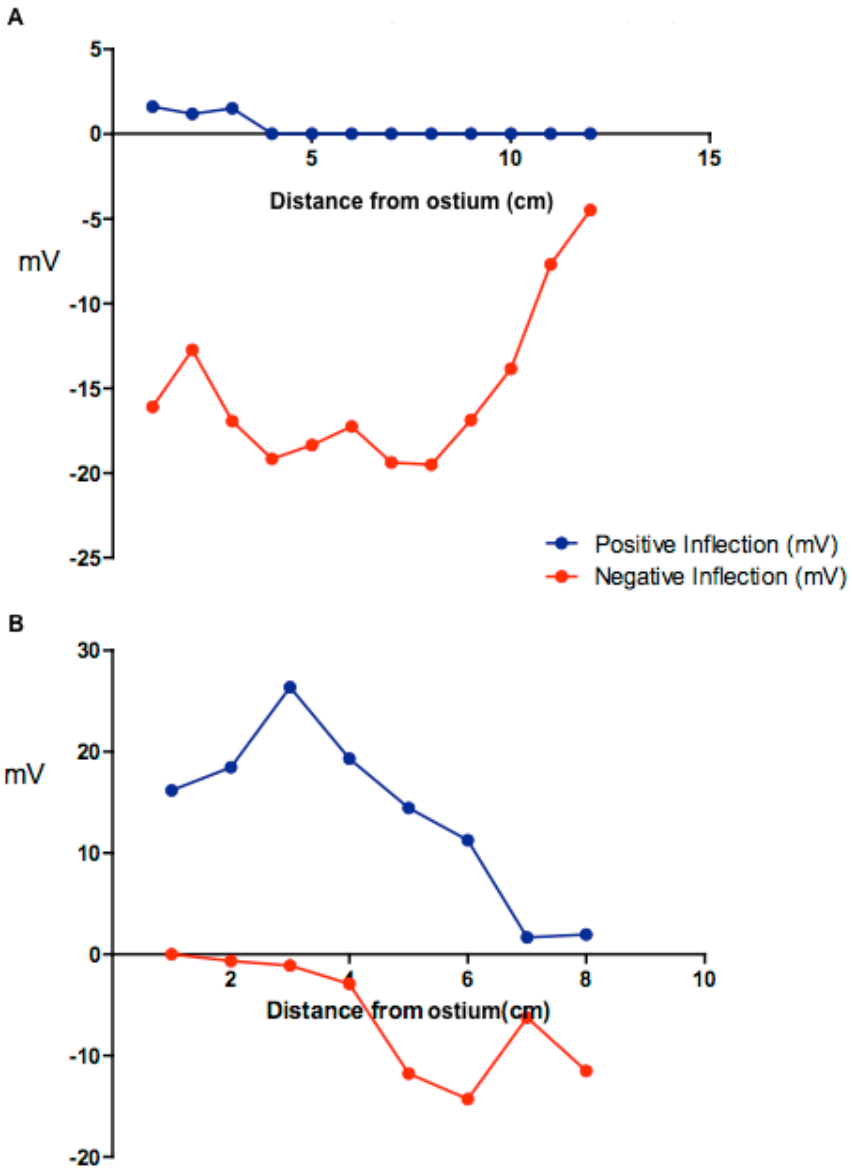

Figure 77: *Graduated pull-back of unipolar trans-coronary electrogram. A – infarct-related LAD vessel, showing diminished overall amplitude, with a marked reduction in positive inflection and a 'step-down' in the negative, and therefore peak-to-peak amplitude in the distal portion of the vessel. B –Reference Cx vessel; Largest peak-to-peak amplitude at the proximal portion of the vessel, but distal peak-to-peak amplitude >13mV.*

Infarct related artery versus reference vessel unipolar voltages

There was a trend of increasing amplitude of TCM electrograms obtained within the patient matched reference vessels, which were sub-tending non-infarcted myocardium (Figure 78). Significant differences in amplitudes were seen when comparing the positive inflection (p=0.02) and peak-to-peak voltages (p=0.05) between IRA and reference vessels. No significant difference was seen with the negative inflection, though a trend of increasing amplitude was also observed (p=0.40).

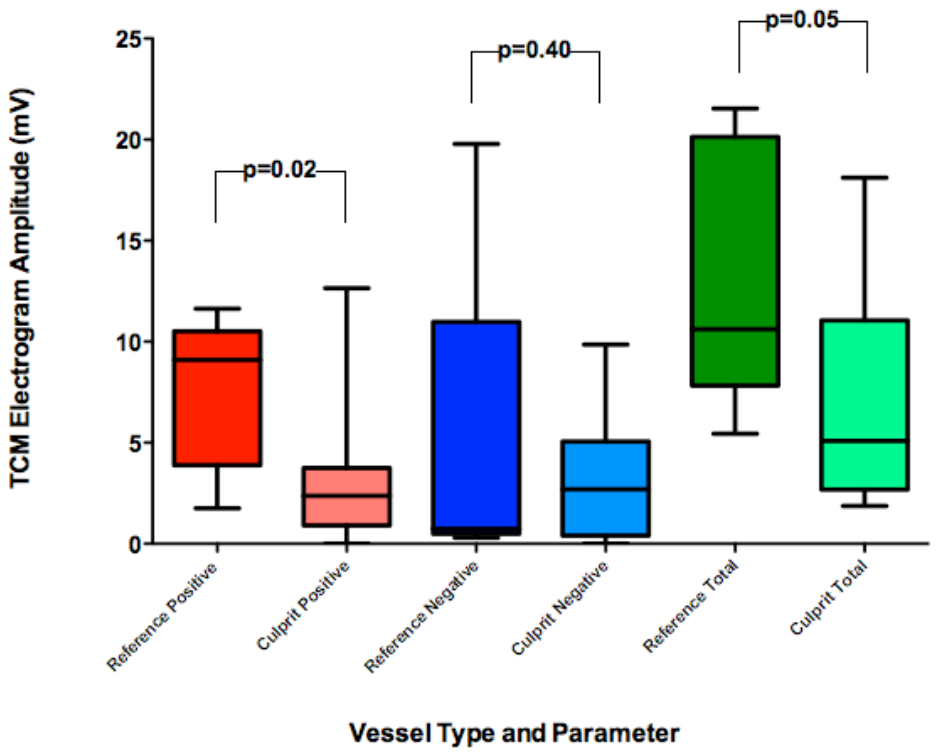

Figure 78: *Reference Vessel versus Infarct-related artery Trans-coronary electrogram; Red – positive inflection; Blue – negative inflection; Green – peak-to-peak*

When considering the voltages of the reference vessels, subtending non-infarcted tissue, there are likely to be systematic variations between voltages in the three main epicardial arteries. The peak-to-peak amplitudes were significantly greater in the reference LAD vessels compared to the RCA (13.2±6.1 vs. 11.1±3.7 mV, p=0.02), but no difference observed between Cx (12.3±5.6 mV, p=0.18).

4.1.6 DISCUSSION

This study has shown the feasibility of using the novel trans-coronary electrogram mapping technique in the assessment of myocardial infarction. Furthermore, the study indicates that the electrical gradient within an epicardial vessel predicts both severity of infarction and also area at risk, identified by late gadolinium enhancement and T2-weighted oedema CMR imaging respectively. The technique may provide an electrical surrogate of myocardial viability that can be obtained during cardiac catheterization.

Feasibility of Epicardial Electrogram assessment of myocardial infarction

The ability to prospectively risk stratify patients following myocardial infarction is paramount to optimization of outcome. The concept of utilizing the electrophysiological alterations that occur following myocardial infarction to clinically risk stratify patients during percutaneous coronary intervention, would allow a 'real-time' adjunct in the assessment of viability. The current study has provided a validation of the methodology and technique used in obtaining epicardial electrograms during PCI through trans-coronary unipolar mapping, demonstrating

successful translation of a concept initially derived in animal models,[92] extrapolated to human endocardial electrical mapping[97] and subsequently to the current trans-coronary mapping technique. All patients that underwent trans-coronary mapping completed the protocol, with no adverse events secondary to the procedure. Additionally, the traces obtained from the study were of good standard with adequate diagnostic quality. Further developmental work is required to refine the technique, the collection of a greater intensity of data points per vessel to increase the electro-spatial resolution, as presented in the sub-group of patients in this study, is likely to yield an improvement understanding of the electrical-myocardial interaction when interrogated using the trans-coroanry approach. Additional development of an automated 'pull-back' system, that would provide a more standardised measurement protocol.

Epicardial Electrogram gradients

Following acute coronary syndrome coronary revascularization leads to an improvement in regional wall motion, which is typically identified through non-invasive imaging such as echocardiography,[213, 214] however the electrogram amplitude observed through endocardial mapping has previously been suggested as a parameter that can identify myocardial viability, invasively.[94-96] Whilst the endocardial approach provides a detailed three-dimensional source of electro-mechanical mapping, performing this during routine PCI is not logistically feasible and includes the acquisition of additional femoral arterial vascular access. Valhaus et al[101] provided a seminal demonstration of the relationship of epicardial electrical activity with myocardial function, in the setting of patients undergoing coronary artery bypass grafting (CABG). This study using a specially designed 'jacket' of bipolar electrodes, placed on

the epicardial surface of the heart intra-operatively, observing that increased epicardial electrical activity corresponded with echocardiographic improvement in regional ventricular function 3-10 months following the procedure. Whilst this highlighted the validity of using epicardial rather than endocardial electrical activity as a marker of myocardial fucntion, it did not provide a method of performing such an assessment during routine percutaneous revascularization procedures. Subsequently, Segal et al[106], adapted an angioplasty guide-wire, in addition with a temporary pacing wire placed in the inferior vena cava to create a unipolar electrogram from within the epicardial coronary vessel; using this to assess regions of epicardial scar to identify potential scar substrate for ventricular arrhythmias during ablation procedures. The current study extended this technique to be used in the PCI setting, following ACS. Whilst focal electrograms obtained within the IRA epicardial vessel were not representative of infarction, the change in electrical activity between the distal third and middle third of the vessel, corresponded to both infarct and area at risk estimation. This electrical 'gradient' within an epicardial vessel may provide a more robust electrophysiological marker of infarction, as this marker intrinsically includes the electro-mechanical relationship with the underlying myocardial mass being interrogated through the coronary vessel. Furthermore, rather than using the maxima or minima in voltage, the area of the electrogram, a function of both electrical voltage and duration, was shown to be more accurate in determining the CMR indices of infarction in our study, and may provide a more complete electrical indicator of function.

Unipolar Voltage mapping - limited field of view

Previous demonstration by Hutchinson et al,[215] using a direct pericardial approach to assess the ability of unipolar voltages determining regions of scar in comparison with bipolar voltage suggested that a low unipolar voltage (<8.27mV) was predictive in 61% of cases of endocardial scar demonstrated by bipolar voltage mapping. However, the field of view of unipolar voltage mapping may be less than previously estimated, with recent demonstration by Piers et al[216] in a cohort of non-ischaemic cardiomyopathy patients, that unipolar voltages may not be reliable in determining sub-endocardial scar, though intra-mural scar was reliably indentified, suggesting that in an ischaemic population, larger infarcts may be more likely to correlate with the TCM technique. Though, the more homogenous scar present following infarction, compared to fibrotic, inhomogeneous scar observed in the non-ischaemic setting may have reduced the accuracy of the epicardial technique further. Therefore, further investigation is required to definitively assess the field of view unipolar voltages provide.

Infarcted versus normal myocardial epicardial electrograms

There are numerous electrophysiological alterations that occur following myocardial infarction, including a decrease in action potential amplitude and duration, diminution of the resting membrane potential and a reduction in the rate of depolarization.[85-87] In addition as a result of structural cellular dysfunction, there is the uncoupling of intra-cellular gap junctions. This study provided the first demonstration of direct, within patient, comparison of the epicardial electrical activity obtained via a trans-coronary approach in epicardial arteries subtending both infarcted and non-infarcted myocardium. The peak-to-peak

amplitudes of the IRA were significantly diminished compared to the reference vessel electrograms, reaffirming the electrical changes that are heralded by an ischaemic insult and subsequent infarction. Whilst this demonstration is in a small cohort of patients, the ability to differentiate infracted from non-infarcted myocardium has important potential clinical implications. Current revascularization practice focuses on treatment of the IRA, a technique which could differentiate which myocardial territories had suffered an acute insult, would aid risk stratification and individualisation of therapy. Furthermore, significant differences between the LAD and RCA voltages obtained from non-infarcted, reference vessels were observed, suggesting that the degree of electrical activity may be dependent on the myocardial mass subtended by the artery. A greater understanding about the normal trans-coronary epicardial electrophysiology is required to be able to accurate and reproducibly compare to infarct zone arteries.

4.1.7 LIMITATIONS

This was a small, single centre study but is the first in human study to examine the relationship and effects of recent myocardial infarction on epicardial electrogram activity via a novel trans-coronary electrogram mapping method. Despite being a cross-sectional study, patients with prior MI, and those with CMR signs suggestive of non-ischemic myocardial disease or valvular heart disease were excluded, to minimise confounders. Although methodically feasibility was demonstrated, the TCM technique employed uses unipolar electrogram activity, rather than the more spatially specific bipolar electrogram. Current technological limitations prevent adopting the more accurate electrical signal in TCM. Moreover, the myocardium has a continuously changing wall thickness from base to apex[217]

which provides a diverse expression of electrical physiology on the epicardium. Therefore TCM morphology may differ between major coronary arteries, and direct comparison of diseased culprit vessels with healthy reference vessels as done in this study can pose significant bias. Additionally, patients recruited in to the study had relatively small degrees of infarction, with a modest mean LGE derived infarct mass of 7.2% of total myocardium. Therefore the TCM's performed within this study were subjected to testing at high sensitivities, compounding the risk of type 2 errors and potentially diluting the technique's ability to distinguish between infarcted and non-infarcted myocardium. Finally, the voltage analysis performed in the current study was limited to parameters related to the duration and amplitude of the electrograms, a more detailed analysis of the variations in electrogram morphology,[216] performed at higher processing speeds may provide an improved epicardial assessment of myocardial infarction.

4.1.8 FUTURE WORK

One of the limitations of the current method is the inability to directly correlate the position within the vessel with the location on the epicardial surface. Contemporary endocardial mapping systems, have the advantage of providing a three dimensional model to enable clear delineation of the infarct zone. Future work would consist of increasing the standardization of the TCM methodology by developing a automated 'pull-back' device and in conjunction with this develop a method of co-registering this angiographically obtained trans-coronary electrogram data with CMR cine or late-gadolium enhancement scar imaging; improved accuracy and precision, in addition to providing a more individualized diagnostic technique. Moreover, as the nature of epicardial unipolar voltages remains incompletely understood, significant inter- and intra-patient differences are likely to be present, therefore

a ‘library’ of normal reference vessel voltage maps will be collected to understand potential trends that may be present, providing greater insight when comparing with infarct zone voltage maps.

4.1.9 CONCLUSION

Trans-coronary electrogram mapping during PCI is technically feasible and may provide an electrophysiological marker of viability, during cardiac catheterization. There is a reducing gradient in unipolar voltage, within the epicardial vessel, which is in proportion with both infarct size and oedematous mass, identified with late-gadolinium enhancement and T2-weighted CMR imaging. Further prospective investigation in to development of the technique and determining its clinical accuracy is required to confirm these findings.

5. SYNTHESIS

The purpose of this synthesis is to summarize the major findings and implications of the studies that are presented in this thesis.

5.1 Aims of this Thesis

Ischaemic stress causes a number of deleterious affects on myocardial function, which are primarily governed by the interaction with the microcirculation. Technological advancements have allowed an increased understanding of the haemodynamic and functional adaptations that occur at the microvascular and myocyte level. The aim of this thesis was to examine the physiological adaptations that occur following infarction on micrvascular haemodynamics and electrophysiological alterations in dysfunctional myocardium.

The experimental models used to interrogate the microcirculation in this thesis were based upon invasive physiological measurements, as previous understanding of the microcirculation has been as a result of work performed in a variety of animal or non-invasive models.[218-220] The *in vivo* simultaneous pressure-flow assessment during PCI represents a unique model in the haemodynamic assessment of the coronary and microcirculation. Furthermore, to delineate the haemodynamic alterations that may occur with left ventricular dysfunction, a spectrum of patients were assessed; from those with acute myocardial infarction to a subset with chronic myocardial infarction, whose haemodynamics were augmented by intra-aortic balloon counterpulsation therapy. The

novel mathematical model of wave intensity anlaysis in these settings was adopted for the first time, with comparison of these wave energy indices with clinically relevant markers of infarct size and ventricular function assessed by cardiac magnetic resonance.

Myocardial electrophysiology was investigated through a novel trans-coronary electrogram method of perfoming a unipolar voltage map from within the epicardial coronary vessel, in a cohort of patients who were undergoing percutaneous revascularization for acute myocardial infarction. This study assesses the potential utility of an invasive marker of myocardial infarction and viability, through an adaptation of the coronary guidewire to produce a unipolar electrogram.

5.2 Summary of Main Findings

5.2.1 Wave energy in acute coronary syndromes

Phasic interrogation of the coronary microcirculation with the use of wave intensity analysis, following myocardial infarction has not previously been performed. Using this novel mathematical model, the nature of energy transfer within the coronary circulation was determined. This study showed that the energy emanating specifically from the microcirculatory-end of the circulation was impeded by myocardial infarction. Two important observations were made; the first was that there was an inversely proportional reduction in microcirculatory energy with increasing infarct size, identified by both Troponin T biomarker and late-gadolinium enhancement cardiac MRI analysis. The second was that the microcirculatory energy was an accurate predictor of regional myocardial recovery three-months following percutaneous coronary revascularization. The findings suggest that

WIA may provide a more detailed and integrated assessment of myocardial function and coronary vascular haemodynamics. The results from this study reinforce the concept that the microcirculation is a hugely important element in the integrity of myocardial function, with the strength of the relationship between the microcirculatory energy parameters and the markers of infarct size re-emphasizing the synergy between the microcirculation and the myocardium.

5.2.2 Coronary and Microvascular Phsyiology during intra-aortic balloon counterpulsation

Intra-aortic balloon counterpulsation is the most commonly utilized mechanical assisst device during percutnaeous revascularization procedures. The ability to augment diastolic coronary pressure has been the mainstay in the physiological basis for the devices' utilization. However recent clinical trials have questioned the efficacy of the device in common clinical scenarios.[170, 171, 221] The interaction of the haemostatic coronary autoregulatory function on the device and its resultant efficacy has not previously been investigated, particularly with contemporary invasive physiological assessment methods adopted in this thesis. Wave intensity analysis provided the first demonstration of the effect of balloon inflation in diastole on coronary wave energy, by causing an acceleratory, aorta-originating (forward) compression wave. During adenosine-induced hyperaemia, innate autoregulation is modulated, mimicking an ischaemic response. In this experimental condition, the magnitude of the wave energy derived by balloon inflation related proportionately to the increase in coronary flow velocity. Importantly, however, during, basal conditions, in the presence of a functioning autoregulation, no such relationship was observed, with the inference that the interaction of the device and microvascular

haemodynamics mitigates the expected increase in flow. Further investigation using pulse wave and mean-derived indices, suggest that during basal conditions, the increased coronary pressure conferred by balloon inflation leads to an increase in microvascular resistance, resulting in a minimal change in net coronary flow velocity. This study has provided the rationale for why the device has limited efficacy when used routinely in patients whose physiology remains within the functioning autoregulatory range, and provides insight into the potential focused use of the device in those in the extreme-end of the physiological spectrum.

5.2.3 Impact of Coronary wave speed

The mathematical solution that wave intensity analysis is based upon relies on appreciation of the coronary wave speed. Previous use of wave intensity used the assumptions inherent in the single-point estimate of wave speed, validated within the aorta by Davies et al.[158] Definitive assessment of directly measured, 'foot-to-foot' coronary wave speed has not previously been performed, and no comparison has been made with this and the currently widely used single-point method. Through adaptation of coronary guiding catheter equipment, and with the use of a high fidelity pressure in addition to a dual sensor pressure-flow guidewire were used to perform the first direct comparison of the measured and single-point method. This showed that during baseline conditions, the two methods provided equivalent results, however, wave speed estimate using the single-point was erroneous during hyperaemic conditions. This study also provided an insight into how coronary wave speed behaves during altering transmural pressure and under different pharmacologic conditions. Importantly for on-going work in this field, the study identified that single-point

wave speed at baseline was numerically equivalent to the directly measured hyperaemic wave speed, therefore, the baseline single-point estimate can be used and extrapolated to other conditions, without effecting the separated wave intensity analysis.

5.2.4 Trans-coronary Electrogram Mapping during Percutaneous Coronary Intervention: A Novel Electrophysiological Assessment of Myocardial Infarction

The electrophysiological alterations that occur following myocardial infarction provide a unique facet for assessing myocardial viability. However, invasive interrogation of electrical parameters during percutaneous intervention is not currently available. This study developed a trans-coronary unipolar voltage mapping (TCM) technique that was performed successfully in all patients recruited to the study, with, a subset, undergoing comparison with to late-gadolinium enhancement cardiac MRI scar imaging. The current results suggest there are recurring differences between infarcted and normal myocardial tissue, with regard to peak-to-peak amplitude and area of electrograms in the infarct-related vessel. The study suggests that TCM's is feasible, and with further development of the data analysis, may yield a dynamic, and spatially referenced marker of infarction and viability. On-going work regarding how epicardial voltages correlate with the reference standard, endocardial mapping, will provide further insights into the pathophysiological relationship between epi- and endo-cardial electromechanical function.

5.3 Conclusion

The affects of ischaemia and infarction on microvascular haemodynamics and myocardial functional integrity have been explored in this thesis with a number of varied clinical experiements. Wave energetics has been shown to provide an integrated marker of microvasular haemodyanmics and myocardial function, with the microcirculatory derived waves relating closely with the severity of myocardial infarction, being predictive of regional ventricular recovery. The importance of the microcirculation in its interaction with mechanical assist devices has been highlighted with the absence of a significant augmentation of coronary flow velocity with intra-aortic balloon counterpulsation in the presence of functioning autoregulation. The methods surrounding calculation of coronary wave speed, an important determinant of separated wave energy in wave intensity analysis, was investigated, showing the limitations of the single-point estimate of wave speed. Finally trans-coronary voltage mapping, was developed and seen to be technically feasible during PCI, though further work is required to understand the unique electrograms obtained through this method of epicardial voltage mapping.

6 . FUSION OF TRANS-CORONARY EPICARDIAL AND ENDOCARDIAL ELECTROGRAMS WITH THREE-DIMENSIONAL 3 TESLA CMR SCAR IMAGING - A FEASIBILITY STUDY

Kalpa De Silva[1], Michael Truong[2], Radomir Chabiniok[2], Markus Henningsson[2], Kawal Rhode[2], Rene Botnar[2], Matthew Wright[1], Michael Cooklin[1], Jaswinder Gill[1], Simon Redwood[1], Sven Plein[2,3], Divaka Perera[1]

Affiliations:

[1] King's College London BHF Centre of Excellence, NIHR Biomedical Research Centre at Guy's and St. Thomas' NHS Foundation Trust, Cardiovascular Division, The Rayne Institute, London, UK

[2] King's College London BHF Centre of Excellence, NIHR Biomedical Research Centre and Welcome Trust and EPSRC Medical Engineering Centre at Guy's and St. Thomas' NHS Foundation Trust, Division of Imaging Sciences, The Rayne Institute, London, UK

[3]Multidisciplinary Cardiovascular Research Centre, Leeds Institute of Genetics, Health and Therapeutics University of Leeds, Leeds, UK.

6.1 ABSTRACT

BACKGROUND

Revascularisation of coronary artery disease (CAD) is only beneficial if myocardium subtended by the diseased epicardial artery is viable. Viability assessment is poorly undertaken and can only be performed via non-invasive techniques prior to revascularisation. At present there is no method of 'on-table' assessment in the cardiac catheterisation labababrotory in those undergoing percutaneous coronary intervention (PCI). The aim of this study was to assess the feasibility of correlating the novel technique of trans-coronary electrogram mapping (TCM) during PCI to the reference standard of endocardial electro-anatomical mapping, whilst uniquely fusing and overlaying this data with 3D cardiac magnetic resonance (CMR) scar imaging.

METHODS

Four patients, with ischaemic cardiomyopathy, undergoing eldctive PCI for stable angina were recruited. Each had a pre-procedural 3-Tesla CMR scan; with acquisition of steady state free-precession cine imaging, a navigated free-breathing coronary-enhanced sequence and a 3D whole heart late-gadolinium-enhancement scar sequence; assessing myocardial recruitment and viability, gross coronary anatomy and delineating scar severity, respectively. TCM were obtained post-PCI, using a routine intra-coronary angioplasty guide-wire with a non-inflated over-the-wire balloon insulating the length of the wire except the distal 5mm and temporary pacing wire (placed in the inferior vena cava, acting as an indifferent electrode), creating unipolar electrograms captured on the integrated Siemans SENSIS integrated electrophysiology monitoring system. CARTO endocardial mapping was then

performed to allow correlation with the TCM measurements. The datasets were fused and volume-rendered to simultaneously display coronary anatomy, myocardial scar and epi- and endo-cardial unipolar electrograms.

RESULTS

Mean age was 61 ± 12 years. The tri-phase, CMR, TCM and CARTO, protocol was completed in all cases. The CMR confirmed viability was present in the intended revascularization territory with proximal- and mid-coronary artery anatomy identifiable in all cases. There was a electrical correlation between the endocardial and epicardial identified scar regions in the three-dimensional rendered ventricular cavity, in terms of unipolar electrical activity identified by the two modalities.

CONCLUSION

Fused volume rendered three-dimensional myocardial scar and coronary imaging is clinically feasible and allows the anatomical distribution of the coronary anatomy to be understood on an individual basis. This may be valuable in the planning and optimizing of PCI procedures.

Key words

Co-registration; data fusion; trans-coronary electrogram mapping; CARTO mapping; myocardial scar; CMR

6.2 INTRODUCTION

The utility of integrated imaging and interventional systems

Patients with impairment of left ventricular function often undergo PCI, aiming to improve regional and global systolic performance.[31, 137] Three-dimensional vascular imaging, particularly with the use of Computed Tomography (CT) imaging, has been shown to be of value in identifying potential arterial targets.[222, 223] However, imaging of the vascular supply alone is insufficient in determining the suitability for revascularization, and is reliant on the presence and severity of myocardial scar. The presence of viability is of paramount importance in deciding whether revascularization therapy is appropriate in these circumstances. Transmural scar in myocardial segments subtended by the disease vessel mitigates the benefit of revascularization.[26, 62] Therefore whilst anatomic information about the coronary artery may assist in identifying an appropriate target for revascularisation, the integrity of the underlying myocardial tissue must also be considered. Angiographic examination allows a two-dimensional assessment of the coronary anatomy, which remains the gold-standard method of detecting coronary disease, but does not provide information regarding the underlying myocardium. Therefore, a method to integrate x-ray angiography with high resolution imaging modalities would be of great research and clinical significance.

Three-dimensional CMR Fused with X-ray Coronary Angiography

There has been much research to augment X-ray fluoroscopy by overlaying better soft-tissue-contrast 3D information of the heart using 2D-3D image registration.[224-227] A pre-calibrated hybrid X-ray/MR system can achieve registration within an accuracy of 5 mm;[224]

however, these systems are not widely available outside research environments. Surrogate structures such as fiducial skin markers (Figure 79), visible in both X-ray and the 3D modality, provide another means of registration.[225] However, accuracy of this technique may be compromised as the relative position between the markers and the heart may change throughout the cardiac and respiratory cycles that may lead to some inaccuracies in the registration.

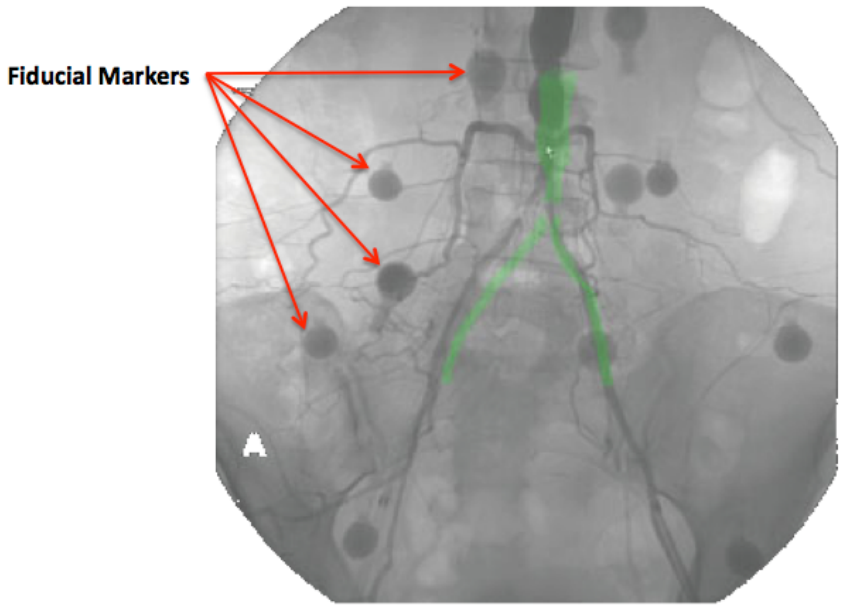

Figure 79: *Fiducial Marker based approach of X-ray-CMR co-registration – with MRI derived overlay shown in green. (Adapted from Gutiérrez et al)*[225]

Both of these issues could be avoided if registration was achieved by using features of the heart itself, or of devices placed inside it such as catheters or wires. Sra et al[228] was the first to propose using the catheters placed inside the heart for registration. This was in the context of electrophysiology studies performed for atrial fibrillation ablation procedures. It represented an attractive method of using catheters that were part of the procedure, as the constraint for registration. As the catheters and wires placed in vessels of the heart remain in situ throughout the procedure, to enable continuous electrical data collection, this

provided the ideal internal reference point for registration. This registration process was performed by first projecting the coronary sinus (CS) segmented from CT onto the fluoroscopy, and then matching the centreline of the projected vessel to a CS catheter in 2D. For the purpose of the current study, to avoid out-of-plane translation errors associated with projections, Truong et al[229, 230] performed the registration process in three-dimensions with the inclusion of a catheter reconstruction step. Briefly, a 2D to 3D image registration method has been developed, to consolidate the advantages of both modalities by overlaying the 3D images onto the fluoroscopy by using the guidewires placed in the coronary arteries of the heart, as positional markers. Conceptually, 2D-3D image registration takes 3D information and overlays it onto the X-ray image. Registration of X-ray-CMR images requires that the relationship between the patient's positions while in the MR scanner and when on the X-ray table is known. The images acquired are cardiac and respiratory gated in both modalities, and it is assumed that the heart returns to the same shape at the same phase and therefore is mathematically described as a *rigid-body transformation*; schematically this consists of a rotation and translation, followed by a perspective projection (Figure 80).

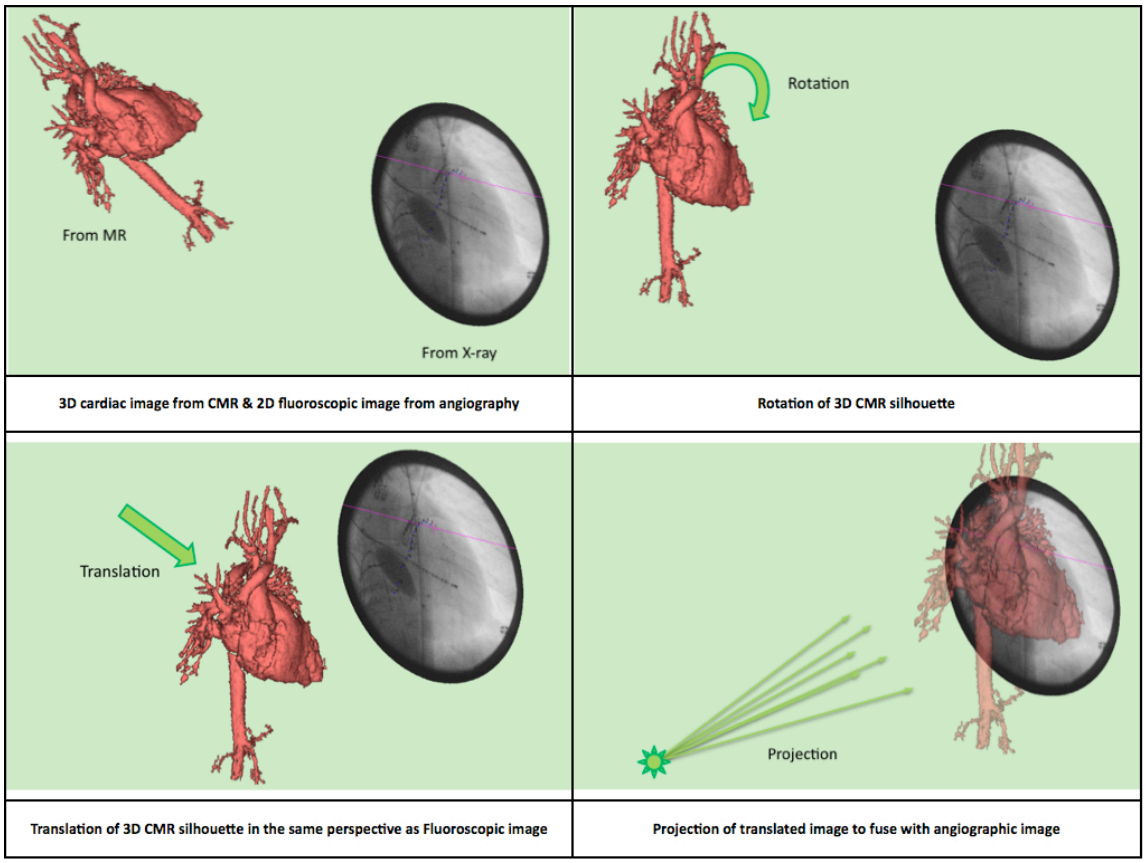

***Figure 80**: Concept of Developing a 2D to 3D fused dataset – using the Rigid-Body Transformation Method; The CMR data is rotated, translated and then projected on to the fluoroscopic X-ray image.*

To achieve registration, Truong et al[229] have developed an automatic global-fit algorithm which minimizes the root-mean-square distance error of the wire to the medial line of its respective vessel. Data has previously been processed for clinical cases in venous system, such as those undergoing pacemaker implantation, with accurate registration, validated by visual inspection (Figure 81).

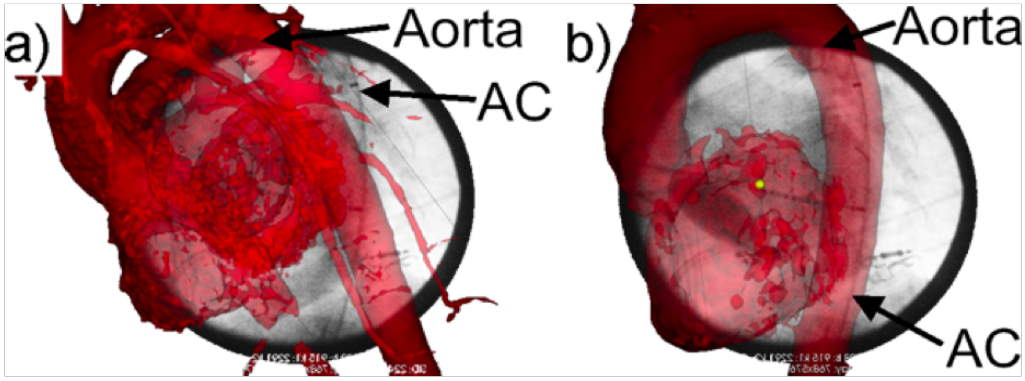

Figure 81: *a) Model of the heart (red) overlaid on the x-ray using the Coronary sinus catheter to constrain the registration, but is misaligned. b) Both the CS and aortic catheter (AC)/vessel pairs are then used, resulting in a more accurate registration.*

Trans-coronary Electrogram & CARTO ™ Endocardial Mapping Fused with CMR

We have demonstrated the technical feasibility of Trans-coronary electrogram mapping (TCM) measurements during PCI, as a potential method of assessing myocardial viability (Chapter 4). However, whilst TCM provides a spatially mapped measure of viability within an epicardial vessel, it remains unclear how this correlates anatomically with other imaging modalities. Furthermore, endocardial mapping provides the reference standard in electrical mapping of the ventricular cavity, and represents an accurate and reproducible method of assessing infarct related diminution in electrical activity. The relationship between epicardial and endocardial electrogram activity has not previously been established, and this study aims to assess this association. Cardiac MRI (CMR) provides the most detailed mode of infarction assessment, with late-gadolinium enhancement being the most utilized technique in this scenario. The ability to correlate the invasively obtained endo- and epi-cardial electrogram maps with the high spatial resolution infarction assessment provided by CMR

would allow greater understanding of the electro-mechanical relationship in the myocardium following myocardial infarction.

6.3 AIMS

The aim of this study was to assess the correlation between TCM and two distinct reference standards for scar, namely endocardial electro-anatomical non-contact mapping (CARTO™, Biosense Webster, USA) and LGE-CMR. The study also assesses the feasibility of providing spatially matched datasets simultaneously displaying coronary anatomy, myocardial scar and epi- and endo-cardial unipolar electrograms, through x-ray angiography (with TCM), 3-dimensional (3D) CMR, and CARTO mapping (Figure 82).

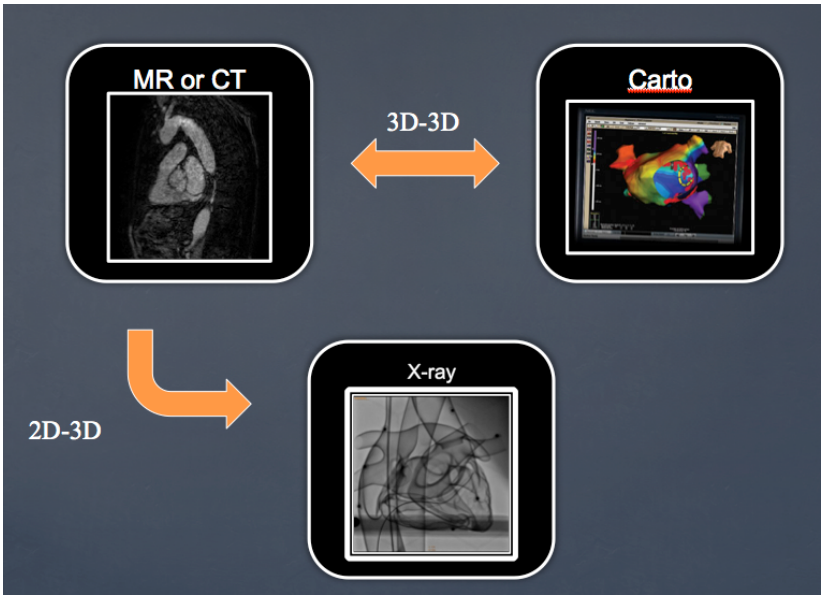

Figure 82: *Planned data fusion modalities*

6.4 STUDY DESIGN

6.4.1 Inclusion Criteria

Patients scheduled to undergo planned coronary angiography and revascularization for stable angina, with impaired LV function (LVEF ≤40%) secondary to prior myocardial infarction were recruited. Figure 83 shows the study data acquisition stream.

6.4.2 Exclusion Criteria

Patients were not considered for recruitment if a prior diagnosis of significant (>moderate) valvular disease had been made. Additional exclusions were if persistent intra-procedural arrhythmias or hemodynamic instability occurred. Patients with contraindications to CMR at study entry, such as pacemakers, implantable defibrillators, claustrophobia, or metallic intracranial implants, were also excluded.

6.4.3 Ethical Approval

The study protocol was approved by the institutional research ethics committee (REC ref 09/H0804/75). All participants were provided with an information sheet detailing the study protocol prior to obtaining informed consent.

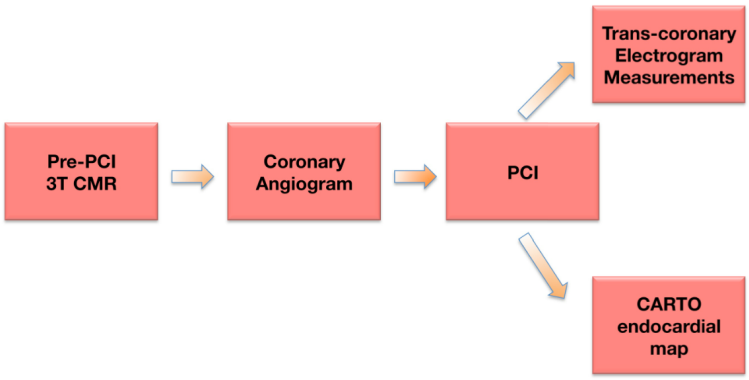

Figure 83: *Data Acquisition Stream*

6.4.4 Cardiac Magnetic Resonance Imaging

CMR studies were performed prior to admission for the planned PCI. The scans were performed on a 3 Tesla cardiac MRI scanner (Achieva, Phillips Healthcare, Best, Netherlands) equipped with dual-RF transmission technology and a 32-channel phase array body coil. Cine images were acquired using a standard steady state free precession (SSFP) cine technique in two-, three- and four-chamber orientations and in a left-ventricular (LV) short-axis stack covering the LV from apex to base. The acquisition pulse sequence provided a typical spatial resolution of 1.5 x 1.7 x 8 mm with a 2mm inter-slice gap and a temporal resolution of 40 frames per second. A 3D whole-heart, inversion-recovery gradient echo pulse sequence with a respiratory navigator pulse placed over the diaphragm was used to obtain both an early (coronary-enhanced) and late (scar-enhanced) dataset. Fat suppression was used to minimise pericardial fat signal. A 3D whole heart stack of images Late gadolinium enhanced (LGE) sequence was acquired was performed using an inversion recovery fast gradient echo sequence 10 min after the intravenous administration of 0.2 mmol/kg body weight of gadobutrol (Gadovist, Bayer Schering Pharma, Berlin, Germany). LGE acquisition was guided by a Look-Locker sequence with a typical pre-pulse delay of 200-330ms.

6.4.5 Cardiac catheterization, trans-coronary electrogram and CARTO mapping

All patients where given loading doses of aspirin (300mg) and clopidogrel (600mg) as per standard clinical practice, prior to coronary intervention. IV unfractionated heparin was given at the start of the procedure (70 IU/kg), with the activated clotting time (ACT) measured every 20 minutes, being maintained at ≥250 seconds for the duration of the procedure.

Cardiac Catheter Laboratory Set-up

After the patient is placed on the catheter laboratory table, a CARTO magnetic patch is placed on the back of the supine patient. The X-ray fluoroscopic C-arm is positioned over chest iso-centred between the x-ray tube and the detector. Coronary angiography was performed through an 8F sheath via a femoral artery approach. A 7F venous sheath was placed in the femoral vein at the outset of the procedure, to be used for the temporary wire (TPW) placed in the inferior vena cava, acting as the indifferent electrode for trans-coronary electrogram mapping to be performed. 0.5mg-1mg intracoronary nitroglycerin was administered as per routine practice after selective intubation of each coronary system, to reduce the effect of coronary vasospasm. Coronary angiography was performed according to the following standard fluoroscopic views; posterior-anterior (PA) view, left anterior oblique (LAO) cranial, right anterior oblique (RAO) cranial, RAO caudal and LAO caudal. The method and extent of PCI was at the discretion of the operator, including type of stent (BMS or DES). Following completion of the PCI procedure, the x-ray table remains in a chosen fixed position, to ensure movement of the patient relative to the x-ray system is minimized,

decreasing potential inaccuracies when the co-registration process takes place. Trans-coronary electrogram mapping is performed, as described in chapter 4.1. Briefly, an uncoated angioplasty guide-wire, with an un-inflated over-the-wire balloon insulating the entire length except for the distal 5mm tip is placed in the distal target vessel. A TPW is placed sub-diaphragmatically in the IVC to complete the unipolar circuit. The wire is then sequentially withdrawn within the coronary artery, with continuous electrogram recordings being obtained. Each wire position was documented with a non-contrast enhanced fluroscopic acquisition in two orthogonal views e.g. PA and RAO caudal angles (Figure 84). Each x-ray sequence contained at least one respiratory cycle, enabling the diastolic phase to be captured in expiration, to allow the registration of angiographic data with CMR data; the latter is principally obtained in diastole.

Following completion of the TCM measurments, acquisition of the endocardial mapping points is performed in accordance with standard clinical practice. Briefly, the CARTO™ catheter is introduced into the arterial circulation via the 8F femoral sheath and retrogradely placed into the left ventricular cavity via the aortic valve. Endocardial electrical activation and voltage maps (set to unipolar setting) were constructed using approximately 80-100 recording points, focusing on region of prior infarction, and a region designated as a normal reference. Mapping points were obtained in the left ventricular outflow tract and aorta at the level of the sinus of valsalva/tubular-junction, to increase the spatial resolution for the registration process.

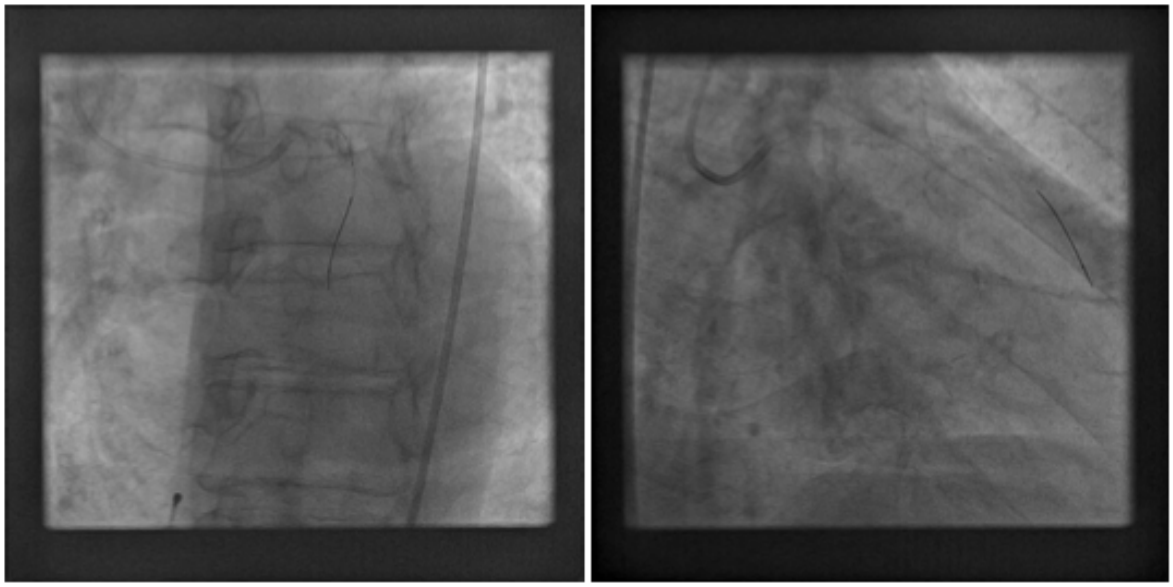

a) Posterior-anterior view of the left anterior descending (LAD) artery

b) Right anterior oblique view of the LAD

Figure 84: *Orthogonal angiographic views of the TCM guidewire, as part of the datset required for co-registration*

6.4.6 Data analysis

Registration workflow

The registration process is divided into three parts.[229] First, the coronary artery's medial line is extracted from CMR. Following this, the coronary guide-wire is reconstructed in 3D from a sequential biplane X-ray pair. Finally, a transformation that minimizes the root-mean-square (RMS) distance error between the medial line of the guide-wire and the catheter reconstruction. This transformation, combined with a calibrated and tracked X-ray system, allows the overall 2D-3D registration to be performed.

The co-registration of the angiographic data to both forms of electrophysiological data (the CARTO maps and the epicardial electrical mapping) was spatially registered by members of the Imaging Sciences Biomedical Engineering department (M Truong and K Rhode) using

their previously determined registration protocol. The development of the CMR sequences and the angiographic acquisition of the data during the interventional procedure was performed by myself. Endocardial mapping was performed by J Gill, M Wright and M Cooklin, whilst trans-coronary mapping was performed by D Perera and S Redwood.

CMR Analysis

Quantitative analysis was performed offline, by blinded observers, using dedicated CMR viewing software (CMR 42, Circle Cardiovascular Imaging, Calgary, Canada). The area of hyperenhancement was quantitatively determined using a previously described signal intensity method,[26, 138] where infarcted tissue is defined as an area of myocardium with LGE signal intensity greater than 5 S.D. Endo-epi-cardial contours were drawn (excluding papillary muscles) to derive total LV mass. Infarct mass was expressed as the absolute mass of infarcted tissue (in grams) and as the percentage of the total LV mass.

CMR Coronary Artery Segmentation

Coronary artery images obtained through the 3D navigated whole heart sequence were then manually segmented, using in-house segmentation software, Cardioclick, which was developed within the Biomedical Engineering department, KCL (Figure 85).

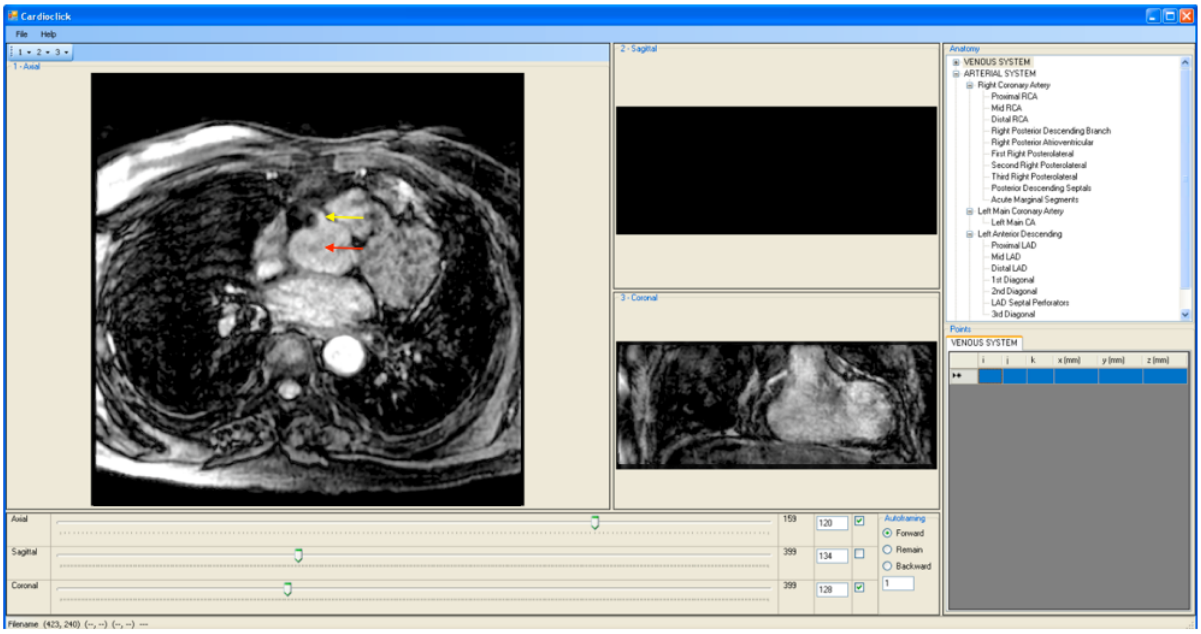

Figure 85: *A single slice from the Cardioclick coronary artery segmentation software – Enlarged image is the axial cross-sectional view. The red arrow indicating the aorta, and yellow arrow highlighting the ostium of the right coronary artery. A manually placed mark is placed in each slice identifying the location of the coronary artery being analysed (not seen in this image)*

This software allowed the coronary artery to be visually tracked in three planes, sagittal, axial and coronal views. Each point provides an x, y and z co-ordinate, which allows the path of arteries in the CMR sequence to be cross-referenced with that of the x-ray coronary angiogram, in the corresponding x, y and z planes, and can then be co-registered.[229]

6.5 RESULTS

BASELINE CHARACTERISTICS

Four patients (61 ± 12 years) completed the pre-procedural CMR and combined invasive electrical assessment with TCM epicardial and CARTO endocardial mapping. The mean left ventricular ejection fraction was 36±5%. Mean heart rate at the time of CMR was 69±12bpm, with all patients being in sinus rhythm. Quantitatively determined percentage diameter stenosis of the target vessel lesion was 81±13% (Table 14). The data presented below is from a single patient, graphically highlighting the process undertaken and the result of the fused data.

Variable	n
Age, Mean (±SD)	61 (12)
Clinical characteristics	
Male, n (%)	4 (100)
Hypertension, n (%)	3 (75)
Diabetes mellitus, n (%)	2 (50)
Hypercholesterolemia, n (%)	4 (100)
Smokers, n (%)	1 (25)
BMI[*] (kg/m²), Mean (±SD)	28 (3)
Prior MI[†], n (%)	4 (100)
Previous PCI[‡], n (%)	2 (50)
Peripheral Vascular Disease, n (%)	1 (25)
Quantified coronary angiography, % (±SD)	81 (13)
Cardiac MRI	
Sinus rhythm	4 (100)
Mean heart rate, bpm (±SD)	69(12)
Left ventricular Ejection Fraction, % (±SD)	36 (5)
LV end-diastolic volume, ml (±SD)	202 (104)
LV end-systolic volume, ml (±SD)	141 (84)
LV mass, g (±SD)	153 (62)
Total scar volume, % of of LV mass (±SD)	14 (11)

Table 14: Patient Characteristics

3D late-gadolinium enhancement imaging dataset

Figure 86 below shows a typical three dimensional whole heart LGE stack obtained on the 3 Tesla MRI scanner.

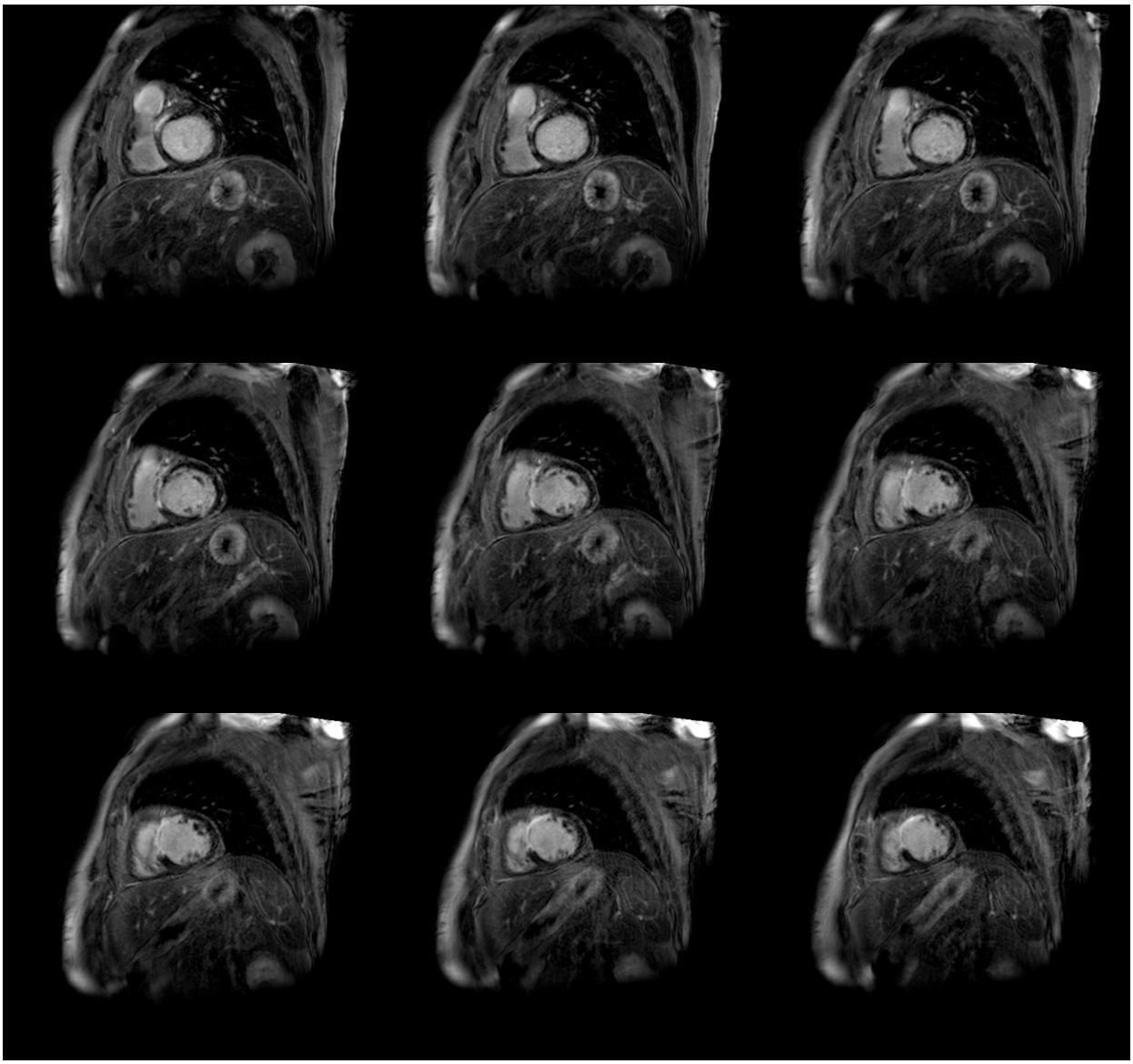

Figure 86: *Three-dimensional whole heart late-gadolinium enhancement imaging; Top row left – basal slices; middle row – mid-ventricular slices; bottom row – apical slices. Images depict a subendocardial infarctio in the basal anterior-septal wall, with transmural infarction in the mid-ventricular-apical slices. Viability of the basal anterior wall was confirmed with increased contractility with low-dose dobutamine stress.*

2D X-ray angiography -3D CMR ventricular co-registration

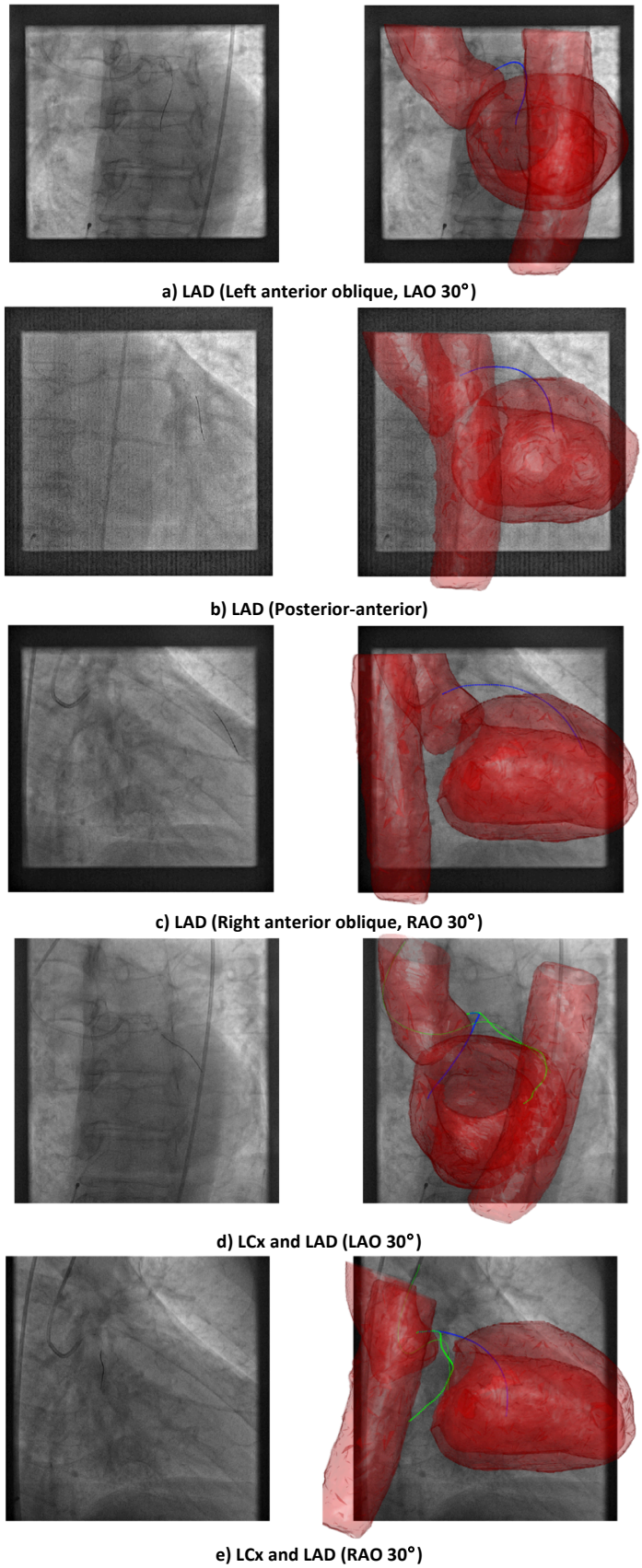

Figure 87: *2D X-ray -3D CMR ventricular modeling; Blue line demonstrating path of Left anterior descending artery and Green line-Circumflex vessel*

Trans-coronary epicardial map and CARTO endocardial map fused with CMR overlay

Figure 88 shows the final result in this case, with the unipolar voltages (mV) taken with CARTO™ and interpolated over the CMR endocardial surface using a principle-component-based 3D-3D registration algorithm. Trans-coronary epicardial electrogram unipolar voltages (mV), with spatial location reconstructed from X-ray and registered to the CMR segmentation using a catheter-based 2D-3D registration algorithm are overlayed on the image to demonstrate the relationship to the scar evident on CMR and CARTO. The anatomical surface of the epicardium (and the aorta) is represented by the light red shell structures, which was obtained via co-registration of x-ray angiogram with volume rendered CMR. The endocardial surface is represented by the dark red inner cavity. The areas identified by both LGE-CMR and endocardial voltage mapping are depicted in colour, varying according to the unipolar voltage observed via the endocardial method, with the range shown on the right of the image. The course of the coronary guidewire is shown by the blue dashed line, with the unipolar voltages obtained from each corresponding point shown above the acquisition point. Due to the limited number of endocardial points mapped, not all regions of infarction were mapped, giving an appearance of inhomongenous or discontinuous scar, which is contrary to the LGE images obtained in this case. The endocardial surface is predominantly dark red, representing a unipolar voltage of 12mV, which was used as the standard for the ventricular cavity, in the absence of data points to discern the exact value. However, the basal most epicardial voltage is 4mV, which corresponds with the 4-5mV observed via the endocardial approach. The apical epicardial electrogram is 7mV, which is comparable to the apical endocardial voltage of 8mV.

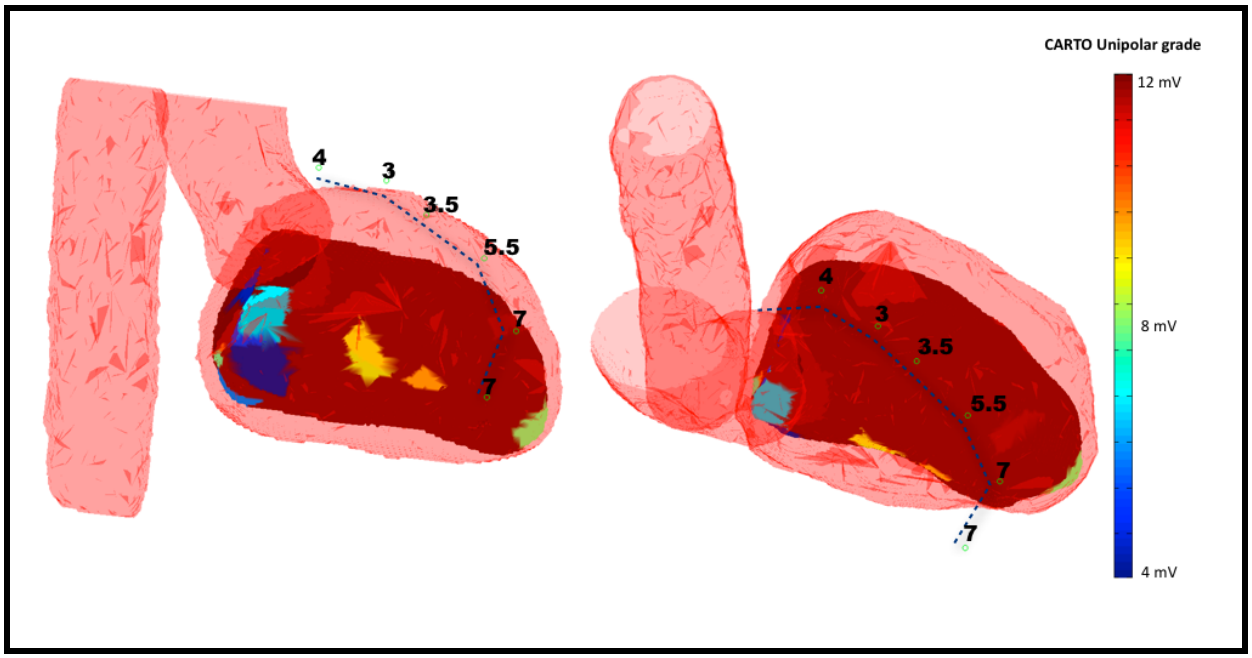

Figure 88: *TCM-CARTO-CMR overlay; TCM epicardial guide-wire position highlighted in dashed blue line, with corresponding voltages. CARTO derived scar map and unipolar voltage grading on right of image. Two orientations are shown in this fused overlay. The epicardial electrogram signals range from 4mV proximally (at the basal level of the myocardium) to 7mV*

6.6 DISCUSSION

This preliminary work suggests that accurate registration of clinical data from multiple sources can be achieved. However, further analysis and quantification of the results is required to determine the accuracy of the techniques employed in this study. The epicardial voltages obtained through trans-coronary mapping show a promising correlation with the endocardial mapped equivalent, in the single case analysed. The 2D-3D registration algorithm utilized in this study, combined with the tracked c-arm method may allow improved visualization of fluoroscopic guided cardiac catheterisation procedures.

Correlation of Trans-coronary epicardial and Endocardial Electrograms

The currently adopted trans-coronary electrogram mapping technique is limited in its electro-spatial resolution, as only focal points, rather than a cluster of data points, within the epicardial vessel are obtained. This limits the accuracy of the technique to precisely map the underlying epicardium, unlike the comparative endocardial method, which allows the operator to identify and readily demarcate the area of infarction by the variation of electrical activity.[107] However, the fused dataset demonstrated in this study shows there is likely to be a numerical correlation in unipolar voltages between the epicardial and endocardial modes of assessment.

The main detraction from the TCM method is the inability to define the exact anatomical location on the epicardial surface that is being interrogated. The fusion of LGE-CMR to this would greatly improve the methods accuracy, however, the dataset presented in this study, does not seem to show a visual anatomical congruence between the CMR identified scar and the spatial position of the coronary vessel, and the TCM guide-wire, despite the complex mathematical modelling performed. However, the numerical unipolar voltage values of the epicardial electrograms are similar to those obtained from the CARTO mapping system. Furthermore, the LGE-CMR in the case depicted suggested a large degree of transmural myocardial infarction in the anterior wall, which is reflected in the diminished nature of the electrogram activity observed through both modalities. Interestingly, the voltage range observed suggests that the myocardium is, in the main, non-viable, when related to previously demonstrated electromechanical studies, stating that myocardial unipolar voltages less than 8mV were unlikely to represent viable tissue.[94, 95, 231, 232] The average epicardial peak-to-peak voltage obtained in this case was 4.3mV, with a range of 4-12mV

from the CARTO endocardial method. Further analysis of the epicardial technique is required to determine whether the trend observed in this case is replicated, and whether it predicts viability, which will require assessment of regional ventricular function following revascularization.

Computational feasibility of co-registering data

One of the main assumptions made in the computational registration of data from various sources, is that the heart behaves in accordance to 'rigid-body dynamics'. Inaccuracies in the technique are likely to stem from the nature of the beating heart, in that it is a highly deformable structure which undergoes complex motion during each cardiac cycle. As such, any phase mismatches between the CMR and x-ray images may compromise accuracy. Moreover, the algorithm employed in this study assumes that the coronary guide-wire lies close to the medial line of the vessel which may not be hold true, particularly, in those vessels which have a large diameter. Furthermore, the effect of increasing numbers of wires or catheters on the registration process remains untested, and may deleteriously affect the accuracy of the process, which will need further evaluation. However, a combined three-dimensional imaging technique, spatially registering both myocardial scar and coronary anatomy may offer advantages for the planning of complex interventional procedures, particularly if these techniques could be developed to allow real-time, intra-procedural evaluation of the myocardium.

6.7 LIMITATIONS

The global-fit method of registration is a protracted, and labour intensive computational process, which is prone to sources of error that result from assumptions made in regard to the 'rigid-body' dynamics of the beating heart. Nonetheless, this study provides a platform for further development into the acquisition of this type of novel, individualised data. Additionally, navigated free breathing 3T MRA sequences, whilst previously tested on phantom models and in young healthy volunteers,[233, 234] do not currently provide a reproducible method of imaging the coronary tree with a high degree of spatial and temporal resolution, due to considerable variability in navigator accuracy, predominantly because of abnormal breathing patterns observed in patients with underlying cardiovascular pathology.

6.8 FUTURE WORK

This study represents a novel development in the interface between invasive and non-invasive diagnostic and therapeutic management of coronary revascularization. An important sub-set of patients, such as those with complex coronary anatomy and multiple regions of myocardial scar, would benefit from the ability to determine regions of viable and non-viable scar through an invasive electrophysiological parameter, such as trans-coronary mapping, whilst having the ability to accurately determine the exact regions of infarction through fusion of this data with the higher resolution CMR data.

Further work on the three remaining datasets that have been collected are to be analysed, with a view of developing a semi-quantitative method of analyzing anatomically correlation

of this merged data, by the use of coronary artery maps to plot the exact location in the epicardial vessel during angiography, and then, using a blind observer, do the same with during the MRA acquisition. Further work on the development of the methods outlined in this study will be undertaken to improve the robustness and efficiency of the technique. Specifically, in reference to the improvement of the MRA sequences used in the patient setting, as this is integral in the development of this body of work.

6.9 CONCLUSION

Fused volume rendered three-dimensional myocardial scar and coronary imaging is clinically feasible and allows the anatomical distribution of the coronary anatomy to be understood on an individual basis. This may be valuable for the planning PCI procedures when regionality of myocardial scar optimizes therapeutic success. Further investigation and development is required in assessing the accuracy of the computational co-registration technique applied in this study and also improved reproducibility of the magnetic resonance coronary angiography undertaken on a 3 Tesla magnet should be sought.

7. RESEARCH OUTPUTS RELATING TO THIS THESIS

Prizes

- **American College of Cardiology (ACC) Young Investigator Finalist (Physiology, Pathology, Pharmacology section) – '***Coronary Physiological Adaptations in the presence of Left ventricular dysfunction: Insights from Coronary Wave Intensity analysis*', San Francisco, March 2013
- **King's College London Graduate Research Showcase Oral Presentation Prize**; 'Utility of *Wave Intensity Analysis in Acute Coronary Syndromes'*, June 2011
- **1st Prize BHF Cardiovascular Division Postgraduate Symposium, Oral Presentation**; '*Wave Intensity Analysis in Acute Coronary Syndromes'*; King's College London, May 2011.

International Oral Presentations

- *Usefulness of Dynamic Coronary Signals in Ischaemic Heart Disease* - International Union of Physiological Sciences (IUPS) Satellite Symposium – Royal Dutch Academy of Sciences, Amsterdam, Netherland, July 2013.
- *Coronary Physiological Adaptations in the presence of Left ventricular dysfunction – a Wave Intensity analysis perspective*; ACC, San Francisco, USA, Mar 2013.
- *Can Wave Intensity Analysis Predict Infarct Size in Acute Coronary syndromes?;* AHA, Orlando, USA, Nov 2011.
- *Three-dimensional MR Perfusion Imaging Using k-t SENSE*; EuroCMR, Florence, Italy, May 2010.

Publications

- Rolandi M, **De Silva K**, Lumley M, Lockie T, Clapp B, Spaan J, Perera D, Siebes M. *Wave speed in human coronary arteries is not influenced by microvascular vasodilation: Implications for wave intensity analysis*. In Press January 2014, Basic Res Cardiol.
- **De Silva K**, Lumley M, Kailey B, Alastruey J, Guilcher A, Assress K, Plein S, Marber M, Redwood S, Perera D. *Coronary and Micorvascular Physiology during Intra-aortic balloon counterpulsation*. In Press October 2013, JACC Interventions.
- Jogiya R, Morton G, **De Silva K**, Hachamovitch R, Kozerke S, Nagel E, Underwood R, Plein S. *Ischemic burden by three-dimensional myocardial perfusion CMR – comparison with myocardial perfusion scintigraphy*. Under review at Circ Imaging. December 2013.
- **De Silva K**, Perera D. *The Utility of Hyperaemic Stenosis Resistance in the Functional Assessment of Coronary Artery Disease*. Heart & Metabolism. In Press
- **De Silva K**, Foster P, Guilcher A, Bandara A, Jogiya R, Lockie T, Chowiencyzk P, Nagel E, Marber M, Redwood S, Plein S, Perera D. *Coronary Wave Energy: A Novel Predictor of Functional Recovery following myocardial infarction.* Circ Cardiovasc Interv; Mar 2013: PMID: 23476044
- Lockie TP, Rolandi MC, Guilcher A, Perera D, **De Silva K**, Williams R, Asrress KN, Patel K, Plein S, Chowienczyk P, Siebes M, Redwood SR, Marber M. *Synergistic adaptations to exercise in the systemic and coronary circulations that underlie the warm-up angina phenomenon.* Circulation. 2012 Nov 27;126(22):2565-74.
- **De Silva K**, Morton G, Sicard P, Chong E, Indermuehle A, Clapp B, Thomas M, Redwood S, Perera D. *Prognostic Utility of the BCIS Myocardial Jeopardy Score for Classification of*

Coronary Disease and Completeness of Revascularization. Am J Cardiol; Jan 2013; 15;111(2):172-7. PMID: 23102883

- Morton G, **De Silva K**, Ishida I, Chiribiri A, Indermuehle A, Schuster A, Redwood S, Nagel E, Perera. Validation of the BCIS-1 Myocardial Jeopardy Score Using Cardiac Magnetic Resonance Perfusion Imaging. *Clinical Physiology and Functional Imaging*. Mar 2013;33(2):101-8. PMID: 23383687
- Perera D, Stables R, Clayton T, **De Silva K**, Lumley M, Clack L, Thomas M, Redwood S. *Late Benefit of Intra-Aortic Balloon Counterpulsation during High-risk Percutaneous Coronary Intervention: Long-term Mortality Data from the Balloon pump-assisted Coronary Intervention Study (BCIS-1)*. *Circulation, Sept 2012.*
- Jogiya R, Kozerke S, Morton G, **De Silva K**, Redwood S, Perera D, Nagel E, Plein S. *Validation of Dynamic 3- Dimensional Whole Heart Magnetic Resonance Myoardial Perfusion Imaging Against Fractional Flow Reserve for the Detection of Significant Coronary Artery Disease.* JACC 2012.
- **De Silva K**. *The Utility of Cardiac MRI in Myocardial Infarction*. www.bcs.com. May 2012
- Lumley M, **De Silva K**, Perera D. *Wave Intensity Analysis in Aortic Stenosis*. Circulation. 2012 Apr 24;125(16):e612. PMID: 22529071
- **De Silva K**, Webb I, Sicard P, Lockie T, Pattinson S, Redwood S, Perera D. *Does left ventricular function continue to influence mortality following contemporary percutaneous coronary intervention?*; Coron Artery Dis. March 2012; PMID: 22395238
- **De Silva K**, Baker J, Kidambi, A, Perera, Plein S*. Magnetic Resonance Imaging the Microcirculation in Acute Coronary Syndromes.* Heart & Metabolism. *April 2012*.
- Lumley M, **De Silva K**, Perera D. *Wave Intensity Analysis in Aortic Stenosis*. Circulation. 2012;Apr 24;125(16)

- **De Silva K**. "Is Counter-pulsation Counterproductive?"www.BCS.com (British Cardiovascular Society Educational Editorial) December 2011.
- Lockie T, Ishida M, Perera D, Chiribiri A, **De Silva K**, Kozerke S, Marber M, Nagel E, Rezavi R, Redwood S, Plein S. *High-Resolution Magnetic Resonance Myocardial Perfusion Imaging at 3.0-Tesla to Detect Hemodynamically Significant Coronary Stenoses as Determined by Fractional Flow Reserve*. JACC Vol. 57, No. 1, Jan 2011.
- **De Silva K**, Perera D. *Intra-aortic balloon counterpulsation to support percutaneous coronary intervention: what do the trials tell us?* Interventional Cardiology. Dec 2010, Vol. 2, No. 6, Pages 761-763 , DOI 10.2217/ica.10.88.
- Lockie T, Perera D, **De Silva K**, Webb I, Pattinson S, Redwood S. *Impact of Measuring Fractional Flow Reserve on Decision-Making in the Cath Lab in a Cohort of Patients Being Considered for Coronary Revascularization*. J Invasive Cardiol 2010;22:413–416.

Book Chapters

- **De Silva K** & Perera D. *Physiology of Myocardial ischaemia*; Landmark Papers in Cardiovascular Medicine. Oxford University Press. 2012.

Accreditations

- Society of Cardiac Magnetic Resonance - **Level 3 accreditation in Cardiovascular Magnetic Resonance Imaging**

REFERENCES

1. WHO. Non-communicable disease statistics. *WHO*. Available at: http://www.who.int/gho/ncd/en/index.html, 2013.
2. Chilian WM. Microvascular pressures and resistances in the left ventricular subepicardium and subendocardium. *Circ Res.* 1991;69(3):561-570.
3. Feliciano L, Henning RJ. Coronary artery blood flow: physiologic and pathophysiologic regulation. *Clin Cardiol.* 1999;22(12):775-786.
4. Kuo L, Davis MJ, Chilian WM. Longitudinal gradients for endothelium-dependent and -independent vascular responses in the coronary microcirculation. *Circulation.* 1995;92(3):518-525.
5. Kuo L, Davis MJ, Chilian WM. Myogenic activity in isolated subepicardial and subendocardial coronary arterioles. *Am J Physiol.* 1988;255(6 Pt 2):H1558-1562.
6. Jones CJ, Kuo L, Davis MJ, Chilian WM. Regulation of coronary blood flow: coordination of heterogeneous control mechanisms in vascular microdomains. *Cardiovasc Res.* 1995;29(5):585-596.
7. Siebes M. Coronary flow and physiology beyond the stenosis. *Heart & Metabolism.* 2013(58):4-9.
8. Kern MJ, Lerman A, Bech JW, De Bruyne B, Eeckhout E, Fearon WF, Higano ST, Lim MJ, Meuwissen M, Piek JJ, Pijls NH, Siebes M, Spaan JA. Physiological assessment of coronary artery disease in the cardiac catheterization laboratory: a scientific statement from the American Heart Association Committee on Diagnostic and Interventional Cardiac Catheterization, Council on Clinical Cardiology. *Circulation.* 2006;114(12):1321-1341.
9. Gould KL, Lipscomb K, Hamilton GW. Physiologic basis for assessing critical coronary stenosis. Instantaneous flow response and regional distribution during coronary hyperemia as measures of coronary flow reserve. *Am J Cardiol.* 1974;33(1):87-94.
10. Gould KL, Kirkeeide RL, Buchi M. Coronary flow reserve as a physiologic measure of stenosis severity. *J Am Coll Cardiol.* 1990;15(2):459-474.
11. Chilian WM. Coronary microcirculation in health and disease. Summary of an NHLBI workshop. *Circulation.* 1997;95(2):522-528.
12. Krug A, Du Mesnil de R, Korb G. Blood supply of the myocardium after temporary coronary occlusion. *Circ Res.* 1966;19(1):57-62.
13. Ito H, Maruyama A, Iwakura K, Takiuchi S, Masuyama T, Hori M, Higashino Y, Fujii K, Minamino T. Clinical implications of the 'no reflow' phenomenon. A predictor of complications and left ventricular remodeling in reperfused anterior wall myocardial infarction. *Circulation.* 1996;93(2):223-228.
14. Wu KC, Zerhouni EA, Judd RM, Lugo-Olivieri CH, Barouch LA, Schulman SP, Blumenthal RS, Lima JA. Prognostic significance of microvascular obstruction by magnetic resonance imaging in patients with acute myocardial infarction. *Circulation.* 1998;97(8):765-772.
15. Mather AN, Lockie T, Nagel E, Marber M, Perera D, Redwood S, Radjenovic A, Saha A, Greenwood JP, Plein S. Appearance of microvascular obstruction on high resolution first-pass perfusion, early and late gadolinium enhancement CMR in patients with acute myocardial infarction. *J Cardiovasc Magn Reson.* 2009;11:33.

16. Nijveldt R, Beek AM, Hirsch A, Stoel MG, Hofman MB, Umans VA, Algra PR, Twisk JW, van Rossum AC. Functional recovery after acute myocardial infarction: comparison between angiography, electrocardiography, and cardiovascular magnetic resonance measures of microvascular injury. *J Am Coll Cardiol.* 2008;52(3):181-189.

17. Kloner RA, Ganote CE, Jennings RB. The "no-reflow" phenomenon after temporary coronary occlusion in the dog. *J Clin Invest.* 1974;54(6):1496-1508.

18. Buja LM. Myocardial ischemia and reperfusion injury. *Cardiovasc Pathol.* 2005;14(4):170-175.

19. Maxwell SR, Lip GY. Reperfusion injury: a review of the pathophysiology, clinical manifestations and therapeutic options. *Int J Cardiol.* 1997;58(2):95-117.

20. Engler RL, Dahlgren MD, Morris DD, Peterson MA, Schmid-Schonbein GW. Role of leukocytes in response to acute myocardial ischemia and reflow in dogs. *Am J Physiol.* 1986;251(2 Pt 2):H314-323.

21. Saber RS, Edwards WD, Bailey KR, McGovern TW, Schwartz RS, Holmes DR, Jr. Coronary embolization after balloon angioplasty or thrombolytic therapy: an autopsy study of 32 cases. *J Am Coll Cardiol.* 1993;22(5):1283-1288.

22. Tennant R, Wiggers CJ. Effect of coronary occlusion on myocardial contraction. *American Journal of Physiology.* 1935;112:351-361.

23. Braunwald E, Kloner RA. The stunned myocardium: prolonged, postischemic ventricular dysfunction. *Circulation.* 1982;66(6):1146-1149.

24. DeBoer FWV IJ, Kloner RA, Braunwald E. Prolonged Derangements of Canine Myocardial Purine Metabolism after a brief coronary artery occlusion not associated with anatomic evidence of necrosis. *Proc Natl Acad Sci U S A.* 1980;77:5471.

25. Tarakji KG, Brunken R, McCarthy PM, Al-Chekakie MO, Abdel-Latif A, Pothier CE, Blackstone EH, Lauer MS. Myocardial viability testing and the effect of early intervention in patients with advanced left ventricular systolic dysfunction. *Circulation.* 2006;113(2):230-237.

26. Kim RJ, Wu E, Rafael A, Chen EL, Parker MA, Simonetti O, Klocke FJ, Bonow RO, Judd RM. The use of contrast-enhanced magnetic resonance imaging to identify reversible myocardial dysfunction. *N Engl J Med.* 2000;343(20):1445-1453.

27. Bolli R, Triana JF, Jeroudi MO. Prolonged impairment of coronary vasodilation after reversible ischemia. Evidence for microvascular "stunning". *Circ Res.* 1990;67(2):332-343.

28. Camici PG, Prasad SK, Rimoldi OE. Stunning, hibernation, and assessment of myocardial viability. *Circulation.* 2008;117(1):103-114.

29. Rahimtoola SH. Coronary bypass surgery for chronic angina--1981. A perspective. *Circulation.* 1982;65(2):225-241.

30. Carluccio E, Biagioli P, Alunni G, Murrone A, Giombolini C, Ragni T, Marino PN, Reboldi G, Ambrosio G. Patients with hibernating myocardium show altered left ventricular volumes and shape, which revert after revascularization: evidence that dyssynergy might directly induce cardiac remodeling. *J Am Coll Cardiol.* 2006;47(5):969-977.

31. Allman KC, Shaw LJ, Hachamovitch R, Udelson JE. Myocardial viability testing and impact of revascularization on prognosis in patients with coronary artery disease and left ventricular dysfunction: a meta-analysis. *J Am Coll Cardiol.* 2002;39(7):1151-1158.

32. Heusch G, Schulz R, Rahimtoola SH. Myocardial hibernation: a delicate balance. *Am J Physiol Heart Circ Physiol.* 2005;288(3):H984-999.

33. Vatner SF. Correlation between acute reductions in myocardial blood flow and function in conscious dogs. *Circ Res.* 1980;47(2):201-207.
34. Gallagher KP, Matsuzaki M, Koziol JA, Kemper WS, Ross J, Jr. Regional myocardial perfusion and wall thickening during ischemia in conscious dogs. *Am J Physiol.* 1984;247(5 Pt 2):H727-738.
35. Schulz R, Rose J, Martin C, Brodde OE, Heusch G. Development of short-term myocardial hibernation. Its limitation by the severity of ischemia and inotropic stimulation. *Circulation.* 1993;88(2):684-695.
36. Gerber BL, Melin JA, Bol A, Labar D, Cogneau M, Michel C, Vanoverschelde JL. Nitrogen-13-ammonia and oxygen-15-water estimates of absolute myocardial perfusion in left ventricular ischemic dysfunction. *J Nucl Med.* 1998;39(10):1655-1662.
37. Pagano D, Townend JN, Parums DV, Bonser RS, Camici PG. Hibernating myocardium: morphological correlates of inotropic stimulation and glucose uptake. *Heart.* 2000;83(4):456-461.
38. Fath-Ordoubadi F, Beatt KJ, Spyrou N, Camici PG. Efficacy of coronary angioplasty for the treatment of hibernating myocardium. *Heart.* 1999;82(2):210-216.
39. Conversano A, Walsh JF, Geltman EM, Perez JE, Bergmann SR, Gropler RJ. Delineation of myocardial stunning and hibernation by positron emission tomography in advanced coronary artery disease. *Am Heart J.* 1996;131(3):440-450.
40. Maki M, Luotolahti M, Nuutila P, Iida H, Voipio-Pulkki LM, Ruotsalainen U, Haaparanta M, Solin O, Hartiala J, Harkonen R, Knuuti J. Glucose uptake in the chronically dysfunctional but viable myocardium. *Circulation.* 1996;93(9):1658-1666.
41. Selvanayagam JB, Jerosch-Herold M, Porto I, Sheridan D, Cheng AS, Petersen SE, Searle N, Channon KM, Banning AP, Neubauer S. Resting myocardial blood flow is impaired in hibernating myocardium: a magnetic resonance study of quantitative perfusion assessment. *Circulation.* 2005;112(21):3289-3296.
42. Afridi I, Kleiman NS, Raizner AE, Zoghbi WA. Dobutamine echocardiography in myocardial hibernation. Optimal dose and accuracy in predicting recovery of ventricular function after coronary angioplasty. *Circulation.* 1995;91(3):663-670.
43. Rahimtoola SH, Dilsizian V, Kramer CM, Marwick TH, Vanoverschelde JL. Chronic ischemic left ventricular dysfunction: from pathophysiology to imaging and its integration into clinical practice. *JACC Cardiovasc Imaging.* 2008;1(4):536-555.
44. Shimoni S, Frangogiannis NG, Aggeli CJ, Shan K, Quinones MA, Espada R, Letsou GV, Lawrie GM, Winters WL, Reardon MJ, Zoghbi WA. Microvascular structural correlates of myocardial contrast echocardiography in patients with coronary artery disease and left ventricular dysfunction: implications for the assessment of myocardial hibernation. *Circulation.* 2002;106(8):950-956.
45. Camici PG, Crea F. Coronary microvascular dysfunction. *N Engl J Med.* 2007;356(8):830-840.
46. Ragosta M, Camarano G, Kaul S, Powers ER, Sarembock IJ, Gimple LW. Microvascular integrity indicates myocellular viability in patients with recent myocardial infarction. New insights using myocardial contrast echocardiography. *Circulation.* 1994;89(6):2562-2569.
47. Kaul S, Jayaweera AR. Myocardial contrast echocardiography has the potential for the assessment of coronary microvascular reserve. *J Am Coll Cardiol.* 1993;21(2):356-358.

48. Ito H, Tomooka T, Sakai N, Yu H, Higashino Y, Fujii K, Masuyama T, Kitabatake A, Minamino T. Lack of myocardial perfusion immediately after successful thrombolysis. A predictor of poor recovery of left ventricular function in anterior myocardial infarction. *Circulation.* 1992;85(5):1699-1705.

49. Taylor AJ, Al-Saadi N, Abdel-Aty H, Schulz-Menger J, Messroghli DR, Friedrich MG. Detection of acutely impaired microvascular reperfusion after infarct angioplasty with magnetic resonance imaging. *Circulation.* 2004;109(17):2080-2085.

50. Suryapranata H, Zijlstra F, MacLeod DC, van den Brand M, de Feyter PJ, Serruys PW. Predictive value of reactive hyperemic response on reperfusion on recovery of regional myocardial function after coronary angioplasty in acute myocardial infarction. *Circulation.* 1994;89(3):1109-1117.

51. Ragosta M, Powers ER, Samady H, Gimple LW, Sarembock IJ, Beller GA. Relationship between extent of residual myocardial viability and coronary flow reserve in patients with recent myocardial infarction. *Am Heart J.* 2001;141(3):456-462.

52. Bax M, de Winter RJ, Schotborgh CE, Koch KT, Meuwissen M, Voskuil M, Adams R, Mulder KJ, Tijssen JG, Piek JJ. Short- and long-term recovery of left ventricular function predicted at the time of primary percutaneous coronary intervention in anterior myocardial infarction. *J Am Coll Cardiol.* 2004;43(4):534-541.

53. Claeys MJ, Vrints CJ, Bosmans J, Krug B, Blockx PP, Snoeck JP. Coronary flow reserve during coronary angioplasty in patients with a recent myocardial infarction: relation to stenosis and myocardial viability. *J Am Coll Cardiol.* 1996;28(7):1712-1719.

54. Shimada K, Sakanoue Y, Kobayashi Y, Ehara S, Hirose M, Nakamura Y, Fukuda D, Yamagishi H, Yoshiyama M, Takeuchi K, Yoshikawa J. Assessment of myocardial viability using coronary zero flow pressure after successful angioplasty in patients with acute anterior myocardial infarction. *Heart.* 2003;89(1):71-76.

55. Meuwissen M, Chamuleau SA, Siebes M, Schotborgh CE, Koch KT, de Winter RJ, Bax M, de Jong A, Spaan JA, Piek JJ. Role of variability in microvascular resistance on fractional flow reserve and coronary blood flow velocity reserve in intermediate coronary lesions. *Circulation.* 2001;103(2):184-187.

56. Beleslin B, Ostojic M, Djordjevic-Dikic A, Vukcevic V, Stojkovic S, Nedeljkovic M, Stankovic G, Orlic D, Milic N, Stepanovic J, Giga V, Saponjski J. The value of fractional and coronary flow reserve in predicting myocardial recovery in patients with previous myocardial infarction. *Eur Heart J.* 2008;29(21):2617-2624.

57. Serruys PW, di Mario C, Piek J, Schroeder E, Vrints C, Probst P, de Bruyne B, Hanet C, Fleck E, Haude M, Verna E, Voudris V, Geschwind H, Emanuelsson H, Muhlberger V, Danzi G, Peels HO, Ford AJ, Jr., Boersma E. Prognostic value of intracoronary flow velocity and diameter stenosis in assessing the short- and long-term outcomes of coronary balloon angioplasty: the DEBATE Study (Doppler Endpoints Balloon Angioplasty Trial Europe). *Circulation.* 1997;96(10):3369-3377.

58. Di Mario C, Moses JW, Anderson TJ, Bonan R, Muramatsu T, Jain AC, Suarez de Lezo J, Cho SY, Kern M, Meredith IT, Cohen D, Moussa I, Colombo A. Randomized comparison of elective stent implantation and coronary balloon angioplasty guided by online quantitative angiography and intracoronary Doppler. DESTINI Study Group (Doppler Endpoint STenting INternational Investigation). *Circulation.* 2000;102(24):2938-2944.

59. Kern MJ, Donohue TJ, Aguirre FV, Bach RG, Caracciolo EA, Wolford T, Mechem CJ, Flynn MS, Chaitman B. Clinical outcome of deferring angioplasty in patients with normal translesional pressure-flow velocity measurements. *J Am Coll Cardiol.* 1995;25(1):178-187.

60. Kitabata H, Imanishi T, Kubo T, Takarada S, Kashiwagi M, Matsumoto H, Tsujioka H, Ikejima H, Arita Y, Okochi K, Kuroi A, Ueno S, Kataiwa H, Tanimoto T, Yamano T, Hirata K, Nakamura N, Tanaka A, Mizukoshi M, Akasaka T. Coronary microvascular resistance index immediately after primary percutaneous coronary intervention as a predictor of the transmural extent of infarction in patients with ST-segment elevation anterior acute myocardial infarction. *JACC Cardiovasc Imaging.* 2009;2(3):263-272.

61. Choi KM, Kim RJ, Gubernikoff G, Vargas JD, Parker M, Judd RM. Transmural extent of acute myocardial infarction predicts long-term improvement in contractile function. *Circulation.* 2001;104(10):1101-1107.

62. Beek AM, Kuhl HP, Bondarenko O, Twisk JW, Hofman MB, van Dockum WG, Visser CA, van Rossum AC. Delayed contrast-enhanced magnetic resonance imaging for the prediction of regional functional improvement after acute myocardial infarction. *J Am Coll Cardiol.* 2003;42(5):895-901.

63. Pijls NH, van Son JA, Kirkeeide RL, De Bruyne B, Gould KL. Experimental basis of determining maximum coronary, myocardial, and collateral blood flow by pressure measurements for assessing functional stenosis severity before and after percutaneous transluminal coronary angioplasty. *Circulation.* 1993;87(4):1354-1367.

64. De Bruyne B, Baudhuin T, Melin JA, Pijls NH, Sys SU, Bol A, Paulus WJ, Heyndrickx GR, Wijns W. Coronary flow reserve calculated from pressure measurements in humans. Validation with positron emission tomography. *Circulation.* 1994;89(3):1013-1022.

65. Pijls NH, De Bruyne B, Peels K, Van Der Voort PH, Bonnier HJ, Bartunek JKJJ, Koolen JJ. Measurement of fractional flow reserve to assess the functional severity of coronary-artery stenoses. *N Engl J Med.* 1996;334(26):1703-1708.

66. Bech GJ, De Bruyne B, Pijls NH, de Muinck ED, Hoorntje JC, Escaned J, Stella PR, Boersma E, Bartunek J, Koolen JJ, Wijns W. Fractional flow reserve to determine the appropriateness of angioplasty in moderate coronary stenosis: a randomized trial. *Circulation.* 2001;103(24):2928-2934.

67. De Bruyne B, Pijls NH, Bartunek J, Kulecki K, Bech JW, De Winter H, Van Crombrugge P, Heyndrickx GR, Wijns W. Fractional flow reserve in patients with prior myocardial infarction. *Circulation.* 2001;104(2):157-162.

68. Samady H, Lepper W, Powers ER, Wei K, Ragosta M, Bishop GG, Sarembock IJ, Gimple L, Watson DD, Beller GA, Barringhaus KG. Fractional flow reserve of infarct-related arteries identifies reversible defects on noninvasive myocardial perfusion imaging early after myocardial infarction. *J Am Coll Cardiol.* 2006;47(11):2187-2193.

69. Fearon WF, Balsam LB, Farouque HM, Caffarelli AD, Robbins RC, Fitzgerald PJ, Yock PG, Yeung AC. Novel index for invasively assessing the coronary microcirculation. *Circulation.* 2003;107(25):3129-3132.

70. Lim HS, Yoon MH, Tahk SJ, Yang HM, Choi BJ, Choi SY, Sheen SS, Hwang GS, Kang SJ, Shin JH. Usefulness of the index of microcirculatory resistance for invasively assessing myocardial viability immediately after primary angioplasty for anterior myocardial infarction. *Eur Heart J.* 2009.

71. Aarnoudse W, Fearon WF, Manoharan G, Geven M, van de Vosse F, Rutten M, De Bruyne B, Pijls NH. Epicardial stenosis severity does not affect minimal microcirculatory resistance. *Circulation.* 2004;110(15):2137-2142.

72. Di Mario C, Krams R, Gil R, Serruys PW. Slope of the instantaneous hyperemic diastolic coronary flow velocity-pressure relation. A new index for assessment of the physiological significance of coronary stenosis in humans. *Circulation.* 1994;90(3):1215-1224.

73. de Bruyne B, Bartunek J, Sys SU, Pijls NH, Heyndrickx GR, Wijns W. Simultaneous coronary pressure and flow velocity measurements in humans. Feasibility, reproducibility, and hemodynamic dependence of coronary flow velocity reserve, hyperemic flow versus pressure slope index, and fractional flow reserve. *Circulation.* 1996;94(8):1842-1849.

74. Gregg DE, Sabiston DC, Jr. Effect of cardiac contraction on coronary blood flow. *Circulation.* 1957;15(1):14-20.

75. Spaan JA, Breuls NP, Laird JD. Diastolic-systolic coronary flow differences are caused by intramyocardial pump action in the anesthetized dog. *Circ Res.* 1981;49(3):584-593.

76. Parker KH, Jones CJ. Forward and backward running waves in the arteries: analysis using the method of characteristics. *J Biomech Eng.* 1990;112(3):322-326.

77. Bleasdale RA, Parker KH, Jones CJ. Chasing the wave. Unfashionable but important new concepts in arterial wave travel. *Am J Physiol Heart Circ Physiol.* 2003;284(6):H1879-1885.

78. Savitzky A. Smoothing and differentiation of data by simplified least squares procedures. *Anal Chem.* 1964;36:1627-1639.

79. Davies JE, Whinnett ZI, Francis DP, Manisty CH, Aguado-Sierra J, Willson K, Foale RA, Malik IS, Hughes AD, Parker KH, Mayet J. Evidence of a dominant backward-propagating "suction" wave responsible for diastolic coronary filling in humans, attenuated in left ventricular hypertrophy. *Circulation.* 2006;113(14):1768-1778.

80. Jones CJ, Sugawara M. "Wavefronts" in the aorta--implications for the mechanisms of left ventricular ejection and aortic valve closure. *Cardiovasc Res.* 1993;27(11):1902-1905.

81. Jones CJ, Sugawara M, Kondoh Y, Uchida K, Parker KH. Compression and expansion wavefront travel in canine ascending aortic flow: wave intensity analysis. *Heart Vessels.* 2002;16(3):91-98.

82. Khir AW, Henein MY, Koh T, Das SK, Parker KH, Gibson DG. Arterial waves in humans during peripheral vascular surgery. *Clin Sci (Lond).* 2001;101(6):749-757.

83. Ohte N, Narita H, Sugawara M, Niki K, Okada T, Harada A, Hayano J, Kimura G. Clinical usefulness of carotid arterial wave intensity in assessing left ventricular systolic and early diastolic performance. *Heart Vessels.* 2003;18(3):107-111.

84. Sun YH, Anderson TJ, Parker KH, Tyberg JV. Wave-intensity analysis: a new approach to coronary hemodynamics. *J Appl Physiol.* 2000;89(4):1636-1644.

85. Downar E, Janse MJ, Durrer D. The effect of acute coronary artery occlusion on subepicardial transmembrane potentials in the intact porcine heart. *Circulation.* 1977;56(2):217-224.

86. Janse MJ, Kleber AG. Electrophysiological changes and ventricular arrhythmias in the early phase of regional myocardial ischemia. *Circ Res.* 1981;49(5):1069-1081.

87. Redwood SR, Taggart PI, Sutton PM, Bygrave A, Bashir Y, Purkayastha DD, Camm AJ, Treasure T. Effect of magnesium on the monophasic action potential during early ischemia in the in vivo human heart. *J Am Coll Cardiol.* 1996;28(7):1765-1769.

88. Kleber AG, Janse MJ, van Capelle FJ, Durrer D. Mechanism and time course of S-T and T-Q segment changes during acute regional myocardial ischemia in the pig heart determined by extracellular and intracellular recordings. *Circ Res.* 1978;42(5):603-613.

89. Ben-Haim SA, Osadchy D, Schuster I, Gepstein L, Hayam G, Josephson ME. Nonfluoroscopic, in vivo navigation and mapping technology. *Nat Med.* 1996;2(12):1393-1395.

90. Callans DJ, Ren JF, Michele J, Marchlinski FE, Dillon SM. Electroanatomic left ventricular mapping in the porcine model of healed anterior myocardial infarction. Correlation with intracardiac echocardiography and pathological analysis. *Circulation.* 1999;100(16):1744-1750.

91. Gepstein L, Goldin A, Lessick J, Hayam G, Shpun S, Schwartz Y, Hakim G, Shofty R, Turgeman A, Kirshenbaum D, Ben-Haim SA. Electromechanical characterization of chronic myocardial infarction in the canine coronary occlusion model. *Circulation.* 1998;98(19):2055-2064.

92. Kornowski R, Hong MK, Gepstein L, Goldstein S, Ellahham S, Ben-Haim SA, Leon MB. Preliminary animal and clinical experiences using an electromechanical endocardial mapping procedure to distinguish infarcted from healthy myocardium. *Circulation.* 1998;98(11):1116-1124.

93. Fuchs S, Kornowski R, Shiran A, Pierre A, Ellahham S, Leon MB. Electromechanical characterization of myocardial hibernation in a pig model. *Coron Artery Dis.* 1999;10(3):195-198.

94. Kornowski R, Hong MK, Leon MB. Comparison between left ventricular electromechanical mapping and radionuclide perfusion imaging for detection of myocardial viability. *Circulation.* 1998;98(18):1837-1841.

95. Koch KC, vom Dahl J, Wenderdel M, Nowak B, Schaefer WM, Sasse A, Stellbrink C, Buell U, Hanrath P. Myocardial viability assessment by endocardial electroanatomic mapping: comparison with metabolic imaging and functional recovery after coronary revascularization. *J Am Coll Cardiol.* 2001;38(1):91-98.

96. Botker HE, Lassen JF, Hermansen F, Wiggers H, Sogaard P, Kim WY, Bottcher M, Thuesen L, Pedersen AK. Electromechanical mapping for detection of myocardial viability in patients with ischemic cardiomyopathy. *Circulation.* 2001;103(12):1631-1637.

97. Perin EC, Silva GV, Sarmento-Leite R, Sousa AL, Howell M, Muthupillai R, Lambert B, Vaughn WK, Flamm SD. Assessing myocardial viability and infarct transmurality with left ventricular electromechanical mapping in patients with stable coronary artery disease: validation by delayed-enhancement magnetic resonance imaging. *Circulation.* 2002;106(8):957-961.

98. Reimer KA, Jennings RB. The "wavefront phenomenon" of myocardial ischemic cell death. II. Transmural progression of necrosis within the framework of ischemic bed size (myocardium at risk) and collateral flow. *Lab Invest.* 1979;40(6):633-644.

99. Gerber BL, Garot J, Bluemke DA, Wu KC, Lima JA. Accuracy of contrast-enhanced magnetic resonance imaging in predicting improvement of regional myocardial

function in patients after acute myocardial infarction. *Circulation.* 2002;106(9):1083-1089.

100. Reddy VY, Wrobleski D, Houghtaling C, Josephson ME, Ruskin JN. Combined epicardial and endocardial electroanatomic mapping in a porcine model of healed myocardial infarction. *Circulation.* 2003;107(25):3236-3242.

101. Vahlhaus C, Bruns HJ, Stypmann J, Tjan TD, Janssen F, Schafers M, Scheld HH, Schober O, Breithardt G, Wichter T. Direct epicardial mapping predicts the recovery of left ventricular dysfunction in chronic ischaemic myocardium. *Eur Heart J.* 2004;25(2):151-157.

102. Edwards RJ, Redwood SR, Lambiase PD, Tomset E, Rakhit RD, Marber MS. Antiarrhythmic and anti-ischaemic effects of angina in patients with and without coronary collaterals. *Heart.* 2002;88(6):604-610.

103. Abaci A, Oguzhan A, Topsakal R, Seyfeli E, Yilmaz Y, Eryol NK, Basar E, Ergin A. Intracoronary electrocardiogram and angina pectoris during percutaneous coronary interventions as an assessment of myocardial viability: comparison with low-dose dobutamine echocardiography. *Catheter Cardiovasc Interv.* 2003;60(4):469-476.

104. Balian V, Galli M, Marcassa C, Cecchin G, Child M, Barlocco F, Petrucci E, Filippini G, Michi R, Onofri M. Intracoronary ST-segment shift soon after elective percutaneous coronary intervention accurately predicts periprocedural myocardial injury. *Circulation.* 2006;114(18):1948-1954.

105. Kumagai K, Takahashi A, Yamauchi Y, Aonuma K. Ventricular tachycardia originating from the epicardium identified by intracoronary mapping using a PTCA guidewire. *J Cardiovasc Electrophysiol.* 2006;17(6):670-673.

106. Segal OR, Wong T, Chow AW, Jarman JW, Schilling RJ, Markides V, Peters NS, Wyn Davies D. Intra-coronary guidewire mapping-a novel technique to guide ablation of human ventricular tachycardia. *J Interv Card Electrophysiol.* 2007;18(2):143-154.

107. Samady H, Liu YH, Choi CJ, Ragosta M, Pfau SE, Cleman MW, Powers ER, Kramer CM, Wackers FJ, Beller GA, Watson DD. Electromechanical mapping for detecting myocardial viability and ischemia in patients with severe ischemic cardiomyopathy. *Am J Cardiol.* 2003;91(7):807-811.

108. Spaan JA, Piek JJ, Hoffman JI, Siebes M. Physiological basis of clinically used coronary hemodynamic indices. *Circulation.* 2006;113(3):446-455.

109. Tonino PA, De Bruyne B, Pijls NH, Siebert U, Ikeno F, van' t Veer M, Klauss V, Manoharan G, Engstrom T, Oldroyd KG, Ver Lee PN, MacCarthy PA, Fearon WF. Fractional flow reserve versus angiography for guiding percutaneous coronary intervention. *N Engl J Med.* 2009;360(3):213-224.

110. De Bruyne B, Pijls NH, Kalesan B, Barbato E, Tonino PA, Piroth Z, Jagic N, Mobius-Winkler S, Rioufol G, Witt N, Kala P, MacCarthy P, Engstrom T, Oldroyd KG, Mavromatis K, Manoharan G, Verlee P, Frobert O, Curzen N, Johnson JB, Juni P, Fearon WF. Fractional flow reserve-guided PCI versus medical therapy in stable coronary disease. *N Engl J Med.* 2012;367(11):991-1001.

111. Hartley CJ, Cole JS. An ultrasonic pulsed Doppler system for measuring blood flow in small vessels. *J Appl Physiol.* 1974;37(4):626-629.

112. Spaan JA. Mechanical determinants of myocardial perfusion. *Basic Res Cardiol.* 1995;90(2):89-102.

113. Verhoeff BJ, Siebes M, Meuwissen M, Atasever B, Voskuil M, de Winter RJ, Koch KT, Tijssen JG, Spaan JA, Piek JJ. Influence of percutaneous coronary intervention on coronary microvascular resistance index. *Circulation.* 2005;111(1):76-82.

114. Meuwissen M, Siebes M, Chamuleau SA, van Eck-Smit BL, Koch KT, de Winter RJ, Tijssen JG, Spaan JA, Piek JJ. Hyperemic stenosis resistance index for evaluation of functional coronary lesion severity. *Circulation.* 2002;106(4):441-446.

115. Siebes M, Verhoeff BJ, Meuwissen M, de Winter RJ, Spaan JA, Piek JJ. Single-wire pressure and flow velocity measurement to quantify coronary stenosis hemodynamics and effects of percutaneous interventions. *Circulation.* 2004;109(6):756-762.

116. McGeoch RJ, Oldroyd KG. Pharmacological options for inducing maximal hyperaemia during studies of coronary physiology. *Catheter Cardiovasc Interv.* 2008;71(2):198-204.

117. Brunckhorst CB, Delacretaz E, Soejima K, Maisel WH, Friedman PL, Stevenson WG. Impact of changing activation sequence on bipolar electrogram amplitude for voltage mapping of left ventricular infarcts causing ventricular tachycardia. *J Interv Card Electrophysiol.* 2005;12(2):137-141.

118. Hundley WG, Bluemke DA, Finn JP, Flamm SD, Fogel MA, Friedrich MG, Ho VB, Jerosch-Herold M, Kramer CM, Manning WJ, Patel M, Pohost GM, Stillman AE, White RD, Woodard PK. ACCF/ACR/AHA/NASCI/SCMR 2010 expert consensus document on cardiovascular magnetic resonance: a report of the American College of Cardiology Foundation Task Force on Expert Consensus Documents. *J Am Coll Cardiol.*55(23):2614-2662.

119. Kelle S, Hamdan A, Schnackenburg B, Kohler U, Klein C, Nagel E, Fleck E. Dobutamine stress cardiovascular magnetic resonance at 3 Tesla. *J Cardiovasc Magn Reson.* 2008;10(1):44.

120. Wellnhofer E, Olariu A, Klein C, Grafe M, Wahl A, Fleck E, Nagel E. Magnetic resonance low-dose dobutamine test is superior to SCAR quantification for the prediction of functional recovery. *Circulation.* 2004;109(18):2172-2174.

121. Klein C, Schmal TR, Nekolla SG, Schnackenburg B, Fleck E, Nagel E. Mechanism of late gadolinium enhancement in patients with acute myocardial infarction. *J Cardiovasc Magn Reson.* 2007;9(4):653-658.

122. Hillenbrand HB, Kim RJ, Parker MA, Fieno DS, Judd RM. Early assessment of myocardial salvage by contrast-enhanced magnetic resonance imaging. *Circulation.* 2000;102(14):1678-1683.

123. Ricciardi MJ, Wu E, Davidson CJ, Choi KM, Klocke FJ, Bonow RO, Judd RM, Kim RJ. Visualization of discrete microinfarction after percutaneous coronary intervention associated with mild creatine kinase-MB elevation. *Circulation.* 2001;103(23):2780-2783.

124. Laissy JP, Hyafil F, Feldman LJ, Juliard JM, Schouman-Claeys E, Steg PG, Faraggi M. Differentiating acute myocardial infarction from myocarditis: diagnostic value of early- and delayed-perfusion cardiac MR imaging. *Radiology.* 2005;237(1):75-82.

125. Beek AM, van Rossum AC. Cardiovascular magnetic resonance imaging in patients with acute myocardial infarction. *Heart.*96(3):237-243.

126. Kwong RY, Korlakunta H. Diagnostic and prognostic value of cardiac magnetic resonance imaging in assessing myocardial viability. *Top Magn Reson Imaging.* 2008;19(1):15-24.

127. Aletras AH, Tilak GS, Natanzon A, Hsu LY, Gonzalez FM, Hoyt RF, Jr., Arai AE. Retrospective determination of the area at risk for reperfused acute myocardial infarction with T2-weighted cardiac magnetic resonance imaging: histopathological and displacement encoding with stimulated echoes (DENSE) functional validations. *Circulation.* 2006;113(15):1865-1870.

128. Abdel-Aty H, Cocker M, Meek C, Tyberg JV, Friedrich MG. Edema as a very early marker for acute myocardial ischemia: a cardiovascular magnetic resonance study. *J Am Coll Cardiol.* 2009;53(14):1194-1201.

129. Friedrich MG, Kim HW, Kim RJ. T2-weighted imaging to assess post-infarct myocardium at risk. *JACC Cardiovasc Imaging.*4(9):1014-1021.

130. Ganame J, Messalli G, Dymarkowski S, Rademakers FE, Desmet W, Van de Werf F, Bogaert J. Impact of myocardial haemorrhage on left ventricular function and remodelling in patients with reperfused acute myocardial infarction. *Eur Heart J.* 2009;30(12):1440-1449.

131. Basso C, Corbetti F, Silva C, Abudureheman A, Lacognata C, Cacciavillani L, Tarantini G, Marra MP, Ramondo A, Thiene G, Iliceto S. Morphologic validation of reperfused hemorrhagic myocardial infarction by cardiovascular magnetic resonance. *Am J Cardiol.* 2007;100(8):1322-1327.

132. Lowe JE, Reimer KA, Jennings RB. Experimental infarct size as a function of the amount of myocardium at risk. *Am J Pathol.* 1978;90(2):363-379.

133. Christian TF, Schwartz RS, Gibbons RJ. Determinants of infarct size in reperfusion therapy for acute myocardial infarction. *Circulation.* 1992;86(1):81-90.

134. Braunwald E. Myocardial reperfusion, limitation of infarct size, reduction of left ventricular dysfunction, and improved survival. Should the paradigm be expanded? *Circulation.* 1989;79(2):441-444.

135. Eitel I, Desch S, de Waha S, Fuernau G, Gutberlet M, Schuler G, Thiele H. Long-term prognostic value of myocardial salvage assessed by cardiovascular magnetic resonance in acute reperfused myocardial infarction. *Heart.*97(24):2038-2045.

136. Eitel I, Desch S, Fuernau G, Hildebrand L, Gutberlet M, Schuler G, Thiele H. Prognostic significance and determinants of myocardial salvage assessed by cardiovascular magnetic resonance in acute reperfused myocardial infarction. *J Am Coll Cardiol.*55(22):2470-2479.

137. Rahimtoola SH. The hibernating myocardium. *Am Heart J.* 1989;117(1):211-221.

138. Schuijf JD, Kaandorp TA, Lamb HJ, van der Geest RJ, Viergever EP, van der Wall EE, de Roos A, Bax JJ. Quantification of myocardial infarct size and transmurality by contrast-enhanced magnetic resonance imaging in men. *Am J Cardiol.* 2004;94(3):284-288.

139. Wu E, Judd RM, Vargas JD, Klocke FJ, Bonow RO, Kim RJ. Visualisation of presence, location, and transmural extent of healed Q-wave and non-Q-wave myocardial infarction. *Lancet.* 2001;357(9249):21-28.

140. Cerqueira MD, Weissman NJ, Dilsizian V, Jacobs AK, Kaul S, Laskey WK, Pennell DJ, Rumberger JA, Ryan T, Verani MS. Standardized myocardial segmentation and nomenclature for tomographic imaging of the heart: a statement for healthcare professionals from the Cardiac Imaging Committee of the Council on Clinical Cardiology of the American Heart Association. *J Nucl Cardiol.* 2002;9(2):240-245.

141. Romero J, Xue X, Gonzalez W, Garcia MJ. CMR imaging assessing viability in patients with chronic ventricular dysfunction due to coronary artery disease: a meta-analysis of prospective trials. *JACC Cardiovasc Imaging.* 2012;5(5):494-508.

142. Kwong RY, Schussheim AE, Rekhraj S, Aletras AH, Geller N, Davis J, Christian TF, Balaban RS, Arai AE. Detecting acute coronary syndrome in the emergency department with cardiac magnetic resonance imaging. *Circulation.* 2003;107(4):531-537.

143. Nowosielski M, Schocke M, Mayr A, Pedarnig K, Klug G, Kohler A, Bartel T, Muller S, Trieb T, Pachinger O, Metzler B. Comparison of wall thickening and ejection fraction by cardiovascular magnetic resonance and echocardiography in acute myocardial infarction. *J Cardiovasc Magn Reson.* 2009;11:22.

144. Arai AE. Gadolinium can depict area at risk and myocardial infarction: a double-edged sword? *JACC Cardiovasc Imaging.*4(6):619-621.

145. Lee KS, Marwick TH, Cook SA, Go RT, Fix JS, James KB, Sapp SK, MacIntyre WJ, Thomas JD. Prognosis of patients with left ventricular dysfunction, with and without viable myocardium after myocardial infarction. Relative efficacy of medical therapy and revascularization. *Circulation.* 1994;90(6):2687-2694.

146. White HD, Chew DP. Acute myocardial infarction. *Lancet.* 2008;372(9638):570-584.

147. Anderson JL, Adams CD, Antman EM, Bridges CR, Califf RM, Casey DE, Jr., Chavey WE, 2nd, Fesmire FM, Hochman JS, Levin TN, Lincoff AM, Peterson ED, Theroux P, Wenger NK, Wright RS, Smith SC, Jr., Jacobs AK, Halperin JL, Hunt SA, Krumholz HM, Kushner FG, Lytle BW, Nishimura R, Ornato JP, Page RL, Riegel B. ACC/AHA 2007 guidelines for the management of patients with unstable angina/non ST-elevation myocardial infarction: a report of the American College of Cardiology/American Heart Association Task Force on Practice Guidelines (Writing Committee to Revise the 2002 Guidelines for the Management of Patients With Unstable Angina/Non ST-Elevation Myocardial Infarction): developed in collaboration with the American College of Emergency Physicians, the Society for Cardiovascular Angiography and Interventions, and the Society of Thoracic Surgeons: endorsed by the American Association of Cardiovascular and Pulmonary Rehabilitation and the Society for Academic Emergency Medicine. *Circulation.* 2007;116(7):e148-304.

148. Hamm CW, Bassand JP, Agewall S, Bax J, Boersma E, Bueno H, Caso P, Dudek D, Gielen S, Huber K, Ohman M, Petrie MC, Sonntag F, Uva MS, Storey RF, Wijns W, Zahger D, Bax JJ, Auricchio A, Baumgartner H, Ceconi C, Dean V, Deaton C, Fagard R, Funck-Brentano C, Hasdai D, Hoes A, Knuuti J, Kolh P, McDonagh T, Moulin C, Poldermans D, Popescu BA, Reiner Z, Sechtem U, Sirnes PA, Torbicki A, Vahanian A, Windecker S, Achenbach S, Badimon L, Bertrand M, Botker HE, Collet JP, Crea F, Danchin N, Falk E, Goudevenos J, Gulba D, Hambrecht R, Herrmann J, Kastrati A, Kjeldsen K, Kristensen SD, Lancellotti P, Mehilli J, Merkely B, Montalescot G, Neumann FJ, Neyses L, Perk J, Roffi M, Romeo F, Ruda M, Swahn E, Valgimigli M, Vrints CJ, Widimsky P. ESC Guidelines for the management of acute coronary syndromes in patients presenting without persistent ST-segment elevation: The Task Force for the management of acute coronary syndromes (ACS) in patients presenting without persistent ST-segment elevation of the European Society of Cardiology (ESC). *Eur Heart J.*32(23):2999-3054.

149. Crowe E, Lovibond K, Gray H, Henderson R, Krause T, Camm J. Early management of unstable angina and non-ST segment elevation myocardial infarction: summary of NICE guidance. *BMJ.*340:c1134.

150. Maes A, Van de Werf F, Nuyts J, Bormans G, Desmet W, Mortelmans L. Impaired myocardial tissue perfusion early after successful thrombolysis. Impact on myocardial flow, metabolism, and function at late follow-up. *Circulation.* 1995;92(8):2072-2078.

151. Iliceto S, Galiuto L, Marchese A, Colonna P, Oliva S, Rizzon P. Functional role of microvascular integrity in patients with infarct-related artery patency after acute myocardial infarction. *Eur Heart J.* 1997;18(4):618-624.

152. De Silva K, Webb I, Sicard P, Lockie T, Pattinson S, Redwood S, Perera D. Does left ventricular function continue to influence mortality following contemporary percutaneous coronary intervention? *Coron Artery Dis.* 2012.

153. Fearon WF, Shah M, Ng M, Brinton T, Wilson A, Tremmel JA, Schnittger I, Lee DP, Vagelos RH, Fitzgerald PJ, Yock PG, Yeung AC. Predictive value of the index of microcirculatory resistance in patients with ST-segment elevation myocardial infarction. *J Am Coll Cardiol.* 2008;51(5):560-565.

154. Davies JE, Sen S, Broyd C, Hadjiloizou N, Baksi J, Francis DP, Foale RA, Parker KH, Hughes AD, Chukwuemeka A, Casula R, Malik IS, Mikhail GW, Mayet J. Arterial pulse wave dynamics after percutaneous aortic valve replacement: fall in coronary diastolic suction with increasing heart rate as a basis for angina symptoms in aortic stenosis. *Circulation.* 2011;124(14):1565-1572.

155. Krams R, Sipkema P, Westerhof N. Varying elastance concept may explain coronary systolic flow impediment. *Am J Physiol.* 1989;257(5 Pt 2):H1471-1479.

156. Wiggers CJ. The interplay of coronary vascular resistance and myocardial compression in regulating coronary flow. *Circ Res.* 1954;2(3):271-279.

157. Lee TH, Rouan GW, Weisberg MC, Brand DA, Acampora D, Stasiulewicz C, Walshon J, Terranova G, Gottlieb L, Goldstein-Wayne B, et al. Clinical characteristics and natural history of patients with acute myocardial infarction sent home from the emergency room. *Am J Cardiol.* 1987;60(4):219-224.

158. Davies JE, Whinnett ZI, Francis DP, Willson K, Foale RA, Malik IS, Hughes AD, Parker KH, Mayet J. Use of simultaneous pressure and velocity measurements to estimate arterial wave speed at a single site in humans. *Am J Physiol Heart Circ Physiol.* 2006;290(2):H878-885.

159. DeLong ER, DeLong DM, Clarke-Pearson DL. Comparing the areas under two or more correlated receiver operating characteristic curves: a nonparametric approach. *Biometrics.* 1988;44(3):837-845.

160. McGeoch R, Watkins S, Berry C, Steedman T, Davie A, Byrne J, Hillis S, Lindsay M, Robb S, Dargie H, Oldroyd K. The index of microcirculatory resistance measured acutely predicts the extent and severity of myocardial infarction in patients with ST-segment elevation myocardial infarction. *JACC Cardiovasc Interv.*3(7):715-722.

161. Eitel I, Wohrle J, Suenkel H, Meissner J, Kerber S, Lauer B, Pauschinger M, Birkemeyer R, Axthelm C, Zimmermann R, Neuhaus P, Brosteanu O, de Waha S, Desch S, Gutberlet M, Schuler G, Thiele H. Intracoronary Compared With Intravenous Bolus Abciximab Application During Primary Percutaneous Coronary Intervention in ST-Segment Elevation Myocardial Infarction: Cardiac Magnetic Resonance Substudy of the AIDA STEMI Trial. *J Am Coll Cardiol.* 2013;61(13):1447-1454.

162. Downey JM, Kirk ES. Inhibition of coronary blood flow by a vascular waterfall mechanism. *Circ Res.* 1975;36(6):753-760.

163. Spaan J, Kolyva C, van den Wijngaard J, ter Wee R, van Horssen P, Piek J, Siebes M. Coronary structure and perfusion in health and disease. *Philos Transact A Math Phys Eng Sci.* 2008;366(1878):3137-3153.

164. Allen DG, Orchard CH. Myocardial contractile function during ischemia and hypoxia. *Circ Res.* 1987;60(2):153-168.

165. Hirsch A, Nijveldt R, Haeck JD, Beek AM, Koch KT, Henriques JP, van der Schaaf RJ, Vis MM, Baan J, Jr., de Winter RJ, Tijssen JG, van Rossum AC, Piek JJ. Relation between the assessment of microvascular injury by cardiovascular magnetic resonance and coronary Doppler flow velocity measurements in patients with acute anterior wall myocardial infarction. *J Am Coll Cardiol.* 2008;51(23):2230-2238.

166. Iwakura K, Ito H, Takiuchi S, Taniyama Y, Nakatsuchi Y, Negoro S, Higashino Y, Okamura A, Masuyama T, Hori M, Fujii K, Minamino T. Alternation in the coronary blood flow velocity pattern in patients with no reflow and reperfused acute myocardial infarction. *Circulation.* 1996;94(6):1269-1275.

167. Grayson AD, Moore RK, Jackson M, Rathore S, Sastry S, Gray TP, Schofield I, Chauhan A, Ordoubadi FF, Prendergast B, Stables RH. Multivariate prediction of major adverse cardiac events after 9914 percutaneous coronary interventions in the north west of England. *Heart.* 2006;92(5):658-663.

168. Moscucci M, Kline-Rogers E, Share D, O'Donnell M, Maxwell-Eward A, Meengs WL, Kraft P, DeFranco AC, Chambers JL, Patel K, McGinnity JG, Eagle KA. Simple bedside additive tool for prediction of in-hospital mortality after percutaneous coronary interventions. *Circulation.* 2001;104(3):263-268.

169. Wallace TW, Berger JS, Wang A, Velazquez EJ, Brown DL. Impact of left ventricular dysfunction on hospital mortality among patients undergoing elective percutaneous coronary intervention. *Am J Cardiol.* 2009;103(3):355-360.

170. Perera D, Stables R, Thomas M, Booth J, Pitt M, Blackman D, de Belder A, Redwood S. Elective intra-aortic balloon counterpulsation during high-risk percutaneous coronary intervention: a randomized controlled trial. *JAMA.* 2010;304(8):867-874.

171. Patel MR, Smalling RW, Thiele H, Barnhart HX, Zhou Y, Chandra P, Chew D, Cohen M, French J, Perera D, Ohman EM. Intra-aortic balloon counterpulsation and infarct size in patients with acute anterior myocardial infarction without shock: the CRISP AMI randomized trial. *JAMA.* 2011;306(12):1329-1337.

172. Thiele H, Zeymer U, Neumann FJ, Ferenc M, Olbrich HG, Hausleiter J, Richardt G, Hennersdorf M, Empen K, Fuernau G, Desch S, Eitel I, Hambrecht R, Fuhrmann J, Bohm M, Ebelt H, Schneider S, Schuler G, Werdan K. Intraaortic balloon support for myocardial infarction with cardiogenic shock. *N Engl J Med.*367(14):1287-1296.

173. De Silva K, Foster P, Guilcher A, Bandara A, Jogiya R, Lockie T, Chowiencyzk P, Nagel E, Marber M, Redwood S, Plein S, Perera D. Coronary wave energy: a novel predictor of functional recovery after myocardial infarction. *Circ Cardiovasc Interv.*6(2):166-175.

174. De Silva K, Morton G, Sicard P, Chong E, Indermuehle A, Clapp B, Thomas M, Redwood S, Perera D. Prognostic Utility of BCIS Myocardial Jeopardy Score for Classification of Coronary Disease Burden and Completeness of Revascularization. *Am J Cardiol.*111(2):172-177.

175. Califf RM, Phillips HR, 3rd, Hindman MC, Mark DB, Lee KL, Behar VS, Johnson RA, Pryor DB, Rosati RA, Wagner GS, et al. Prognostic value of a coronary artery jeopardy score. *J Am Coll Cardiol.* 1985;5(5):1055-1063.

176. Buckberg GD, Fixler DE, Archie JP, Hoffman JI. Experimental subendocardial ischemia in dogs with normal coronary arteries. *Circ Res.* 1972;30(1):67-81.

177. Komaru T, Kanatsuka H, Shirato K. Coronary microcirculation: physiology and pharmacology. *Pharmacol Ther.* 2000;86(3):217-261.

178. Bassenge E, Heusch G. Endothelial and neuro-humoral control of coronary blood flow in health and disease. *Rev Physiol Biochem Pharmacol.* 1990;116:77-165.

179. Mosher P, Ross J, Jr., McFate PA, Shaw RF. Control of Coronary Blood Flow by an Autoregulatory Mechanism. *Circ Res.* 1964;14:250-259.

180. Patel MR, Smalling RW, Thiele H, Barnhart HX, Zhou Y, Chandra P, Chew D, Cohen M, French J, Perera D, Ohman EM. Intra-aortic balloon counterpulsation and infarct size in patients with acute anterior myocardial infarction without shock: the CRISP AMI randomized trial. *JAMA.*306(12):1329-1337.

181. Remmelink M, Sjauw KD, Henriques JP, de Winter RJ, Koch KT, van der Schaaf RJ, Vis MM, Tijssen JG, Piek JJ, Baan J, Jr. Effects of left ventricular unloading by Impella recover LP2.5 on coronary hemodynamics. *Catheter Cardiovasc Interv.* 2007;70(4):532-537.

182. Kolyva C, Pantalos GM, Giridharan GA, Pepper JR, Khir AW. Discerning aortic waves during intra-aortic balloon pumping and their relation to benefits of counterpulsation in humans. *J Appl Physiol.* 2009;107(5):1497-1503.

183. Kolyva C, Pantalos GM, Pepper JR, Khir AW. How much of the intraaortic balloon volume is displaced toward the coronary circulation? *J Thorac Cardiovasc Surg.*140(1):110-116.

184. Asmar R, Rudnichi A, Blacher J, London GM, Safar ME. Pulse pressure and aortic pulse wave are markers of cardiovascular risk in hypertensive populations. *Am J Hypertens.* 2001;14(2):91-97.

185. Weber T, Auer J, O'Rourke MF, Kvas E, Lassnig E, Berent R, Eber B. Arterial stiffness, wave reflections, and the risk of coronary artery disease. *Circulation.* 2004;109(2):184-189.

186. Arts T, Kruger RT, van Gerven W, Lambregts JA, Reneman RS. Propagation velocity and reflection of pressure waves in the canine coronary artery. *Am J Physiol.* 1979;237(4):H469-474.

187. Megnien JL, Simon A, Valensi P, Flaud P, Merli I, Levenson J. Comparative effects of diabetes mellitus and hypertension on physical properties of human large arteries. *J Am Coll Cardiol.* 1992;20(7):1562-1568.

188. Naka KK, Tweddel AC, Doshi SN, Goodfellow J, Henderson AH. Flow-mediated changes in pulse wave velocity: a new clinical measure of endothelial function. *Eur Heart J.* 2006;27(3):302-309.

189. Nichols WW, Singh BM. Augmentation index as a measure of peripheral vascular disease state. *Curr Opin Cardiol.* 2002;17(5):543-551.

190. Parker KH. An introduction to wave intensity analysis. *Med. Biol. Eng. Comput.* 2009;47:175-188.

191. De Silva K, Foster P, Guilcher A, Bandara A, Jogiya R, Lockie T, Chowiencyzk P, Nagel E, Marber M, Redwood S, Plein S, Perera D. Coronary wave energy: a novel predictor

of functional recovery after myocardial infarction. *Circ Cardiovasc Interv.* 2013;6(2):166-175.

192. Khir AW, O'Brien A, Gibbs JS, Parker KH. Determination of wave speed and wave separation in the arteries. *J Biomech.* 2001;34(9):1145-1155.

193. Davies JE, Whinnett ZI, Francis DP, Willson K, Foale RA, Malik IS, Hughes AD, Parker KH, Mayet J. Use of simultaneous pressure and velocity measurements to estimate arterial wave speed at a single site in humans. *Am J Physiol Heart Circ Physiol.* 2005;290(2):878-885.

194. Kolyva C, Spaan JA, Piek JJ, Siebes M. Windkesselness of coronary arteries hampers assessment of human coronary wave speed by single point technique. *Am. J. Physiol. Heart Circ. Physiol.* 2008;295(H):482-490.

195. Arts T, Kruger TI, Van Gerven W, Lambregts JAC, Reneman RS. Propagation velocity and reflection of pressure waves in the canine coronary artery. *American Journal of Physiology Heart and Circulatory Physiology.* 1979;234:H469-H474.

196. Rumberger JA, Nerem RM, Muir WW. Coronary artery pressure development and wave transmission characteristics in the horse. *Cardiovascular Research.* 1979;13(7):413-419.

197. Megnien JL, Simon A, Valensi P, Flaud P, Merli I, Levenson J. Comparative effects of diabetes mellitus and hypertension on physical properties of human large arteries. *J Am Coll Cardiol.* 1992;20:1562-1568.

198. Naka KK, Tweddel AC, Doshi SN, Goodfellow J, Henderson AH. Flow-mediated changes in pulse wave velocity: a new clinical measure of endothelial function. *European Heart Journal.* 2006;27(3):302-309.

199. Ting CT, Chang MS, Wang SP, Chiang BN, Yin FCP. Regional pulse wave velocities in hypertensive and normotensive humans. *Cardiovascular Research.* 1990;24(11):865-872.

200. Sanz J, Prat-Gonzalez S, Macaluso F, Fuster V, Garcia M. 155 Quantification of pulse wave velocity in the pulmonary artery in patients with pulmonary hypertension. BioMed Central Ltd.; 2008.

201. Murgo JP, Westerhof N, Giolma JP, Altobelli SA. Aortic input impedance in normal man: relationship to pressure wave forms. *Circulation.* 1980;62(1):105-116.

202. Rolandi MC, Nolte F, van de Hoef TP, Remmelink M, Baan J, Jr., Piek JJ, Spaan JA, Siebes M. Coronary wave intensity during the Valsalva manoeuvre in humans reflects altered intramural vessel compression responsible for extravascular resistance. *J Physiol.* 2012;590(Pt 18):4623-4635.

203. Savitzky A, Golay MJE. Smoothing and Differentiation of Data by Simplified Least Squares Procedures. *Analytical Chemistry.* 1964;36(8):1627-1639.

204. Parker KH, Jones CJ. Forward and backward running waves in the arteries: analysis using the method of characteristics. *J Biomech.Eng.* 1990;112(3):322-326.

205. Kolyva C, Spaan JA, Piek JJ, Siebes M. Windkesselness of coronary arteries hampers assessment of human coronary wave speed by single point technique. *American Journal of Physiology Heart and Circulatory Physiology.* 2008;295(H):482-490.

206. Harder DR, Belardinelli L, Sperelakis N, Rubio R, Berne RM. Differential effects of adenosine and nitroglycerin on the action potentials of large and small coronary arteries. *Circ Res.* 1979;44(2):176-182.

207. Feldman RL, Marx JD, Pepine CJ, Conti CR. Analysis of coronary responses to various doses of intracoronary nitroglycerin. *Circulation.* 1982;66(2):321-327.

208. Murgo JP, Westerhof N, Giolma SA. Aortic input impedance in normal man; relationship to pressure waveforms. *Circulation.* 1980;62:105-116.

209. Rolandi MC, Nolte F, van de Hoef TP, Remmelink M, Baan J, Piek JJ, Spaan JAE, Siebes M. Coronary wave intensity during the Valsalva manoeuvre in humans reflects altered intramural vessel compression responsible for extravascular resistance. *The Journal of Physiology.* 2012;590(18):4623-4635.

210. White JA, Fine N, Gula LJ, Yee R, Al-Admawi M, Zhang Q, Krahn A, Skanes A, MacDonald A, Peters T, Drangova M. Fused whole-heart coronary and myocardial scar imaging using 3-T CMR. Implications for planning of cardiac resynchronization therapy and coronary revascularization. *JACC Cardiovasc Imaging.* 2010;3(9):921-930.

211. Kornowski R, Hong MK, Shiran A, Fuchs S, Pierre A, Collins SD, Elahham S, Leon MB. Electromechanical characterization of acute experimental myocardial infarction. *J Invasive Cardiol.* 1999;11(6):329-336.

212. Younger JF, Plein S, Barth J, Ridgway JP, Ball SG, Greenwood JP. Troponin-I concentration 72 h after myocardial infarction correlates with infarct size and presence of microvascular obstruction. *Heart.* 2007;93(12):1547-1551.

213. Presti CF, Gentile R, Armstrong WF, Ryan T, Dillon JC, Feigenbaum H. Improvement in regional wall motion after percutaneous transluminal coronary angioplasty during acute myocardial infarction: utility of two-dimensional echocardiography. *Am Heart J.* 1988;115(6):1149-1155.

214. Nienaber CA, Brunken RC, Sherman CT, Yeatman LA, Gambhir SS, Krivokapich J, Demer LL, Ratib O, Child JS, Phelps ME, et al. Metabolic and functional recovery of ischemic human myocardium after coronary angioplasty. *J Am Coll Cardiol.* 1991;18(4):966-978.

215. Hutchinson MD, Gerstenfeld EP, Desjardins B, Bala R, Riley MP, Garcia FC, Dixit S, Lin D, Tzou WS, Cooper JM, Verdino RJ, Callans DJ, Marchlinski FE. Endocardial unipolar voltage mapping to detect epicardial ventricular tachycardia substrate in patients with nonischemic left ventricular cardiomyopathy. *Circ Arrhythm Electrophysiol.* 2011;4(1):49-55.

216. Piers SR, van Huls van Taxis CF, Tao Q, van der Geest RJ, Askar SF, Siebelink HM, Schalij MJ, Zeppenfeld K. Epicardial substrate mapping for ventricular tachycardia ablation in patients with non-ischaemic cardiomyopathy: a new algorithm to differentiate between scar and viable myocardium developed by simultaneous integration of computed tomography and contrast-enhanced magnetic resonance imaging. *Eur Heart J.* 2013;34(8):586-596.

217. Anderson RH, Becker AE, Tranum-Jensen J, Janse MJ. Anatomico-electrophysiological correlations in the conduction system--a review. *Br Heart J.* 1981;45(1):67-82.

218. Tillmanns H, Ikeda S, Hansen H, Sarma JS, Fauvel JM, Bing RJ. Microcirculation in the ventricle of the dog and turtle. *Circ Res.* 1974;34(4):561-569.

219. Ashikawa K, Kanatsuka H, Suzuki T, Takishima T. Phasic blood flow velocity pattern in epimyocardial microvessels in the beating canine left ventricle. *Circ Res.* 1986;59(6):704-711.

220. de Silva R, Camici PG. Role of positron emission tomography in the investigation of human coronary circulatory function. *Cardiovasc Res.* 1994;28(11):1595-1612.

221. Thiele H, Zeymer U, Neumann FJ, Ferenc M, Olbrich HG, Hausleiter J, Richardt G, Hennersdorf M, Empen K, Fuernau G, Desch S, Eitel I, Hambrecht R, Fuhrmann J,

Bohm M, Ebelt H, Schneider S, Schuler G, Werdan K. Intraaortic Balloon Support for Myocardial Infarction with Cardiogenic Shock. *N Engl J Med.* 2012.

222. Gulbins H, Reichenspurner H, Becker C, Boehm DH, Knez A, Schmitz C, Bruening R, Haberl R, Reichart B. Preoperative 3D-reconstructions of ultrafast-CT images for the planning of minimally invasive direct coronary artery bypass operation (MIDCAB). *Heart Surg Forum.* 1998;1(2):111-115.

223. Gasparovic H, Rybicki FJ, Millstine J, Unic D, Byrne JG, Yucel K, Mihaljevic T. Three dimensional computed tomographic imaging in planning the surgical approach for redo cardiac surgery after coronary revascularization. *Eur J Cardiothorac Surg.* 2005;28(2):244-249.

224. Rhode KS, Sermesant M, Brogan D, Hegde S, Hipwell J, Lambiase P, Rosenthal E, Bucknall C, Qureshi SA, Gill JS, Razavi R, Hill DL. A system for real-time XMR guided cardiovascular intervention. *IEEE Trans Med Imaging.* 2005;24(11):1428-1440.

225. Gutierrez LF, Silva R, Ozturk C, Sonmez M, Stine AM, Raval AN, Raman VK, Sachdev V, Aviles RJ, Waclawiw MA, McVeigh ER, Lederman RJ. Technology preview: X-ray fused with magnetic resonance during invasive cardiovascular procedures. *Catheter Cardiovasc Interv.* 2007;70(6):773-782.

226. Ector J, De Buck S, Adams J, Dymarkowski S, Bogaert J, Maes F, Heidbuchel H. Cardiac three-dimensional magnetic resonance imaging and fluoroscopy merging: a new approach for electroanatomic mapping to assist catheter ablation. *Circulation.* 2005;112(24):3769-3776.

227. De Buck S, Maes F, Ector J, Bogaert J, Dymarkowski S, Heidbuchel H, Suetens P. An augmented reality system for patient-specific guidance of cardiac catheter ablation procedures. *IEEE Trans Med Imaging.* 2005;24(11):1512-1524.

228. Sra J, Ratnakumar S. Cardiac image registration of the left atrium and pulmonary veins. *Heart Rhythm.* 2008;5(4):609-617.

229. Truong MVN AA, Ginks M, Rinaldi CA, Rezavi R, Penney GP, Rhode KS. 2D-3D Registration of Cardiac Images Using Catheter Constraints. *2009.* 2009.

230. Truon MVN AA, Ginks M, Rinaldi CA, Rezavi R, Penney GP, Rhode KS. 2D-3D Registration of Cardiac Images Using Cardiac Constraints. *Computing in Cardiology.* 2009.

231. Koch KC, Wenderdel M, Stellbrink C, Hanrath P, vom Dahl J. Electromechanical assessment of left ventricular function following successful percutaneous coronary revascularization. *Catheter Cardiovasc Interv.* 2001;54(4):466-472.

232. Samady H, Choi CJ, Ragosta M, Powers ER, Beller GA, Kramer CM. Electromechanical mapping identifies improvement in function and retention of contractile reserve after revascularization in ischemic cardiomyopathy. *Circulation.* 2004;110(16):2410-2416.

233. Henningsson M, Koken P, Stehning C, Razavi R, Prieto C, Botnar RM. Whole-heart coronary MR angiography with 2D self-navigated image reconstruction. *Magn Reson Med.*67(2):437-445.

234. Henningsson M, Smink J, Razavi R, Botnar RM. Prospective respiratory motion correction for coronary MR angiography using a 2D image navigator. *Magn Reson Med.*69(2):486-494.